Exploring the Role of P2X7 Receptor in Regulation of Microglial Function and Behaviour

Hanna Bielecka

A thesis presented for the degree of Doctor of Philosophy at the University of East Anglia, Norwich, UK

School of Chemistry, Pharmacy and Pharmacology

September 2025

Abstract

P2X7 is a purinergic receptor and a non-selective ion channel that becomes activated by high levels of extracellular ATP. Predominantly expressed by immune cells, P2X7 plays a vital role in facilitating immune and inflammatory responses, as well as cell death. In microglia, the resident immune cells of the CNS, P2X7 expression has been linked to various functions beyond inflammation, such as survival, metabolic switch, phagocytosis, and cytokine release. Microglia perform vital functions from development to aging. As such, they are highly adaptable and flexible, responding to the demands in their environment. Modifying microglial responses in health and disease is a promising target for the management of neuroinflammation, neurodegenerative, and neurodevelopmental diseases, yet the full understanding of how microglia function is still to be unravelled. The aim of this thesis was to shed light on the role of the P2X7 receptor in microglia.

The project demonstrated that P2X7 expression, in the BV-2 murine microglial cell line, or in the transfected HEK 293 cell line, does not have a trophic effect and does not affect proliferation. An Alamar blue metabolic assay revealed an interesting advantage of P2X7-expressing cells related to cellular metabolism. P2X7 did not affect cell activation or the expression of polarisation markers in BV-2 cells. P2X7 itself was upregulated with pro-inflammatory stimulants LPS and IFN-γ.

P2X7 expression was shown to promote multinucleation and giant cell (GMC) formation in BV-2 microglia. The GMCs were more numerous and reached larger sizes in the 72h incubation time when P2X7 was expressed. GMCs could be induced with pro-inflammatory stimuli such as LPS, but not with IL-4 or IL-13, and would also form spontaneously without any induction. The effect of pharmacological modulation and inhibition of P2X7 was explored in GMC formation. Microglial GMC morphology, protein expression, and function were evaluated in the BV-2 and BV-2^{P2X7-} model system.

Table of contents

List of figures

List of tables

Acknowledgements

First and foremost, I would like to thank my primary supervisor, Dr Leanne Stokes, for going above and beyond in her guidance, insight, and enthusiasm for the project. Her mentorship and support allowed me to grow and develop my confidence and scientific judgement. It has been a pleasure and a privilege to complete my Master's and my PhD degrees in the Stokes Lab.

I would also like to acknowledge my secondary supervisors, Dr Julie Sanderson and Dr Anastasia Sobolewski, whose feedback was always insightful and greatly appreciated.

Many thanks to Dr Serena Monaco for her collaboration on the NMR metabolomics assay and to Dr Emily Hobson for her collaboration on the NQO1 activity assay.

I would also like to thank Prof Maria O'Connell and Dr Stefan Bidula, who were not part of my project, yet always extended their kind support during my time at the university.

I was blessed with working alongside truly wonderful team members in our lab – many thanks to Dr Elizabeth Allum, Dr Jack Newman, Jacob Browne, and Sarah Bouyabs, for keeping me positive, inspired, and enthusiastic about our purinergic research.

Finally, I would like to thank my dear friends Jack, Sean, Emily, and my wonderful partner, Pedro, who showed me immense love and support as I was finishing my PhD.

I met some of the kindest and most inspiring people here at UEA, and made friendships and connections that changed my life. Thank you, everyone!

*

I would like to dedicate this thesis to my parents. To my dad, Paweł, who would have been happy to know that I pursued a PhD in science at a UK university, and to my mum, Anna, who fiercely supported me as I did.

Declaration by the candidate

I hereby declare that this thesis is my own work. Where other sources of information have been used, or contributions have been made in collaboration, they have been duly acknowledged. I also declare that this thesis does not surpass the permitted word limit.

List of abbreviations

AD	Alzheimer's disease
ADP	Adenosine diphosphate
ALS	Amyotrophic lateral sclerosis
AMP	Adenosine monophosphate
ANOVA	Analysis of variance
ASC	Apoptosis associated speck like protein
ATP	Adenosine triphosphate
APP	Amyloid precursor protein
BBB	Blood brain barrier
BSA	Bovine serum albumin
BzATP	Benzoyl-benzoyl adenosine 5'-triphosphate
CCL2	Chemokine (C-C motif) ligand 2
cDNA	Complementary deoxyribonucleic acid
CNS	Central nervous system
CRISPR	Clustered regular interspaced short palindromic repeats
DAMPs	Damage associated molecular patterns
DMEM	Dulbecco's Minimum Essential Medium
DMSO	Dimethyl sulfoxide
DNA	Deoxyribonucleic acid
dNTP	Deoxynucleotide triphosphate
ER	Endoplasmic reticulum
FBGC	Foreign body giant cell
FBS	Foetal bovine serum
GMC	Giant multinucleated cell
GMC+	Giant multinucleated cell rich (cell cultures)
HEK 293	Human Embryonic Kidney 293 Cells
IFN	Interferon
IL	Interleukin
LGC	Langhan's giant cell
LPS	Lipopolysaccharide
MCP-1	Monocyte chemoattractant protein 1
mRNA	Messenger ribonucleic acid
MTS	3-(4,5-dimethylthiazol-2-yl)-5-(3-carboxymethoxyphenyl)-2-(4 sulphophenyl)-2H-tetrazolium
MTS	Methanethiosulfonate
NF-κB	Nuclear factor kappa B
NLRP3	NOD-, LRR- and pyrin domain-containing protein 3
PAMPs	Pathogen associated molecular patterns
PBS	Phosphate buffered saline
PCR	Polymerase chain reaction
PD	Parkinson's disease
PKC	Protein kinase C
PLD	Poly-D-Lysine
PMA	Phorbol 12-myristate 13-acetate

Poly (I:C)	Polyinosinic:polycytidylic acid
qPCR	Quantitative Polymerase Chain Reaction
RANKL	Receptor activator of nuclear factor kappa-B ligand
RNA	Ribose nucleic acid
ROS	Reactive oxygen species
TLR4	Toll-like receptor 4
TNF	Tumour Necrosis Factor
UDP	Uridine 5'-diphosphate Uridine 5'-triphosphate 221
YO-PRO-1	4-[(3-methyl-1,3-benzoxazol-2(3H)-ylidene)methyl]-1-[3 (trimethylammonio)propyl]quinolinium diiodide

Chapter 1- Introduction

1.1 The immune system of the CNS

The immune system is vastly complex and involves many specialized cell types and mechanisms to provide homeostasis maintenance for the body. It does so by detecting and responding to any arising perturbances such as injury, danger signals, invading pathogens, or cancer cells. The immune cells facilitate tissue repair and often perform organ-specific functions (Marshall et al., 2018). The brain parenchyma is uniquely separated from the rest of the body by the blood brain barrier (BBB) and thereby the brain, apart from the meninges, is effectively isolated from the peripheral immune system (Norris & Kipnis, 2019). The immune system of the CNS is instead managed by specialized cells of myeloid descent called the microglia (Norris & Kipnis, 2019).

Research now shows that the interaction between the immune system, the microglia and the brain is important in not only disease and pathology, but also in health (Kettenmann et al., 2013; Deczjowska et al., 2018). Local cytokine release by peripheral immune cells such as $CD4^+$ T cells in the meningeal spaces, has been shown to interact and modify the responses and recruitment of microglia in the bordering tissue, and influence neuronal function. (Filiano et al., 2017; Kipnis, 2016).

Finally, the non-parenchymal border-associated macrophages (BAMs) also play a role in immune responses of the CNS. BAMs are mostly located in the perivascular spaces, the choroid plexus, and the meningeal spaces. In immune-mediated neuropathologies, they contribute to neuroimmune responses associated with the blood-brain and blood-CSF barriers (Sun & Jiang, 2024).

1.2 Microglia

Microglia, accounting for approximately 5-15% of the cell population of the CNS depending on their exact location, are the tissue-resident macrophages of the brain (Healy et al., 2022; Ochocka & Kaminska, 2021). Microglia differentiate from myeloid progenitor cells of the yolk sac and become the immunocompetent cells which form the first line of defense in the CNS, independently of developing macrophage populations (Kettenmann et al., 2011). Early on during embryonic development (as early as day 9 in mice) microglia migrate to the brain and the CNS parenchyma where they establish local populations and continue to self-renew throughout the adult life (Bruttger et al., 2015). Therefore, microglia colonize the brain before astrocytes, and

days earlier than the first cortical neurons begin to develop (Miller & Gauthier, 2007). In humans, it has been documented that from 4.5 weeks gestation, microglial cells with amoeboid morphology and expressing Iba1, CD68, CD45, and MHC-II markers, enter the cerebral wall from the leptomeninges and the ventricular lumen (Monier et al., 2007; Rezaie et al., 2005).

A balance of proliferation and apoptosis sustains the self-regulated populations of microglia, with enough plasticity to serve the demands of the developing, adult, and aging brain, unlike some other tissue-resident macrophages, whose populations are frequently supported by peripheral monocyte-derived pools (Ajami et al., 2007; Hoeffel et al., 2015; Zhan et al., 2019).

The maintenance of the proliferating microglial populations in the early brain has been associated with interleukin 34 (IL-34) signalling, which is important in microglia homeostasis, and its receptor, CSF 1 receptor (M-CSF-R) (Squarzoni et al., 2014a; Y. Wang et al., 2012). M-CSF-R can also be stimulated by macrophage colony-stimulating factor 1 (CSF-1) and CSF-1 knockout animals show a dramatic reduction in microglia numbers (Hattori, 2022). ATP and P2Y12 have been shown to be important for migration of microglia in the adult brain (Lin et al., 2021) and ATP signaling has been shown to be important for microglial infiltration during development (Maeda et al., 2016, Casano et al., 2016). However, studies on P2Y12 knockout animals suggest that this is not the only mechanism for microglial colonization of the brain (Haynes et al., 2006). PU.1 – a commonly used marker for microglial identity is also key in the microglial differentiation and colonisation of the brain (Kierdorf et al., 2013). PU.1 knockout mice have no parenchymal microglia present in their brains (Kierdorf et al., 2013). Furthermore, downstream of PU.1 signalling, interferon regulatory factor 8 contributes to differentiation and function of developing microglia (Kierdorf et al., 2013). As the cells mature the expression of surface proteins and signalling pathways changes. As discussed above, microglia form separately from macrophage populations and in addition to sharing some key marker genes with other myeloid cells (such as CD11b, CD68, CX3CR1, F4/80 and IBA1) microglia distinctly express PU.1, P2Y12, TMEM19, HexB, Sall1, FCRLS – which are expressed in a lower proportion on macrophages (Jurga et al., 2020). Microglia also have low CD45 and low CD206 (Jurga et al., 2020). This is illustrated in the Figure 1.1 below.

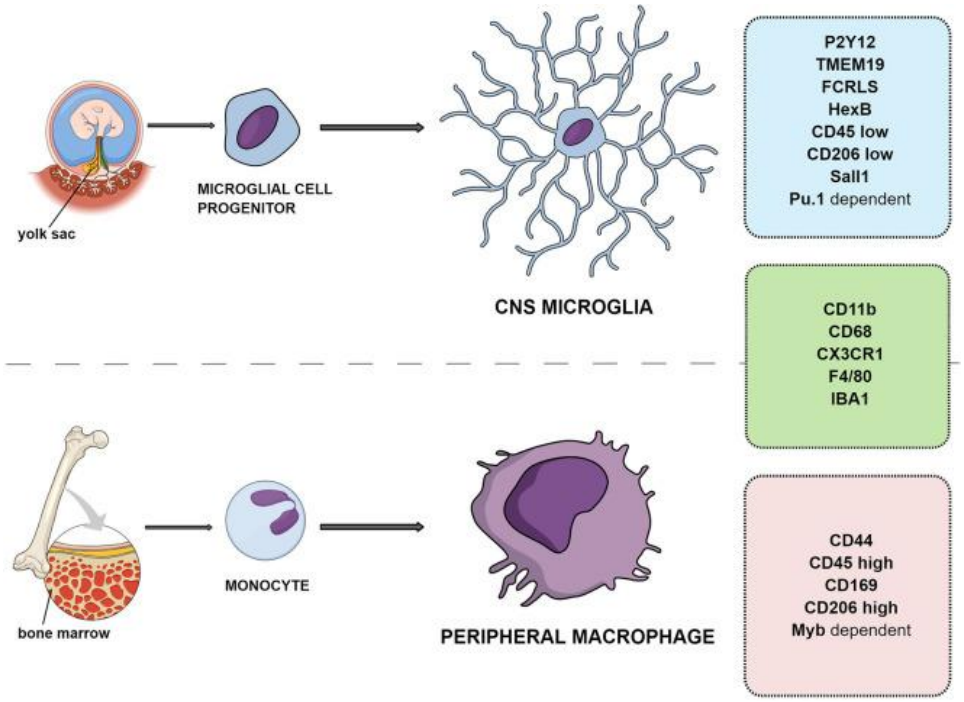

Figure 1.1 Expression of key markers of mature microglia and macrophages. *Microglia derive from the yolk sac in a separate pathway from the macrophages, which originate in the bone marrow. Both types of cells express similar markers (green box), although their expression levels may vary. Certain proteins and receptors are commonly used as markers for each cell type, based on levels of expression. Figure taken from (Jurga et al., 2020).*

Microglia shape cortical development in the brain (Squarzoni et al., 2014b). During development microglia are involved in regulation of neuronal numbers via engulfing neuronal precursors, in remodeling of neuronal connections, pruning of synapses and angiogenesis (Luis Marín-Teva et al., 2004; Perez-Pouchoulen et al., 2015). They are the phagocytes of the CNS; therefore, any accumulated debris, dead cells, or cytotoxic proteins may be cleared up by microglia (Vilhardt, 2005) . Microglia can also bring about cell death upon detecting neuronal malfunction. Filipello et al., (2018) showed that TREM2 receptor expressed by microglia is important for their phagocytic activity during development. At the same time, microglia can have a protective function on their microenvironment. They can release anti-inflammatory cytokines and recruit and trigger regeneration, repair, and neuroprotection (Hermann & Gunzer, 2021).

Microglia are constantly surveilling and monitoring their environment and initiate inflammatory responses upon detection of DAMPs or pathogens (Kettenmann et al., 2011). The cytokine release by microglia recruits and mobilizes surrounding cells to elicit appropriate responses and a tightly controlled inflammatory cascades (Frank et al., 2019; Hermann & Gunzer, 2021; S. J. Yang et al., 2018). Surface receptors on microglia are able to recognize subtle alterations in their

surroundings, such as complement fragments, adhesion molecules, immunoglobulins, chemokine receptors (CCRs), purinoceptors, Toll-like receptors (TLRs), fractalkine (Fc), and scavenger receptors (Frank et al., 2019).

Heterogeneity of microglia is not surprising in view of their many functions, which are well reviewed by (Hughes, 2012; Cronk and Kipnis, 2013; Colonna and Butovsky, 2017; Salter and Stevens, 2017). Microglial distribution, morphology and function vary greatly depending on the location in the CNS and the cells' activation status, and differs greatly in homeostatic vs pathologic conditions (Kettenmann et al., 2011).

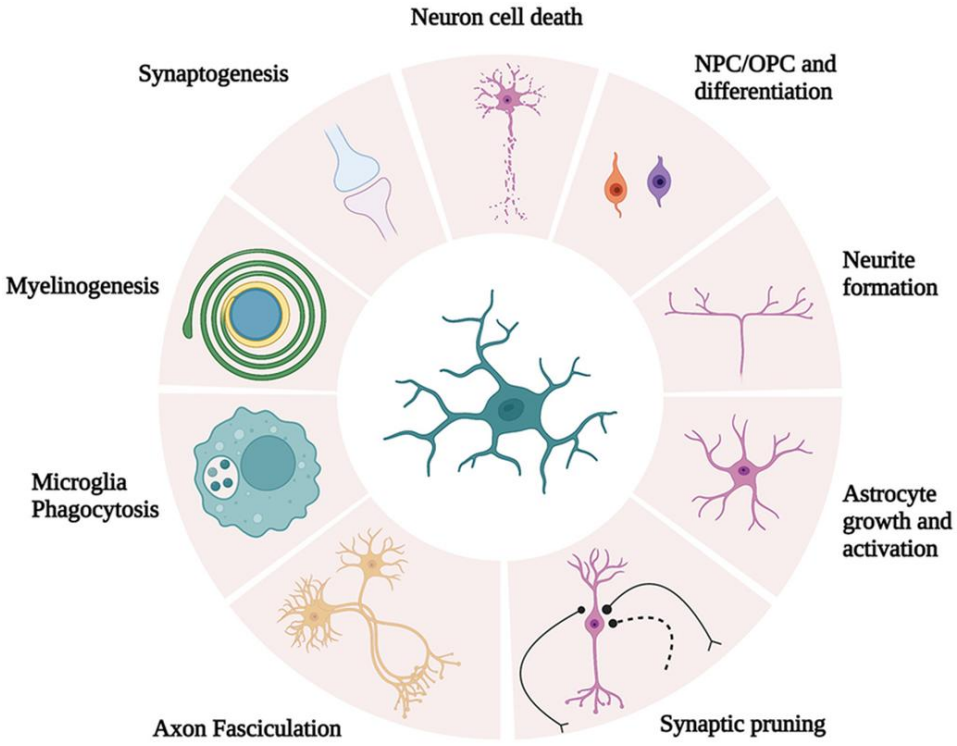

***Figure 1.2* Various functions of microglia in the CNS.** *Microglia adopt a variety of roles in CNS across the lifespan. In development, they assist with axon fasciculation, myelinogenesis, synaptogenesis and neurite formation. They perform phagocytic functions to engulf any pathogens and cell debris resulting from injury, neuron cell death, or tissue remodelling. Microglia play key roles in synaptic pruning, neuronal precursor cell (NPC) regulation, and promote astrocyte growth and activation. Figure taken from Saucier et al., (2023).*

Microglia switch flexibly between resting and activated states displaying different pro or anti-inflammatory and phagocytic profiles (Kettenmann et al., 2011; Paolicelli et al., 2022). Differences are also observed between male and female microglia (Kettenmann et al., 2011). Age is also an important factor to consider, as microglial phenotypic tendencies vary in developing vs adult vs an aging brain, and are key in correct pruning of synaptic connections (Wendimu & Hooks, 2022), self-renewal ability and proliferation (Réu et al., 2017). Microglia also play a role in the development of neuronal terminals, guiding cell migration and axonal growth of neurons via release of substances and cell-to-cell contact. In the adult brain this activity is mostly downregulated and microglia are found predominantly in a resting state until presented with a pathological or homeostatic challenge (Vilhardt, 2005). Kettenmann et al., (2013) and Salter and Stevens, (2017) describe how in neuropathologies microglia drive excessive synaptic and neuronal clearance, which may amplify the dysfunction of neurones, ultimately worsening functional and cognitive function. Disease-associated microglia not only perform activated functions such as phagocytosis or cytokine release, but also modulate the microenvironment at the incident site, which affects surrounding cells and their phenotypes and behaviour (Deczkowska et al., 2018).

1.2.1 Microglial activation and polarisation

Microglia are similar to macrophages in the functions they perform, such as their phagocytic ability, production and release of growth factors, nitrogen compounds, and free radicals, or their responses to chemokines, migrating capacity, release of cytokines, and antigen presentation (Prinz et al., 2014). Pattern-associated molecular patterns (PAMPs), danger-associated molecular patterns (DAMPs), and other signals trigger appropriate response mechanisms to pathogens and damage in the microglial environment, causing microglia to assume different phenotypes and characteristics to perform their many functions (Norris & Kipnis, 2019). A system describing polarisation of macrophages as M1 and M2 phenotypes has been previously developed to aid experimental guidelines by simplifying and classifying stages of macrophage polarisation and activation (Murray et al., 2014), and the same system has been applied by many authors to microglia. Phenotypic polarisation is thought to be regulated and influenced by the tissue microenvironment, as well as extrinsic and intrinsic cellular pathways, such as metabolic changes (Bernier, York, & MacVicar, 2020; Norris & Kipnis, 2019; Orihuela et al., 2016). However, researchers now widely agree that microglia and macrophages would be more accurately described as existing in a flexible spectrum of phenotypes, rather than being permanently committed to a restricted, narrow panel of behaviours and expressed receptors and markers

(Flowers et al., 2017; Healy et al., 2022). A recent paper by Paolicelli et al., (2022) has classified the old categorisation system as outdated and counterproductive to understanding the true nature of microglia, as it implies conformity to just the three rigid and limited phenotypes. Instead, it is now proposed that microglia exist on a fluid spectrum and constantly update the expression and synthesis of proteins in response to environmental cues as well as 'memory' of previous events, resulting in carefully tailored adaptations and responses. Figure 1.3 depicts the spectrum of microglial activation and varied phenotypic display.

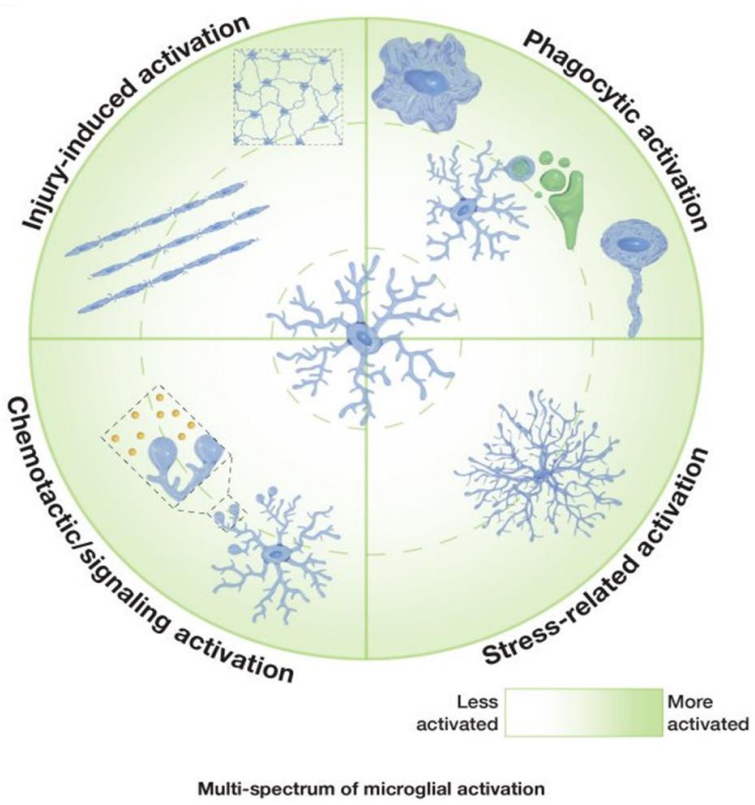

Figure 1.3 Microglial polarisation and activation resembles a spectrum. *Cells vary their response depending on the level of activation and the required activity. Stress or injury-related activation bares specific characteristics and differs from chemotactic activation or phagocytic phenotype. In each activated state, the cells express specific markers that may be upregulated or downregulated and associated with morphological changes or release of cytokines and signalling factors. Figure taken from Vidal-Itriago et al., (2022).*

However, in a simplified view, convenient for a laboratory set-up, microglia can be polarised into two main activated states from their quiescent, resting state. Under homeostatic conditions they

are found in a ramified shape with small, round cell bodies with little cytoplasm and extensive branching processes. In this dominant state, they are constantly probing their microenvironment with their processes. However, the activated microglia assume a different 'ameboid' shape and a rounded cell body with thicker and shorter pseudopodia, upon detection of danger signals, which results in efficient chemotaxis to the area, and activity such as the release of cytotoxic substances and phagocytosis. Depending on the duration of the inflammatory status or signals and strength of activation, microglia will exist in various intermediate states between the quiescent and activated phenotypes (Kettenmann et al., 2011). It is worth emphasizing that the expression of different proteins and their functional profile at any time highly depends on the microenvironment and does not conform to either extreme. While the classification of M0/M1/M2 phenotypes allows for a convenient reference system, more recent publications have now moved away from this system.

Activation of microglia can be brought about by exogenous PAMPs, LPS, pathogen genetic material, viruses, or endogenous signals such as DAMPs, protein aggregates, e.g. amyloid β and senile plaques, apoptotic cells, or recognition of 'find me', 'eat me', or 'do not eat me' signals, which bring on expression of genes associated with bringing on the pro-inflammatory responses (Korzhevskii & Kirik, 2016; Vilhardt, 2005). Chemokines such as CCL-2 and cytokines such as TNF-α, and IFN-γ can also trigger a further propagation of pro-inflammatory responses including release of IL-1β, or higher expression of iNOS and recruit further microglia creating autocrine loops (Deczkowska et al., 2018; Flowers et al., 2017; Frank et al., 2019; Tsuda, 1959). While anti-inflammatory factors such as IL-4 and IL-13 can induce an anti-inflammatory phenotype and promote expression and release of the brain-derived neurotrophic factor (BDNF) and other neuroprotective factors (Hanisch, 2002; Jurga et al., 2020). This is illustrated in Figure 1.4 and further discussed in the introduction to Chapter 4 which addresses microglial activation. Contact with other cells, such as neurons, also appears to be important in inducing activation. For example, the interaction of the cluster of designation 200 (CD200) protein on neuronal membranes with the myeloid cell receptor (CD200R) downregulates microglial activation via an inhibitory signal (Vilhardt, 2005).

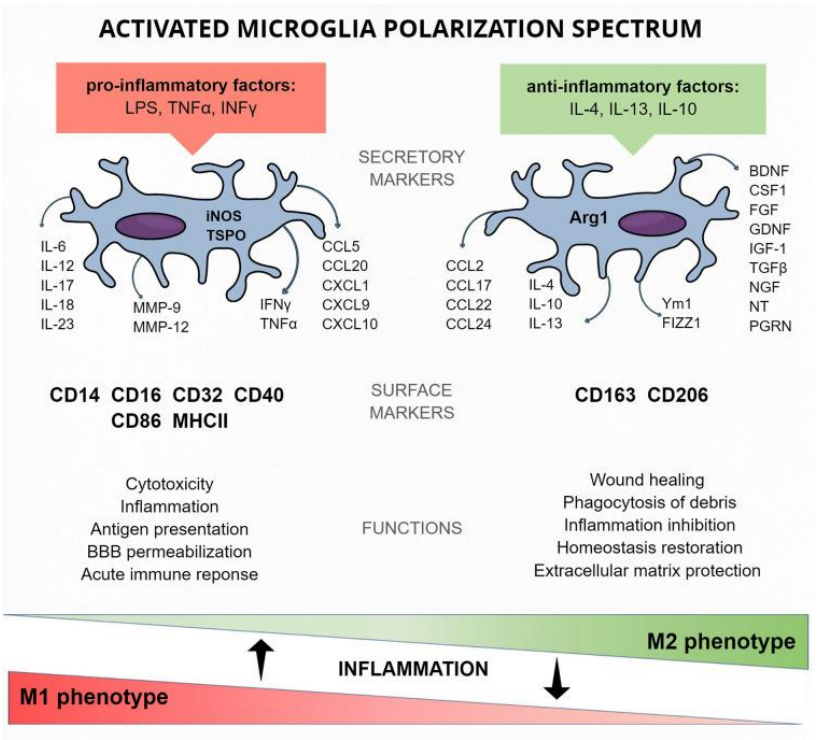

Figure 1.4 Microglial activation and expression of classical pro- and anti-inflammatory markers. *Expression levels of markers and receptors on microglia vary depending on the activation phenotype of the cells. They can be induced by proinflammatory factors (red) or anti-inflammatory factors (green) and are associated with specific functions. Figure taken from Jurga et al., (2020).*

A few studies have looked into the property of microglia to multinucleate and form giant cells, which have been noted in some neurological conditions and animal models of neurological diseases (Fendrick et al., 2007; Fu et al., 2024; Hornik et al., 2014; Suzumura et al., 1999; Wei et al., 2020). This quality is known in macrophages, and in the case of macrophage-derived osteoclasts, it allows the cells to undergo adaptations to perform their highly specialized function (Sabe et al., 2024). Very little is known about this property in microglia, however, the literature suggests that these cells arise in inflammatory conditions and may be associated with enhanced phagocytic function (Milde et al., 2015). Although giant multinucleated cells form only a low percentage of the total microglial population, their identity and function should be better understood, and this gap in research should be addressed with further studies. Further information on multinucleation can be found in Chapter 5, where a full introduction to the topic is given.

1.2.2 Microglial metabolism

Highly plastic and adaptable, microglia have the ability to rapidly switch their metabolism to match the demands of their environment and function (Jung et al., 2019; Orihuela et al., 2016). Depending on nutritional availability, microglia can utilize glycolysis or glutaminolysis (Ghosh et al., 2018). With their main metabolic pathway being oxidative glycolysis, in times of increased demand and inflammation, microglia can shift towards aerobic glycolysis (Bernier, York, & MacVicar, 2020). Immunometabolism studies show that metabolic maladaptation in microglia directly affects numerous neurological conditions and diseases (Bernier, York, & MacVicar, 2020; Jung et al., 2019; Mithaiwala et al., 2021). Microglial metabolism is well reviewed by Bernier et al., (2020). Research also suggests that the correct metabolic shift in microglia is necessary for the required nitric oxide (NO) and cytokine output(Bernier, York, & MacVicar, 2020). L. Wang et al., (2019) showed that inhibition of the glucose transporter GLUT1 receptor reduces polarized response to LPS and IFN-γ. Inhibition of the glycolysis pathway using 2-deoxy-d-glucose (2-DG) can be used to eliminate microglia completely from neuronal and astrocytic cocultures (Vilalta & Brown, 2014), and to reduce IL-1β, TNF-α, and IL-6 transcription from primary microglia induced with LPS (Yan et al., 2020;Liu et al., 2023). LPS treatment is generally associated with lowered oxidative phosphorylation (OXPHOS) in multiple models of microglia (Nair et al., 2019).

PAMPs and DAMPs, as well as cytokines, can induce metabolic changes in microglia and modify their responses, and the mTOR pathway specifically has been linked to regulation of this glycolytic switch in microglia, which was also demonstrated on BV-2 cells (Hu et al., 2020; Liu et al., 2023), and possibly occurs via HIF-1α signalling, which has been shown in Alzheimer's disease (Baik et al., 2019). Transcription factors regulate the preferential metabolic pathways by maintaining expression levels of key metabolic enzymes such as PFKFB3 and accumulation of metabolic TCA metabolites (O'Neill et al., 2015). The relationship between activation of microglia and metabolic pathways inside the cells are believed to drive cycles of neuroinflammation, when dysregulated. This is shown in Figure 1.5

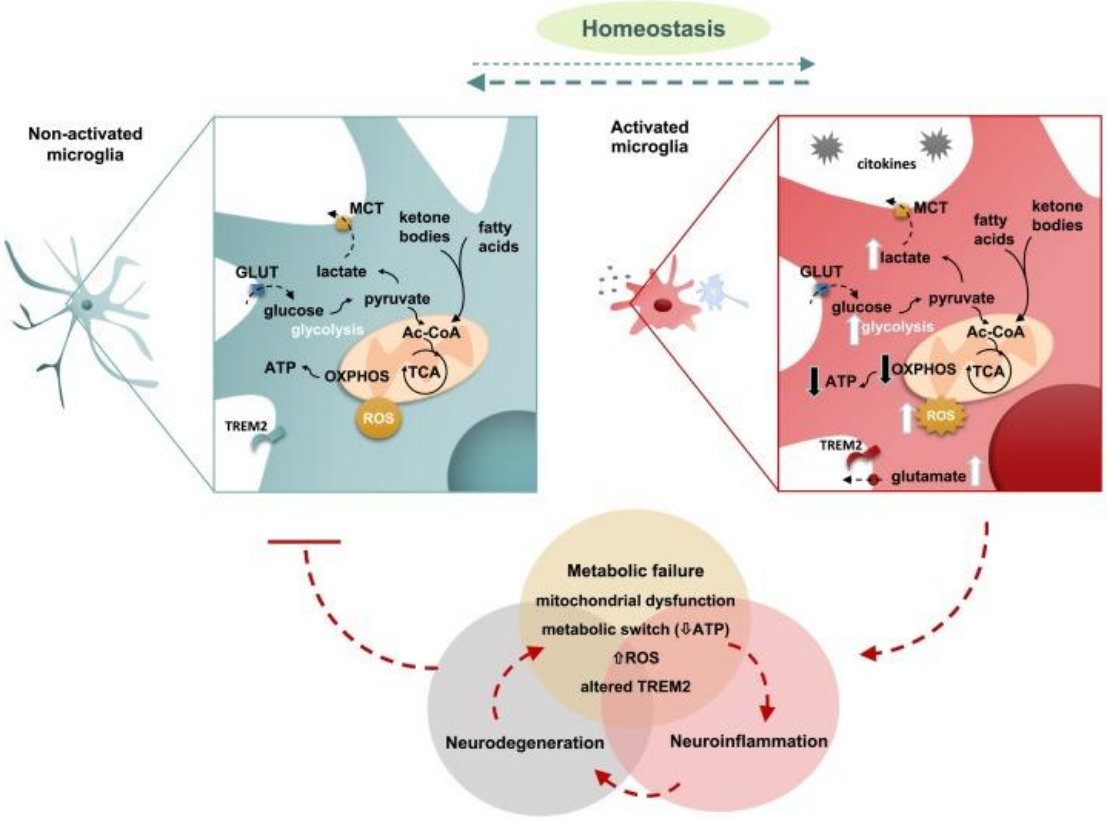

Figure 1.5 Microglial activation is associated with a metabolic switch in favor of glycolysis and away from oxidative phosphorylation (OXPHOS). *The acute microglial neuroinflammatory responses involve release of several inflammatory mediators, cytokines, and ROS. This acute response is beneficial to the CNS, as it can resolve damage and promote repair. However, chronic microglial activation can propagate cycles of neuroinflammation, and neurodegeneration. Oxidative stress and proinflammatory mediators can damage mitochondrial enzymes and mitochondrial DNA. At the same time, mitochondrial dysfunction accompanied and increased ROS production can activate neighbouring microglia. Microglial activation and mitochondrial dysfunction have been linked to molecular pathways of neuronal degeneration. Figure taken from Aldana., (2019).*

1.2.3 Microglia in aging

Aging microglia may often resemble an activated, pro-inflammatory state(Flowers et al., 2017). For example, studies on rodents indicate that levels of activation markers on microglia in older animals, such as MHC II, CD45 and CD4 are expressed at a higher level throughout the brain (Antignano et al., 2023). Aged microglia are believed to be in a phenotypic state ready to strongly respond to a pro-inflammatory stimulus. This priming is thought to occur via downregulation of homeostatic genes, which otherwise inhibit inflammatory responses, (e.g. CD200, CXCL1, sialic acid and CD47) (Divangahi et al., 2021) and simultaneous upregulation of

MHC, CD86, CD68, CR3, Clec7a and TLRs, which are all associated with pro-inflammatory behaviour (Divangahi et al., 2021; Niraula et al., 2017). The morphology of the microglia may also appear altered and cytoskeletal changes have been noted(Deczkowska et al., 2018; Flowers et al., 2017). Motility of the cells and phagocytosis ability is affected and as a result older microglia struggle to remove debris material in the brain (Antignano et al., 2023). It should be noted that most of the studies available to date have been carried out on mouse microglia which may not be reflective of human aging, however, these studies suggest that complement system C3 and C1q levels as well as pro-inflammatory cytokines such as IFN-γ may be important (Antignano et al., 2023). Metabolic changes are also discussed in many studies. Lipid metabolism is different in aging microglia and lipid laden microglia have been associated with neurodegenerative diseases and reduced phagocytosis (Marschallinger et al., 2020). Metabolic changes may be further exacerbating local inflammatory microenvironment (Minhas et al., 2021).

1.2.4 Implicating microglia in disorders

It is not surprising that faulty regulation of microglial activation and polarization or an enduring inflammatory state may result in cytotoxicity to the surrounding neural tissue by exposing the CNS to cytokines and ROS species, chemokines, and complement proteins released by microglia, which can have neurotoxic effects in case of a chronic and ongoing exposure (Norden and Godbout, 2013a). The pro-inflammatory factors secreted by activated microglia can easily exacerbate and drive neurodegenerative diseases by triggering neuronal death, and microgliosis has been an area of research in understanding of numerous neuropathologies (Niraula et al., 2017; Wendimu & Hooks, 2022). Microglial-associated inflammation is linked with neurodegenerative conditions such as Alzheimer's Disease (AD), prion diseases, multiple sclerosis (MS), and Amyotrophic Lateral Sclerosis (ALS) (Kuntzel and Bagnard, 2022).

An alternatively activated phenotype of microglia is associated with autophagy and promotion of repair. Like macrophages, in simplified terms, microglia's immediate response to damage is pro-inflammatory, which then shifts towards pro-resolving (Vilhardt, 2005). AD is an example where promoting the transition into a pro-resolving phenotype, allowing for enhanced autophagy and reduction of the pro-inflammatory action, could provide a way of targeting AD-associated neuroinflammation and plaque buildup. Shifting or influencing the microglial phenotype itself presents a promising pharmacological target, and therefore, careful distinction of the phenotypes is important.

Furthermore, the link between microglia and depression is strong, since microglia affect synaptic plasticity and neural network formation, as well as inflammation, in the brain, all of which impact depressive disorders (H. Wang et al., 2022). Changes in the microglia in the brain regions associated with depression, such as the amygdala, the prefrontal cortex, and the anterior cingulate cortex, have been observed in clinical studies. In suicide victims, increased microglial activation and priming, as well as increased microglial cell numbers, have been found in white matter areas associated with depression (Torres-Platas et al., 2014). Microglial activation and neuroinflammation has been also linked to the pathogenesis of anxiety, schizophrenia, and autism symptoms (Yirmiya et al., 2015). NLRP3 inflammasome, in particular, is being explored as a possible target in treatment of affective disorders (Xia et al., 2023). According to H. Wang et al., (2022) microglial changes which contribute to the pathology of depression involve the regulation of inflammatory response, such as NLRP3 inflammasome recruitment, decreased neurogenesis, and altered tryptophan metabolism via the kynurenine pathway. In this way, microglial behaviour severely affects neurons and leads to affective and cognitive symptoms.

Microglia and neuroinflammation have also been linked to chronic pain (Karavis et al., 2023). Neuropathic pain is associated with changes in the physiological processing of sensory stimuli, and common features include allodynia and hyperalgesia (Campbell & Meyer, 2006). Studies report that in response to peripheral nerve damage, an increase in microglia numbers in the spinal cord is frequently observed (Karavis et al., 2023). CSF-1 mediated signalling from injured neurons recruits and activates microglia to the site, where it leads to increased proliferation of microglia (Guan et al., 2015). Activity and inflammatory cascades initiated by microglia have been proposed to facilitate the transition from acute to chronic pain, as microglia participate in mediation, expansion of pain, and sensitization, via mechanisms involving ATP and fractalkine pathways (Campbell & Meyer, 2006; Tsuda, 1959). In the brains of animal models of chronic neuropathic pain, activation of microglia and microgliosis has been observed in the brain areas associated with chronic pain, such as the thalamus and somatosensory cortex (Taylor et al., 2017). P2X7 activation and downstream release of pro-inflammatory cytokines TNF-α, IL-6, and IL-1β has been linked to pathogenesis of neuropathic pain (Teixeira et al., 2010), while P2X7 knockout mice show a reduced sensitivity to pain (Chessell et al., 2005; J. Zhang et al., 2024).

1.3. Purinergic signalling and P2X7 receptor

1.3.1 Purinergic signalling

As well as being the primary intracellular source of energy for cells, nucleotides such as ATP perform an important function as extracellular signaling molecules (Burnstock, 2018; Idzko et al., 2014). Cells release low amounts of ATP and its metabolites under homeostatic conditions as a form of signaling (Burnstock, 2018). Under certain conditions such as mechanical stress, in dangerous environment such as hypoxia, cells can release large amounts of purinergic ligands ATP, ADP, UTP, and UDP (Burnstock, 2018). Purinergic signaling comprises a family of receptors- P1, P2, PY, and PX, which were first described by Burnstock in 1976, and subsequently categorized and described in detail (Hoult et al., 1979). G-protein coupled receptors, which can be activated by various purinergic ligands, have been named P2Y receptors (P2Y 1,2,4,6,11,12,13,14), and the ligand-gated ion channels, which are predominantly activated by ATP, comprise the P2X receptors (P2X 1,2,3,4,5,6,7) (Abbracchio and Burnstock, 1994; Burnstock, 2007). Purinergic receptors and their ligands are summarized in Figure 1.6 B. Evolutionary conservation of purinergic signaling highlights its importance and involvement in vital functions. In mammalian organisms, the immune system, endocrine and exocrine systems, platelet aggregation, pain signaling, inflammation cascades, vasodilation, and even cell proliferation and differentiation, all rely on purinergic signaling (Burnstock, 2018). Purinergic regulation and modulation of the immune system and inflammation has gained particular interest and attention in research since its discovery (Kaczmarek-Hájek et al., 2012). Under physiological conditions, the average levels of nucleotides in the blood are below 0.1 µM, however, under stress and cellular injury, local concentration of nucleotides can increase rapidly, as rupturing cells release their cytosolic ATP which inside the cell can reach up to 5mM, which triggers purinergic receptors in a variety of ways since they have different sensitivities and roles in health and disease (Di Virgilio et al., 2003). ATP and purinergic signalling is summarised in the Figure 1.6 below. Normally ATP is present at low concentration in the extracellular space. ATP can be released by exocytosis, membrane channels such as P2X7, connexin-43 hemichannels, and pannexin-1 channels, or by specific transporters such as ATP-binding cassette (ABC) transporters. ATP in the extracellular space is broken down into different metabolites which include adenosine diphosphate (ADP), and adenosine; by ectonucleotidases (e.g. ectonucleoside triphosphate diphosphohydrolase family (E-NTPDases)), ectonucleotide pyrophosphatase/phosphodiesterase family (E-NNP), and alkaline phosphatases (ALP) (Burnstock, 2018; Gil et al., 2022). ATP release can rapidly increase with cell death, inflammation and even with increased neuronal activity in the CNS. ATP signalling and especially

perhaps the P2X7 purinergic receptor is now recognised as a key player in neuroinflammation and neurodegenerative pathologies (Gil et al., 2022).

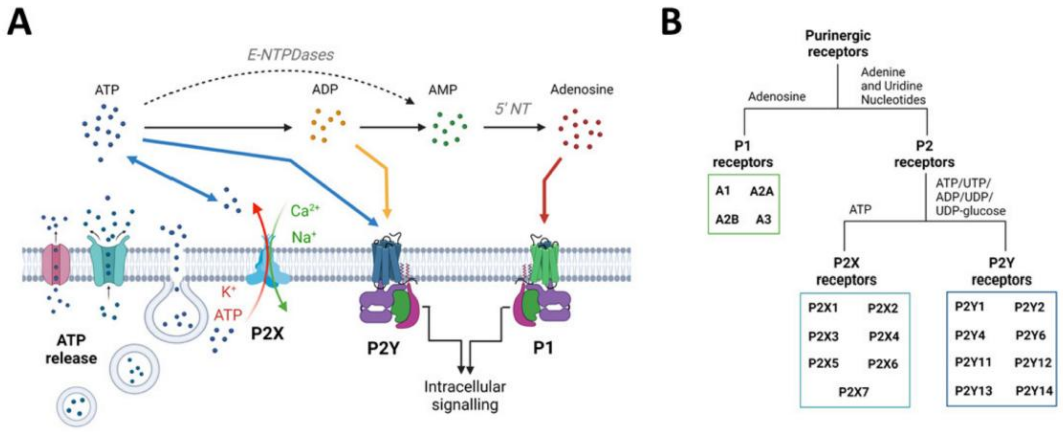

Figure 1.6 Purinergic signalling. A *ATP is released from transporters, membrane channels and via exocytosis from neurons and glial cells. Ectozymes such as NTPDases, NPPases, and alkaline phosphatases convert ATP into ADP and AMP. ATP in the extracellular space acts on P2X (ligand gated) and P2Y (G protein coupled) receptors, while ADP also acts via subtypes of P2Y receptors, and Adenosine acts via P1 (G protein coupled) receptors.* ***B*** *Purinergic receptors are divided into adenosine-sensitive P1 receptors (further categorized into A1, A2A, A2B, and A3 receptors) and nucleotide-sensitive P2 receptors, which include the inotropic P2X and the metabotropic P2Y receptors. All seven mammalian P2X receptor subtypes respond to ATP. The eight different P2Y receptor subtypes respond to ATP, ADP, UTP, UDP, or UDP-glucose, depending on the subtype. Taken from Gil et al., (2022).*

1.3.2 P2X7 structure and activation

First cloned in 1996, in earlier literature, P2X7 is sometimes termed P2Z, as it was originally classified separately from other P2X ion channels due to its distinctive characteristics (Suprenant et al., 1996). P2X7 is expressed in immune cells at high levels (this includes macrophages, mast cells, T-cells, and microglia in the CNS) and is also expressed in other cells, such as epithelial cells (Savio et al., 2018). In the nervous system, studies have shown P2X7 function in microglia, Schwann cells, oligodendrocytes, and even astrocytes and neurons, although the evidence for expression in neurons is more contradictory (Kopp et al., 2019). P2X7 has been shown to play a role in bone tissue maintenance, and it is expressed by both osteoclasts (Grol et al., 2009), and osteoblasts (Orriss et al., 2012). The human P2X7 gene is located on chromosome 12 and comprises 13 exons (Buell & Rassendren, 1998). Several splice variants of P2X7 exist, and as a result of single nucleotide polymorphisms, different expression and function levels of P2X7 are

present in humans (Cheewatrakoolpong et al, 2005; Sluyter & Stokes, 2011), with altered binding properties of the ATP agonist and different downstream signaling outcomes (Xu et al, 2012).

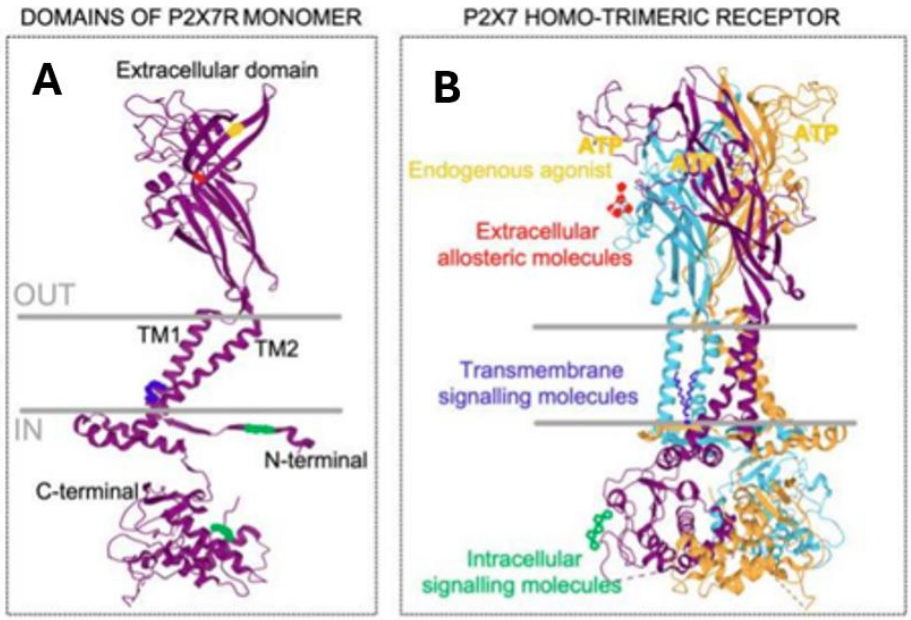

Figure 1.7 P2X7 structure. ***A*** *Structure of the P2X7 monomer composed of five domains; extracellular domain, transmembrane 1 (TM1), transmembrane 2 (TM2), intracellular C-terminus, and intracellular N-terminus. The colours into the domains represent possible specific molecular recognition sites.* ***B*** *Homotrimeric P2X7 receptor composed of three monomers (purple, blue, and orange) position into the trimeric receptor showing possible signaling and activating molecules. Intracellular messengers interact with P2X7 at the N- and/or C- termini (green), membrane residues at the transmembrane domains (blue), and the endogenous agonist adenosine triphosphate (ATP, yellow), and allosteric modulators (red) bind the extracellular domain. Figure taken from Martinez-Cuesta et al., (2020).*

P2X7 is a non-selective cation channel that does not typically desensitize. Upon sustained activation, it results in a macropore formation, which facilitates Na^+, Ca^{2+} influx, K^+ efflux, and allows large molecules (up to 900 Da in size) such as fluorescent dye YO-PRO-1 or ethidium bromide to enter the cell (North and Surprenant, 2000). Human P2X7 is a homotrimeric channel, comprising three membrane-spanning subunits. Although it has also been shown in a heteromeric combination with P2X4 subunits (Antonio et al., 2011), there is also evidence in the literature showing that native P2X7 does not exist as heteromers (Nicke, 2008). The structure of P2X7 is shown in Figure 1.7. P2X7 monomeric structure comprises a large extracellular domain, and two transmembrane domains, with C- & N- termini on the cytoplasmic intracellular side (Kopp et al., 2019).

The C terminus has been implicated in positioning of the receptor in membrane microdomains and in facilitating contact with signaling molecules (Kopp *et al.*, 2019). The sequence of the C terminus holds regulatory mechanisms for many abilities of the receptor, such as the characteristic lack of desensitization (Costa-Junior et al., 2011). The C-terminus is also thought to be linked to the receptor's cytolytic activity and a putative binding site for bacterial lipopolysaccharide (LPS) (Denlinger et al., 2001a).

The C terminus is involved in pore formation, and its truncation or deletion was shown to highly interfere with P2X7-mediated properties such as large dye uptake or membrane blebbing (Smart et al., 2003; Kopp et al., 2019). The exact mechanism underlying the formation of this large pore is still debated (Di Virgilio, Schmalzing, and Markwardt, 2018). Different ideas have been put forward to explain the mechanism underlying this macropore formation. It has been proposed that other transmembrane channel proteins, such as Pannexin 1, may be recruited in the process (Pelegrin & Surprenant, 2006), however, more studies are now suggesting that the dilation of the pore is intrinsic and a property of the P2X7 ion channel independently of pannexin (Di Virgilio et al., 2018). The N terminal has also been proposed to regulate pore dilation and diameter (Allsopp & Evans, 2015;Yan 2008). Di Virgilio et al. (2017) showed that the N-terminus and the transmembrane domains of P2X7 are crucial for the gating and dilation of the pore.

The ATP binding site is located in the large extracellular domain between adjacent subunits and its binding leads to a sequence of conformational changes that pull the channel open (Kopp et al., 2019). Three ATP molecules are required to bind the receptor to initiate the opening, and each ATP binding propagates the conformational changes of the subsequent ATP molecules (Jiang et al, 2012).

Although, ATP is the only known physiological agonist of P2X7 receptors, a synthetic agonist BzATP is also frequently used in research experiments to elicit responses, with an approximately 30-fold greater potency than ATP (North and Surprenant, 2000). P2X7 is the only P2X receptor that is exclusively activated by high levels of extracellular ATP (0.3-2.5 mM) (Suprenant 1996; Di Virgilio et al., 2017). Under physiological conditions, the extracellular levels of ATP remain relatively low; however, in inflammatory, stressed, or tumour environments, the cells release high levels of ATP, which in these conditions functions as a DAMP signaling molecule activating P2X7 (Di Virgilio et al., 2003).

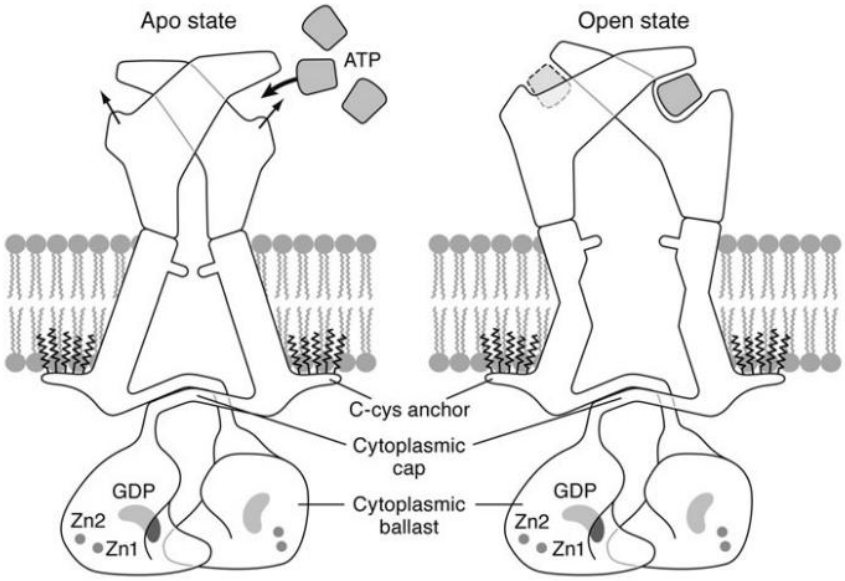

Figure 1.8 Gating of the P2X7 receptor. *P2X7 receptor subtype does not normally desensitize. Three molecules of ATP are required for the channel to open. The conformational change opens the transmembrane channel. Major features of the cytoplasmic domain include: the palmitoylation moieties in the C-cys anchor, and the high-affinity guanosine nucleotide binding site and dinuclear zinc ion complex, both located in the cytoplasmic ballast. Figure taken from McCarthy et al., (2019).*

1.3.3 Pharmacology of P2X7

While ATP is the only known endogenous agonist of P2X7, and BzATP is the only commonly used, more potent synthetic agonist, there are many antagonists and allosteric modulators of P2X7 that have been developed. Both ATP and ADP molecules activate other purinergic receptors as well at low concentrations, while P2X7 is activated by relatively high concentrations. In fact, selective P2X7 agonists are not currently known. Main Pharmacological modulators of P2X7 are listed in Table 1.1 below.

Allosteric modulators act at a different site of the receptor than the orthosteric, agonist binding site. They enhance or inhibit the activity and sensitivity of the receptor to its agonist, often via inducing conformational changes of the receptor protein, or blocking the agonist binding site indirectly. There is a lack of selective modulators of P2X7 since many of those compounds act on other purinergic receptors as well. The known NAMs and PAMs of P2X7 are well reviewed by Müller & Namasivayam, (2022).

Since only very high concentrations of ATP are capable of activating P2X7, it has been proposed that positive allosteric modulators (PAMs) may play a role in pathological and physiological conditions (Walker, 2022). Various phospholipids at high concentrations are capable of enhancing ATP potency (Karasawa Akira et al., 2017). Human P2X7 has also shown potentiation to arachidonic acid (Barbieri et al., 2008).

There are also some known endogenous negative modulators of P2X7. Intracellular ions are capable of modulating P2X7 activity- for example, extracellular magnesium ions reduce the pore activity (Harkat et al., 2017), while extracellular divalent cations affect the conformational plasticity of the pore (Khakh and North, 2006; Wang et al., 2020). Peverini et al., (2018) talked about the importance of lipid composition in the cell membrane for P2X7 activation, emphasising that lipids such as sphingomyelin and phosphatidylglycerol positively impact the passage of large cations through P2X7, while cholesterol inhibits the process. In peripheral cells, lithocholic acid has been described as an endogenous modulator of P2X7 (Sivcev et al., 2020), and intercellular pH has been shown to influence P2X7 activation (X. Liu et al., 2009; Sekar, Huang, Chang, et al., 2018). A newly published paper (Mou et al., 2025) provides evidence for NADPH acting as a modulator of P2X7, important in the inflammatory responses of microglia. The authors demonstrate that NADPH binds to P2X7 directly and inhibits the downstream activation of the NLRP3 inflammasome.

Several pharmacological compounds, such as polymyxin B (Ferrari et al., 2004), clemastine (Nörenberg et al., 2011a), ivermectin (Nörenberg et al., 2012), and natural compounds from Panax ginseng, such as ginsenosides (Piyasirananda et al., 2021), have been reported in literature as positive modulators of P2X7.

P2X7 antagonists have been an active topic of research over the past years. The first generation NAMs used in research included Brilliant Blue G (BBG), calmidazolium, and KN-62 (Walker, 2022). Since then, a selection of CNS-penetrant, more potent, and highly selective NAMs has been discovered (Kwak et al., 2018). Examples include AZ10606120, which is a quinoline derivative with high water-solubility. Preclinical studies on mice show antiangiogenic effects and anti-tumour activity of this compound (Kan et al., 2023). JNJ-47965567, a pyridine derivative, is an example of a brain-permeable NAM. It effectively inhibits P2X7-mediated calcium influx and IL-1β release, and in preclinical animal studies in rat models, JNJ-47965567 had moderate effects on treating neuropathic pain, and attenuated hyperactivity in an-amphetamine-induced model (Bhattacharya et al., 2013).

Table 1.1 Selected examples of P2X7 agonists, antagonists and modulators. *Example reported EC50/IC50 values are provided for human (h), mouse (m) and rat (r) P2X7 receptor from selected literature.*

Selected Compounds with P2X7 activity	Reported EC_{50}/IC_{50} values (μM)	References
Agonists		
ATP	541(h) 130(r) 2400(m)	(Müller & Namasivayam, 2022)
BzATP	0.370–4.7(h) 10(r) 100(m)	
Positive Allosteric Modulators (PAMs)		
Ivermectin	0.056(h) >3(r) >3(m)	(Müller & Namasivayam, 2022; Nörenberg et al., 2012)
Polymyxin B	25 (h)	(Ferrari et al., 2004, 2007)
Clemastine	10 (h)	(Nörenberg et al., 2011a)
Tenidap	n/a	(Sanz et al., 1998)
Abcavir	n/a	(Collado-Díaz et al., 2021)
HEI3090	n/a	(Douguet et al., 2021)
Ginsenoside CK	61.6 (h)	(Piyasirananda et al., 2021)
Endogenous PAMs		
Arachidonic acid	n/a	(Barbieri et al., 2008)
Lithocholic acid	n/a	(Sivcev et al., 2020)
sphingomyelin	n/a	(Karasawa Akira et al., 2017)
phosphatidylglycerol	n/a	(Karasawa Akira et al., 2017)
Negative Allosteric Modulators (NAMs)		
KN-62	12.7 (h)	(Gargett & Wiley, 1997)
Brilliant Blue G (BBG)	0.2 (h) 10 (r)	(L.-H. Jiang et al., 2000)
Calmidazolium	0.1 (h)	(Chessell et al., 1998)
Oxidised ATP	n/a	(Müller & Namasivayam, 2022)
AZ 10606120	0.0014(h) 0.019(r)	
A-740003	0.04–0.08(h) 0.004–0.059(r) 0.250(m)	
A-804598	0.010–0.060(h,r,m)	
GW 791343	0.063–0.126(h)	
JNJ 47965567	0.005–0.0350(h) 0.0047–0.098(r) 0.00065(m)	
AZD9056	0.0035–0.015(h) 0.0044–0.130(r) 1.70(m)	
[^{11}C]SMW139	0.0046(h) 0.0206(r)	
CE-224,535	0.001–0.014(h) 0.470(r) 0.660(m)	
JNJ-42253432	0.020(h) 0.016(r) 0.079(m)	
JNJ54175446	0.003(h)	
[^{11}C]JNJ-54173717	0.0077(h) 0.010(r)	
[^{18}F]JNJ-64413739	0.001–0.0159(h) 0.002–0.0027(r)	
JNJ55308942	0.010(h) 0.015(r)	
[^{3}H]JNJ-54232334	0.0003–0.0005(h) 0.0316(r)	
A438079	0.0126–2.10(h) 0.20–0.91(r) 2.90(m)	
A-839977	0.020(h) 0.042(r) 0.150(m)	
GSK1482160	0.03–0.119(h) 0.250–1.90(r) 2.30(m)	
Endogenous NAMs		
Metal cations and protons (Ca^{2+}, Mg^{2+}, Cu^{2+}, H^{+})	$MgCl_2$ 409 (h) 270 (m) $NiCl_2$ 153 (h) 65.1 (m) $ZnCl_2$ 168 (h) 183 (m) $CuCl_2$ 9.18 (h) 12.5 (m) $CaCl_2$ 1680 (h) >7000 (m)	(Fujiwara et al., 2017)
cholesterol	n/a	(Karasawa Akira et al., 2017; Robinson et al., 2014)
NADPH	n/a	(Mou et al., 2025)

Finally, bacterial LPS is also reported to modulate P2X7 activity downstream of multiple pathways. In mouse cells, LPS indirectly via caspase-11 and the cleavage of pannexin-1, results in an increase in extracellular ATP (D. Yang et al., 2015). Loureiro et al., (2022); and Rusiecka et al., (2022) demonstrate that when pannexin-1 facilitates ATP release, P2X7-resulting activation, leads to an increase in IL-6 expression and caspase-3/7-mediated apoptosis (Loureiro et al., 2022; Rusiecka et al., 2022). Moreover, some studies propose that intracellular LPS may interact with the putative LPS-binding domain on the C-terminus, causing conformational changes which reduce the receptor's activation threshold to its agonist ATP (Watters et al., 2001; Yang et al., 2015). However, more work is needed to definitively confirm this.

1.3.3 P2X7 signalling pathways

The activation and function of P2X7 is predominantly associated with bringing about inflammatory responses, such as P2X7-driven cleavage of caspases, activation of the NLRP3 inflammasome, which leads to release of pro and anti-inflammatory cytokines (including interleukins IL-1β, and IL-18), and reactive oxygen species (ROS) production; ultimately bringing about cell death, which can be mediated via multiple pathways including autophagy, pyroptosis, necrosis and apoptosis (Orioli *et al.*, 2017). P2X7 downstream signalling pathways are shown in Figure 1.9 below.

Signalling pathways and cascades downstream of P2X7 activation follow from P2X7 mediated Ca^{2+} influx and K^{+} efflux. Extracellular ATP causes Na^{+} and Ca^{2+} to rush into the cell via the open P2X7 channel, consequently driving membrane depolarisation in the cell. Thus, P2X7 signalling contributes to maintenance of intracellular Ca^{2+} levels in microglia, which indirectly implicates P2X7 in many downstream pathways and functions. The resulting intracellular Ca2+ increase, triggers downstream cellular processes, including release of TNF-α (Hide et al., 2000; Suzuki et al., (2004), transcription factor NFAT activation (Ferrari et al., 1999), cell cycle progression (Bianco et al., 2006), and even disruption to the cytoskeleton of the cell (Mackenzie et al., 2005).

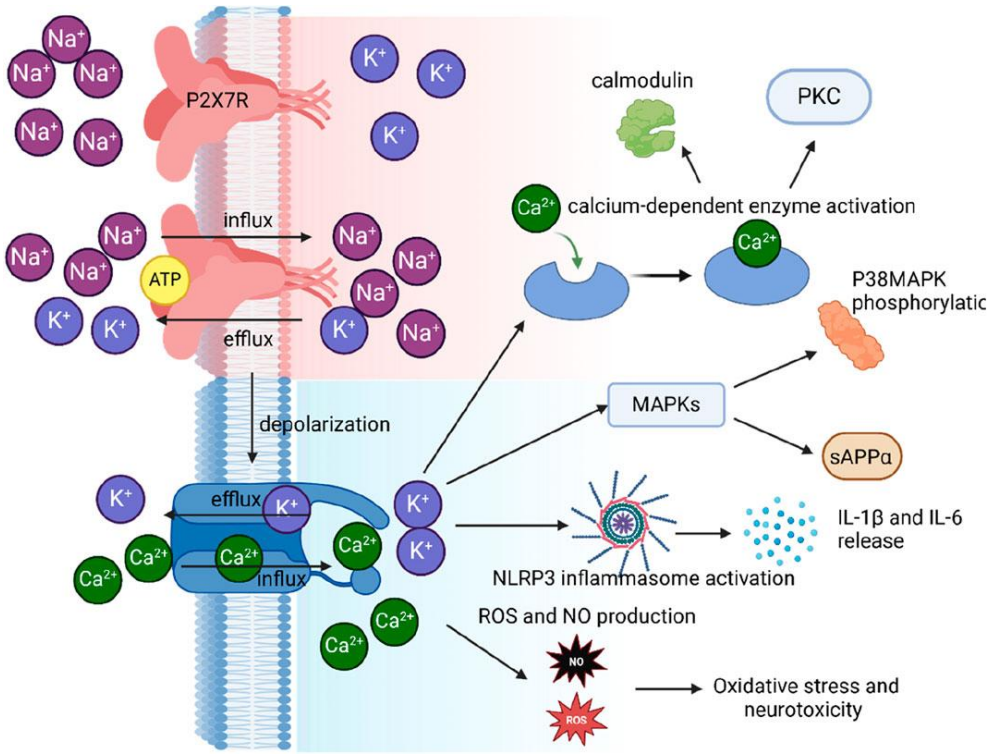

Figure 1.9 P2X7 downstream signalling pathways. *P2X7 activation in microglial cells facilitates ion flux, depolarization, and downstream signalling pathways such as calcium-dependent enzyme activation – calmodulin and PKC, MAPKs activation and phosphorylation, NLRP3 inflammasome activation, cytokine maturation and release, ROS and NO production. Figure taken from Liu et al., (2024)*

P2X7 can also regulate the intracellular Ca^{2+} concentration by another mechanism, namely via modulation of the store-operated calcium entry (SOCE), which becomes activated by depletion of intracellular Ca2+ stores and is an important mechanism for calcium influx in non-excitable cells such as microglia (Kodakandla et al., 2023). SOCE can amplify calcium signaling in microglia further. P2X7 channel also results in activation of PKC and calmodulin, which are both calcium-dependent enzymes(X. Liu et al., 2024). The mitochondrial apoptotic pathway can also be activated via P2X7-dependent calcium signaling. This pathway, ultimately leading to cell death, involves release of cytochrome c, and activation of caspases (Pelegrin and Surprenant, 2007). Sustained activation P2X7 by long term exposure to high levels of ATP is believed to result in Ca^{2+} overload and lead to apoptosis (Pelegrin and Surprenant, 2006). However, under transient stimulation, P2X7 calcium signaling supports the cell function (Di Virgilio et al., 2017). It has been suggested that P2X7 may interact with receptors which restore intracellular Ca2+ to the resting state, avoiding the overload (Stojilkovic et al., 2014). Plasma membrane Ca2+-ATPase (PMCA) and the sarco/endoplasmic reticulum Ca2+-ATPase (SERCA) work by pumping Ca2+ ions out of the cell's cytoplasm and into the endoplasmic reticulum, respectively (Recourt et al., 2020), and they

have been proposed to become activated with P2X7-mediated Calcium signaling (Kopp et al., 2019). Thus, Calcium signalling-dependent behaviour in microglia, such as phagocytosis, migration, and cytokine production, is all affected by P2X7 activation (Kettenmann et al., 2013).
K+ efflux downstream of P2X7 activation, promotes maturation and subsequent release of IL-1β, and IL-18 (Di Virgilio, 2007). Maturation and release of IL-1β has been the most widely studied result of P2X7 activation in immune cells (Burnstock, 2016) stimulated by PAMPs such as LPS binding to TLR4. This step is referred to as 'priming' in the literature (Das et al., 2016). Priming induces the transcription factor NF-kB, which in turn induces pro-IL-1β synthesis and NLRP3 inflammasome assembly, ready for activation which initiates caspase cleavage. The NLRP3 inflammasome is an intracellular multiprotein complex comprising NLRP3 pattern recognition receptor, cysteine protease caspase, an adaptor apoptosis-associated speck-like protein with a caspase recruitment domain (ASC), and never-in-mitosis A related kinase 7 (Franceschini et al., 2015; Kouba et al., 2023). ATP and DAMPs induce IL-1β release, which was shown to be closely dependent on K^+ efflux from the cell and co-driven by P2X7 (Ferrari *et al.*, 2006). Studies demonstrate that in microglia, P2X7 directly interacts with NLRP3 inflammasome (Franceschini *et al.*, 2015), and the literature suggests that LPS priming and P2X7 activity stimulated by ATP are both needed for IL-1β release from different microglia models *in vitro* (Campagno et al., 2025; He et al., 2017a; Stojilkovic et al., 2014). P2X7, however, is not the only channel responsible for K+ efflux in microglia and subsequent NLRP3 activation, as THIK-1 has been shown to facilitate this pathway in microglia (Drinkall et al., 2022; Ossola et al., 2023).

IL-6 was also shown to be released with a contribution from P2X7 activation. For example, the mechanosensitive up-regulation of IL-6 and its subsequent release from the cells of the retina-astrocytes and retinal ganglion cells, was linked to P2X7 (Lu et al 2017).

ROS production by the mitochondrial electron transport chain and by activation of NADPH oxidases plays an important function in immune responses and killing of phagocytosed pathogens. In microglia, as well as macrophages, P2X7 activation has been proposed to initiate ROS production via facilitating activation of NADPH oxidases by subunit phosphorylation (Kopp *et al.*, 2019).

Mitogen activated protein kinases (MAPKs), are a family of pathways regulating gene expression and differentiation of cells in response to stress or survival stimuli (Cargnello & Roux, 2011). In microglia, LPS-induced pro-inflammatory changes and behaviours are activated via p38, JNK and ERK, which are all examples of kinases from the MAPK family. P2X7 activation is associated with phosphorylation of MAPK, and P2X7 inhibition was shown to reduce inflammatory function, such

as cytokine production via MAPK (Franceschini et al., 2015; Giuliani et al., 2017). For example, TNF-α mRNA production is linked to JNK and ERK, while p38 regulates TNF transport to the cytoplasm and initiates its release from microglial cells downstream of P2X7 (Hide, 2003; Suzuki et al., 2004). Wang et al., (2017) showed that P2X7 inhibition reduces microglial activation and prevents phosphorylated 38MAPK-driven neurodegeneration in Parkinson's disease models. P2X7 signaling has also been linked to the modulation of amyloid precursor protein (APP), involved in the progression of neurodegenerative diseases, processing via the MAPK-dependent pathways (Camden et al., 2005; Surprenant and North, 2009).

Protein Kinase C (PKC) is involved in initiating cellular signalling following P2X7 stimulation (Bradford & Soltoff, 2002). In neuronal progenitor cells isolated from rat brains, P2X7 activation mediated differentiation of the cells via PKC-dependent ERK phosphorylation and translocation of PKCα and PKCγ (Tsao 2013). Shiratori et al., (2010) looked at PKC pathway in BV-2 microglia. They demonstrated that the ATP signalling via P2X7 induced mRNA expression and release of the chemokine CXCL2. The authors further showed that P2X7 activates the calcineurin–NFAT and PKC/MAPK pathways, and show that PKC inhibitors suppress the ATP-induced chemokine CXCL2 expression in this cell line.

An interaction between P2X7 and P2X4 has been proposed by a few authors. Phagosome and autophagy function in immune cells has been proposed to involve a possible interaction of P2X7 with P2X4 receptors (Kopp et al., 2019). P2X4 activation was shown to affect the P2X7-mediated IL-1β maturation and release (Pérez-Flores et al., 2015).

Involvement of P2X7 in phagocytosis has been previously shown. In the absence of ATP, P2X7 may be acting as a scavenger receptor for aiding phagocytosis(Gu & Wiley, 2018). Transient and low activation of P2X7 aids a reversible phosphatidyl serine (PS) translocation, which is a signal for phagocytosis, while prolonged P2X7 activation and the irreversible exposure of PS brings about cell death (Mackenzie et al., 2005). The exact mechanisms of PS exposure still need to be confirmed, however they may involve Ca^{2+} signalling and interaction with other receptors such as Ano6 (Ousingsawat et al., 2015).

It was shown that PS exposure is required for metalloprotease activity (such as ADAM17) (Sommer et al., 2016), which via the described P2X7 signalling pathways- dependent phosphorylation by ERK and p38 and membrane trafficking, is linked to P2X7.

P2X7 stimulation with P2X7 receptor agonist BzATP has been shown to increase lysosomal pH in BV-2 microglia (Sekar et al., 2018) and in a different microglial cell line MG6, stimulation with the endogenous agonist ATP deacidified lysosomes (Takenouchi et al., 2009). At the same time P2X7 receptor antagonists can prevent the de-acidification, supporting the role for the P2X7 in modulating lysosomal pH (Takenouchi et al., 2009). However, in macrophages, P2X7 stimulation of cells infected with bacteria, resulted in acidified lysophagosomes (Fairbairn et al., 2001). Lysosomal pH in microglia is dynamic and reported to be higher than in other types of cells, such as macrophages (Majumdar et al., 2007). An increase in lysosomal pH will usually negatively impact the rates of autophagy or degradation (Kahali et al., 2025). The literature suggests that P2X7 activation may reduce autophagosome-lysosome fusion, which reduces clearance (Campagno & Mitchell, 2021a). One theory is that P2X7 can activate the NLRP3 inflammasome by Cathepsin B leakage due to disruption of lysosomal integrity (Santos et al., 2022). This was also investigated in BV-2 cells (Sekar et al., 2018), however, more research is needed to confirm this theory and to fully understand the mechanism of interaction between P2X7, lysosomal health, and function of microglia.

P2X7 has also been reported as a fusogen in osteoclasts and transfected HEK cells (Falzoni et al., 2000; Pellegatti et al., 2011) In osteoclast formation, which results from cell fusion of macrophages, P2X7 knockout was shown to negatively impact the fusing behaviour (Ma et al., 2022a).

1.3.4 Trophic role of P2X7

Multiple studies suggests that P2X7 has a trophic effect. This has been researched in many cell lines, including transfected HEK 293 cells (Amoroso et al., 2012a), cancer cell lines (Di Virgilio et al., 2009; Kan et al., 2024), and murine microglia models (Monif et al., 2009).
In cancers, including glioma, P2X7 antagonists have shown antiproliferative activity (Drill et al., 2021; Kan et al., 2019). In osteosarcoma, Giuliani et al., (2014) demonstrated the trophic activity of a naturally occurring isoform A and B of the P2X7 receptor.

Adinolfi et al. (2005) showed that P2X7-transfected HEK 293 cells retain the ability to proliferate in serum-free media. The authors proposed that a tonic stimulation of P2X7 by low levels of ATP can elevate the resting mitochondrial membrane potential, increase mitochondrial Ca^{2+} levels, and lead to an overall increase in the cells' ATP content, thus exerting trophic effects (Adinolfi et al., 2005). Amoroso et al., (2012) further showed that P2X7 expression in transfected HEK 293

cells supports survival in the challenging conditions of serum withdrawal and low-glucose media, by regulating aerobic glycolysis and facilitating a metabolic switch away from oxidative phosphorylation- towards glycolysis- similar to the Warburg effect observed in cancer cells. P2X7 interaction with hypoxia inducible factor α (HIF-1α) has also been investigated in relation to P2X7 regulating the growth of neuroblastoma (Amoroso *et al.* 2015). It was shown that P2X7 downmodulation reduced HIF-1α. In another study, HIF-1α has also been proposed to regulate the expression of P2X7 in a hypoxic microenvironment (Tafani et al., 2011).

Trophic role of P2X7 in microglial cells was also reported by Monif et al. (2009), who attributed the proliferative activity to the P2X7 macropore. The authors showed that P2X7 overexpression in hippocampal cultures was driving microglial activation and proliferation. Furthermore, the authors demonstrated that when the P2X7 pore-forming ability was ablated, via a point mutation, the trophic activity was lost. This suggests that the trophism observed in N9 microglia is driven by the P2X7 macropore formation activity, rather than the ion channel conduit (Monif et al., 2010).

1.3.5. P2X7 as a pharmacological target in neurological diseases

Enhanced microglial activation together with increased expression of P2X7 is a feature observed in many neurodegenerative and neuroinflammatory disorders (T. Jiang et al., 2015a; Orioli et al., 2017; Savio et al., 2018; Stokes et al., 2015). Activation of microglia is associated with enhanced production of inflammatory factors and exposes surrounding neurons to high levels of chemokines, cytokines, ROS, and complement proteins, which can have challenging and damaging effects on healthy tissues (X. Liu et al., 2024). P2X7 is emerging as a pharmacological target in manipulating microglial activation and neuroinflammation-driven disorders, including conditions such as AD, prion diseases, MS, and ALS (X. Liu et al., 2024). Monif et al. (2010) propose a cycle in their review where the activation of P2X7 drives microglial proliferation and activation of the cells. Pro-inflammatory substances released through the P2X7 macropore, for example IL-1β and TNF-α, lead to a self-propagating cycle of inflammation as IL-1β acts in an autocrine fashion to activate more microglia (Monif et al., 2010).

Inflammation has long been linked to the development of Major Depressive Disorder (MDD) (Troubat et al., 2021). NRLP3 inflammasome and microglial activation have recently been identified as key players in the pathogenesis of MDD, and it has been proposed that these processes, inducing a state of 'sterile' inflammation, not associated with pathogen activation,

form the underlying neuropathology (Ratajczak et al., 2019). As the NLRP3 inflammasome is known to be driven by P2X7 activation (Franceschini et al., 2015), the receptor presents itself as a novel pharmacological target in the treatment of this frequent and prevalent psychiatric condition. Many studies confirm the link between P2X7 and depression (Stokes et al., 2015; Troubat et al., 2021; M. Wang et al., 2025). Studies exploring polymorphisms in the gene encoding P2X7 suggest an increased risk of developing MDD and bipolar disorder. (Roger et al., 2010; Stokes et al., 2015). P2X7 knockout studies have also shown that mice lacking the receptor show a lower sensitivity to stress (Csolle et al., 2013). Psychological stress has been linked to activation of the inflammasome via P2X7 and ATP signalling (Iwata et al., 2016). Use of P2X7 antagonists has also been shown to have antidepressant effects on depressive-like behaviour in mice in a model of depression and LPS challenge (Farooq et al*.,* 2018; Ma, Ren, Zhang, & Hashimoto, 2014). P2X7 antagonists with activity in the CNS are being developed to target neurological diseases driven by inflammation, such as depression. JNJ-54175446, a CNS penetrant selective P2X7 antagonist, has recently been assessed in clinical trials for depressive disorders, where it effectively lowered IL-1β levels in healthy volunteers and improved anhedonia, which is a common depressive symptom, induced by sleep deprivation in the study subjects (Recourt et al., 2023).

P2X7 expression has been linked to survival, and enhanced proliferation and migration in many cancer cell lines (Kan et al., 2019; Matyśniak et al., 2022). In glioblastoma cells, the evidence for the role P2X7 plays is still contrasting, some studies showing an inhibitory potential and others a detrimental effect of the receptor overexpression and activation on tumour progression (Kan et al., 2019). The presence and activity of microglia and macrophages in the glioma environment influence the disease outcomes and pathology (Hambardzumyan et al., 2015). P2X7 is expressed on both the tumour cells and the infiltrating microglia, and thus plays a key role in influencing glioma microenvironment and mediating a range of effector functions (Burnstock & Knight, 2018). P2X7 likely has a dual role in cancer as it may contribute to setting up a tumour-inhibitory or tumour-protective and promoting microenvironment (Kan et al., 2019).

A recent study by Matyśniak et al., (2022) demonstrated, in a glioblastoma cell line, that P2X7 stimulation increases cell viability and proliferation, as well as promotes cell adhesion, depolarization of mitochondria, and enhanced ROS production. An increasing number of studies focus on the use of P2X7 antagonists in the development of tumour treatment methods (Drill et al., 2021). For example, the P2X7 antagonist AZ10606120 was shown to deplete glioblastoma cells in an *in vitro* model (Kan et al., 2024). JNJ-54175446, a CNS penetrant selective P2X7 antagonist, has been found to be effective for seizure treatment in a preclinical study in mice (Mamad et al.,

2023). Many P2X7 modulators are being researched in preclinical studies for various conditions, including sepsis and neuropathic pain (Drill et al., 2021; Ou et al., 2018; Santana et al., 2015).

It is apparent that P2X7 mediates multiple effects directly and indirectly via signalling as an ion channel, via regulating intracellular calcium levels, modulating transcription of factors, supporting the maturation and release of cytokines, and interacting with proteins. As such, P2X7 is a key player in setting the inflammatory milieu in the CNS, and its expression dictates the microenvironment in the brain parenchyma, influencing countless neurological diseases (X. Liu et al., 2024). As pharmacological tools are being developed to target P2X7, more needs to be understood about the long-term indirect effects of blocking P2X7 signalling, as well as the potential benefits of enhancing its activity in a targeted fashion.

1.4. Aims of the project and significance

This thesis explores the role purinergic receptor P2X7 plays in the control of microglial function, survival, and inflammation. Microglia, performing so many important homeostatic and key functions within the CNS, are also naturally involved in numerous neuropathologies. Research suggests that P2X7 may be a potential target for modulating effects such as proliferation, microglia recruitment, phagocytosis, and metabolic plasticity, thus mitigating neuroinflammation, a driver of diseases such as depression and neurodegeneration. More information is needed to understand the role of P2X7 in microglial proliferation, activation, phenotypic differentiation, and function in health and disease. This project explores the role of P2X7 in the commonly used research model of mouse microglia- BV-2 cells. The advantages and limitations of this cell line are discussed in Chapter 2.1 Cell model.

Aim 1) Role of P2X7 in microglial proliferation

Some studies suggest that P2X7 has a trophic effect in microglia and allows for enhanced survival under serum deprivation and reduced glucose conditions (Amoroso et al., 2012; Monif et al., 2009). Some studies suggest that part of this effect may be attributed to P2X7 contributing to a metabolic switch in challenging conditions. The main aim was to demonstrate a trophic role of P2X7 in BV-2 cells by comparing them to a P2X7-deficient cell line. A series of assays were designed to understand whether P2X7 could influence proliferation of microglia.

Aim 2) Role of P2X7 in microglial functions

The second aim of the project was to investigate factors secreted following P2X7 activation in different environmental conditions such as glucose deprivation, serum reduction or the inflammatory milieu stimulated by bacterial LPS or pro-inflammatory cytokines using the P2X7-deficient BV-2 cell line. Shieh et al., (2014) linked CCL2 release to P2X7 activation and release of the chemokine CCL2, and the cytokine IL-1β was to be investigated in the BV-2 cell line. Microglia-specific functions such phagocytosis were to be assessed by flow cytometry analysis of uptake of fluorescent particles to investigate a role for P2X7 in this process.

Aim 3) Role of P2X7 in giant multinucleated cell formation

In microglia populations, under certain conditions, presence of giant multinucleated cells (GMCs) has been noted in both in-vivo and in-vitro models. BV-2 and BV-2^{P2X7} cell lines were to be investigated for their ability to form GMCs.

The hypothesis of the thesis was that P2X7 purinergic receptor affects and modulates microglial activity, such as proliferative capacity, survival in challenging conditions, cell activation behaviour related to inflammatory responses, cytokine secretion, and phagocytosis, as well as plays a role in multinucleated giant cell formation.

Chapter 2- Materials and methods

2.1 Cell model

BV-2 cells are a useful *in vitro* model for studying microglial functions and behaviour, however, the limitations of this model should be noted, as they may not fully represent the complexity of human microglial cells in the brain in vivo. BV-2 is a mouse-derived immortalized microglial cell line, which is commonly used in neuroscience research. It is a useful *in vitro* model to study neurodegenerative diseases and neuroinflammation as an alternative model system for primary microglia. BV-2 microglial cell line comes from microglia of neonatal C57/BL6 mice. The cells have been immortalized by J2 retrovirus infection with v-raf/v-myc oncogene (Peng et al., 2021) enabling continuous growth and fast division in this adherent cell line making them a convenient model for in vitro testing. Unstimulated BV2 cells are reported to exhibit a more activated and inflammatory morphology and resting state than primary microglia (Sarkar et al., 2018). However, the cells still possess many useful characteristics such as expression of F4/80, CD11b and Iba 1 (Gao et al., 2020; Sarkar et al., 2018) -essential biomarkers of primary microglia, which makes them similar to primary microglia. Since this is a mouse derived and an immortalized cell line the applicability to human-specific conditions is obviously limited. Furthermore, being derived from neonatal cells this may not be the most robust model for aging microglia. However, as a primary tool in high throughput screening and in the initial stages of research this is a convenient model to use. Commonly, in later stage pre-clinical research it is essential to consider using additional models such as primary microglia or iPSC lines to verify the data and translate the findings into human models.

BV-2 is an immortalized murine microglial cell line that naturally expresses P2X7. These cells form a convenient *in vitro* model, as they have been extensively described in the literature in terms of inflammatory responses and behaviour. P2X7 knockout (BV-2^{P2X7-}) has been generated in the wildtype BV-2 cell line, and validated as a functional microglial model by Dhuna et al., (2019); and Felgate, (2019) using the clustered regularly interspaced short palindromic repeats (CRISPR) gene editing technique. Subjecting the two cell lines to different functional and activity assays in parallel provides vital information for the role of P2X7 in eliciting microglial responses. A recent research paper by (Janks et al 2018) on primary human microglia demonstrates that P2X7 expression and behaviour is very comparable to that of mouse model cell lines, in terms of ion channel and dye uptake activity, as well as caspase induction and phagocytic behaviour, thus validating cells like BV-2 as a useful model for target validation and research concerning the role of P2X7 in neuroinflammation.

2.2 Materials and reagents

All materials and reagents are listed on the table below showing the suppliers.

Table 2.1 List of suppliers of chemicals and materials used. *The following materials and reagents were used, unless otherwise indicated in the individual figure legends.*

2NBDG	Abcam
ATP, ADP, UDP, AMP, UDP-glucose (UDT)	Sigma-Aldrich
Az10606120	Tocris Bioscience
BSA	Thermo Fisher
CCL2	PeproTech
CellTrace Deep Red	Thermo Fisher
CellTrace Yellow	Thermo Fisher
CFSE	Biolegend
Clemastine	Tocris Bioscience
CLI096	Invivogen
DMEM:F12 cell culture media microglia DMEM:F12 cell culture media HEK293 cells RPMI 1640 cell culture media RAW 264.7	Thermo Fisher Thermo Fisher Thermo Fisher
DMSO	Sigma-Aldrich
E coli pHrodo	Thermo Fisher
Fetal Bovine Serum (FBS) microglia Fetal Bovine Serum (FBS) HEK293 cells	Sigma-Aldrich PAN Biotech
Fura-2 acetoxymethyl ester (AM)	HelloBio
Glucose	Sigma-Aldrich
Hoechst 33342	Thermo Fisher
IFNg	PeproTech
IL-1β	PeproTech
IL-4	PeproTech
JNJ-47965567	Tocris Bioscience
Lactate	Sigma-Aldrich
LPS 055: B5 strain	Sigma-Aldrich
Lysotracker	Thermo Fisher
MitoSox	Thermo Fisher
Mitotracker Deep Red	Thermo Fisher
Mitotracker Green	Thermo Fisher
Neurosteroids: Allopregnanolone, pregnenolone, pregnanolone, progesterone, testosterone, DHEA, 17-β-estradiol glucuronide, DHEA,THC	Sigma-Aldrich
Nigericin	Sigma-Aldrich
PBS	Sigma-Aldrich
Penicillin-Streptomycin antibiotic	Thermo Fisher
Phalloidin	Thermo Fisher (a gift from Dr Isabel Hamshaw)
PMA	Sigma-Aldrich
Poly (I:C)	Sigma-Aldrich
Poly-D lysine	Merck
Polymyxin B	Sigma-Aldrich
RANKL	Pepro Tech
Resazurin	Sigma-Aldrich
Sulfinpyrazone	Sigma-Aldrich
Sulfinpyrazone	Sigma-Aldrich
TMRM	Thermo Fisher
TNFa	PeproTech
YO-PRO-1 dye	HelloBio
Zymosan	Thermo Fisher
β-Mercaptoethanol	Sigma-Aldrich

2.3 Cell culture

A bank of cells was created and stored in –80 °C to use throughout this work. Cells were only used for approximately 12 weeks, and then a new batch would be thawed. Cells were passaged routinely 2-3 times a week depending on requirements. Cells were frozen in cryogenic vials in 5% DMSO in FBS.

Microglial cell model. BV-2 cells, the immortalised murine microglial cell line which naturally expresses P2X7 was used. A P2X7 deficient clone in BV-2 cell line was previously generated by CRISPR editing and verified as an effective model by Stokes lab (Dhuna et al., 2019; Felgate, 2019). Cells were maintained in Dulbecco's modified Eagle's medium (DMEM) F:12 (Gibco, Thermo Fisher) containing penicillin/streptomycin (Thermo Fisher) and 10% fetal bovine serum (Sigma, F4135) for BV2 cells. The cells were passaged 2-3 times a week using 0.25% Trypsin EDTA (Gibco, Thermo Fisher) (up to approximately passage 36). Care was taken to ensure the conditions and procedures the cells were exposed to were identical for all culture flasks and performed at the same time for P2X7 expressing and deficient pairs. Where indicated, cells were pre-grown at a specific density in sterile dishes overnight, prior to seeding for an experiment to further eliminate variability. Some variability is introduced naturally as time goes by. It was observed that BV-2 cells become more adherent with each passaging and this effect is more pronounced when P2X7 is expressed. Some phenotypic changes such as accumulation of giant cells over time were also noticed. Therefore, care was taken to change growth flasks frequently (maximum 4 passages) and not extend the 36 passages window when working with BV-2 microglia.

P2X7 transfected HEK-293 cells. HEK-293 cell lines highly expressing mouse (m) or human (h) P2X7 were previously generated by Stokes lab, including one in a HEK-293 cell line model where P2Y2 was also knocked out by CRISPR (20e6-hP2X7). These model cell lines were used alongside the P2X7 deficient HEK-293 cells for verification of data obtained on BV-2 cells with respect to P2X7 activity. Cells were maintained in Dulbecco's modified Eagle's medium (DMEM) F:12 (Gibco, Thermo Fisher) containing penicillin/streptomycin (Thermo Fisher) and 10% fetal bovine serum (PAN Biotech). Care was taken to ensure the conditions and procedures the cells were exposed to were identical for all culture flasks and performed at the same time for P2X7 expressing and deficient pairs.

RAW 264.7 and J774 murine macrophages. RAW 264.7 and J774 murine macrophages express P2X7. They were used in a few experiments as a comparison model of macrophages to microglia.

The cells were cultured in RPMI 1640 (Gibco, Thermo Fisher) containing penicillin/streptomycin (Thermo Fisher) and 10% fetal bovine serum (PAN Biotech). The cells were cultured till 80% confluency and passaged twice a week by scraping in PBS or media.

Media, **serum and glucose stocks.** Heat inactivated Fetal Bovine Serum (Sigma, F4135) was purchased in bulk of three bottles from one supplier, aliquoted and frozen prior to starting the cell cultures. The stock served all experiments on BV-2 cell lines. Whenever a batch of cells was thawed, a fresh aliquot of serum and an aliquot of 1 mM glucose were kept in the fridge to serve the series of upcoming experiments from the same stock, to use in the experimental setups which required varying concentrations of serum or glucose.

Cell culture. Cells were grown in 75 cm^3 flasks (NuncTM EasYFlaskTM, Thermo Scientific) and incubated at 37°C, 5% CO_2 in humidified incubators. Cells would be passaged 2-3 times per week after reaching 80% confluency. Experiments run in pairs, i.e., all experiments comparing P2X7-expressing to P2X7-deficient cells, were handled in parallel, passaging at the same time and re-seeding to the same density in the flasks, using the same media and reagent stocks.

Passaging. Media was aspirated, and 5 mL of 0.25% Trypsin-EDTA solution (Thermo Fisher) was added and incubated for approximately 5 minutes. An equal volume of 10% FBS DMEM/F-12 was then used to deactivate trypsin. The cell suspension was transferred to an aseptic 15 mL centrifuge tube and centrifuged at 300 x G for 5 minutes to form a cell pellet. The supernatant was aspirated, and the pellet was re-suspended in 1ml of 10% FBS DMEM/F-12. Re-suspended cells
were then counted using a haemocytometer and seeded back into the flask (flasks were used for up to 5 passages, or a new flask was used). Passage numbers were recorded. Alternatively, the cells were plated in 2 mL dishes or multi-well plates and used in experiments.

2.4 Experimental designs

Plating for experiments

Cells were obtained using trypsin, in the method described above, from 80 % confluent culture flasks or 2mL dishes. Cells were counted using a haemocytometer and plated at densities shown in Table 2.2, specified for each plate and assay type.

Coating plates for P2X7 activity fluorometric assays. 96-well plates were coated with poly-D lysine made up in sterile water to 50 µg/mL. 50 µL –100 µL of poly-D lysine solution was used per well. The plates were incubated overnight in the fridge. Next day, the wells were washed with 200 µL/well of sterile water and allowed to dry, before seeding the cells.

Table 2.2 Experimental designs in different plates. *For every experiment a standard design plate was used, unless otherwise indicated in the figure legend. Seeding numbers in 24-well design were scaled up and proportional to 6000 or 9000 cells/well in a 96-well plate.*

Assay	Plate	Plating density	Plating volume
Viability (Alamar Blue/MTS, NQO1,)	96-well	6000 cells/well 9000 cells/well 12 000 cells/well	200 µL
BrDU	96-well	9000 cells/well	200 µL
Fura-2 AM	96-well (Poly-D lysine coated)	2 x 10^4 cells/well	100 µL
YOPRO	96-well (Poly-D lysine coated)	2 x 10^4 cells/well	100 µL
Immunofluorescence (imaging in plates)	96-well	9000 cells/well	200 µL
Immunofluorescence (imaging on cover slips)	6-well 24-well	20 000 cells/coverslip	200 µL
Staining (flow cytometry)	24-well	54690 cells/well	1 mL
CellTrace Yellow	24-well	35600 cells/well 54690 cells/well	1 mL
ELISA	24-well	70 000 cells/well	1 mL
qPCR	24-well	54690 cells/well	1 mL

Plating on coverslips. Coverslips were placed inside wells of a 6-well plate or 24-well plate. Cells were counted and resuspended to a desired density in 0.5% serum media using the method described above. Cells were seeded on glass coverslips by releasing a 500 µL droplet of the cell suspension onto a glass coverslip. Cells were allowed to settle and adhere for 1h in the incubator. The well was then covered with media.

Challenging conditions. Cells were challenged with serum and glucose reduction in experimental designs.

Serum deprivation. Dulbecco's modified Eagle's medium (DMEM) F:12 (Gibco, Thermo Fisher) containing penicillin/streptomycin (Thermo Fisher) was supplemented with fetal bovine serum (Sigma, F4135) to desired serum percentage. Care was taken to ensure that the same aliquot of

made up media containing the low % of serum served both compared cell lines per experiment. For serum deprivation experiments cells were plated into 0.5% or 1% serum containing media for the duration of 24h, 48h or 72h.

Glucose reduction. Glucose-free Dulbecco's modified Eagle's medium (DMEM) F:12 (Gibco, Thermo Fisher) containing penicillin/streptomycin (Thermo Fisher) was used. Aliquots of 4 mM glucose media were prepared using the same stock of 1 M glucose. Care was taken to ensure the same aliquot of made-up media containing the low glucose and supplemented with the desired serum concentration served both compared cell lines per experiment. For glucose deprivation experiments, cells were pre-cultured in 4 mM glucose, 10% serum media, and plated into 4mM glucose, 0.5% serum media for the duration of 24h or 48h.

Exposure to ATP and other nucleotides. Cells were exposed to nucleotides at a range of concentrations 3 mM, 1 mM, and 300 µM. DMSO was used as a vehicle control. Nucleotides were added directly to 500 µL of media on top of the cells in a 24-well plate. The media contained 0.5% serum. Cells were exposed for 30 minutes.

Exposure to steroids, cytokines, lactate and multinucleating factors. Cells were exposed to a range of cytokines, steroid compounds pro-inflammatory molecules, and lactate for 48h or 72h. Images were recorded every 24h using a light microscope EVOS or Nikon Ti Eclipse, using x 10 or x 20 magnification to capture a representative image of the morphological changes in the population across the well. Some plates were set up in doubles, and the second plate was used for Alamar blue assay. Neurosteroids were used at 10µM. Lactate was used at 1 mM, 5 mM and 10 mM. Cytokines and proinflammatory factors were used at the following concentrations: IL-4 and IL-13 20 ng/mL, TNFα 50 ng/mL, IFNg 20 ng/mL, CCL2 10 ng/mL, LPS 100ng/mL, Poly(I:C) 100 ng/mL. Multinucleating factors were used at the following concentrations: PMB 100ng/mL, RANKL 100 ng/mL, All suppliers are listed in Table 2.1.

Exposure to P2X7 pharmacological modulators. Cells were exposed to a range of compounds for 48h or 72h. For giant cell imaging, images were recorded at 72h using a light microscope EVOS or Nikon Ti Eclipse, using x 10 or x 20 magnification to capture a representative image of the morphological changes in the population across the well. For P2X7 activity assays, cells were pre-incubated with the compounds at desired concentrations for 15 minutes to 1 hour.

2.5 P2X7 activity fluorometric assays

Calcium signaling (Fura-2 AM). Fura-2 AM assay was used to measure intracellular Ca^{2+} levels. Cells were plated in poly-D lysine coated 96 well plates at density 2x 10^4 cells/well in complete media, volume 100 µL per well, and incubated overnight. Cells were loaded with Fura-2 AM dye for 45 minutes using low divalent cation buffered saline solution (ELDV) (composition: 147 mM NaCl, 0.2 mM $CaCl_2$, 2 mM KCl, 13 mM glucose, 10 mM HEPES; pH 7.3) containing Fura-AM dye at concentration of 2 µM and 250 µM sulfinpyrazone. After 45 minutes the loading buffer was removed and replaced with E-calcium buffer (composition: 147 mM NaCl, 2 mM $CaCl_2$, 2 mM KCl, 1 mM $MgCl_2$, 13 mM glucose, 10 mM HEPES, pH 7.3) containing 250 µM sulfinpyrazone, 180 µL per well. Prior to the recording, the cells were left to warm up and pre-incubate with tested compounds for 15 minutes at 37°C. The Drugs were prepared at 10x final concentration in a separate drug plate. ATP was injected at 30s and responses were measured on Flexstation 3 microplate reader. The excitation and emission wavelengths were 340 nm and 510 nm, respectively (Lm1); and 380 nm, 510 nm (Lm2). The fluorescence ratio Lm1/Lm2 was taken and expressed as area under curve 30-300s. ATP concentration range to obtain a full dose-response curve was: 1 µM, 10 µM, 30 µM, 100 µM, 300 µM, 500 µM.

YO-PRO-1 dye uptake. Cells were plated in poly-D lysine-coated 96-well plates at density 2x 10^4 cell/well, in complete media, volume 100µl per well, and incubated overnight. The media was removed and replaced with 180µl per well low divalent cation buffered saline solution (ELDV) (composition: 147 mM NaCl, 0.2 mM $CaCl_2$, 2 mM KCl, 13 mM glucose, 10 mM HEPES; pH 7.3) containing 2 µM YO-PRO-1 dye. Prior to the recording, the cells were left to warm up and pre-incubate with compounds being tested for 20 min at 37 °C. The ATP was prepared at 10x final concentration in a separate drug plate. ATP was injected at 40s and responses were measured on Flexstation 3 microplate reader. The excitation and emission wavelengths were 490nm and 520nm, respectively. The fluorescence ratio was measured and expressed as area under curve 50-300s. ATP concentration range for full dose-response was: 10 µM, 20 µM, 50 µM, 100 µM, 200 µM, 500 µM, 1 mM.

Data for P2X7 activity was obtained on Flexstation 3 plate reader was analysed using SoftMax Pro 5.4.6 software (Molecular Devices), and expressed as fluorescence ratio, area under curve 30-300s for Fura-2 AM recordings; and as area under curve 50-300s for YO-PRO-1 dye uptake recordings. For Fura-2 AM the data was normalised, zero baseline (3 point) was set; for YO-PRO-1 data zero baseline was set (1 point).

2.6 Cell number quantification

Alamar blue cell viability. Metabolic assay Alamar blue was used to assess the effect of P2X7 expression on cell viability in challenging conditions of reduced serum and low glucose media. Cells were plated in 96-well plates at desired density (6000, 9000 or 12000 cells/well), volume 200 µL per well, and incubated over a set time period of 24h, 48h or 72h. 20 µL of the metabolic dye Alamar blue dye (resazurin) (Sigma Aldrich) at the concentration of 0.1 mg/mL was added to each well and incubated for 2h or 4h at the final concentration of 10 µg/mL, at which point fluorescence was measured on a Flexstation 3 plate reader using the excitation 570 nm and emission at 600 nm. The background fluorescence was subtracted for each experiment from the average of three wells which contained only media and Alamar Blue dye. Each individual experiment comprised three to nine repeats and the data shown were collated from one to three independent experiments performed.

MTS metabolic activity assay. Cells were plated in 96-well plates at desired density of 9000 cells per well (200 µL per well) and incubated over a set time period of 24h or 48h. 20 µL of the metabolic MTS dye (5-[3-(carboxymethoxy)phenyl]-3-(4,5-dimethyl-2-thiazolyl)-2-(4-sulfophenyl)-2H-tetrazolium inner salt) was added to each well and incubated for 2h or 4h, at which point fluorescence was measured on a Flexstation 3 plate reader, absorbance setting 490nm. Background signal was subtracted for each experiment from an average of three wells which contained only media and MTS dye. Each individual experiment was performed with 6 replicates. Three independent experiments were done to collate the data.

For viability/metabolic assays, plates were read on Flexstation 3 plate reader and data was obtained using SoftMax Pro 5.4.6 software (Molecular Devices). The background fluorescence was recorded with each plate in wells containing media only. Respective background values were subtracted from each well as the data was analysed.

CellTrace Yellow dye retention. CellTrace Yellow (Thermo Fisher) was used to follow cell divisions over time by Flow Cytometry. Cells were stained in PBS with 5 µM CellTrace Yellow dye for 20 min, counted and plated in 0.5% serum containing media and 0.5% serum, 4 mM glucose containing media at density 35640 or 53460 cells/well in a 24-well plate. The densities chosen were the result of scaling up from a 96-well plate to best mimic those conditions, and equivalent to the starting densities 6000 and 9000 cells/well used in Alamar blue assay in a 96-well plate design, respectively. Cells were trypsinised out of a well and washed into 0.5% BSA in PBS at each

time point. Flow cytometry was performed immediately. Fluorescence was recorded through the PE channel. Readings were taken at various time points over 48h. A gate was set to capture average size cells. 20000 events were recorded at each measurement in the gate and median fluorescence values were obtained for each sample measured. Each set of experiments was performed three times independently and the data shown is the collated average of those.

BrdU incorporation ELISA. The assay was performed with BrdU cell proliferation kit from Sigma-Aldrich, used according to the protocol provided by the manufacturer. Cells were seeded in 0.5% serum media at the density 9000 cells/well in a 96-well plate. BrdU label was added at dilution 1:20000 in 0.5% serum media for the last 1-2h of the 48h incubation time. Media was removed and the cells were fixed with the fixing solution provided. Anti-BrdU antibody was used at 1:100 dilution and secondary antibody was used at dilution 1:400 in the diluent solutions provided. The plate was washed 3 times with wash solution provided, between each step. The plate was lastly washed with distilled water and 100 µL per well of substrate solution was added. The plate was incubated for 15 mins in the dark and 100 µL per well of stop solution was added. Absorbance was measured on Flexstation 3 set at 450 nm. The background readings were subtracted. The assay was performed three times with three replicates each. The data presented shows an average of the collated experiments.

Haemocytometer cell counts. Cells were seeded in 2.5mL culture growth flasks at density 4.5 x 10^4 cell/mL and left to incubate for 72h. Cells were trypsinised as normal, centrifuged, resuspended in 1ml of fresh media and counted using a hemocytometer. An average of 4 counts was calculated and the results of three to five independent experiments were collated.

2.7 Mitochondrial mass and health measured by fluorescent staining and flow cytometry

BV-2 and BV-2^{P2X7-} cells were plated in 0.5% serum containing media or complete media at density 35640 or 53460 cells/well in a 24-well plate. The densities chosen were the result of scaling up from a 96-well plate to best mimic those conditions, and equivalent to the starting densities 6000 and 9000 cells/well used in Alamar blue assay in a 96-well plate design, respectively. After 48h incubation cells were trypsinised out, counted and staining was performed following the manufacturers' protocols.

Mitotracker Deep Red. Mitotracker Deep Red dye (Thermo Fisher) was used to stain mitochondria in approx. $1x10^6$ BV-2 or BV-2^{P2X7-} cells. The dye concentration used was 100 nM. Cells were stained in complete media at 37 °C for 30 minutes, protected from light. Flow cytometry was performed immediately. A large gate was set to include the total population (i.e. cells of small, average and giant size) and two smaller gates were set to separate out small and giant cells. A minimum of 10 000 events were captured in each gate in APC-A channel.

TMRM. TMRM dye (Thermo Fisher) was used to stain mitochondria in approx. $1x10^6$ BV-2 or BV-2^{P2X7-} cells. The dye concentration used was 100nM. Cells were stained in complete media at 37°C for 30 mins protected from light. Flow cytometry was performed immediately. A gate was set to include healthy cells of average size and 20 000 events were captured in the gate in FITC-A Channel.

Mitotracker Green. Mitotracker Green dye (Thermo Fisher) was used to stain mitochondria in approx. $1x10^6$ BV-2 or BV-2^{P2X7-} cells. The dye concentration used was 100 nM. Cells were stained in complete media at 37°C for 30 mins protected from light. Flow cytometry was performed immediately. A gate was set to include healthy cells of average size and 20 000 events were captured in the gate in FITC-A channel.

MitoSOX. MitoSOX dye (Thermo Fisher) was used to stain mitochondria in approx. $1x10^6$ BV-2 or BV-2^{P2X7-} cells. The dye concentration used was 100 nM. Cells were stained in complete media at 37°C for 30 mins protected from light. Flow cytometry was performed immediately. A gate was set to include healthy cells of average size and 20 000 events were captured in the gate in PE-A channel.

2.8 Staining for surface markers of activation by flow cytometry

Flow cytometry was used to stain for surface receptors and markers of cell activation in BV-2 cells. Cells were plated in 0.5% serum media at 53460 cells/well in a 24-well plate (equivalent to 9000 cells/well in a 96-well plate) with 100 ng/mL LPS and 50 ng/mL IFN-γ to achieve LPS + IFN-γ activated phenotype; or with 20 ng/mL IL-4 to achieve +IL-4 activated phenotype; or with 'nothing' to achieve the resting phenotype. After 48h cells were trypsinised out, counted and resuspended in PBS/ BSA 0.5% in Eppendorf tubes for staining with approximately 2×10^5 cells in each tube. All antibodies used are listed in Table 2.3.

Table 2.3 Antibodies. *Antibodies used for staining by flow cytometry and their respective dilutions.*

Antibody	Dilution
Hano43 rat anti-mouse P2X7 (Enzo Biosciences)	1:10
Rat anti-mouse P2Y12 (Biolegend)	1:100
Rat anti-mouse CD11b (Biolegend)	1:200
Alexa Fluor 488 (goat anti-rat IgG2b) (Biolegend)	1:200
Anti-mouse CD86 antibody conjugated to fluorescent APC tag (Biolegend)	1:80
Anti-mouse CD206 antibody conjugated to fluorescent FIT-C tag (Biolegend)	1:400

P2X7, P2Y12, CD11b. Primary antibodies were used at their respective dilutions shown in Table 2.3. Secondary antibody used was Alexa Fluor 488 (goat anti-rat IgG2b) dilution 1:200. Isotype control was also used at concentration 1 µg/mL. The procedure was performed on ice with 1h incubation with each antibody and washing with PBS/ 0.5% BSA buffer. Flow cytometry was performed straight away. A gate was set to capture healthy cells of average size. 20 000 events in the gate were recorded in the FITC-A channel. This was performed in three independent experiments.

CD86 and CD206. The antibodies conjugated to fluorescent tags were purchased from Biolegend. Antibodies were used at dilutions indicated in Table 2.3. The procedure was performed on ice with 1h incubation with the antibody and washing with PBS/ 0.5% BSA buffer. Unstained cells were used as control. Flow cytometry was performed straight away. A gate was set to capture healthy cells of average size. 20 000 events in the viable gate were recorded through appropriate channels. This was performed in three independent experiments.

2.9 2-NBDG glucose uptake by flow cytometry

BV-2 and BV-2^{P2X7-} cells were assessed for glucose uptake following one hour incubation with fluorescent 2-NBDG glucose. Cells were plated in 24-well plates at a density of 53460 cells/well (the equivalent of 9000 cells/well) in 0.5% serum conditions and incubated for 48h. The cells were trypsinised, washed into 0.5% serum glucose-free media, and incubated with 2-NBDG glucose or 'nothing' (control media) for one hour. Fluorescence was measured by flow cytometry in a gated population of cells of interest in the sample. 10,000 - 20,000 events were recorded in the viable cell gate on PE-A channel.

2.10 Phagocytosis assays by flow cytometry

Fluorescent beads uptake by flow cytometry- Zymosan. Uptake of fluorescent Zymosan particles was measured by flow cytometry. Cells were seeded in 0.5% serum media in a 96-well plate to achieve 70% confluency and allowed to settle overnight. Cells were fed Zymosan particles following the manufacturer's protocol, exposing each cell to approximately 50 particles per cell. Cells were left in the incubator for one hour. Three wells were stained with nuclear dye Hoechst (2 µg/mL) 10 minutes before taking the images. Representative images were taken with a x60 objective using a fluorescent microscope Nikon Ti Eclipse and image processing software Nikon NIS Elements. For the remaining three wells, using flow cytometry, average fluorescent signal of phagocytosed Zymosan particles was recorded in different gated populations of interest. 10,000 - 20,000 events were recorded in each gate of viable cells through PE-A channel.

Fluorescent *E. coli* pHrodo uptake. *E. coli* pHrodo particles become fluorescent once inside the acidic lysosomes. *E. coli* pHrodo uptake was measured by flow cytometry. Cells were seeded in 0.5% serum media in a 96-well plate to achieve 70% confluency and allowed to settle overnight. Cells were fed *E. coli* pHrodo particles following the manufacturer's protocol, exposing each cell to approximately 50 particles per cell. Cells were left in the incubator for one hour. Three wells were stained with nuclear dye Hoechst (2 µg/mL) 10 minutes before taking the images. Representative images were taken with a x60 objective using a fluorescent microscope Nikon Ti Eclipse and image processing software Nikon NIS Elements. For the remaining wells, using flow cytometry, average fluorescent signal of phagocytosed *E. coli* pHrodo particles was recorded in different gated populations of interest. 10,000 - 20,000 events were recorded in each gate of viable cells through PE-A channel.

All flow cytometry data was obtained by measuring fluorescence on a CytoFLEX flow cytometer (Beckman Coulter). Data were analysed using CytExpert Software (Beckman Coulter).
For GMC experiments, gating was performed according to cells' size. A gate was created for small cells, giant cells and total cells, and fluorescence shift was measured within each gate, normalised to a respective unstained control in each gate. An example of gating is shown below (Figure 2.1).

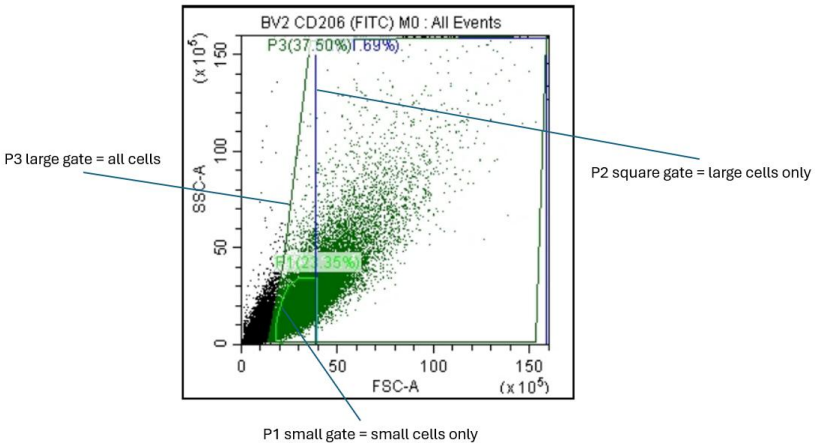

Figure 2.1 Example of gating for flow cytometry experiments. *For flow cytometry experiments, when average cells were stained (Chapter 3 and 4), a small gate (P1, bright green) was set that captured 20 000 events in a viable population of cells, capturing the average cells representative of the population. In Chapter 5 cells were gated according to size. A large square gate (P2, navy blue) was also set to capture large cells, and a total population was gated that included small and large cells (P3, dark green).*

2.11 Cytokine secretion by ELISA

IL-1β ELISA. Cells were plated in 24-well plates at a density 70 000 cells/well in 0.5% serum media and incubated for 48h. Cells were then primed with LPS (100 ng/mL) or 'nothing' (control) in duplicate repeats and incubated for 4 hours. Next, the cells were stimulated with ATP (3 mM, 1 mM, 0.3 mM) for 30 minutes. Nigericin (10 µM) was used as a positive control. Cells were next lysed with 1% Triton. Supernatants were collected and centrifuged to remove any cell material. Supernatants were used in the standard ELISA protocol (Thermo Fisher), which was followed according to the manufacturer's guidelines. The development time for the colour change was 45 minutes. Absorbance was read immediately at 450 nm. A standard curve was run on the same plate, and the data was interpolated.

CCL2 ELISA. Cells were plated in 24-well plates at a density 70 000 cells/well in 0.5% serum media and incubated for 48h. Next, the cells were stimulated with ATP (3 mM, 1 mM, 0.3 mM) for 4, 8 or 24 hours, as indicated in figure legends. LPS (100ng/mL) was used as a positive control. Cells were lysed with 1% Triton, where indicated. Supernatants were collected and centrifuged to remove any cell material. Supernatants were used in the standard ELISA protocol (Invitrogen), which was followed according to the manufacturer's guidelines. Absorbance was read immediately at 450 nm. A standard curve was run on the same plate and data was interpolated.

For colorimetric sandwich ELISA experiments, the plates were read on Flexstation 3 plate reader and data was retrieved using SoftMax Pro 5.4.6 software (Molecular Devices).

NQO1 activity. NQO1 activity assay was kindly performed by Dr Emily Hobson on a confluent 96-well plate of BV-2 and BV-2^{P2X7-} cells, following the manufacturer's protocol (Sigma-Aldrich), with extended development time of 4h. The plating conditions were optimised to 20 000 cells/well in a 96-well plate. The cells were plated and incubated under the required conditions for 24h or 48h in 0.5% serum, and handed over to Dr Hobson for the assay procedure.

2.12 Fluorescent imaging for morphological features of giant multinucleated cells

All imaging was carried out on Nikon Eclipse Ti and the images were captured and processed in Nikon NIS Elements software.

Nuclear stain Hoechst 33342. The cells were stained with Hoechst 33342 dye at the final concentration 2 µg/mL. After addition of the dye, the cells were incubated for 7 minutes in the dark at 37 °C and imaged using Nikon Eclipse Ti microscope and Nikon NIS Elements software. For each replicate three images were taken that comprised the middle of the well, top right corner and top left corner of the well. A fluorescent image and a phase image was taken in each instance and the images were overlapped for analysis. Every cell containing more than two nuclei was considered a multinucleated cell. The images were quantified by counting the giant cells in the field of view as a percentage of the total cell population. The replicates were averaged across three repeats.
For size quantification, in each image, five largest giant cells were selected. The outline was highlighted and the area was calculated using Nikon NIS Elements Software.

F-actin staining with phalloidin. Phalloidin staining was used to observe different morphologies in GMCs and mononucleated cells. Cells were stained with Alexa Fluor 488 phalloidin to fluorescently label F-actin (green) and with nuclear dye Hoechst (blue) to label the nuclei. Cells were seeded at density 9000 cells/well and grown in 0.5% serum media, stimulated with LPS 100 ng/mL for 72h or 'nothing' for control wells and spontaneously arising GMCs. Cells were grown in plastic wells of a 96-well plate or on a glass coverlip. Cells were stained with phalloidin (1:1000 dilution) in PBS for 30 minutes, following formaldehyde fixation, following the manufacturer's protocol. Stained with Hoechst nuclear dye 2 µg/mL as the final step. Images were taken using

x60 objective. Images were taken with a fluorescent microscope Nikon Ti Eclipse and Nikon NIS Elements software to capture and edit the images.

Cell fusion imaging. GMC formation and cell fusion was assessed by imaging. Cells were stained with two different dyes CellTrace Far Red (red) and CFSE (green)/ CellTrace Yellow (green), according to the manufacturers' protocols. Cells were pelleted and incubated with 1 µM dye in PBS at 37 °C for 30 minutes. Cells were washed, quenched in complete media and resuspended. Cells were counted and mixed 1:1 in a bijoux in 0.5% ser media. Cells were then seeded at total density of 12 000 cells/well in 0.5% serum media and stimulated with 'nothing' (spontaneous GMC formation) or LPS 100 ng/mL for 72h to induce GMC formation. Images were taken at 72h using fluorescent microscope Nikon Ti Eclipse and Nikon NIS Elements imaging software. Images were overlapped. The overlapping colours indicated cell fusion during the formation of GMCs in the well.

2.13 Gene expression in giant multinucleated cells

qPCR was used to determine the expression of fusogens and cytokines in BV-2 and BV-2^{P2X7-} cells forming GMCs. RAW 264.7 macrophages were also used as GMC-forming controls. Cells were plated in complete media, or 0.5% serum +/- LPS 100 ng/mL at a density of 53460 cells/well in 24-well plates for 72h. Spontaneously forming microglial GMCs were collected from GMC-rich flasks or 2 cm dishes. Cells were lysed in wells and harvested in lysis buffer RLT + β-Mercaptoethanol (1 µl per 1 mL of buffer) and stored at –80 °C.

RNA extraction. RNA was extracted using a Qiagen RNeasy kit following the manufacturer's instructions. Cells were pelleted and first passed through a shredding column.

cDNA synthesis. cDNA was synthesised using cDNA Tetro kit following manufacturers' protocols. RNA concentration was measured using a Nanodrop NS-1000 Spectrophotometer and reagents were added in appropriate corresponding amounts following the manufacturer's protocol for 1 µg of total RNA per sample. Total volumes for the PCR reaction mix were made up to 20 µL using RNA-free water and contained 1 µL 10 mM dNTP mix, 1 µL Primer Oligo (dT), 1 µL Ribosafe RNase Inhibitor, 1 µL Tetro Reverse Transcriptase (200 u/L) and 4 µL 5x RT Buffer. PCR cycle was run on a LifeECO PCR machine using the programme settings of 45 °C for 30 minutes, followed by 85 °C for 5 minutes, and chilled at 4 °C. Samples were stored in the fridge.

qPCR. The qPCR was performed using Rotor Gene Q (Qiagen). The reaction mix contained 5 µL SensiFAST SYBR (Bioline, Scientific Lab Supplies), 0.5 µL 5 µM reverse and forward primers for each gene, 1 µL cDNA sample, and 3 µL RNA-free water. This was made up in a 0.1 mL strip tube and cap (Starlab). QPCR was performed using the program settings: hold at 95 °C for 2 minutes, cycle through 95 °C for 5 seconds, 60 °C for 10 seconds, and 72 °C for 20 seconds- repeated 40 times. The cycle ended with a melt stage, which rises from 72 °C to 95 °C before finishing. The data were obtained and analysed using the Rotor-Gene Q series Software. Ct for each technical triplicate was obtained. Standards were run for each gene in technical duplicates. Melt curves and standard curves were obtained and checked for each gene. Two housekeeping genes (beta actin and GAPDH) were run. The fold change in mRNA was calculated for each gene using the delta-delta Ct method (2-ΔΔCt). The primers used are listed in Table 2.4.

Table 2.4 Primer sequences used in qPCR.

Gene	***Primer sequences***
DCSTAMP	Forward Sequence TTTGCCGCTGTGGACTATCTGC Reverse Sequence GCAGAATCATGGACGACTCCTTG
CCR2	Forward Sequence GCTGTGTTTGCCTCTCTACCAG Reverse Sequence CAAGTAGAGGCAGGATCAGGCT
SIPRA	Forward Sequence TCATCTGCGAGGTAGCCCACAT Reverse Sequence ACTGTTGGGTGACCTTCACGGT
CD47	Forward Sequence GGTGGGAAACTACACTTGCGAAG Reverse Sequence CTCCTCGTAAGAACAGGCTGATC
MMP9	Forward Sequence GCTGACTACGATAAGGACGGCA Reverse Sequence TAGTGGTGCAGGCAGAGTAGGA
CLEC10A (CD301)	Forward Sequence ATGGGTGGATGGGACCGACTTT Reverse Sequence GGAAGGTTCTCTGGCAGACATC
TREM2	Forward Sequence CTACCAGTGTCAGAGTCTCCGA Reverse Sequence CCTCGAAACTCGATGACTCCTC
TYROBP (DAP12)	Forward Sequence GTGACTTGGTGTTGACTCTGCTG Reverse Sequence GATAAGGCGACTCAGTCTCAGC
CTSK (Cathepsin K)	Forward Sequence AGCAGAACGGAGGCATTGACTC Reverse Sequence CCCTCTGCATTTAGCTGCCTTTG
ACP5 (TRAP)	Forward Sequence GCGACCATTGTTAGCCACATACG Reverse Sequence CGTTGATGTCGCACAGAGGGAT
CD9	Forward Sequence CTGTGGCATAGCTGGTCCTTTG Reverse Sequence AGACCTCACTGATGGCTTCAGG
CD81	Forward Sequence CCACCATACTGAGGAACAGCCT Reverse Sequence GCTACCACAATGGCTGCAATTCC
CD44	Forward Sequence CGGAACCACAGCCTCCTTTCAA Reverse Sequence TGCCATCCGTTCTGAAACCACG
CCL2	Forward Sequence GCTACAAGAGGATCACCAGCAG Reverse Sequence GTCTGGACCCATTCCTTCTTGG
IL1B	Forward Sequence TGGACCTTCCAGGATGAGGACA Reverse Sequence GTTCATCTCGGAGCCTGTAGTG

2.14 NMR metabolomics

Cells were seeded at 54690 cells/well in a 24-well plate in 0.5% and incubated for 48h. The supernatants were collected and centrifuged to remove any debris, kept on ice, whenever possible during the procedure, and analysed on 800 MHz NMR spectrometer with Bruker TopSpin software.

NMR metabolomic experiments were done in collaboration with Dr Serena Monaco, School of Chemistry, Pharmacy and Pharmacology, University of East Anglia, who kindly ran the samples and analysed the data.

2.15 Data processing and statistical analysis

All data analysis was performed using GraphPad Prism 6. Error bars on graphs indicate standard deviation. The data was analysed by Ordinary One-way ANOVA and Šídák's multiple comparisons test, unless otherwise indicated. (Statistical significance denoted by * $p<0.05$, ** $p<0.01$, *** $p<0.001$, **** $p<0.0001$, ns not statistically significant). Where standard curves were plotted, EC50 values were calculated, and half-maximal responses (EC50 values) were generated in GraphPad Prism with 95% confidence intervals.

Chapter 3- Investigating the role of P2X7 in microglial proliferation

3.1 Introduction

This chapter looks at the role of P2X7 in promoting survival, cell proliferation and growth in challenging conditions in microglia. The aspect of P2X7 supporting metabolism of the cells is also considered.

Trophic activity of P2X7 was previously documented in various studies. P2X7 has long been considered a possible target in treatment of cancer (Di Virgilio et al., 2009; Drill et al., 2021). Giuliani et al., 2014 described the trophic activity of P2X7 in osteosarcoma. A growth-promoting role was documented in primary rat microglia and the mouse N9 microglial cell line (Bianco et al., 2006; Monif et al., 2009), in lymphoid cells (Baricordi et al., 1999), and HEK 293 cells (Amoroso et al., 2012a) with regard to P2X7.

Adinolfi et al., (2005) worked with P2X7 transfected HEK 293 cells and proposed that while strong ATP stimulation results in cell death by causing mitochondrial Ca^{2+} overload and ultimately a mitochondrial membrane potential collapse, a tonic stimulation by constant low levels of ATP signaling hyperpolarizes the mitochondria by increasing mitochondrial Ca2+ levels resulting in an overall increase in the cellular ATP content, thus exerting trophic effects. The authors showed that P2X7-transfected cells retain the ability to proliferate in serum-free media.

A trophic role of P2X7 in microglia was also reported by Monif et al. (2009), who attributed the activity to the macropore. The authors showed that microglial activation and proliferation in hippocampal cultures could be driven by P2X7 overexpression. Furthermore, they used a full-length P2X7 receptor construct containing a single point mutant, which lacked the pore-forming ability but was capable of normal ion channel conductance and cellular trafficking with normal ATP sensitivity, to demonstrate that the activation and trophism observed were driven by the macropore formation activity, rather than the ion channel conduit (Monif et al., 2009).

Giuliani et al., (2014) showed trophic activity of a naturally occurring isoform A and B of P2X7 in osteosarcoma.

P2X7 was proposed to promote survival and proliferation and metabolic reprogramming- switch away from oxidative phosphorylation and towards glycolysis (Amoroso et al., 2012b; Sarti et al., 2021). Amoroso et al., (2012) showed that P2X7-transfected HEK 293 cells had a proliferative

advantage in serum-free and low glucose conditions, implicating P2X7 in the intrinsic ability to reprogram cell metabolism in support of survival.

Interestingly, while tonic low stimulation of P2X7 is suggested to result in trophic activity, P2X7 is also known for bringing about cell death, and in microglia it is proposed to be involved in regulating mitophagy and mitochondrial dysfunction in BV-2 cells (Sekar et al., 2018).

Sharing many similarities with macrophages, microglia are very plastic and flexible in their use of substrates and metabolic pathways and switch phenotypes to meet energy and functional demands (Lauro and Limatola, 2020). Specific activated phenotypes are strictly associated with utilized metabolic pathways and are critically important for facilitation of repair mechanisms in CNS injury and neurodegeneration, where conditions in the microenvironment can be highly challenging (Bernier, York, & MacVicar, 2020; Jung et al., 2019).

Homeostatic microglia grown in cell culture preferentially use oxidative metabolism (Lauro and Limatola, 2020). Under normal oxygen supply, the energy is produced in mitochondria through oxidative phosphorylation, and in hypoxic conditions, pyruvate is converted into lactate via anaerobic glycolysis in the cell cytoplasm (Bernier, York, & MacVicar, 2020). While oxidative phosphorylation yields more ATP molecules, glycolysis in activated microglia allows for faster ATP production, which is used for functional support, allowing rapid metabolism and supporting cell growth, production of cytokines, and ROS (Ghosh et al., 2018; Yang et al., 2021).

Glucose is the main energy fuel for microglia, and surface expression of glucose transporters is plastic and responsive to environmental conditions (Bernier, York, & MacVicar, 2020; L. Wang, Pavlou, et al., 2019). An increased microglial expression of GLUT1 glucose transporter is brought about by the activated pro-inflammatory phenotype, achieved with LPS and IFN-γ stimulation (previously referred to as M1), (Wang et al., 2019.) Upregulated expression of GLUT1 promotes glycolysis by facilitating a high uptake of glucose (Gimeno-Bayón et al., 2014; L. Wang, Pavlou, et al., 2019). It is proposed that transcriptional control over microglial activation is regulated by glucose metabolism itself in the cell (Hung et al., 2022; Quan et al., 2011). Glucose availability and the glycolytic rate influence proinflammatory gene and protein expression and thus microglial activity (Nagy et al., 2018)

Peripheral immune cells, such as macrophages, are known to be capable of switching away from oxidative phosphorylation and towards aerobic glycolysis when activated (Bernier, York, Kamyabi, et al., 2020; Lauro & Limatola, 2020; Orihuela et al., 2016). This is an effect similar to the Warburg effect observed in tumor cells to support proliferative activity (Lauro & Limatola, 2020). Several studies have now demonstrated across different microglial models, including BV-2 cells, that a metabolic shift can be brought about by inflammatory stimuli (Maher, 2021). These are well

reviewed in Lauro and Limatola., (2020). Chapter 4 addresses inflammatory stimuli and phenotypic differentiation of the cells in detail.

This Chapter addresses the question of how P2X7 expression in BV-2 cells affects the cells' ability to proliferate and looks for evidence to support the trophic role of P2X7 as suggested in the literature.

3.2 Results

3.2.1 Verification of P2X7 knockout model and P2X7 expression in BV-2 cells by flow cytometry

A P2X7 knock-out cell line model was previously generated by CRISPR/Cas9 editing in BV-2 murine microglia and has been used as an effective model in our laboratory (Dhuna et al., 2019; Falgate, 2020). Flow cytometry staining verified the lack of expression of P2X7 on the cell surface of the model BV-2^{P2X7-} cell line as shown in Figure 3.1.

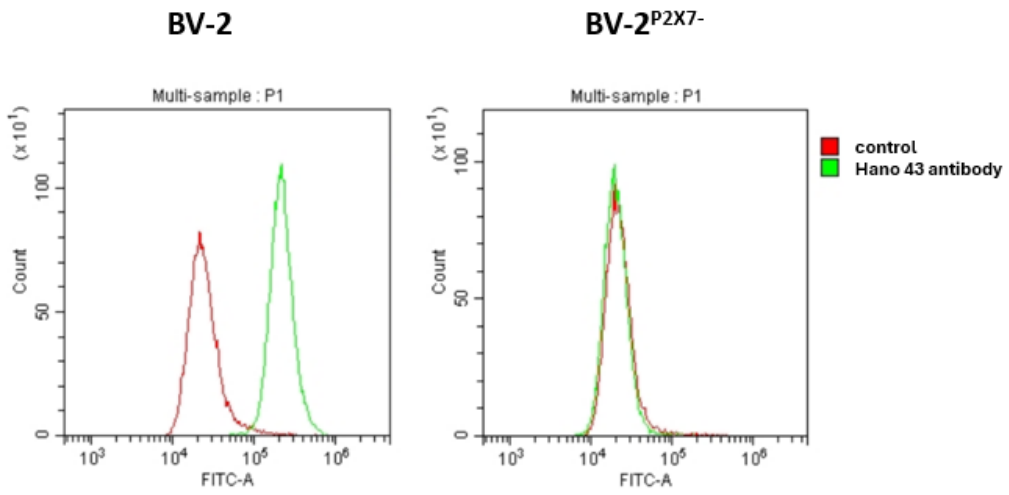

Figure 3.1 P2X7 expression in BV-2 and BV-2P2X7-cells. *Cells were stained to demonstrate lack of expression of P2X7 in BV-2^{P2X7-} cell line using flow cytometry as described in the methods section. Histograms are representative images of three independent experiments.*

3.2.2 Optimization of experimental culture conditions and serum reduction challenge

BV-2 cells are an immortalized murine microglial cell line, frequently used as an *in vitro* experimental model for investigating microglial behavior and responses (Henn et al., 2009). Like all microglial cells, they are heterogeneous within their population and respond to cytokines and environmental cues by differentiating and adapting their morphology and function accordingly, and their classical activation and resting phenotypes have been described (Henn et al., 2009; Maher, 2021). In their resting phenotype in cell culture, BV-2 microglia are frequently characterized by a spindle shape and small size, while in an activated state, they become ameboid or rounded and enlarged. The BV-2 cell morphology (Figure 3.2) was observed over time using a microscope. The magnification of x10 and x20 was preferentially used as it allowed to capture the largest sample of the population in a well, since the cells tend to migrate and form clusters and subpopulations of phenotypically defined groups. Thus using a lower magnification was the most representative method of examining this dynamic and heterogeneous cell line.

The BV-2 cells were cultured in media supplemented with 10% fetal bovine serum as a standard procedure. In experimental designs, however, serum-free media is commonly used. Cells were first subjected to complete serum withdrawal; however, this resulted in a high number of cell death. Serum reduction to 1% or 0.5% serum could be used without resulting in cell death. With reduced serum, the morphology of the cells was affected, resulting in a more rounded activated shape away from the spindly morphology associated with the resting state of the cells (Figure 3.2). The cell numbers were also visibly lower, indicating a slower rate of proliferation with serum reduction. In all the following work, care was taken to use well-mixed serum from the same stocks when setting up experiments with 0.5% or 1% serum that were comparing BV-2 and BV-2^{P2X7-} cell lines.

Different experimental setups in a 96-well plate were explored to find the best growing conditions for the cells over time. The ideal time for cells to incubate in the wells without becoming overcrowded was 48h in complete media and 48h or 72h in 0.5% serum, depending on the initial plating density (Figure 3.2).

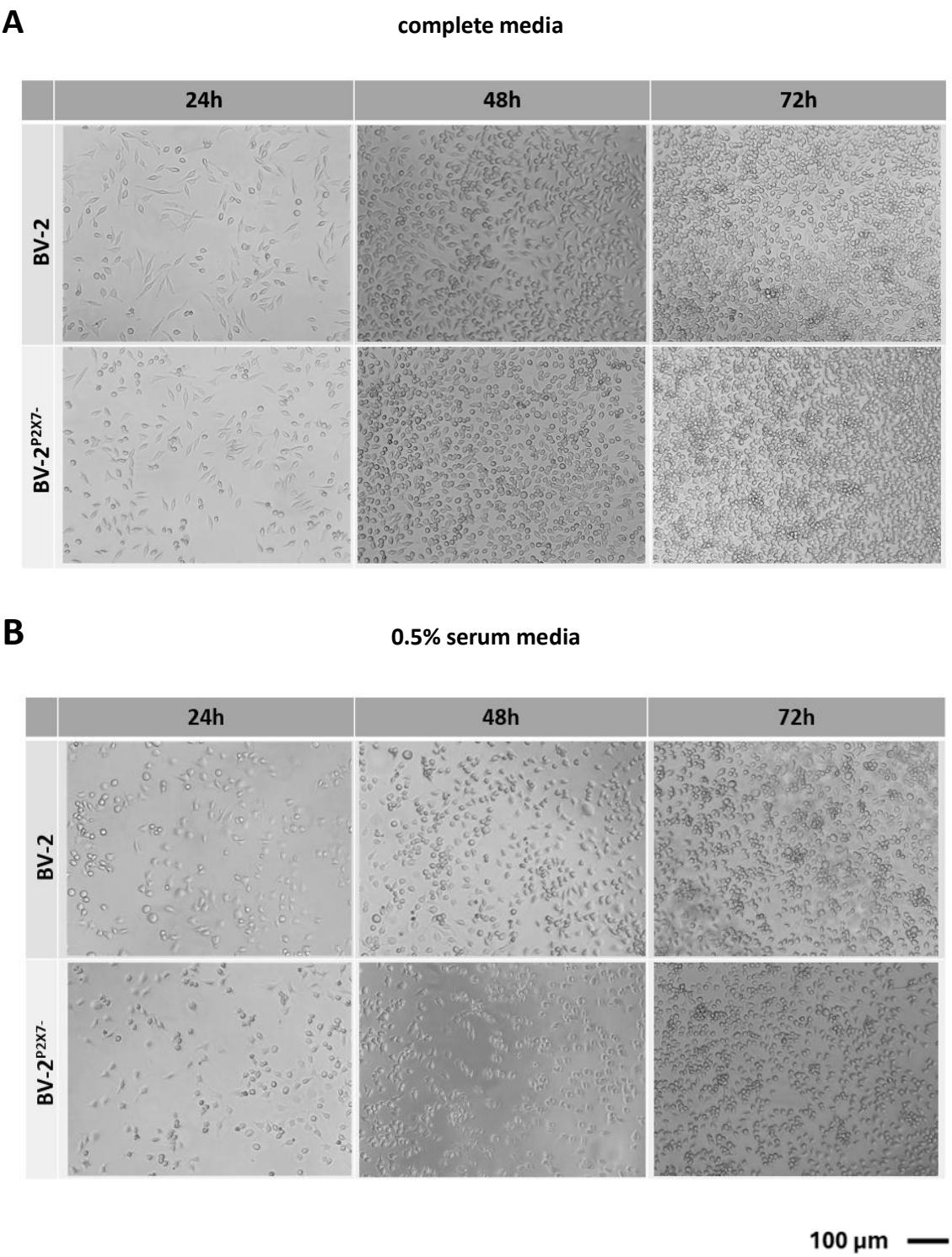

Figure 3.2 The response to serum withdrawal over time in BV-2 cells. *Cells were seeded at 9000 cells/well in a 96-well plate and incubated for 72h in complete media (A) or reduced (0.5%) serum (B). X10 photographs were taken at 24h, 48h, and 72h using a brightfield view on Nikon Ti Eclipse microscope. Images are representative of three independent experiments.*

3.2.2 Effect of P2X7 expression on cell number in challenging conditions of serum deprivation

Alamar blue assay as a readout for cell viability following serum reduction challenges

BV-2 cells are a fast-proliferating model. Serum withdrawal in culture is known to reduce the rate of proliferation (Yao & Fu, 2020). It also 'resets' the cells' circadian clock and leads to cell cycle synchronization in cell culture (Walker, 2011). Alamar blue assay is routinely used to look at cell viability and metabolism by measuring the cells' ability to process Resazurin dye into a fluorescent product (Rampersad, 2012). Alamar blue cellular viability assay was used as an indirect measure of cell number following a period of incubation in reduced serum media, in order to see if P2X7-expressing cells had an advantage at proliferating in challenging conditions. Different densities and different concentrations of serum were tested to ascertain if that had an impact on proliferation.

Cells were set up in a 96-well plate at different densities and in different concentrations of serum. BV-2 cells expressing P2X7 were compared to BV-2^{P2X7-} cells (Figure 3.3, Figure 3.4, and Figure 3.5). A consistent advantage of BV-2 cells over BV-2^{P2X7-} in the resulting Alamar blue fluorescence was observed throughout the work, although under most conditions, this was not statistically significant. The conditions of 0.5% serum concentration and initial plating density of 9000 cells/well, 48h reading, were determined to be the optimum method for eliciting this difference in Alamar Blue assay with statistical significance (Figure 3.3 B and E). Plated at a higher density, the wells would achieve confluency before the 72nd hour, and looked clearly overgrown, although they were still healthy.

Depending on the cell line and assay conditions, Alamar blue takes approximately 1-4h to be processed by the cells into its fluorescent product in high enough quantities for a difference to be registered by the plate reader. The fluorescence of Alamar blue was measured at 2h and 4h for each experiment to see if the difference between the BV-2 cell lines would become statistically significant with more time for the cells to process the dye and a higher amount of fluorescent product. Although with more processing time, RFU values were higher, there was no striking difference between the Alamar blue readings taken at 2h and 4h.

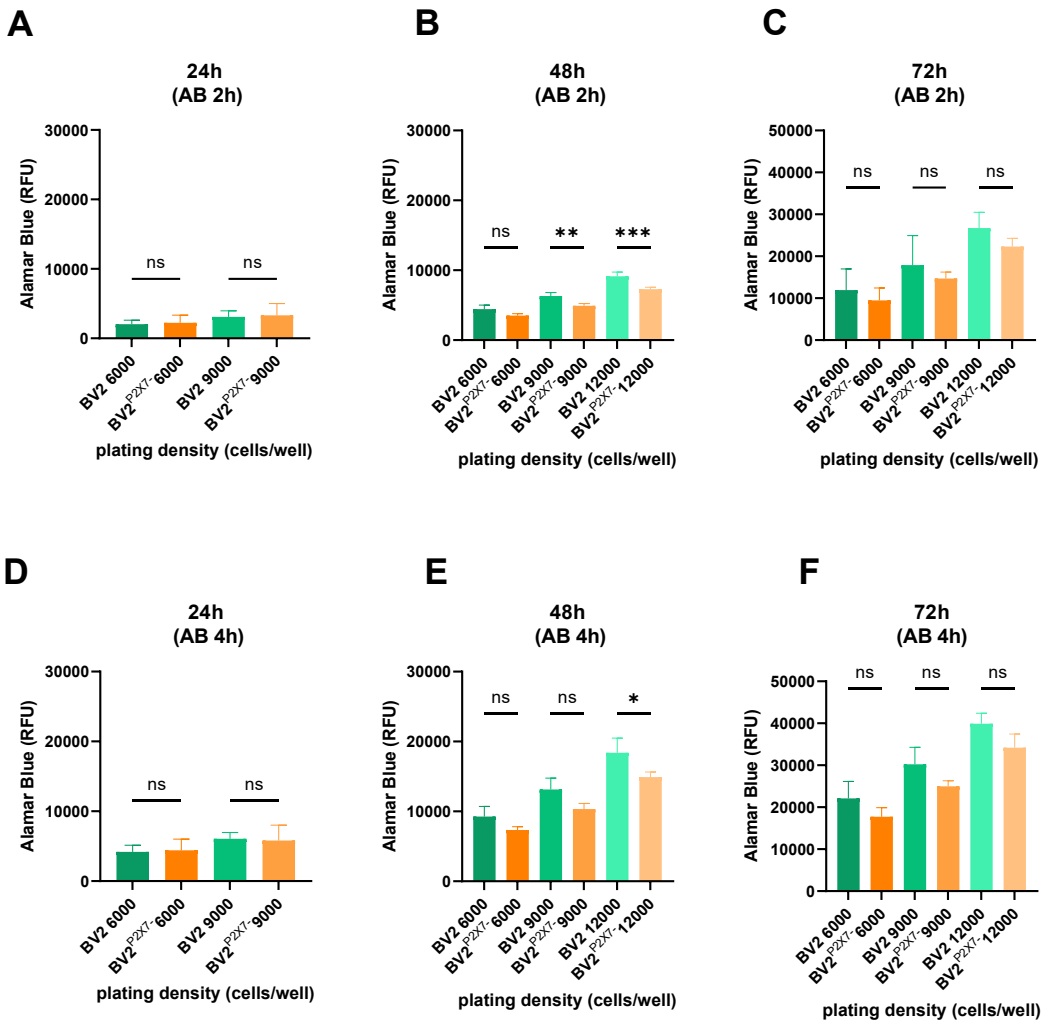

Figure 3.3 Cell viability in Alamar blue assay of BV-2 cells vs BV-2^{P2X7-} in challenging conditions of 0.5% serum- containing media. *Cells were plated in 96-well plates at densities of 6000, 9000, or 12 000 cells/well in complete media or reduced serum media and left to incubate for 24h, 48h, or 72h. Alamar blue assay was performed as described in the method section, with readings taken at 2h and 4h of processing time for the Resazurin dye. Each point represents an average of 3 independent biological experiments with 6-10 technical replicates for each condition.* ***A, D*** *24h 0.5% serum-containing media, 2h, and 4h Alamar blue processing time, respectively.;* ***B, E*** *48h in 0.5% serum-containing media 2h, and 4h Alamar blue processing time, respectively.;* ***C, F*** *72h in 0.5% serum-containing media 2h, and 4h Alamar blue processing time, respectively. Analyzed with Ordinary One-way ANOVA and Šídák's multiple comparisons test. (Statistical significance denoted by * p<0.05, ** p<0.01, *** p<0.001).*

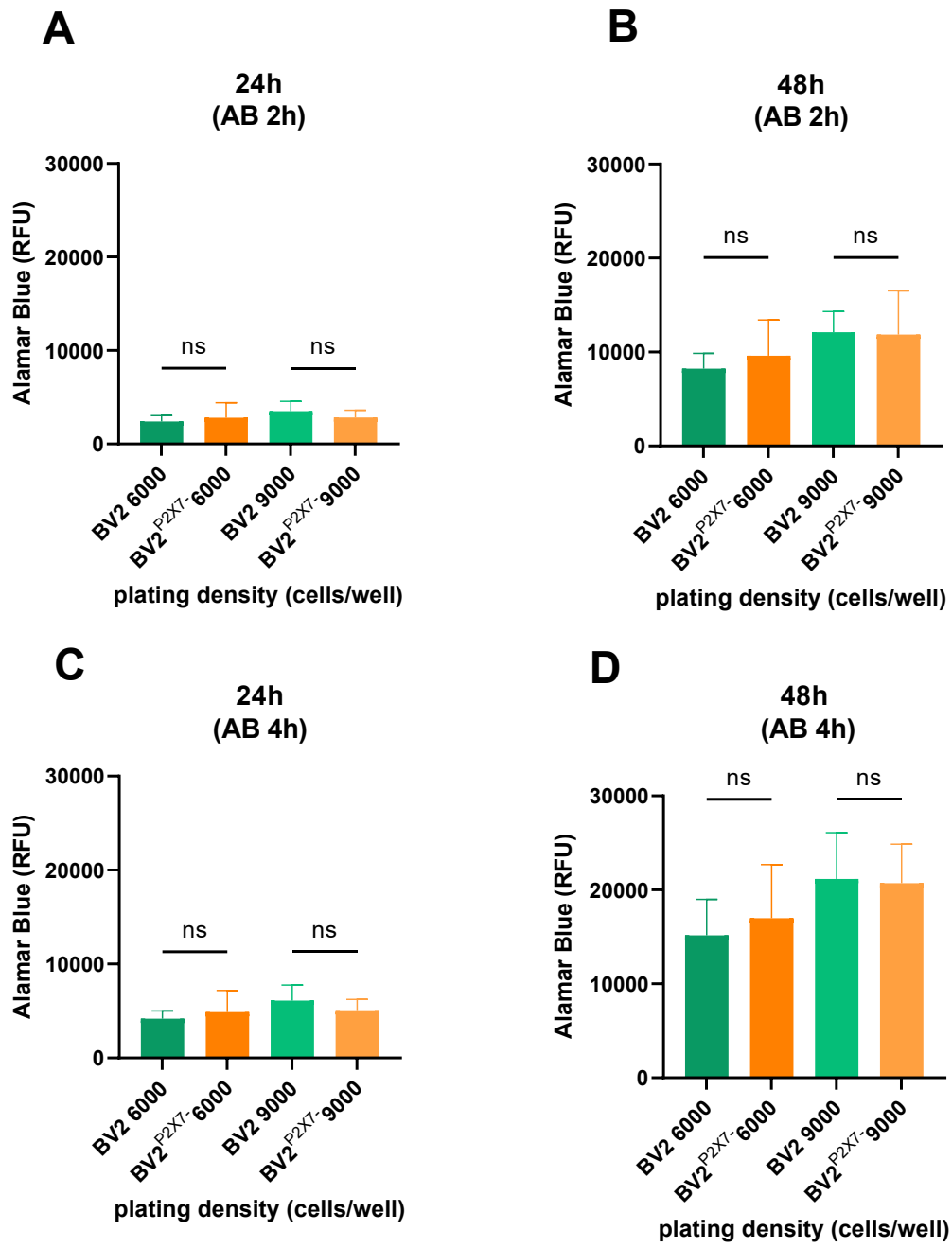

Figure 3.4 Cell viability in Alamar blue assay of BV-2 cells vs BV-2^{P2X7-} in 10% serum (complete media). *Cells were plated in 96-well plates at densities of 6000, 9000, or 12 000 cells/well in complete media or reduced serum media and left to incubate over 24h, 48h, or 72h. Alamar blue assay was performed as described in the method section, with readings taken at 2h and 4h of processing time for the Resazurin dye. Each point represents an average of 3 independent experiments with 6-10 technical replicates for each condition.* ***A, C*** *24h in complete media, 2h, and 4h Alamar blue processing time, respectively.;* ***B, D*** *48h in complete media 2h, and 4h Alamar Blue processing time, respectively. Analyzed with Ordinary One-way ANOVA and Šídák's multiple comparisons test. (Statistical significance denoted by * p<0.05, ** p<0.01, *** p<0.001).*

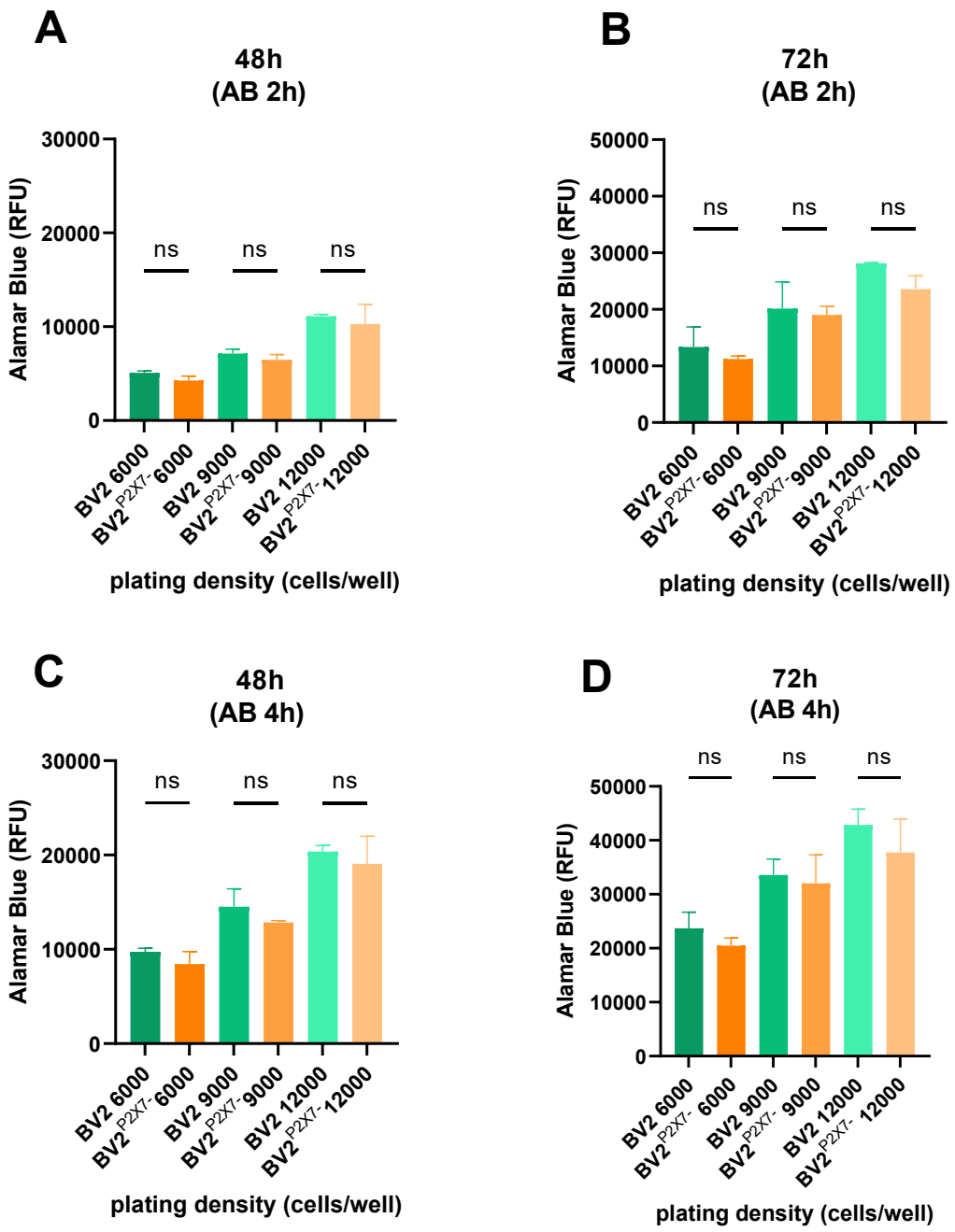

Figure 3.5 Cell viability in Alamar blue assay of BV-2 cells vs BV-2^{P2X7-} in 1% serum- containing media. *Cells were plated in 96-well plates at densities of 6000, 9000, or 12 000 cells/well in complete media or reduced serum media and left to incubate over 24h, 48h, or 72h. Alamar blue assay was performed as described in the method section, with readings taken at 2h and 4h of processing time for the Resazurin dye. Each point represents an average of 3 independent experiments with 6-10 technical replicates for each condition.* ***A, C*** *48h 1% serum-containing media, 2h, and 4h Alamar blue processing time, respectively.;* ***B, D*** *72h in 1% serum-containing media 2h, and 4h Alamar blue processing time, respectively. Analyzed with Ordinary One-way ANOVA and Šídák's multiple comparisons test. (Statistical significance denoted by * p<0.05, ** p<0.01, *** p<0.001).*

It was next investigated whether a trophic effect of P2X7 could be observed in a stably transfected HEK 293 cell line. The Stokes lab had previously generated HEK 293 cells highly expressing human P2X7 (hP2X7) by transfection. This cell line (HEK^{hP2X7}) vs the common HEK 293 cell line (HEK) showed a similar pattern to the BV-2 vs BV-2^{P2X7-} cells, in the Alamar Blue assay under the same experimental conditions (Figure 3.6), although the difference between the cell lines was statistically insignificant.

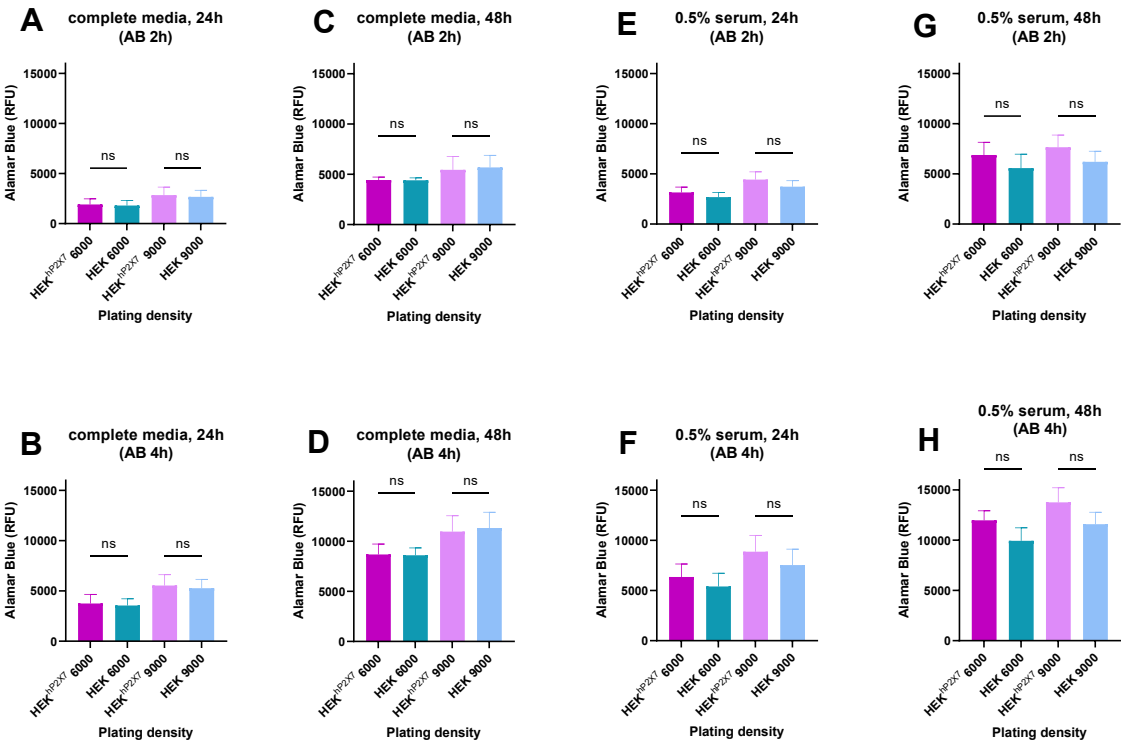

Figure 3.6 Cell viability in Alamar blue assay of HEK 293 cells vs P2X7-transfected HEK^{hP2X7} cells. *Cells were plated in 96-well plates at density 6000, or 9000 cells/well in complete media or reduced serum media and left to incubate over 24h or 48h. Alamar blue assay was performed as described in the method section, with readings taken at 2h and 4h of processing time for the Resazurin dye. Each point represents an average of 3 independent experiments with 10 technical replicates for each condition.* ***A, B*** *24h in complete media, 2h, 4h Alamar blue processing time, respectively.;* ***C, D*** *48h in complete media 2h, 4h Alamar blue processing time, respectively.;* ***E, F*** *24h in 0.5% serum media, 2h, 4h Alamar Blue processing time, respectively.;* ***G, H*** *48h in 0.5% serum media, 2h, 4h Alamar blue processing time, respectively. Analyzed with Ordinary One-way ANOVA and Šídák's multiple comparisons test. The difference between the selected pairs was not significant when the data was collated.*

Experimental conditions may differently affect processing of Resazurin dye. Different cell lines may also process the dye differently. In order to investigate whether both cell lines are equally capable of processing the dye under different experimental conditions, standard curves were plotted.

The standard curves allowed to assess the quantity of the fluorescent product across a range of known cell densities in the cell lines of interest. Initially, the cells were taken from culture growth flasks and plated in different serum concentrations at known densities. Alamar blue was added immediately and the cells were allowed to process the dye over the standard time period (2h and 4h). This is shown in Figure 3.7. This experiment showed that BV-2 and BV-2^{P2X7-} cells taken immediately from culture flasks, have the same ability to process the dye. The variability of the data, reflected in large error bars, may have been due to the shock of serum reduction as the cells were removed from complete media in the growth flasks.

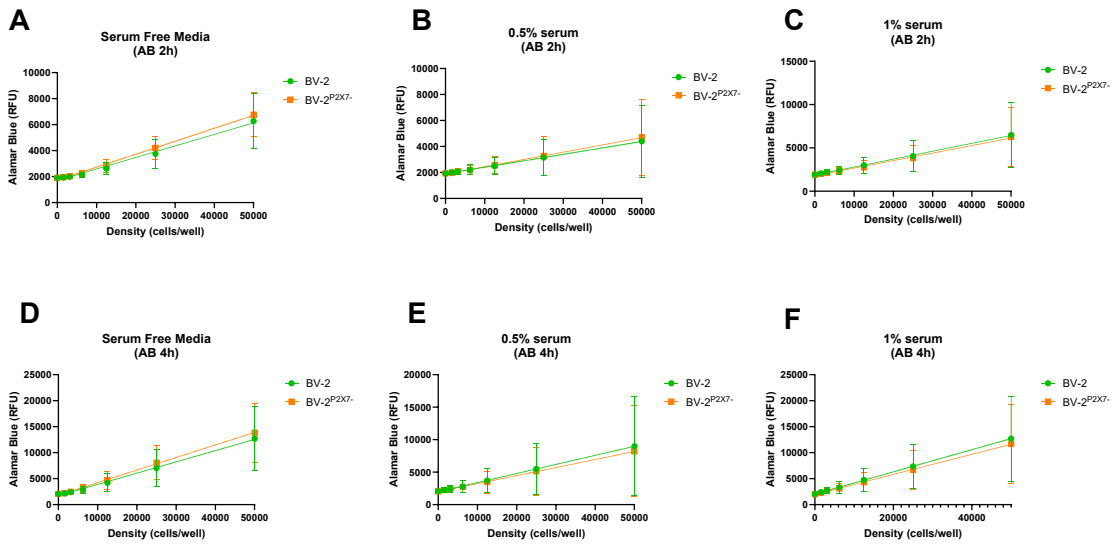

Figure 3.7 Resazurin processing standard curve in BV-2 and BV-2^{P2X7-} cells taken directly from culture flasks. *Cells were trypsinised directly out of culture flasks, counted and plated in serum-free media, 0.5% serum-containing media or 1% serum media, respectively. Known cell densities were prepared by serial dilution starting at 50000 cells/well. Alamar blue assay was performed as described in the method section, and fluorescence was plotted against known cell density. Each point is an average of 3 independent experiments with 3 technical repeats for each condition.* ***A, D*** *Alamar Blue relative fluorescence in serum-free media, BV2 cells 2h and 4h incubation with resazurin, respectively;* ***B,E*** *0.5% serum media, BV2 cells 2h and 4h incubation with resazurin, respectively;* ***C,F*** *1% serum, BV2 cells 2h and 4h incubation with resazurin, respectively.*

It was next considered, whether there may be metabolic changes or adaptations occurring in the cells over the 48h period in reduced serum, that then lead to an advantage in dye processing. For the next series of experiments, the cells were pre-conditioned for 48h in 0.5% serum, and cultured

at a density equivalent to 9000 cells/well in a 96-well plate, in order to mimic the conditions from the initial Alamar blue experiments, where a P2X7-dependent advantage was observed. This is shown in Figure 3.8. No advantage was observed for P2X7-expressing cells.

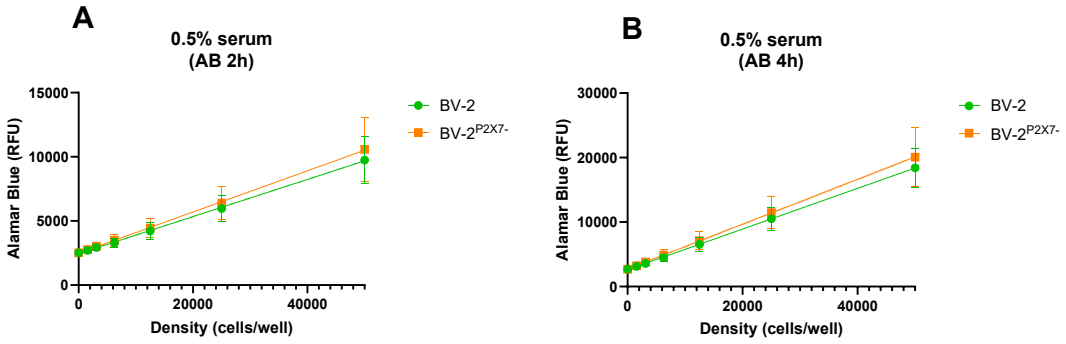

Figure 3.8 Resazurin processing standard curve of BV-2 and BV-2^{P2X7-} cells pre-conditioned in reduced serum and fixed density. *Cells were pre-conditioned by culturing in dishes in 0.5% serum for 48h at a starting density equivalent to 9000 cells/well in a 96-well plate. The cells were then trypsinised, counted and plated in 0.5% serum at known densities prepared by serial dilution starting at 50000 cells/well. Alamar blue was added immediately and allowed to process for 2h (**A**), and 4 hours (**B**). The fluorescence was plotted against known cell density. Each point is an average of 3 independent experiments with 3 technical replicates for each condition.*

Finally, Resazurin processing was investigated in HEK and HEK^{hP2X7} cells pre-conditioned by culturing in 0.5% serum-containing media for 48h, then plated in 0.5% serum media vs HEK and HEK^{hP2X7} cells taken directly from growth flasks, then plated in complete media (Figure 3.9). Both cell lines were equally capable of processing the dye, regardless of the experimental conditions.

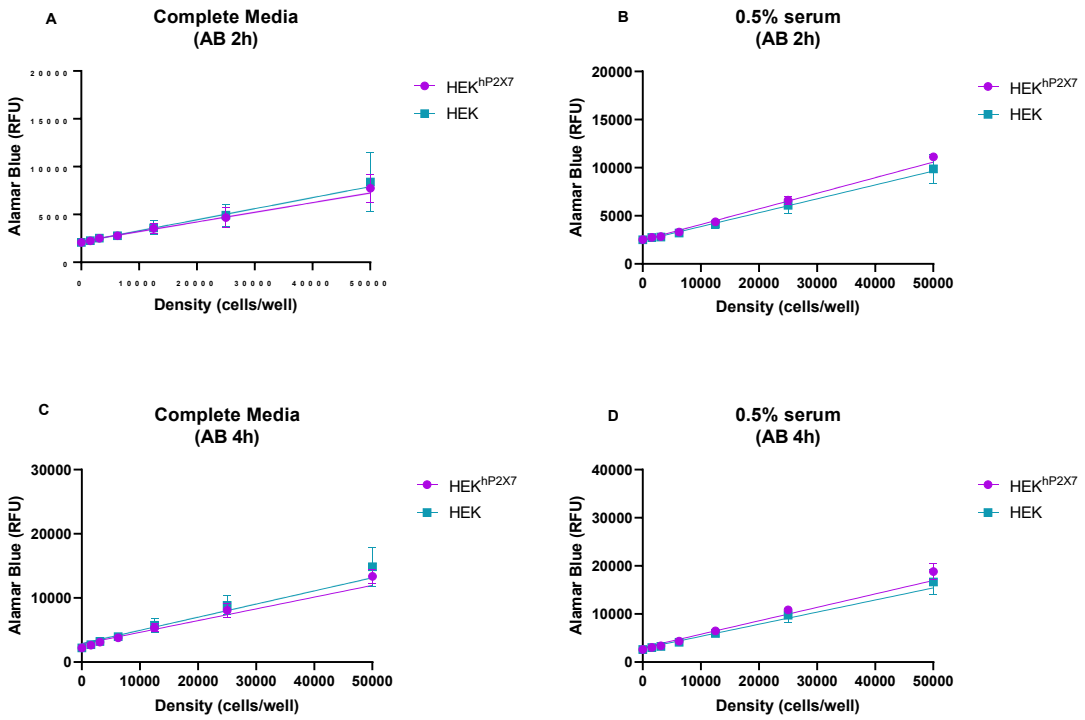

Figure 3.9 Resazurin processing standard curve in HEK and HEK^{hP2X7} cells pre-conditioned in low serum for 48h vs cells from growth flasks in complete media. *Cells were either grown in complete media (**A**,**C**) or pre-conditioned by culturing in dishes in 0.5% serum for 48h at a starting density equivalent to 9000 cells/well in a 96-well plate (**B**,**D**). The cells were then trypsinised, counted, and plated in complete media (**A**,**C**) or 0.5% serum-containing media (**B**,**D**) at known densities prepared by serial dilution starting at 50000 cells/well. Alamar blue was added immediately and allowed to process for 2 and 4 hours, as indicated. Fluorescence was plotted against known cell density. Each point is an average of 3 independent experiments with 3 technical replicates for each condition.*

Various methods of measuring proliferation following serum reduction challenge

Following from the data obtained in Alamar blue assay, which provided an indirect way of assessing the cell number, and revealed an advantage of P2X7-expressing cells in the challenging conditions of serum reduction (0.5%) and 48h incubation time point, more assays were used to look at the cell numbers directly. A selected range of experimental techniques useful to measure proliferation was employed to assess differences between BV-2 and BV-2^{P2X7-} cells. The effect of P2X7 expression on cell proliferation in BV-2 cells under challenging conditions of serum reduction was next investigated by manual cell counting using a hemocytometer and a microscope. This was also performed in the HEK 293 cell line model. All manual counts are shown in Figure 3.10.

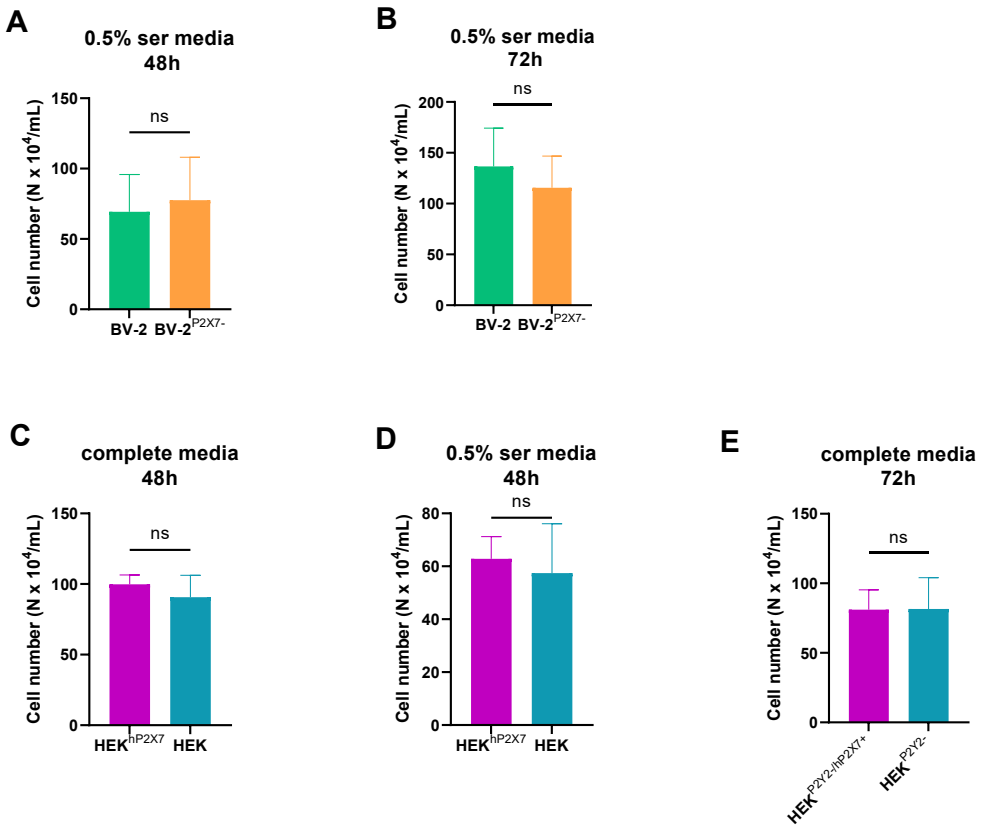

Figure 3.10 Manual cell count as a measure of proliferation. *Cells were seeded in 2.5 mL growth flasks at a starting density equivalent to 9000 cells/well in a 96-well plate, in media containing 0.5% serum or complete media, and left to grow over 72h or 48h. Cells were then trypsinised and counted using a haemocytometer.* ***A*** *shows BV-2/BV-2^{P2X7-} cells at 48h in 0.5% serum-containing media (n=3).* ***B*** *BV-2/BV-2^{P2X7-} in 0.5% serum-containing media for 72h (n=5).* ***C*** *HEK^{hP2X7}/HEK cells in complete media for 48h (n=3).* ***D*** *HEK^{hP2X7}/HEK cells in 0.5% serum-containing media for 48h (n=3).* ***E*** *HEK$^{P2Y2-/hP2X7+}$/HEK^{P2Y2-} cells in complete media for 72h (n=3). Four samples were taken for counting from each sample and averaged. The graphs show collated data of mean result out of 3-5 independent experiments. Data was analyzed with an unpaired t test (ns = not significant).*

The cells were set up in 0.5% serum media for 48h in 2.5mL growth flasks to obtain a sufficient number of cells for counting. No significant difference was found between cell lines dependent on P2X7 expression, neither in BV-2 or HEK 293 cells (Figure 3.10). The microglia proved very difficult to fully trypsinise out of the 2.5 mL growth flasks. Therefore, the time of trypsinization was doubled and the bottom of the well was rinsed several times to thoroughly remove all cells. The empty flasks were also inspected under a light microscope for any leftover adherent cells. The findings on microglial cell line were therefore confirmed in the HEK/ HEK^{hP2X7} cell model, as well as an additional HEK model available - the HEK/ HEK$^{P2Y12-/hP2X7+}$ cell line (P2Y12 receptor knockout), which lift off the bottom of the flask easily after the standard treatment with trypsin/EDTA. This data suggests that the number of cells at the end of the experiment was similar, irrespective of P2X7 expression.

The effect of P2X7 expression on cell division in BV-2 cells under challenging conditions of serum reduction was further investigated over 72h using the CellTrace Yellow Dye Retention Assay. This assay uses a fluorescent dye that stains the cells permanently allowing for a fluorescent signal to be measured by flow cytometry. When samples are taken over time from the stained population, it is possible to observe the dye retention per cell decreasing with every cycle of division. Figure 3.11 shows the data obtained for BV-2 cells over 72h, started at different densities, which were corresponding to 6000 and 9000 cells/well, where we had previously seen a difference in the Alamar blue cell viability assay. Because BV-2 and BV-2^{P2X7-} cells had taken up different amounts of CTY stain (see Figure 3.11 B,C at time '0'), the data was also normalized to allow a better comparison between the cell lines. Following normalisation of the data (Figure 3.11 D and E) it is clear that the rate of divisions in BV-2 and BV-2^{P2X7-} cells is the same; in fact, the plots perfectly overlap. Interestingly, though, BV-2 cells show a higher signal at time 0 (raw data shown in Figure 3.11 B and C), which suggests a higher dye uptake per cell when P2X7 is expressed.

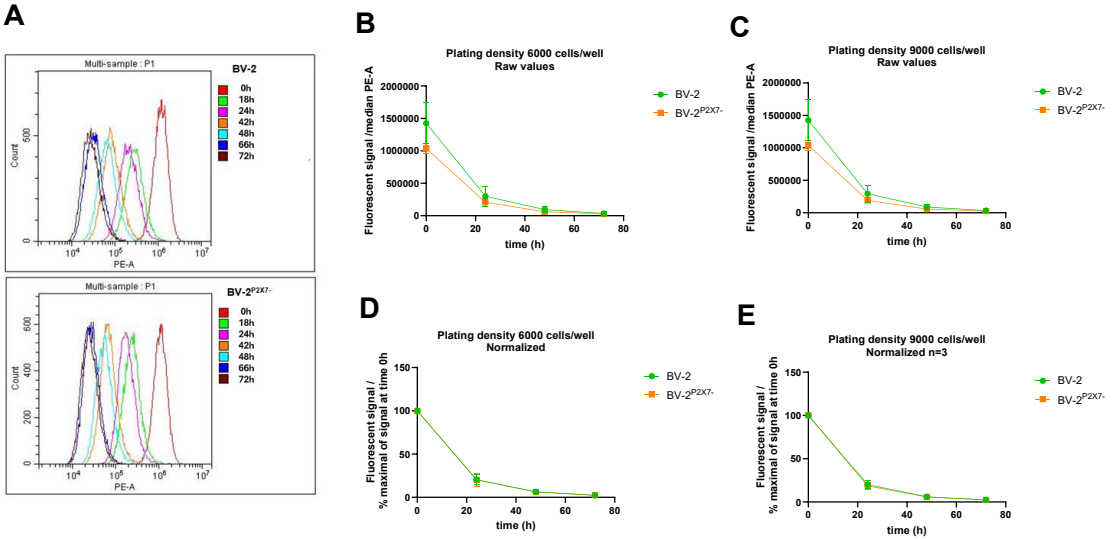

Figure 3.11 CellTrace Yellow dye retention assay as measure of cell divisions over time over 72h of growth in reduced serum. *BV-2 and BV-2^{P2X7-} cells were stained with CellTrace Yellow dye following the manufacturer's protocol, washed and plated in 24-well plates in 0.5% serum containing media at the starting density 35640 and 53460 cells/well (equivalent to 6000 and 9000 cells/well in a 96-well plate). The cells were then trypsinised at different timepoints over the next 72h and CellTrace Yellow fluorescence was measured by flow cytometry as described in the method section. Each point is an average of 3 independent experiments.* ***A*** *shows representative histograms capture for BV-2 and BV-2^{P2X7-} cells where plating density was equivalent to 9000 cells/well.* ***B*** *and* ***D*** *show dye retention over 72h in cells where plating density was equivalent to 6000 cells/well in a 96 well plate, depicted by fluorescence signal (raw data) and normalized (percentage of maximum signal at time 0h), respectively.* ***C*** *and* ***E*** *show dye retention over 72h in cells plated at starting density equivalent to 9000 cells/well in a 96 well plate, depicted by median fluorescence signal (raw data) and normalized data (percentage of maximum signal at time 0h), respectively.*

The time point 0-24h, when the initial dye uptake is higher in BV-2 cells than BV-2^{P2X7-} cells, was investigated more closely in Figure 3.12. Although the dye uptake is different, the figure shows that the rate of divisions shown by the slope of the curve is the same for both cell lines.

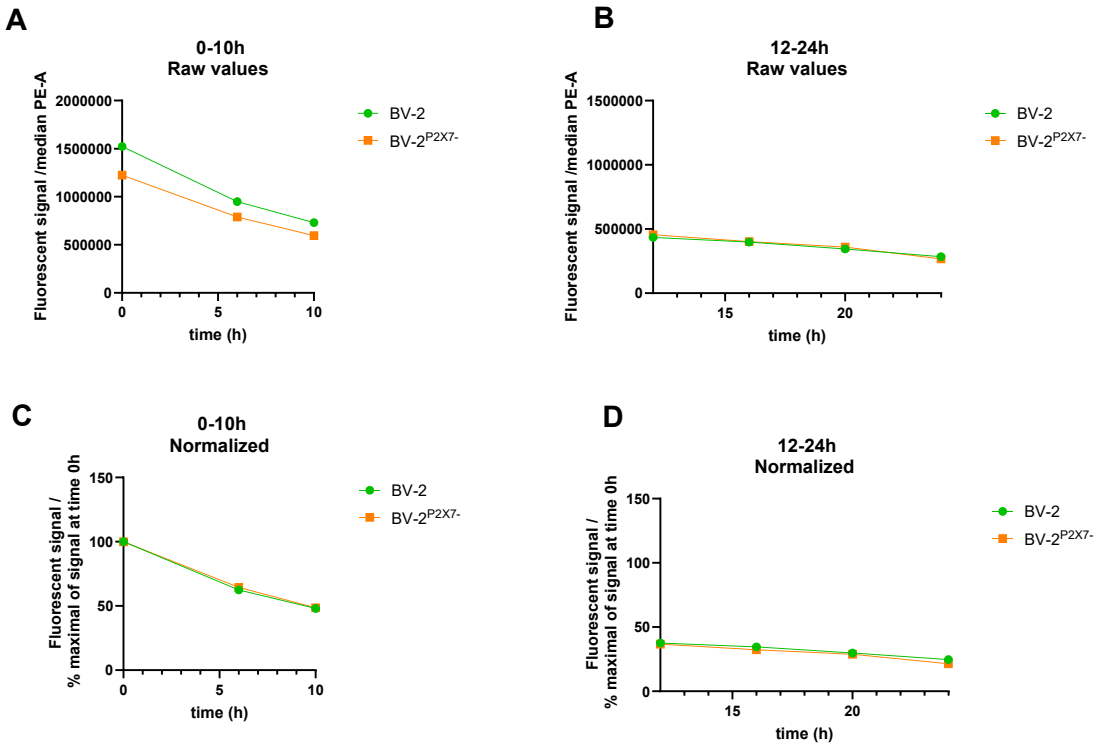

Figure 3.12 CellTrace Yellow dye retention assay as measure of cell divisions over time over the first 24h of growth in reduced serum. *BV-2 and BV-2^{P2X7-} cells were stained with CellTrace Yellow dye following the manufacturer's protocol, washed and plated in 24-well plates in 0.5% serum containing media at the starting density 35640 and 53460 cells/well (equivalent to 6000 and 9000 cells/well in a 96-well plate). The cells were then trypsinised at different timepoints over the next 24h and CellTrace Yellow fluorescence was measured by flow cytometry as described in the method section. Each point is a representative of a single experiment.* ***A*** *and* ***C*** *show dye retention over 0-10h in cells, depicted by fluorescence signal (raw data) and normalized (percentage of maximum signal at time 0h), respectively.* ***B*** *and* ***D*** *show dye retention over 12-24h in cells, depicted by median fluorescence signal (raw data) and normalized data (percentage of maximum signal at time 0h), respectively.*

Next, the effect of P2X7 Expression on Cell Proliferation was measured in BrdU Incorporation Assay and compared to Alamar blue assay 'sister' plate prepared from the same stocks and at the same time. Figure 3.13 A shows that the rate of DNA synthesis, measured by BrDU incorporation in an ELISA assay, is the same in both cell lines, regardless of P2X7 expression. Interestingly, the 'sister' Alamar blue plate (Figure 3.13 B) shows that P2X7-expressing cells display an increased Alamar blue fluorescence. The assay was conducted at the 24h time point (Figure 3.13 A and B) and at the 48h incubation time point (Figure 3.13 C and D).

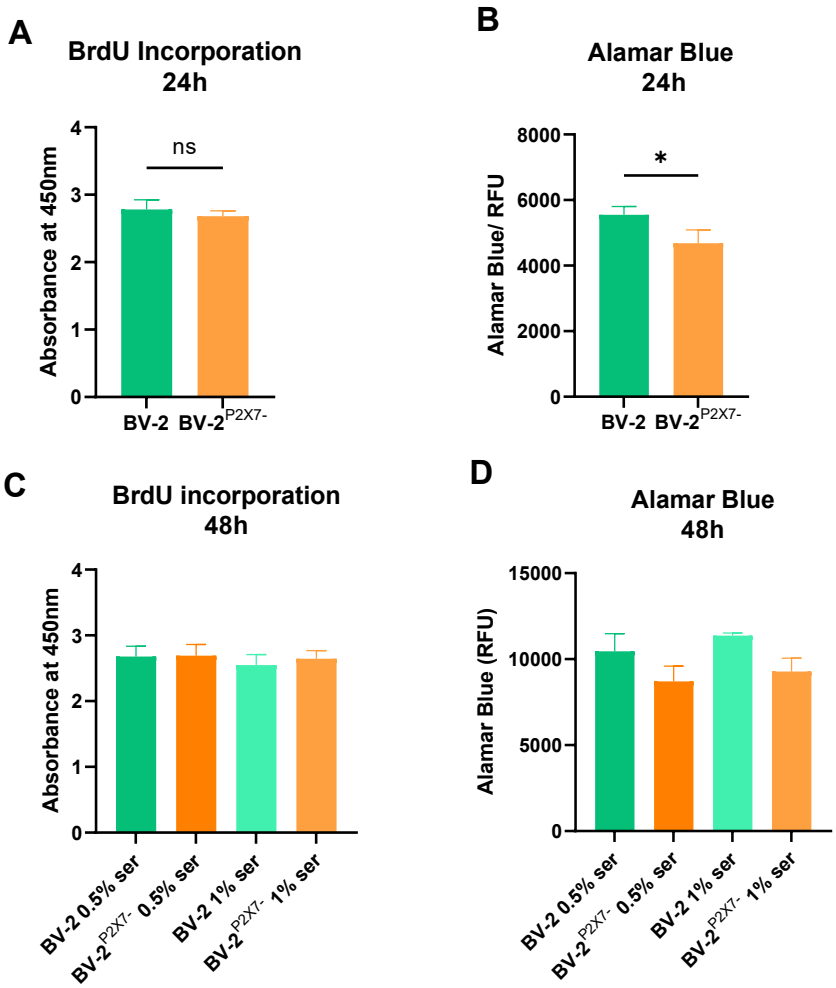

Figure 3.13 BrdU incorporation vs Alamar blue assay. *BV-2 and BV-2^{P2X7-} cells were plated in 0.5% serum containing media at density 9000 cells/well in two identical 96-well plates and allowed to incubate for 22h (**A** and **B**) or 46h (**C** and **D**) at which point BrdU label or Alamar blue was added to the plate for further two hours. **A** Results of BrdU ELISA assay, 24h. **B** Results of Alamar blue assay, 24h. Each point is an average of three independent experiments performed in six and three replicates for each condition in BrdU and Alamar Blue assays, respectively. **C** and **D** are the results of BrDU and Alamar blue assay, respectively, at a 48h time point. The results are from a single experiment performed with 3-6 technical replicates for each condition. Background corrected. Statistical analysis was performed using one-way ANOVA followed by Šídák's multiple comparisons test (* P=0.05) on **A** and **B**.*

Next, the effect of P2X7 expression on cell number in challenging conditions was compared in Alamar blue assay vs another metabolic activity assay, that relies on a colorimetric change and a measure of absorbance, rather than fluorescence- the MTS Assay- to see if the same pattern emerged. Although the difference between the two cell lines did not come out as significant when the data was collated, exactly the same trend was apparent in the MTS assay, as in the Alamar

blue assay (Figure 3.14). This suggests that the P2X7 advantage observed in the Alamar blue assay may be due to a metabolic effect.

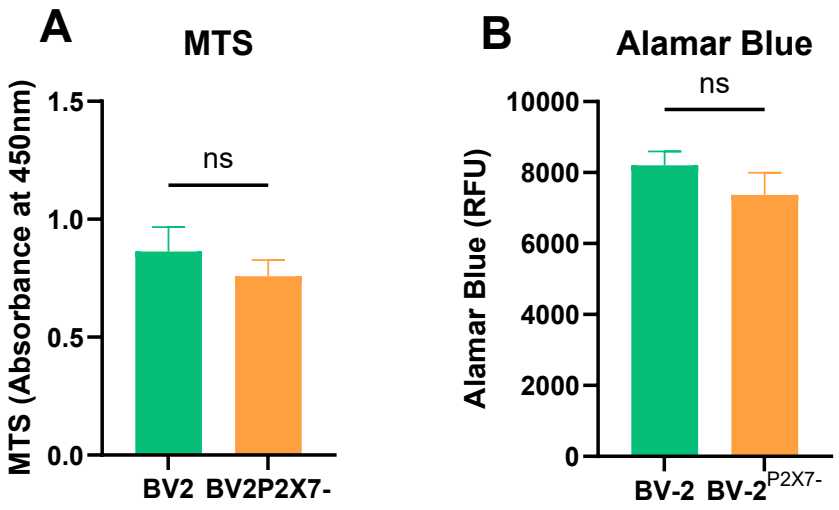

Figure 3.14 MTS viability assay on BV-2/ BV-2^{P2X7-} cells in reduced serum compared to Alamar blue. *The cells were plated at density 9000 cells/well in 0.5% serum containing media and allowed to incubate for 24h. Alamar blue was performed on half of the plate (**A**) and MTS assay on the other half (**B**), allowing 2h for processing of the dye. The data points represent the average of three independent experiments with 8 technical replicates for each condition. Background corrected. Analyzed with one-way ANOVA and Šídák's multiple comparisons test (ns= not significant).*

3.2.3 Effect of experimental conditions on Alamar blue assay

Specific experimental design factors that might affect the Alamar blue assay were considered. An optimum cell density is key in healthy cultures of microglia. The right amount of cell-to-cell contact is important for proliferation, activation, and migration of the cells. Effect of cell-to-cell contact conditioning prior to plating on the final RFU values in Alamar blue assay, was measured by varying the cell density in cell culture prior to experimental set-up (Figure 3.15).

Although the data does not show statistical significance, it can be observed that the values are higher for whichever cell line was pre-cultured at a lower initial density. This could be due to growth-inhibiting signalling which occurs in cell culture at high confluency with a lot of cell-to-cell contact. The data does demonstrate some degree of variability and reinforces that care must be taken that BV-2 microglia are pre-grown at optimum and matched densities before their use in experiments that measure cell number and viability.

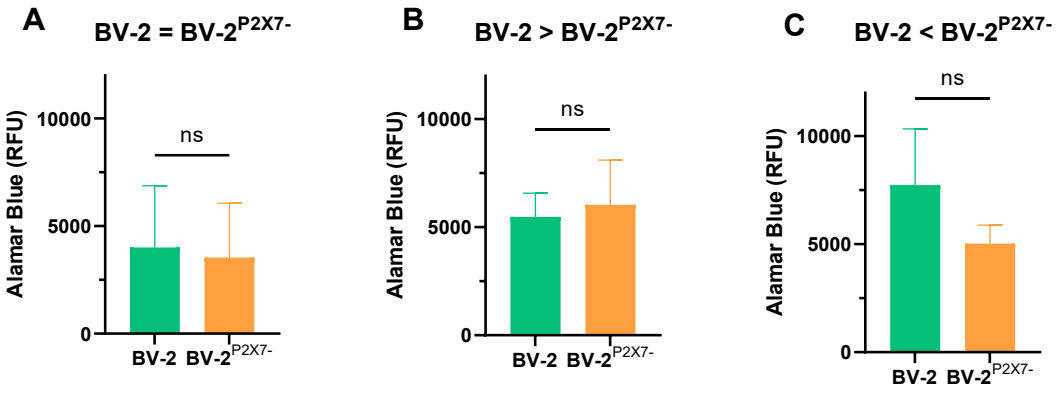

Figure 3.15 Impact of density in cell culture dishes prior to plating on Alamar blue assay results. *BV-2/ BV-2^{P2X7-} cells were pre-cultured in 2 mL dishes overnight prior to use in experimental set up. The relative density in culture was either equal and optimal (approximately 80% confluency in the dish), x2 lower or 2x higher for BV-2 vs BV-2^{P2X7-} cells. On the day of the experiment the cells were plated in 0.5% serum at starting density 9000 cells/well and incubated over 24h. Alamar blue was added within the last 2 hours and allowed to process for 2h before reading. The experiments for B and C were matched and done on the same plate on the same day for better comparison.* ***A*** *Cells pre-grown at equal densities.* ***B*** *BV-2 cells pre-grown at 2X density.* ***C*** *BV-2^{P2X7-} pre-grown at 2X density. Each point represents an average of 3 independent experiments, each conducted with 8-10 technical replicates for each condition. Data analysed with unpaired t-test (ns= not significant).*

Next, the effect of media conditioning by the cells was considered. When the cells are plated and incubated for 24h, 48h or 72h in a small volume of 200 µL of media, they gradually use up available nutrients, change morphologically, release signaling molecules as they respond to the challenge of serum reduction, and some cell death always occurs as population remodeling takes place in response to these challenges. This may have an effect on media composition and pH of the media in the well. It was next considered whether the media is becoming conditioned by the two cell populations differently when P2X7 is expressed or not. This could then have an effect on the processing of the Alamar Blue dye in a routine reading.

To check for major differences in pH, the cells were cultured for 48h in reduced 0.5% serum. They were seeded in a 24-well plate at density equivalent to 9000 cells/well in a 96 well plate (53460 cells/well) to mimic the usual Alamar blue assay conditions. After 48h of incubation the media was removed and centrifuged to remove any cells. It was then tested with a standard pH meter. For BV-2 cells average pH was 8.02 and for BV-2^{P2X7-} it was 8.00. This was the result of an average of two independent experiments with three technical replicates each. This demonstrated that there was no difference in media pH following the 48h culture in reduced serum between the two cell lines.

The effect of the '48h old conditioned media' vs 'fresh media' on Alamar blue readings was next evaluated. The media was taken off from a standard 96-well plate subjected to the usual challenge of serum reduction and applied to a half of a confluent plate of BV-2 vs BV-2^{P2X7-} cells. The other half of the plate received fresh media. Alamar blue was then added and allowed to process for the usual time (2h and 4h). It was visually apparent that the fluorescence values of processed Alamar Blue in fresh media were consistently lower than those in 48h old pre-conditioned media (Figure 3.16), although this was not statistically significant when analysed. Swapping the media did not affect the degree of the difference observed between the readings for the two cell lines investigated.

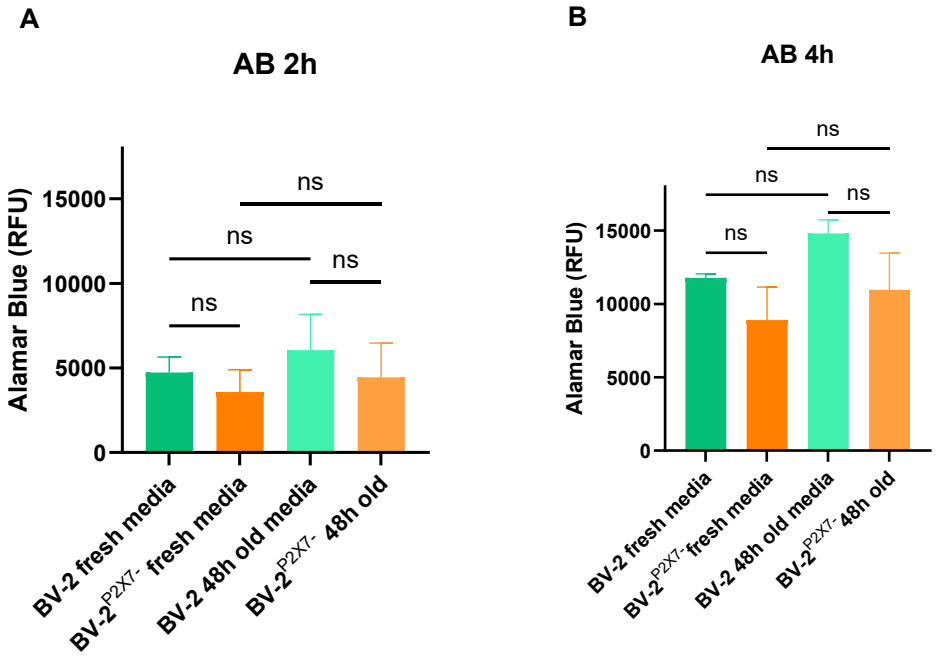

Figure 3.16 Processing of Alamar blue by BV-2 vs BV-2^{P2X7-} cells in fresh media vs 48h old media pre-conditioned by the cells. *BV-2 BV-2^{P2X7-} cells were plated in 96-well plates at density 9000 cells/well in reduced serum 0.5% media and left to incubate over 48h. At 46h half of the plate had media gently removed from the wells and replaced with fresh 0.5% ser media at 37°C. The other half of the plate had its old media left on but gently lifted off and back onto the cells using a multichannel pipette to mimic the swap. Alamar blue assay was performed as described in the method section. Readings were taken at 2h (**A**) and 4h (**B**) of processing time for Resazurin dye. Background fluorescence was subtracted from each well. Each point represents an average of 3 independent experiments with 12 technical replicates for each condition. Analyzed with Ordinary One-way ANOVA and Šídák's multiple comparisons test (ns= not significant).*

The processing of Alamar blue in '48h old media' that had been pre-conditioned by BV-2 and BV-2^{P2X7-} cells vs in 'unchanged HEK 293 media' was next observed on a confluent plate of HEK 293 cells (Figure 3.17).

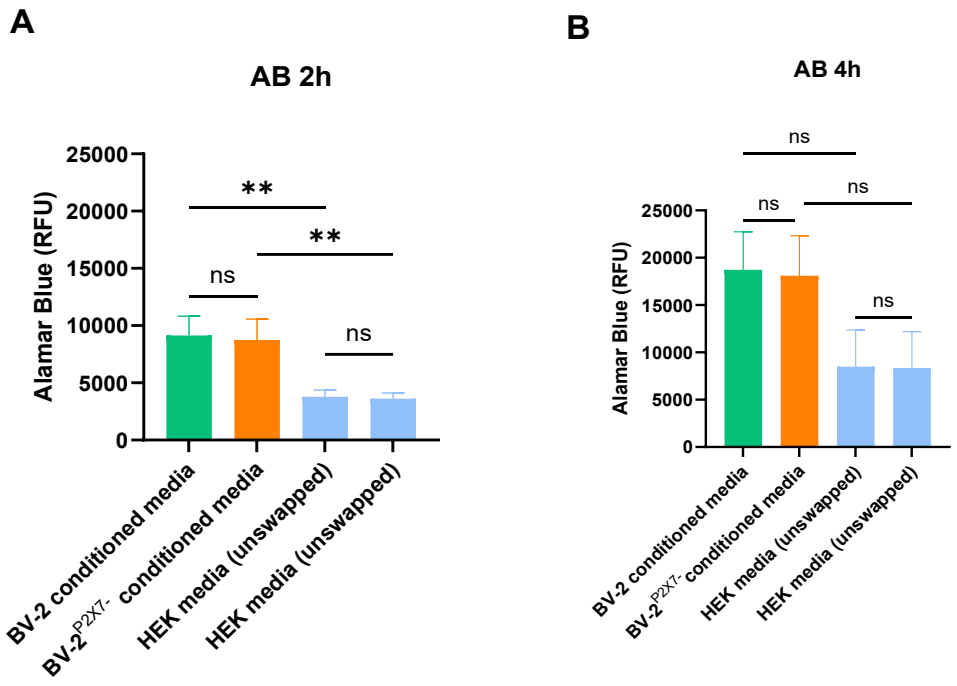

Figure 3.17 Processing of Alamar blue by HEK 293 cells in media pre-conditioned by BV-2 cells vs BV-2^{P2X7-} for 48h, or in unchanged HEK 293 media (control). *A confluent plate of HEK 293 cells was prepared 24h before the experiment. On the day of the experiment half of the plate had its media removed and swapped for media which was pre-conditioned by BV-2 and BV-2^{P2X7-} cells for 48h. The other half of the plate had its old media left on but gently lifted off and back onto the cells using a multichannel pipette to mimic the swap. BV-2 BV-2^{P2X7-} cells were plated in 96-well plates at density 9000 cells/well in reduced serum 0.5% media and left to incubate over 48h. At 46h media was gently removed from the wells and placed onto the empty columns of a confluent plate of HEK cells. Alamar Blue was performed as described in the method section. Readings were taken at 2h (**A**) and 4h (**B**) of processing time for Resazurin dye. Each point represents an average of 3 independent experiments with 12 technical replicates for each condition. Two columns of HEK cells were analysed and plotted to observe if lifting of the media resulted in any subtle differences between the column due to pipetting errors. Analyzed with Ordinary One-way ANOVA and Šídák's multiple comparisons test (Statistical significance denoted by * p<0.05, ** p<0.01, *** p<0.001).*

Figure 3.17 shows that the difference between the Alamar blue reading obtained from HEK 293 cells in the 'HEK 293 control media' and the 'BV-2/ BV-2^{P2X7-} cells pre-conditioned media' is apparent, however there is no difference in how HEK 293 cells were able to process the Alamar blue using the BV-2 vs BV-2^{P2X7-} pre-conditioned media. This is interesting as this media would have come from halves of the plates used in the previous figure (Figure 3.16), where, although not statistically significant, there was a slight difference observed with respect to P2X7 expression.

Finally, as a control, the 48h old media was also taken off the BV-2 and BV-2^{P2X7-} cells, and put into a fresh empty 96-well plate. Alamar blue was added as normal, and the plate was incubated for 4h. No colour change visible to the eye was observed without the presence of viable cells, and

Alamar blue reading shows only a very slight difference compared to fresh media. This could be due to the accidental transfer of viable cells to the plate, however, none were seen under the microscope when the plate was checked. The reading from pre-conditioned media by both cell lines appears to give very minimally higher values than when Alamar blue is added to fresh media (Figure 3.18).

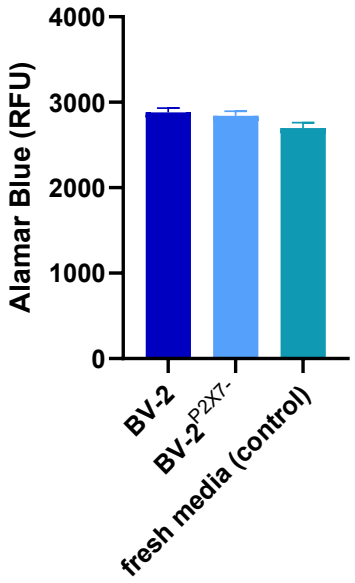

Figure 3.18 Fluorescence of Alamar blue in fresh media vs 48h old media pre-conditioned by BV-2 cells vs BV-2^{P2X7-} cells with cells absent in the plate. *BV-2 BV-2^{P2X7-} cells were plated in 96-well plates at density 9000 cells/well in reduced serum 0.5% media and left to incubate over 48h. At 46h the media was gently removed from the wells and placed in a clean empty 96-well plate. Plate was checked under the microscope for accidental transfer of cells and none were observed. Fresh media was a control. Alamar blue was performed as described in the method section with reading at 4h. These are the results of a single experiment with 6 technical replicates for each condition.*

3.2.4 Effect of reduced glucose on cell survival and cell division

Amoroso et al. (2010) reported the advantage of P2X7 expression in terms of survival when the cells were challenged with low serum and low glucose (4 mM) in the media. The effect of P2X7 Expression on cell survival in challenging conditions of glucose reduction in Alamar blue assay was investigated. The cells were introduced into low-glucose, low-serum media as an additional challenge.

Figure 3.19 shows that reduced glucose challenge did not affect the degree of difference observed between the two cell lines in Alamar blue assay. Rapid glucose reduction coupled with serum

reduction induced a stress response and resulted in high incidence of cell death. This is reflected in Figure 19 A and B, where the error bars are large due to variable but low overall survival. In an alternative experimental approach the cells were cultured in low (4 mM) glucose media in 10% serum for a week, before plating for Alamar blue experiment, where cells were incubated in the plate in 0.5% serum media and low glucose (Figure 3.19 C and D). Figure 3.19 C and D shows the usual pattern of BV-2 cells having slightly higher values than BV-2^{P2X7-} , although the difference between the cell lines is not statistically significant, with expected fluorescence values for a viable population of cells.

CellTrace Yellow assay was next performed to look at the rate of cell divisions between BV-2 and BV-2^{P2X7-} cells in low glucose (4 mM) containing media. This is shown in Figure 3.20. Interestingly, in 4 mM glucose the initial dye uptake was the same in both cell lines, although it could be quite variable (Figure 3.20 A). Normalized to the maximal response at time 0, each replicate followed the same pattern with a gradual reduction in dye retention, indicating no significant differences in the cell division rate between the two cell lines (Figure 3.20 B).

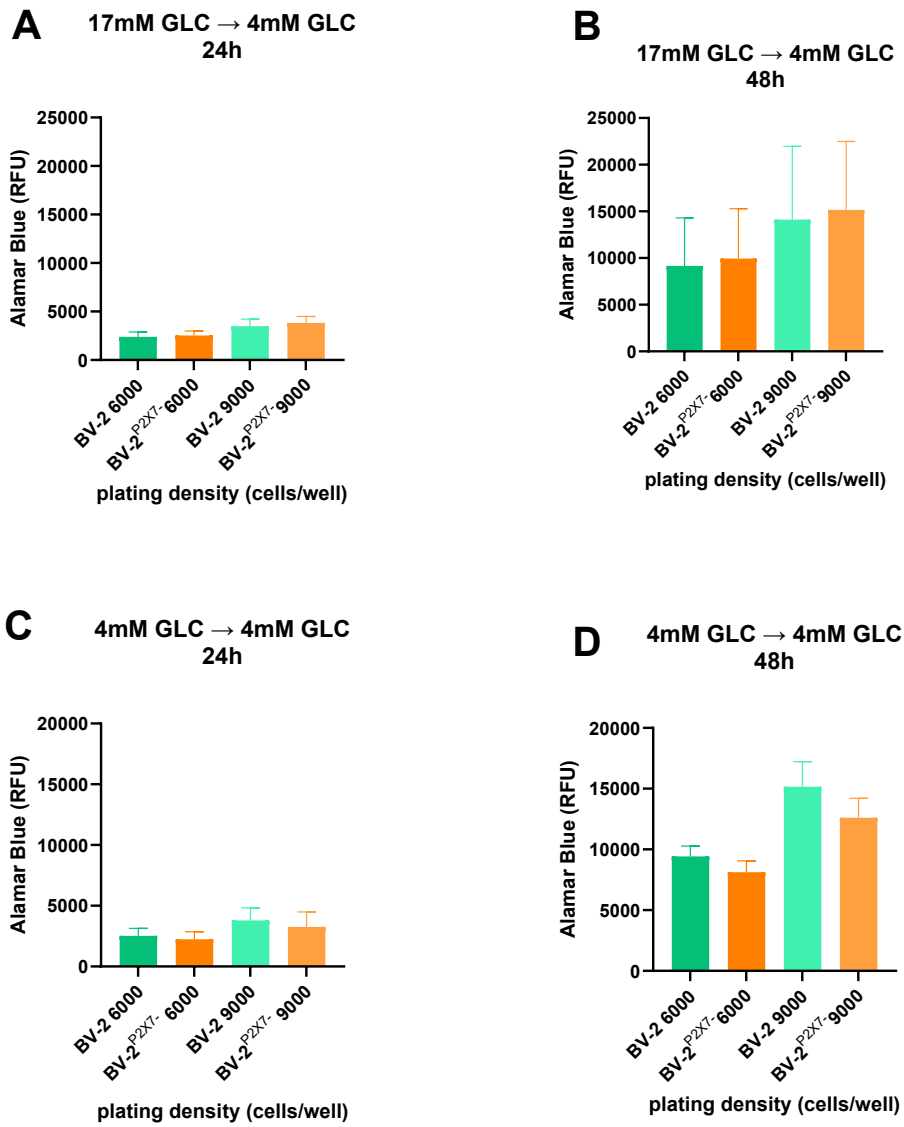

Figure 3.19 Cell viability in Alamar blue assay, of BV2/ BV2^{P2X7-} cells in 0.5% serum introduced to reduced (4 mM) glucose-containing media. *Cells were pre-grown for 24h at equal densities. Cells were plated in 96-well plates at 6000 or 9000 cells/well in 0.5% serum, 4 mM glucose containing media. Alamar Blue was added within the last 4h of the incubation time. Each point represents an average of 2-3 independent experiments, as indicated in brackets, each performed with 8 technical replicates for each condition.* ***A.*** *Cells were cultured in usual high (17 mM) glucose media then plated in reduced (0.5%) serum and 4 mM (low) glucose media incubated for 24h (n=3).* ***B.*** *Cells were cultured in usual high (17 mM) glucose media then plated in reduced (0.5%) serum and 4 mM glucose media and incubated for 48h (n=2).* ***C.*** *Cells were cultured in 4 mM glucose media for a week, on the day of experiment they were plated in reduced (0.5%) serum and 4 mM glucose media and incubated for 24h (n=3).* ***D.*** *Cells were cultured in 4 mM glucose media for a week, on the day of experiment they were plated in reduced (0.5%) serum and 4mM glucose media and incubated for 48h (n=3). All data analyzed with One-way ANOVA and Šídák's multiple comparisons test. Not statistically significant.*

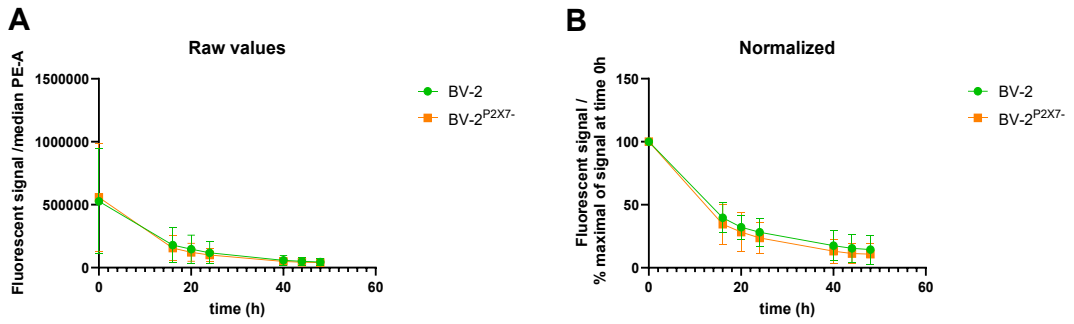

Figure 3.20 CellTrace Yellow dye retention assay as measure of cell division over time over 48h of growth in reduced serum and reduced glucose (4 mM). *Prior to the experiment, BV-2 and BV-2^{P2X7-} cells were set up at equal densities and pre-cultured for 24h in reduced glucose (4 mM from 17 mM) containing media. On the day of the experiment, cells were trypsinised out and stained with CellTrace Yellow dye following the manufacturer's protocol, washed and plated in 24-well plates in 0.5% serum, 4 mM glucose-containing media, at the starting density 35640 and 53460 cells/well (equivalent to 6000 and 9000 cells/well in a 96-well plate). The cells were then trypsinised at different timepoints over the next 48h and CellTrace Yellow assay was performed as described in the method section. Each point is a representative of an average of three independent experiments.* ***A*** *show dye retention over 0-48h in cells, depicted by fluorescence signal (raw data) and* ***B*** *shows the same data normalized (percentage of maximum signal at time 0h), respectively.*

3.2.5 Mitochondrial mass and health

Alamar blue assay detects the reduction of the Resazurin dye into its fluorescent product. The majority of this reduction relies on the mitochondrial activity of the viable cells. This raised a question whether the subtle reduction in Alamar blue fluorescence observed when P2X7 is not expressed in BV-2 cells could be due to mitochondrial numbers or to reduced mitochondrial health in the cells.

To evaluate mitochondrial health, staining with MitoTracker dyes was used to investigate mitochondrial mass in cells under the challenging conditions of serum reduction in BV-2 vs BV-2^{P2X7-} cells (Figure 3.21). The cells cultured in complete media were also compared to the cells cultured in 0.5% serum-containing media for 48h. MitoTracker Deep Red measures mitochondrial mass. MitoSOX measured mitochondrial superoxide levels. TMRM accumulates in mitochondria with high membrane potential.

The most apparent difference was observed with MitoTracker Deep Red between cells cultured in complete media vs reduced serum, although this was not statistically significant. This may suggest that cells are increasing the number of mitochondria when under serum starvation. No statistically significant difference with respect to P2X7 was observed.

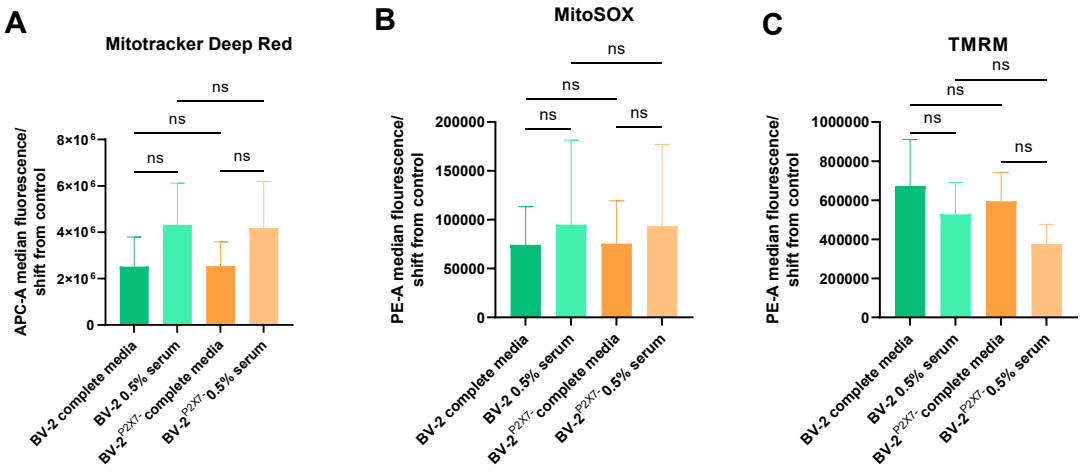

Figure 3.21 Effect of P2X7 expression on mitochondrial mass and health**.** *The cells were stained with mitochondrial dyes MitoTracker Deep Red, MitoSOX and TMRM according to the manufacturer's protocol, and the fluorescent signal was recorded by flow cytometry as described in the method section. Cells were either taken from culture flasks (complete media) or from cultures grown for 48h in 0.5% serum- containing media at density 53460 cells/well in a 24-well plate and pooled together to achieve a larger pellet.* ***A*** *Cells were stained with 100 nM MitoTracker Deep Red dye;* ***B****. Stained with 100 nM MitoSOX;* ***C*** *Cells were stained with 100 nM TMRM. The figures show an average of three independent experiments. Analyzed with One-way ANOVA and Šídák's multiple comparisons test (ns = not statistically significant).*

3.2.6 Effect of P2X7 expression on metabolomics

The effect of P2X7 expression on the metabolite profile of the cells was explored by NMR metabolomics. The cells were cultured under the standard experimental conditions of 48h long incubation in 0.5% serum media, density matched to 9000 cells/well in a 96-well plate, and their supernatants were analyzed by NMR to compare their metabolomic composition with regard to P2X7 expression. The obtained spectra were compared against each other and against a lactate standard, as well as the media control (Figure 3.22). While the spectra looked the same regarding composition, the amount of lactate present in the BV-2 supernatants was slightly higher (0.5 mM lactate) than that of BV-2^{P2X7-} cells (0.3 mM lactate). Extraction of intercellular metabolites was also attempted, however, was not successful and would be an interesting path to explore in the future work.

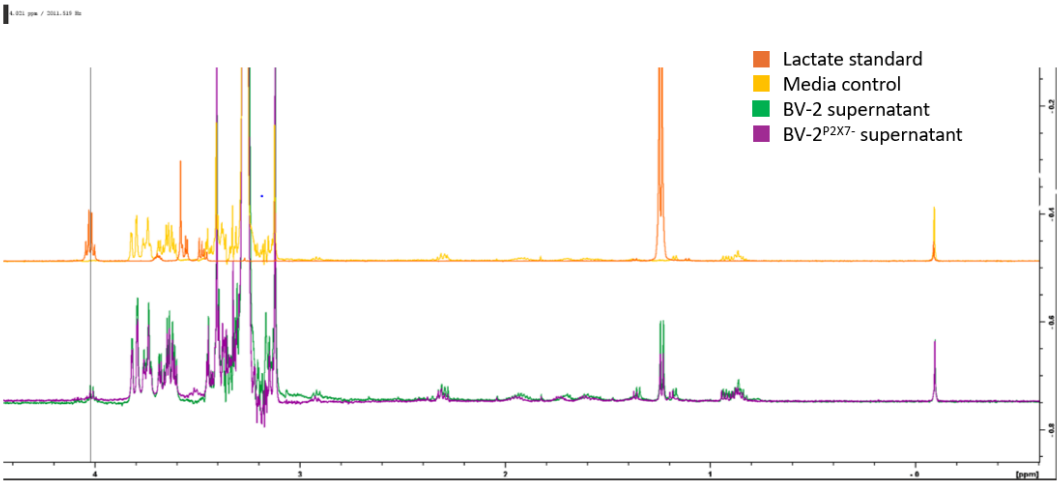

Figure 3.22 Metabolomics comparison by NMR of supernatants from BV-2 cells expressing or lacking P2X7. *Cells were seeded in 24-well plates at density corresponding to 9000 cells/well in a 96-well plate, in 0.5% serum media, and incubated for 48h. Supernatants were collected and centrifuged at maximum speed to remove any cell debris. The supernatants were kindly analyzed by Dr Serena Monaco, School of Chemistry, Pharmacy and Pharmacology, UEA, on 800 MHz NMR spectrometer with Bruker TopSpin software. The spectra were overlapped for comparison against media control and lactate standard. The figure shows representative spectra of an experiment which was repeated independently twice.*

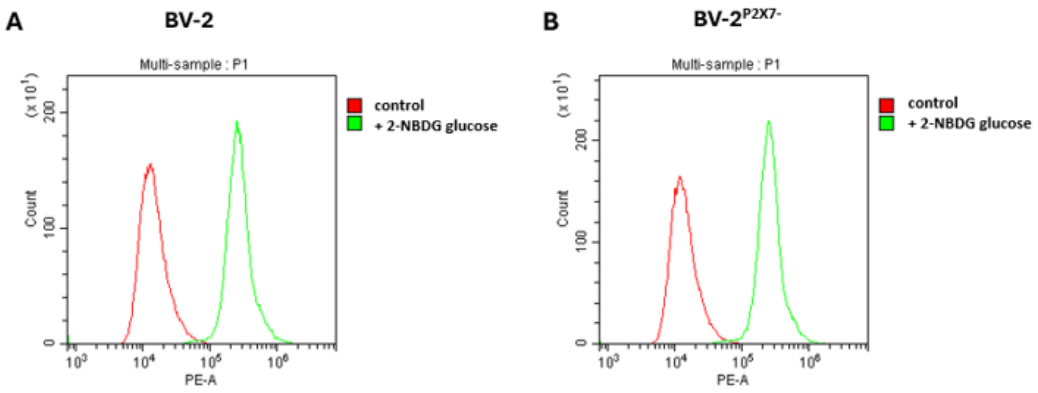

Figure 3.23 Glucose uptake by flow cytometry in BV-2 and BV-2^{P2X7-} following one hour incubation with 2-NBDG glucose. *Cells were plated in 24-well plates at the equivalent of 9000 cells/well in 0.5% serum conditions and incubated for 48h. They were trypsinised and washed into 0.5% serum glucose free media and incubated with 2-NBDG glucose or control media for 1h. Fluorescence was measured by flow cytometry as described in the method section. The figure shows histograms representative of the experiment which was independently repeated twice.*

The NMR experiment suggested a slight metabolic difference with P2X7 expression. Microglial cells are capable of a rapid metabolic switch towards glycolysis and regulate the surface expression of GLUT1 transporters (Wang et al., 2019). Glucose uptake into the cells at 48h in the

challenging conditions of serum reduction (0.5% ser) was investigated in the BV-2 vs BV-2^{P2X7-} cells. Cells were exposed to fluorescent 2-NBDG glucose, which is taken up via glucose transporters but cannot be metabolized by the cells and thus accumulates inside them. No difference was observed in the ability to take up glucose between the two cell lines. Both took up glucose within 10 minutes (data not shown) and showed the same shift away from control at the 1h time point (Figure 3.23).

3.2.7 Effect of P2X7 expression on NQO1 levels

In the final attempt to better understand the P2X7 effect reflected in the Alamar blue assay in BV-2 vs BV-2^{P2X7-} cells, NQO1 activity was considered. The NQO1 assay measures NQO1 (NAD(P)H dehydrogenase (quinone) 1) activity. The activity or available amount of such enzymes may reflect the capacity of the cells to reduce the resazurin dye in Alamar blue assay. NQO1 and Alamar blue assays were set up simultaneously on separate identical 96-well plates. Initially, the intention was to use the conditions of 9000 cells/well in 0.5% serum over 48h, which were previously determined to be optimal for eliciting a statistically significant difference between the two cell lines in the Alamar blue assay. However, the NQO1 assay required a higher confluency of cells per well, and the assays set up at these conditions were failing to produce a color change in preliminary experiments. The initial density of the cells was therefore scaled up to 12,000 cells/ well (Figure 3.24 A and B). NQO1 measurements were successfully achieved at this density, however the cells would reach confluency and start slightly overcrowding the wells of the plate before the 48th hour, which was not optimal as cells would detach and float in media or grow on top of each other. While, in the NQO1 assay, cells are lysed, and this may not be a problem, in the Alamar blue reading, an uneven distribution of cells at the bottom of the well may affect the reading. Also, close cell-to-cell contact may be affecting cells rate of growth, proliferation, and metabolic activity. As a compromise, the cells were set up at 20,000 cells/well (approx. 80% confluent) in 0.5% serum media and incubated overnight (18h) (Figure 3.24 C and D) Then, both assays were done on very confluent but evenly distributed wells.

The results were not what was expected in the Alamar blue assay, as the BV-2 cells were now not showing the usual advantage over the P2X7-deficient clones, however, this is likely due to the cells achieving a very high confluency very quickly under the experimental conditions, as explained above. What the experiments do demonstrate is that NQO1 results mirror the results of Alamar blue assay exactly, suggesting that availability or activity of NAD(P)H is reflected in resazurin reduction in Alamar blue assay.

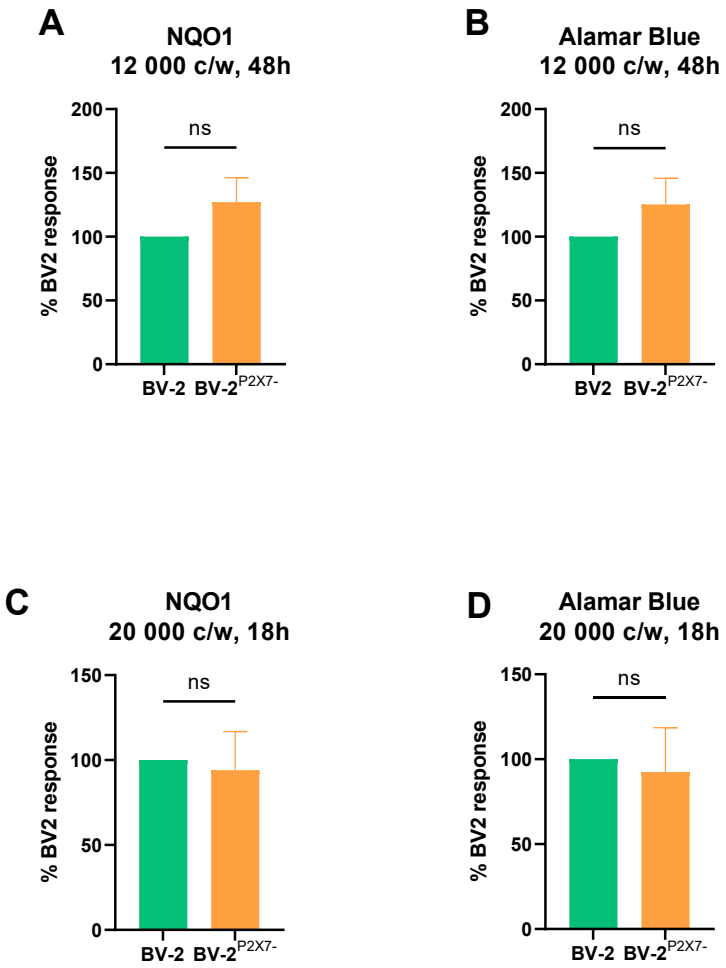

Figure 3.24 NQO1 Activity assay in BV-2 and BV-2^{P2X7-} cells. *Cells were plated simultaneously in identical plates for comparison of NQO1 assay to Alamar Blue resazurin processing.* ***A*** *and* ***B*** *Cells were plated at 12,000 cells/ well (c/w) in 0.5% serum media and incubated for 48h.* ***C*** *and* ***D*** *Cells were plated at 20,000 cells/well in 0.5% serum media and incubated overnight (18h) before performing the assays.* ***A*** *and* ***C*** *NQO1 assay ELISA protocol with processing time 6h.* ***B*** *and* ***D*** *Alamar blue standard protocol with processing time 2h. The NQO1 assay was kindly performed by Dr Emily Hobson, School of Chemistry, Pharmacy and Pharmacology, UEA. Data was normalized and is shown as % response of BV-2. Each point represents an average of 3 independent experiments, each performed with 3 technical replicates for each condition. Analyzed with unpaired t- test (ns= not statistically significant).*

3.3 Discussion

3.3.1. Experimental set-up optimisation and cell culture

Before experiments were started, BV-2 and BV-2^{P2X7-} cell culture was observed under a microscope and assessed by challenging the cells with serum withdrawal. It was observed that serum withdrawal changed the morphology of the cells away from a spindle-shaped and towards a more rounded and activated phenotype. This was in line with literature suggesting that activation of the BV-2 cells results in an enlarged ameboid shape and that serum withdrawal results in slight activation of the microglial cells. Complete serum withdrawal resulted in a high incidence of cell death and was not used.

The Alamar blue assay in particular, showed much variability in terms of the magnitudes of responses obtained from the cells over time. As a general trend, while looking at individual replicates of experiments done over a 14-week period, it was observed that the experiments performed within the middle-aged cells showed a greater magnitude of difference between the cell lines than those carried out on relatively older cells. Freshly thawed/recovering cells were very sensitive to serum deprivation, resulting in a high amount of cell death even in 0.5% serum. Therefore, only cells aged 2-12 weeks were used in experiments, and only 0.5% or higher serum media was used.

It is possible that the changing magnitude of responses observed with Alamar blue assay in particular, was due to the cells aging and undergoing changes which affected their ability to metabolize the dye. Some morphological changes could be observed from week 10 onwards in growth flasks. About 1% of BV-2 cells towards the end of 10th week looked enlarged. As the time went on BV-2 cells expressing P2X7 became more adherent to the surface of the growth flasks than their P2X7 deficient clone. This would affect trypsinization and splitting of the cells while culturing. This was further addressed in Chapter 5 with respect to appearance of spontaneous giant cells and with respect to the expression of adhesion molecules in the BV-2 cells expressing P2X7 and their P2X7-deficient clone. Expression of specific integrins and adhesion molecules, such as CD11a and CD11b has been shown in some studies to be upregulated following activation in BV-2 cells (Norden and Godbout, 2013). This was further addressed in Chapter 4 with respect to polarization and activation of cells. Trypsinisation itself causes mild stress to the cells and can shift the phenotype towards an activated one when cells are overexposed to trypsin. Although normally this does not affect the cells in terms of day-to-day culturing, it is possible that some changes in the cells were occurring with adaptability to handling and culturing conditions over time, or simply the effect of spontaneous mutations as the cells age. However, as microglia are

very plastic and adaptable in challenging conditions, it is interesting to consider these acquired adaptations in terms of possible P2X7-dependent changes, as the P2X7-deficient clones did not show a remarkable increase in cell adhesion with aging. Care was taken throughout the work to account for and to prevent any differences that could arise from these acquired differences between BV-2 and BV-2^{P2X7-} cells, and minimized by brief exposure to trypsin and strict age window for the use of the cell culture.

BV-2 cells becoming more adherent than BV-2^{P2X7-} as the time went on, was also likely to create a difference inside the growth flasks, altering the culture conditions which were aimed to be kept identical for the two cell lines. Although care was taken, when a growth flask was split and used for a second time, the BV2 cells were likely to find themselves at a slightly higher density than BV2^{P2X7-}cells. To remove this effect, cells were pre-grown at a set density in small petri dishes for 24h prior to use for some experiments. Adhesion to the surface of flasks, petri dishes, or microplate wells could, however, affect the experiments, such as cell number count, where the protocol involved a trypsinisation step; and the BrdU assay, which involved media removal prior to fixation and multiple washes of the plate afterwards. Regular inspection of flasks and plates throughout the assays for adherent cells minimized this possibility.

Basal expression of P2X7 was investigated and how it affects the cells over a period of time up to 72h. ATP presence in cell culture with challenging conditions of low serum over such a long period of time resulted in high incidence of cell death and so could not be reliably pursued in this experimental design.

Cell-to-cell contact is important for regulating microglia activity, morphology, motility and proliferation. Contact inhibition of growth is commonly observed in various cell cultures and in vivo models, where cells after reaching a certain density stop proliferating or slow down. In initial experiments (data not shown), it was observed that BV-2 cells grow best at an approximately 60-70% confluency, which is in agreement with the literature (Henn et al., 2009; Maher, 2021). Interestingly, with low or absent serum in the media, BV-2 cells struggled to grow when seeded at confluency 30% or lower (data not shown). Cell contact and density prior to plating were investigated as contributing factors to BV-2 and BV-2^{P2X7-} cells' health and activity, by pre-growing cells at varying densities prior to use in experimental designs (Figure 3.15). Moreover, any possible P2X7-dependent differences arising from cell-to-cell contact or proximity could point to the secretion of factors and should be investigated further. When cells were pre-grown at equal densities prior to plating, the difference between the two cell lines with respect to Alamar blue fluorescence, was observed, with a slight advantage of BV-2 cells over the BV-2^{P2X7-}. Cells were next pre-grown at X2 (or 1/2 density) of the other cell line, for 24h before plating for Alamar blue

assay. Interestingly, whichever cell line was pre-grown at a high density prior to plating, showed a slight disadvantage in Alamar blue assay (RFU). This could point to a high density in cell culture having an inhibitory effect on the cell's proliferation rate and lasting enough to show this after 48h of culture, or it could point to a slight metabolic shift reflected in the cells' ability to reduce the dye. Given that the effect is present in both cell lines, this does not seem to be driven by P2X7.

3.3.2 Investigating the trophic role of P2X7

To investigate whether P2X7 expression results in an advantage to proliferation, metabolic advantage or overall survival, the cells in BV-2/BV-2^{P2X7-} and HEK/HEK^{hP2X7} cell models were subjected to serum reduction or a rapid serum withdrawal and left to incubate and grow over a specified period of time under these challenging conditions, before measuring cell viability and proliferation in an array of assays, some looking at viability and some looking directly at measuring proliferation. Serum withdrawal induces growth arrest in HEK cells, and P2X7 has been previously shown to provide the transfected HEK cells with a proliferative advantage in serum-free conditions (Adinolfi et al., 2005; and Amoroso et al., 2012). Serum reduction results in slowing down of the rate of proliferation in rapidly dividing BV-2 cells, allowing for any difference in the rate of growth to be elicited more easily.

Alamar blue metabolic assay

Alamar Blue is a commonly used viability screening assay convenient for micro-well plate designs. The assay uses a non-fluorescent Resazurin dye which in the mitochondria of viable cells is readily converted to a fluorescent Resofurin product (Rampersad, 2012). The fluorescent signal may then be measured by a plate reader. Thus, Alamar blue assay uses the metabolic activity of the cells to indirectly reflect the number of cells in the wells of a plate. The advantages of the assay are low cost and a convenient way to compare the effect of multiple conditions on multiple cell lines in the same plate. Alamar blue assay experiments performed in BV-2 and HEK cell lines subjected to challenges of low serum demonstrated a clear pattern where P2X7-expressing cells consistently showed a higher RFU value of approximately 20% over the P2X7-deficient clones. However, upon observation, the number of the cells per well appeared the same under a microscope. Counting experiments were carried out on the same cell lines by exposing the cells to matched growth conditions (0.5% serum reduction and a plating density scaled up accordingly from 9000 cells/well in a 96-well plate to match a 2.5mL growth flask). The counting experiments did not reveal a

statistically significant advantage to P2X7-expressing cells, with regard to the cell number at 48h of incubation (Figure 3.10). This was true for both BV-2 and HEK 293 model cell lines.

Standard curves were plotted where a known density of cells was immediately exposed to Alamar blue and allowed to process the dye. These showed that BV-2 and BV-2^{P2X7-} cell lines process the dye in the same way at the densities used (Figure 3.7 and Figure 3.8). As the density of the cells increased to very high and confluent wells, variability was higher in RFU values obtained; however, the lower and middle densities and the slope of the curves looked the same for both cell lines. This was also true for HEK cell models (Figure 3.9), and also tested on cells which had been pre-grown at assay-matched density and reduced serum conditions, and tested in reduced serum conditions (Fig. 3.8 and 3.9). For the cells taken out of the flasks and introduced into low serum conditions to obtain a standard curve, there was an understandable amount of variability, which likely reflected the shock as the cells adapted to new conditions (Figure 3.7). The cells processed the dye in the same way regardless of plating conditions or P2X7 expression.

Direct methods of measuring proliferation

More direct methods of measuring proliferation were employed to look at cell numbers following the serum reduction challenge. BrdU assay was performed to directly measure DNA synthesis in BV-2 vs BV-2^{P2X7-} cells. The conditions chosen were the same as for Alamar blue assay, with the plating density 9000 cells/well and 0.5% serum media, following 24h or 48h incubation time. The results of the BrDU assay showed that BrdU incorporation was the same in BV-2 and BV-2^{P2X7-} cell lines suggesting that there is no difference in proliferation rates driven by expression of P2X7. Interestingly, a matched Alamar Blue 'sister' plate (plated at the same time, and from the same stock, using the same count, media, and cells as the BrDU assay plate) still showed an approximately 20% higher reading for BV-2 cells in the Alamar blue assay.

CellTrace Yellow dilution assay was used to trace cell divisions over time. The assay relies on a fluorescent stain that covalently binds integrins and proteins in the cell membrane, and thus, it is permanently retained by the cell. With each cell cycle and division, the amount of the dye per cell decreases by half. When samples are taken from a stained population of cells over the course of 48h or 72h, the dye retention can be measured by flow cytometry at each time point and generations of cells can be traced by looking at dye dilution. The normalized results (% dye retention) in Figure 11 B and Figure 12 B indicate that there is no difference in cell division rate between BV2 and BV2^{P2X7-} cells in challenging conditions of reduced serum. Interestingly, raw data show that BV-2 cells take up more dye than BV-2^{P2X7-} cells, as shown by the fluorescent signal intensity at time 0 of the assay (Figure 11 A and 12 A). This could be due to differences in the make

up of the cell membranes and expression of proteins or integrins; however, this was not investigated further at this stage. The results of this assay further support the conclusion that P2X7 expression does not affect proliferation in BV-2 cells.

Taken together, the assays discussed above, which directly measure cell division and cell number, suggest that the effect observed in Alamar blue Assay is not due to increased cell number per well. The work carried out in Alamar blue assay may reveal a difference in the metabolic status of the BV2 vs BV2^{P2X7-} cells under challenging conditions or the cells ability to metabolise the resazurin dye. This work provides clear evidence that the discrepancy in Alamar blue assay should be attributed to a metabolic or dye-reducing ability of the cell line, rather than actual cell numbers and proliferative capacity of the respective cell lines.

There is considerable amount of evidence in the literature supporting the idea of a trophic role of P2X7 (Amoroso et al., 2012; Di Virgilio et al., 2009; Giuliani et al., 2014; Kan et al., 2019; Monif et al., 2010; Orioli et al., 2017). Amoroso et al. (2012) showed that P2X7 provides the cells with proliferative advantage, arguing that HEK 293 cells transfected with P2X7 are capable of proliferation in serum-free media. The authors also showed that the effect was enhanced when cells were subjected to low (4 mM) glucose media (Amoroso et al., 2012). The Alamar blue and CellTrace Yellow assays with BV-2/ BV-2^{P2X7-} cells in reduced serum were therefore repeated in low glucose conditions (4 mM glucose) and showed again that P2X7 expression did not affect the rate of cell division in CellTrace Yellow assay (Figure 3.20). Alamar blue assay further showed that the metabolic or reducing advantage to the cells expressing the receptor, cannot even be reliably replicated in 4mM glucose in Alamar Blue assay (Figure 3.19) due to additional stress put on the cells and high rate of cell death, when cells were directly introduced into low glucose and low serum from high glucose and high serum containing media. It is worth noting that Amoroso et al., (2012) used serum-free media for their experiments. Serum-free conditions result in low survival rates and are characterized by low proliferative capacity in HEK 293 cells (Bohlen et al., 2017). In the work carried out here serum-free conditions resulted in very low cell viability and a high incidence of cell death in the wells. For this reason 0.5% or 1% serum media only was used in the experiments described above, and the data from Amoroso et al., (2012) could not be replicated.

The work presented here brings into question the claims in the literature that P2X7 has a trophic effect in microglia and transfected HEK 293 cells. P2X7 may affect the metabolic state and capacity of the cells, however literature claiming P2X7 has a trophic effect applicable to any cell line, should be treated with care.

Alamar blue is a very common, routinely adopted method used to determine cell viability in microplate designs. In principle, the assay relies on a metabolic dye Resazurin, an oxidized form

of 7-hydroxy-3H-phenoxazin-3-1-10-oxide, which is converted to its reduced form, resorufin, by mitochondrial enzymes with diaphorase activity in viable cells (Rampersad, 2012). Therefore, the viability of the cells is assumed to be indirectly proportional to the reduction of the dye and the fluorescent signal produced. There are obvious drawbacks to using an assay which relies on the metabolic activity of the cells, as it is not a direct measure of cell viability but rather a reflection of the cells' health and metabolic status. Proliferative assays, such as BrdU incorporation, rely on measuring actively proliferating cells in the given time point, whereas metabolic assays will detect the quiescent viable cells as well as the actively proliferating ones.

It should be considered that metabolic activity may vary with cell density (Ligasová and Koberna, 2021). This exacerbated effect could explain what is seen at the standard curve where, as the cell density increases the difference between the BV-2 and BV-2^{P2X7-} cells also becomes greater and more apparent (Figure 3.6, Figure 3.7, and Figure 3.8). The greatest difference between the RFU values of BV-2 and BV-2^{P2X7-} cells was observed at the conditions of 0.5% serum, plating density 9000 cells/well, and incubation time 48h (Figure 3.2). This appears to be an optimum point for eliciting a statistically significant discrepancy between the cell lines. At higher time points i.e. 72h or higher plating density i.e. 12 000 cells/well, the difference is more negligible and final RFU values are similar (Figure 3.3).

3.3.3 Mitochondrial mass and health of BV2 and BV2^{P2X7-} cells

The discrepancy between the fluorescence measured in Alamar blue assay in 0.5% serum showed a consistent advantage to P2X7 expressing cells. In viable cells resazurin is reduced to its fluorescent product by any mitochondrial enzymes with diaphorase activity rather than by one specific enzyme (Rampersad, 2012). The discrepancy between the cell lines could therefore be explained by a difference in mitochondria number or function. BV-2 and BV-2^{P2X7-} cells were stained with Mitotracker Deep Red to measure mitochondrial mass, TMRM (a membrane potential-dependent stain), and MitoSOX (measuring mitochondrial superoxide levels). All these are commonly used as markers for mitochondrial mass and health in viable cells. No statistically significant difference was seen between the BV2 and BV2^{P2X7-} cells in the overall mitochondrial mass, indicating that both cell lines express the same levels of healthy mitochondria. The assays were carried out in complete media and also in 0.5% serum, where the cells were exposed to the challenging conditions for 48h. There was an apparent shift in fluorescent signal between the two conditions, although this was not statistically significant, suggesting that the 48h conditioning of the cells to the low serum challenge might be impacting mitochondria, but in equivalent ways in

BV-2 and BV-2^{P2X7-} cell lines when the whole average population was considered. Very little is known about the effect of serum withdrawal on mitochondrial health and mass in cell culture. A study in HeLa cells (Moon Eun-Yi, 2008) shows that mitochondrial activity and mitochondrial enzymes, as well as ROS production, are increased in cells undergoing serum reduction from 10% serum to 3% and 0.5%. Another study in the cell model of adipose-derived stem cells (Giannasi et al., 2023) links serum starvation over 72h, by metabolomic analysis, to mitochondrial dysfunction, upregulation of superoxide dismutase and mitochondrial ROS production. Corroborating with this literature, an increase in mitochondrial superoxide in reduced serum conditions was observed by MitoSOX staining, although this was not statistically significant.

Interestingly, an increase in the number of microglial mitochondria, as well as changes to mitochondrial morphology, have been previously reported in primary rat microglia with pro-inflammatory activation (Banati et al., 2004). As serum deprivation induces activation-like changes in BV-2 cells (Yao & Fu, 2020), mitochondrial biogenesis may be why higher values were observed with MitoTracker staining in the cells exposed to 0.5% serum for 48h. The MitoTracker assays should be followed with more replicates to investigate the effect of reduced serum vs complete media, as some interesting effects may be detected there.

Literature suggests that mitochondria are implicated in facilitating a link between microglial activation and metabolic activity (Banati et al., 2004; Sarti et al., 2021). MitoSOX detects production of superoxide in mitochondria, which can be in part produced by dehydrogenase activity (the same enzymes which catalyse the reduction of the Alamar blue dye). MitoSOX levels could therefore be informative of a difference between the two cell lines which could impact the cells' reducing capacity for the Resazurin dye. The levels of superoxide in BV-2 vas BV-2^{P2X7-} cells, however, appeared to be independent of P2X7 expression.

Some literature suggests that P2X7 may be involved in control of microglial metabolism. Adinolfi et al., (2005) suggest that the trophic effect of P2X7 is partially due to an enhanced mitochondrial energy state and a better handling of ER Ca^{2+}, showing HEK cells transfected with P2X7 displayed more efficient oxidative phosphorylation and proposing that basal expression of P2X7 improves mitochondrial metabolism. The authors further propose that via these effects, low tonic stimulation of P2X7 leads to enhanced survival and promotion of growth, while high continuous stimulation with ATP will lead to P2X7-triggered cell death. Amoroso et al. (2012) implicate P2X7 in the regulation of glycolytic activity in challenging conditions, proposing that it confers an intrinsic ability to induce and enhance the expression of different metabolic features, allowing more effective active glycolytic metabolism and therefore enhancing survival and proliferation.

The reports by Amoroso et al., (2012) and Adinolfi et al., (2005) were found to be not reproducible in this thesis, when addressed in similar experimental conditions of reduced glucose and/or reduced serum, or serum-free conditions, using the BV-2 cell model and the HEK 293 model. Finally, one study on the transfected HEK 293 cell model and P2X7 knockout mice proposes that P2X7 localizes to mitochondria, showing that the lack of the receptor decreases mitochondrial performance, basal respiratory rate, affects expression of oxidative phosphorylation enzymes, and finally even affects cardiac performance (Sarti *et al.*, 2021). In this thesis, mitochondrial staining assays showed no advantage with P2X7 expression in BV-2 cell model.

3.3.4 Metabolic activity of BV-2 and BV-2^{P2X7-} cells

In an attempt to better understand the possible metabolic activity advantage of P2X7-expressing cells in Alamar blue assay, NQO1 Activity assay was performed to measure the NAD(P)H dehydrogenase (quinone) 1 activity in BV-2 and BV-2^{P2X7-} cells (Figure 24). The coenzyme NAD(P)H dehydrogenase is believed to facilitate the conversion of resazurin to fluorescent resofurin in the Alamar blue metabolic assay (Duque-Prata et al., 2024; Ross & Siegel, 2004; Vieira-da-Silva & Castanho, 2023). The NQO1 assay design was difficult to match to the Alamar blue assay conditions, which previously demonstrated the P2X7-driven discrepancy. A very high confluency of BV-2 cells was required for NQO1 detection. This created problems, as the conditions would no longer match the previous Alamar blue experiments. A higher number of cells per well meant that the cells were reaching 100% confluency in the wells very quickly and had to continue growing in an overcrowded environment, which, was reflected in poor morphology of BV-2 cells and may have affected the responses of the cells. While it was interesting to observe that the NQO1 results mirrored exactly the RFU values observed in the Alamar blue assay 'sister' plate (conducted at the same time and from the same cell stocks), the usual P2X7 advantage was not reproduced under these assay conditions. This suggests that both BV-2 and BV-2^{P2X7-} cell lines may have the same reducing capacity, dependent on very sensitive conditions, confluency, and handling on the day. The reduction of resazurin in the Alamar blue assay to its fluorescent product, is likely largely carried out by NAD(P)H 1 in BV-2 cells. It would be interesting to validate this further in a bigger experimental design and following a better optimization of the assay, to explore whether P2X7 expression under certain challenging conditions may influence NQO1 activity. However, based on this experiment it appears to be independent of P2X7 expression. There were, however, significant problems with the performance of this assay such as the need for a high confluency, mentioned above, and a prolonged development time than the advised hours on the ELISA kit manual and

for this reason, it would be interesting to try this assay with another cell line such as HEK vs HEK^{P2X7-}.

The investigation next focused on the metabolic differences between the BV-2 and BV-2^{P2X7-} cell lines. Microglia are known for their high metabolic flexibility, which gives them an enhanced survival capacity in challenging conditions (Bernier, York, & MacVicar, 2020; Orihuela et al., 2016). P2X7 has been linked to the ability of cells to shift their metabolism in favour of glycolysis and away from oxidative phosphorylation (Amoroso et al., 2012; Sarti et al., 2021). It would be interesting in future work to analyse the BV-2 and BV-2^{P2X7-} cells with comprehensive metabolic assay tools such as the Seahorse assay, to look at the oxygen consumption rate or extracellular acidification with regard to P2X7 expression in the BV-2 cell line.

One way of looking for differences in the metabolic activity of the two cell lines is to compare their metabolomic profiles. The metabolomic profile of BV-2 vs BV-2^{P2X7-} cells was compared by NMR metabolomics. The overlaid spectra of intercellular metabolites present in media revealed a slightly higher peak in BV-2 cells compared to BV-2^{P2X7-}, corresponding to extracellular or secreted lactate (Figure 3.22). This may indicate a higher rate of glycolysis, as lactate is a byproduct of glycolytic metabolism. An attempt was made to obtain spectra for intracellular metabolites by performing cell lysis and extraction with methanol; however, this was not successful. It would be interesting to follow this route in future work to obtain a more in-depth picture of the metabolic pathways benefiting from P2X7 expression in BV-2 cells.

A simple experiment which could reveal a glycolytic metabolism difference between the BV-2 and BV-2^{P2X7-} cells was a glucose uptake assay. An inflammatory environment and glycolytic metabolism in microglia has been linked to GLUT 1 receptor upregulation on the cell surface (L. Wang, Pavlou, et al., 2019). It was proposed that P2X7 expression may be facilitating a higher glucose uptake under stress and glucose starvation conditions, as it was shown by Amoroso et al., (2012) that P2X7 regulates glycolysis. BV-2 cells were pre-grown in low glucose and then given a fluorescently labelled 2NBDG glucose in glucose-free media. Uptake was monitored by taking samples over the course of 1h (Figure 3.23), but no difference was observed with regards to P2X7 expression.

3.3.5 Considering the extracellular environment and media conditioning

A theory could be put forward that P2X7-expressing cells have a greater ability to reduce the Alamar blue dye simply due to the composition or conditioning of the media and the extracellular

environment, which happens over the incubation time. Given that P2X7 has the macropore activity, in theory, during a 48h culture, spontaneous activation of P2X7 could facilitate some exchanges and movement of molecules in and out of the cells, on a small scale, in P2X7 expressing cells, which then contributes to conditioning of the media and the cell's advantage to reduce the Alamar blue dye. This could also be due to metabolites present in the media, activity, and levels of enzymes. For example, extracellular lactate concentration was found to be slightly higher in the media of P2X7-expressing BV-2 cells. This is one factor that, in theory could affect pH and conditioning of the media in the well over the time of the cell culture. Thus, the cells' ability to condition the media was considered.

Jabbar et al. (1989) showed that MTT assay showed variability in cells' ability to produce formozan in the media that had been previously inhabited by cells for several days vs fresh media. The authors also reported different pH of the media due to the 'media conditioning' which was occurring as the cells were cultured over the days. Data in Fig. 16 shows that MTS produced a mirrored reading in Alamar blue in BV-2 vs BV-2^{P2X7-}cells. Moreover, Jabbar et al. (1989) showed that Alamar blue fluorescence reading can be affected by factors such as pH.

The conditioning of the media in BV-2 vs BV-2^{P2X7-} cells was investigated in several ways.

Firstly, the pH of the media was compared by using a pH meter to measure the pH of the media following 72h of cell culture. No difference was found between the two cell lines. However, it would be interesting to investigate this by a more precise method.

Secondly, media was taken off the wells of BV-2 and BV-2^{P2X7-} cells of a 96-well plate which had been incubating for 48h and undergoing the standard challenge of serum reduction. This was transferred to an empty 96-well plate along with a column of fresh media, and Alamar blue was added as per usual protocol and the plate was read with a plate reader. No colour difference was observed by eye between the columns, and the RFU values obtained showed no significant advantage to BV-2 cells over BV-$^{2P2X7-}$ for 'conditioned media' over 'fresh media' (Figure 3.16).

To evaluate this further, media swapping experiments were conducted in BV-2 cells, where conditioned media was swapped for fresh (Figure 3.16), and where media of the BV-2 and BV-2^{P2X7-} cells were transferred onto a confluent plate of HEK cells, which then processed the dye in pre-conditioned media vs fresh media (Figure 3.17). Interestingly, the wells with 'pre-conditioned' media did not show any discrepancy between them, but the RFU values obtained from 'fresh' media columns were consistently lower in all experiments.

Taken together, these experiments demonstrate that the Alamar blue assay is sensitive to the conditioning of the media by the cells in the culture. Care needs to be taken, especially with

dynamic and heterogeneous cells such as BV-2, which may condition the media differently based on their activation and metabolic status.

The conditioned media may have been one of the contributing factors to the discrepancy observed between the BV-2 and BV-2^{P2X7-} cell lines in the Alamar blue assay.

Conclusions

P2X7 was not found to have a trophic effect in the BV-2 vs BV-2^{P2X7-} cells. HEK 293 cells transfected with P2X7 also did not carry a proliferative advantage. Literature suggesting that P2X7 expression carries a proliferative and survival advantage in serum reduction and low glucose challenges, was not reproducible.

P2X7 may carry a slight metabolic advantage, which was detected in the Alamar blue assay under specific conditions of 48h incubation with 0.5% serum, and plating density of 9000 cells/well in a 96-well plate. The preliminary NMR experiment revealed an interesting metabolic discrepancy between BV-2 and BV-2^{P2X7-} with respect to extracellular or secreted lactate concentration. It would be interesting to follow this work by looking at the intercellular metabolites in the BV-2 vs BV-2^{P2X7-} model.

Finally, the work demonstrated the sensitivities of the Alamar blue assay in different experimental designs, and the sensitivities of the BV-2 cell line to specific conditions such as confluency in the well and serum levels in the media. Taken together, this work shows how important it is to carefully establish assays and cell models in scientific research; and urges to carefully consider the literature, which suggests that the trophic activity of P2X7 applies to all cell lines and models.

Chapter 4 - Effect of P2X7 expression on microglial function and behaviour

4.1 Introduction

Microglia are incredibly heterogeneous and exhibit different phenotypes, functions, and behaviors depending on environmental cues and demands in the CNS (Healy et al., 2022). This chapter characterizes typical functions and responses of BV-2 cells and compares them to P2X7-deficient BV-2 microglia. The topics researched here include microglial activation, acquisition of classical phenotypes *in vitro*, phagocytosis, and cytokine secretion.

4.1.1 Microglial activation and markers of polarisation

Microglia are well described in the literature, and much of the research was initially based on microglial similarities to macrophages, displaying polarized phenotypes and targeted actions in response to classical activating agents. Just like macrophages, which exist in different phenotypic states and flexibly adapt their characteristics, microglial protein expression on the surface of the cells, and substances released vary depending on the cells' activated state (Kettenmann et al., 2011; Korzhevskii & Kirik, 2016; Murray et al., 2014; Zubova et al., 2022). Please refer to Chapter 1 Introduction to microglial phenotype and activation for more detail (Section 1.2.1). Under normal physiological conditions, microglia surveil the environment in their ramified quiescent state, and constant signals from neighbouring neurons and astrocytes contribute to the maintenance of this phenotype. Activation by pathogens, a physical insult, or dying cells in the vicinity triggers microglia to assume an activated, often enlarged, ameboid shape. It can trigger migration and chemotaxis to an injury site via chemokine signaling, enhanced production of inflammatory factors, upregulated expression of immunomodulatory proteins, or increased expression of receptors that facilitate phagocytosis, as well as proteins and molecules that recruit T cells (Kettenmann et al., 2011; Korzhevskii & Kirik, 2016). As antigen-presenting cells, microglia use class II major histocompatibility complex proteins- MHCII molecules - to present fragments of digested pathogens, so expression of these molecules is upregulated in the activated state (Jurga et al., 2020). Studies also show a relationship between the metabolic state of microglia and their polarized behaviour (Aldana, 2019; Orihuela et al., 2016). All these characteristics provide a valuable set of targets for regulating microglial function in neurodegenerative conditions, aging, and neuroinflammation.

LPS is a bacterial lipoprotein commonly used to induce the activation of microglia and macrophages in laboratory settings via Toll-like receptors (TLR). Although due to the blood-brain barrier, LPS activation is often considered non-physiological, LPS triggers a robust activation in the cell. Because it is well described in the literature, it is a valuable tool that brings about and enhances responses that may not otherwise be detectable in the cell's resting state (Murray et al., 2014).

LPS-activated microglia are generally associated with aggressive, cytotoxic behaviour and inflammation triggering via the release of pro-inflammatory cytokines and chemokines such as TNFα, IL-6, and IL-1β. LPS-activated microglia also express iNOS, MMP-12, MHCII, Fc receptors, and integrins, and NADPH oxidase, which generates superoxide and reactive oxygen species (ROS) (Jurga et al., 2020) This type of activation used to be called M1 in the older literature (Paolicelli et al., 2022). It is commonly induced by combined stimulation with LPS and IFN-γ in microglia and in macrophages (Korzhevskii and Kirik, 2016). These days, scientists agree that, rather than being exclusively committed to either extreme of the polarized state and cell fate, microglia exist in a flexible spectrum, readily adapting and modifying their activity, adjusting to environmental factors at all times (Murray et al., 2014; Paolicelli et al., 2022).

Alternatively activated microglia (which used to be called M2 in older literature (Paolicelli et al., 2022), express a phenotype that promotes recovery, repair, homeostasis, and performs phagocytic activities. These can be further subcategorized depending on the specific activity performed. M2a (induced by IL-4 and IL-13) describes the phenotype involved in regeneration and repair; M2b (inducible by TLR agonists), an immune-regulatory acting phenotype, and M2c (induced by IL-10, TGFβ, and glucocorticoids), which represents an acquired-deactivating phenotype (Jin et al., 2019).

In the laboratory setting, microglial phenotypes, as well as the state of activation, can be discriminated by qualitative expression of markers or quantitative measures of expressed proteins and their ratio (Jurga et al., 2020). General frequently used markers for microglial activation often used to identify microglia in general staining protocols include: ionized calcium-binding adapter molecule 1 (IBA-1); cluster of differentiation receptors CD68, CD11b, CD14, CD45, CD80, CD115; fractalkine receptor (CX3CR1); ferritin; F4/80; high affinity immunoglobulin epsilon receptor subunit gamma (FCER1G) and vimentin; as well as transmembrane protein 119 (TMEM119) and the purinergic receptor P2Y12. The latter two being more specific to yolk sac-derived microglia, while many of the abovementioned markers are also expressed by other cells

in the CNS (Korzhevskii and Kirik, 2016). As in their function, so in their transcriptomic profile, microglia express many of the same markers as macrophages. The main differences are highlighted in the expression of P2Y12 purinergic receptor, CX3CR1 chemokine receptor, and TREM2 receptor, in much higher levels, in microglia. Other useful markers which are commonly used in different studies include CD200R, inducible NO synthase, and CD115 (Korzhevskii & Kirik, 2016). Please refer to main the introduction (Chapter 1) for more detail.

Differences always need to be considered between mouse and human microglia and the specific cell lines and models studied. Some of the key differences worth noting as examples are TLR4 expression which is generally high in rodent but low in human; IFN-γ receptor, F4/80, Ym1, FIZZ1, arginase1 being present in murine but not human microglia; Siglec, CD33 showing species differences; and MHCII which reacts to TGFβ1 in rodent but not human microglia (Luan et al., 2022; Sharma et al., 2021). P2X7 is highly expressed in both human and murine microglia (He et al., 2017b), but minor differences in the receptor sensitivity may vary due to species differences (Hibell et al., 2000; Metzger et al., 2017; Sharma et al., 2021) .

Many of the markers described above are expressed by both activated and quiescent microglia; however, the levels of expression will vary. Thus, an easy way to differentiate between the two states is a semi-quantitative comparison of high vs low levels of the proteins in response to different stimuli. For example, activation with LPS and IFN-γ leads to upregulation of CD86 and P2X7 on the surface of the cells (Jurga et al., 2020; von Mücke-Heim et al., 2023). GLUT1 expression is also increased in LPS and IFN-γ-activated microglia (Wang et al., 2019). The shift towards this phenotype is often accompanied by metabolic reprogramming of the cells (Kong et al., 2019). In this pro-inflammatory state, the metabolism shifts away from oxidative phosphorylation and towards glycolysis (Soto-Heredero et al., 2020; L. Wang, Pavlou, et al., 2019a). In macrophages and microglia, this shift allows the cells to meet the demands of a hypoxic environment, as well as reach microbicidal activity fast by high production of NO (Gimeno-Bayón et al., 2014). In BV-2 microglial cells, Volobouéva et al., (2013) observed increased lactate production, lowered consumption of oxygen in mitochondria, and high extracellular acidification rate in response to LPS stimulation over 3h, as evidence of high glycolysis. NLRP3 inflammasome activation has also been associated with this phenotype and has gained much interest over the past years (Huang et al., 2023; Li et al., 2021; S. J. Yang et al., 2018).

In IL4-activated microglia, high levels of chemokines, such as CCL22, CCL17, and CCL24, are detected, and high upregulation of the mannose receptor, also called CD206, is often used as a marker for this state. (Gimeno-Bayón et al., 2014) showed a reduction in lactate levels produced,

as well as decreased glucose consumption, in line with a lessened demand for anabolic activity of microglia and engagement in phagocytic activity instead.

4.1.2 Phagocytosis

Phagocytosis is one of the key functions of microglia. From pruning of synapses and clearing up cells which undergo programmed death during development, to help with clearing up aggregated material in neurodegenerative conditions associated with aging, microglia carry out the vital maintenance in the CNS via their phagocytic ability (Kettenmann et al., 2011; Vilhardt, 2005). Malfunctioning activity of microglia in this aspect can also lead to exacerbation of demyelinating diseases or synaptic and neuronal loss (Aldana, 2019; Deczkowska et al., 2018; Flowers et al., 2017). It is therefore crucial to understand fully the relationship between activation, polarisation, and behaviour in microglia.

The first steps leading to phagocytosis require recruitment of microglia to the relevant site. This normally happens via 'find me' signals such as chemokine fractalkine (CX3CL1), which is highly expressed in the CNS cells and may be released by neurons, astrocytes, and other microglia. It signals to its corresponding receptor on microglia (CX3CR1) (Kettenmann et al., 2011). The CX3CL1/CX3CR1 axis is studied in many neurodegenerative conditions (Gutiérrez et al., 2025). The microglial P2Y12 receptor is also believed to be important for chemotaxis and chemosensing via ATP released from dying cells (Lin et al., 2021). Microglia express a range of phagocytic receptors on the cell surface, which next become activated (Beiter et al., 2024). A family of receptor tyrosine kinase TAM receptors is believed to bind externalized phosphatidyl serine (PS), exposed on the surface of myelin about to undergo engulfment, or on dead or dying cell bodies, which initiates phagocytosis (M. Wang et al., 2025). The adaptor protein DNAX activating protein 12 (DAP12) interacts with triggering receptor expressed by myeloid cells 2 (TREM2) is also thought to be important to initiate the phagocytic process (Konishi & Kiyama, 2018; M. Wang et al., 2025). Complement receptor 3 (CR3) has been linked to synaptic pruning activity by microglia during development and adolescence (Soteros & Sia, 2022).

Phagoptosis is another form of phagocytosis, where, prior to the engulfment, microglia initiate a target cell's death program (Brown & Neher, 2014). In this way, microglia may even engulf live neurons. This may happen especially during development, where heterogeneous populations of microglia respond with various degrees of sensitivity to signals such as IFN-1, to remodel the developing brain depending on the incoming environmental stimuli (Escoubas et al., 2024).

The balance in the developing brain is thought to be maintained by 'don't eat me signals', which are the negative regulators of phagocytosis (Zengeler & Lukens, 2021). SIRPα receptor on microglia is one of those examples, which, when bound to CD47 on neuronal cells, downregulates phagocytosis (H. Zhang et al., 2015). However, local differences are observed, for example, in the retina, where SIRPα/CD47 axis may initiate pruning activity (D. Jiang et al., 2022).

Mutations in the above-mentioned receptors lead to developmental defects and negatively impact behaviour and social function, demonstrating the importance of the crucial balance in microglial regulation during development and neurological diseases (H. Zhang et al., 2015).

P2X7 has been implicated in phagocytosis, (Campagno & Mitchell, 2021). Transfection with P2X7 is sufficient to allow HEK293 cells to engulf particles (Gu et al., 2010) and using siRNA, to silence P2X7 surface expression and synthesis in human monocytic cells resulted in impairment of phagocytosis (Gu et al., 2011). Intracellular P2X7 receptor has been shown to contribute to phagosome-lysosome fusion events (Fairbairn et al., 2001; Kusner & Barton, 2001).

Gu et al., (2011) showed that extracellular residues (306–320) of the P2X7 receptor can bind to apoptotic cells, bacteria, and beads, while the intracellular regions are connected to non-muscle myosin heavy chain IIA (NMMHC IIA), linking the P2X7 receptor to the cytoskeleton (Gu et al., 2009, 2010). The authors propose that this provides a pathway for engulfment of material into the cell. Interestingly, the authors showed that ATP stimulation reduced phagocytosis via dissociation of NMMHC IIA from P2X7 and thus demonstrated the dual role of P2X7 with and without its agonist.

In microglial cells, unstimulated, P2X7 can act as a scavenger receptor (Ou et al., 2018). The writers propose that this function is specific to microglia and the CNS environment, based on their studies of the effect of serum. (Gu et al., 2012; Gu & Wiley, 2018) found that the protein fraction of serum to have an inhibitory effect on P2X7-mediated phagocytosis. Specifically, the glycoproteins containing copper and/or zinc, ceruloplasmin, amyloid precursor protein and serum amyloid P-component were found to exert this effect. The authors found that in human CSF, which is naturally low in glycoproteins, human monocytic and macrophage cells were able to effectively phagocytose beads or apoptotic cells.

4.1.3 Cytokine release

Cytokine release, especially TNF-α, IL-6, and IL-1β, has been extensively studied in neurodegenerative diseases (W. Y. Wang et al., 2015). Balancing of pro-inflammatory cytokines

has become a therapeutic target in diseases such as Alzheimer's Disease (AD) (Rani et al., 2023). Low levels of IL-10, IL-4, IL-13, and TGF-β are traditionally associated with promoting repair and tissue remodeling, while IL-1β, TNF-α, IL-6, IL-12, IL-23, and ROS are generally linked with loss of neurons and defense against pathogens or invading tumor cells (Norris & Kipnis, 2019; Ochocka & Kaminska, 2021; Smith et al., 2012). A recent study by Adrian et al., (2023) showed that LPS-activated microglia undergo microtubule remodeling pathways to allow for effective trafficking and release of cytokines. Shieh et al., (2014) demonstrated ATP-induced and P2X7-dependent release of cytokines- TNFα, IL-6, and CCL2 - in primary mouse microglia. They showed that this happened without inflammasome activation. During neuroinflammation, the release of IL-1β and TNF-α is high. These enhance other pro-inflammatory cascades and are believed to drive neurodegenerative diseases such as AD and PD (Deczkowska et al., 2018; Smith et al., 2012). High levels of IL-1β were linked to a disrupted blood-brain barrier (Y. Wang et al., 2014).

NLRP3 inflammasome is extensively studied in neuroinflammatory and neurodegenerative diseases such as AD, where amyloid beta deposits are thought to activate microglia and drive neuroinflammation, and in Parkinson's disease, where α-synuclein can trigger NLRP3 activation and high cytokine release (W. Y. Wang et al., 2015). In stroke studies, inflammasome inhibition showed reduction in the severity of functional deficits (S. J. Yang et al., 2018). In animal models, and post mortem studies, NLRP3 activation has been implicated in pathogenesis of major depressive disorder (MDD) and anxiety (Kouba et al., 2023).

DAMs, including ATP and PAMs such as LPS and TLR4 priming, activate the transcription factor, which induces NLRP3 assembly and Pro-IL-1β synthesis (Mehta et al., 2001; Perregaux & Gabels, 1994). K+ depletion was shown by Munoz-Planillo et al., (2013) to be essential for inflammasome activation.

4.1.4 Modulation of polarisation and microglial activity

Many endogenous molecules, in addition to cytokines, PAMs, and DAMs, may further modulate microglial behaviour and influence functions such as activation and cytokine release. In neurodegenerative disorders, protein aggregates such as amyloid beta and alpha-synuclein have been shown to exacerbate pro-inflammatory cytokine release (Nopparat et al., 2023; Smith et al., 2012) . Neurosteroids are an interesting example of endogenous therapeutic candidates for the reprogramming of microglial behaviour, as microglia themselves are capable of synthesizing neurosteroids (Yilmaz et al., 2019). Moreover, some endogenous hormones and synthetic steroids, as well as cholesterol and its metabolites, have been shown to interact with P2X

receptors (Sivcev et al., 2023). 17β-estradiol has been shown to mediate anti-inflammatory effects via ERα and ERβ receptors on microglia and suppress the release of TNFα, IL-6, and expression of iNOS. Progesterone in microglia has been shown to down-regulate activation of the inflammasome and reduce expression of pro-inflammatory genes, including TNFα, iNOS, IL-6, MHCII, and COX2 (Yilmaz et al., 2019). Allopregnanolone and DHEA have been described as reducing neuroinflammation in microglia culture models (Jolivel et al., 2021; Sivcev et al., 2023; Yilmaz et al., 2019).

In summary, P2X7 in its stimulated and inactive state, has been linked to activation and function of microglial cells, such as cytokine release (He et al., 2017; von Mücke-Heim et al., 2023), as well as phagocytic activity (Gu & Wiley, 2018). Whether P2X7 performs these functions in BV-2 microglia is less clear. This chapter sheds light on whether there are consequences to microglial behaviour in response to various stimuli when P2X7 is not expressed.

4.2 Results

4.2.1 Classical microglial polarisation and phenotypic differentiation in BV-2 and BV-2^{P2X7-} cells

Observed morphology

Classical morphological changes were observed in BV-2 cell culture at 48h with exposure to classic polarizing factors. This was captured by imaging using a light microscope throughout this thesis and examples can be seen throughout the text in Figures 4.5, 4.6 and 4.7. BV-2 cells have a tendency to migrate in the wells over the 48h period. Therefore, in all imaging experiments a x 10 or x20 objective was used to capture a good representation of the population of all cells in each well exposed to different conditions.

In the resting state, cells are evenly distributed throughout the well and slightly rounded due to the serum reduction to 0.5% serum, which is sufficient to activate the cells slightly (Yao & Fu, 2020). Cells in the resting state in complete serum are depicted in Figure 3.1. With LPS (100 ng/mL) and IFN-γ (50 ng/mL), a proportion of cells become enlarged and more rounded but still well adherent to the bottom of the plate. Upon stimulation with IL-4, cells assume a small, rounded shape and start to cluster together and frequently detach from the surface of the plate. In the +IL-4 wells, many of the cells have detached from the surface of the well or migrated to the edges of the well, where they have formed clusters. The total number of cells per well looked comparable

amongst the treatments throughout this work. Example images can be seen in Figures 4.5, 4.6 and 4.7.

Changes to the morphology of the cells can be a good indicator of their polarisation and activation. However, a significantly more reliable measure is the quantification of the upregulation or downregulation of key surface markers, which were well described in the literature for each polarised state.

Polarisation and activation

To further verify polarisation in the BV-2 and BV-2^{P2X7-} model, flow cytometry was used to measure the expression of surface protein markers by staining (Figure 4.1). Cells were exposed to classical activating stimuli for 48h, and antibodies for different markers were used to stain the surface proteins expressed. Cells activated by LPS and IFN-γ (LPS+IFN-γ) and cells activated by IL-4 (IL-4) were compared to 'resting cells', which have not been exposed to any cytokines. BV-2 and BV-2^{P2X7-}cell lines were also compared to each other. The data corroborated with the literature showing upregulation of CD206 with the IL-4 phenotype; and the LPS+ IFN-γ phenotype showed upregulation of CD86, as well as P2X7 in the BV-2 cells expressing the receptor. Interestingly, P2Y12 was also upregulated, and so was CD11b, with LPS + IFN-γ phenotype, compared to resting or IL-4 activation. This pattern was the same in both cell lines, suggesting that P2X7 expression does not affect the cells' ability to polarise in response to classical stimuli, and it does not affect expression of the tested protein surface markers. The upregulation/downregulation of surface markers was also already detectable at 24h (data not shown), when morphological changes were still not as apparent and uniform as they were at 48h.

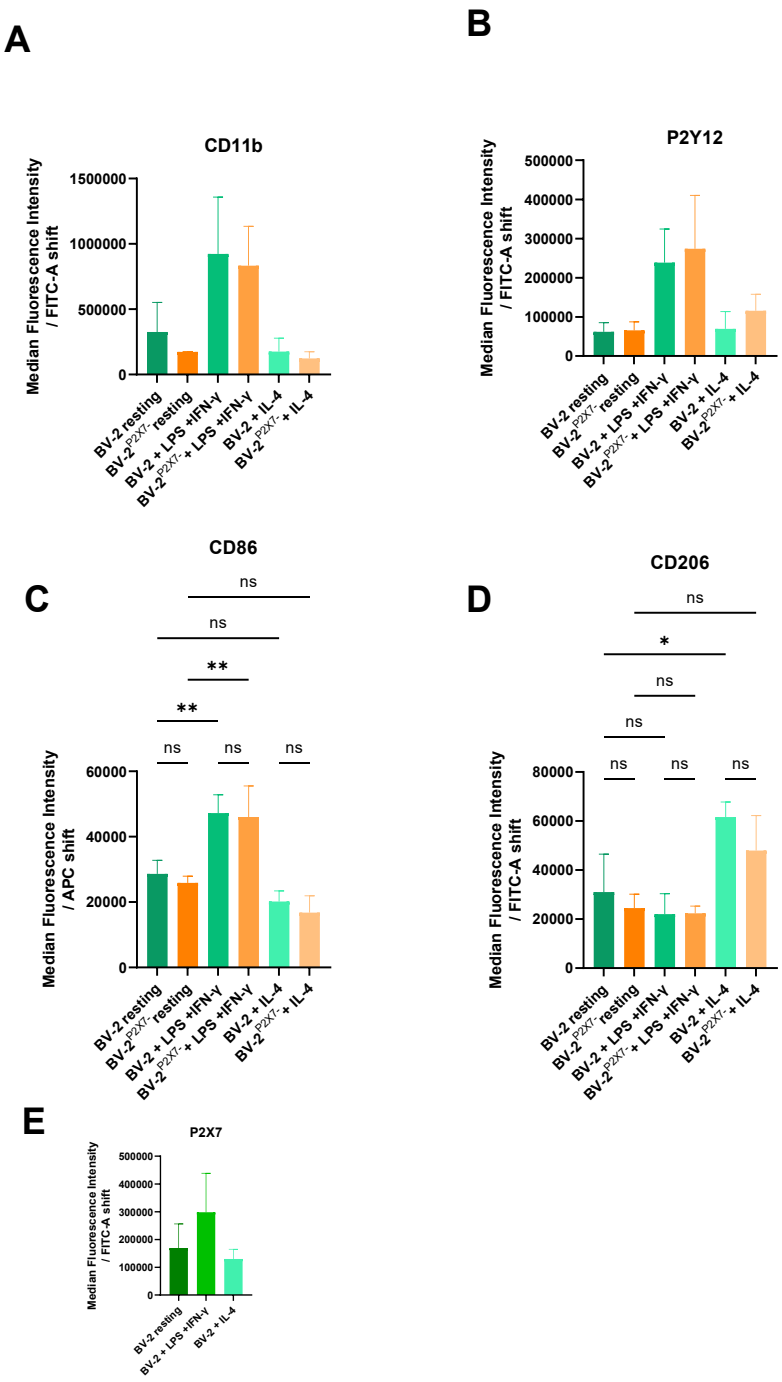

Figure 4.1 Expression of surface protein markers of activation by flow cytometry in BV-2 vs BV2^{P2X7-} cells following 48h incubation with classical stimulating factors. *Cells were cultured in 0.5% serum media and stimulated with 100 ng/mL LPS+ 50 ng/mL IFNγ; 20 ng/mL IL-4, or nothing (resting). Stained with anti-CD11b, anti-CD86, anti-CD206, anti-P2Y12, and anti-P2X7 as described in the method section. Median Fluorescence Intensity was measured by flow cytometry, and a shift away from unstained control was calculated for each sample. Results show a collated average of 2-3 independent experiments, as indicated in the brackets.* ***A*** *CD11b (n=2);* ***B*** *P2Y12 (n=2);* ***C*** *CD86 (n=3);* ***D*** *CD206 (n=3);* ***E*** *P2X7 (n=2). Analyzed with One-way ANOVA followed by Tukey's multiple comparisons test (Statistical significance denoted by * p<0.05, ** p<0.01, *** p<0.001, ns not significant).*

4.2.2 Effect of polarising agents on cell viability, cell division, and function

Knowing that the BV2 and BV2^{P2X7-} cells polarise well and in the same manner, aside from P2X7 expression itself, by displaying morphological and surface expression characteristics at 48h, the cells were subjected to an Alamar Blue assay to evaluate metabolic health and viability (Figure 4.2). The assay showed a previously observed pattern where all the cells expressing P2X7 showed a slightly higher relative fluorescence value than BV2^{P2X7-} cells. The resting cells and cells stimulated with IL-4 showed almost identical RFU values to each other. The LPS and IFN-γ-stimulated cells showed lower RFU values and a greater difference between the P2X7-expressing and P2X7-lacking cells in this group. A visual check confirmed that the wells under this condition contained slightly fewer cells at the end of the 48h period. This concurs with the literature, which suggests that LPS slows down proliferation of BV-2 cells (Yao & Fu, 2020). This was further confirmed in CellTrace Yellow dye retention assay (Figure 4.3).

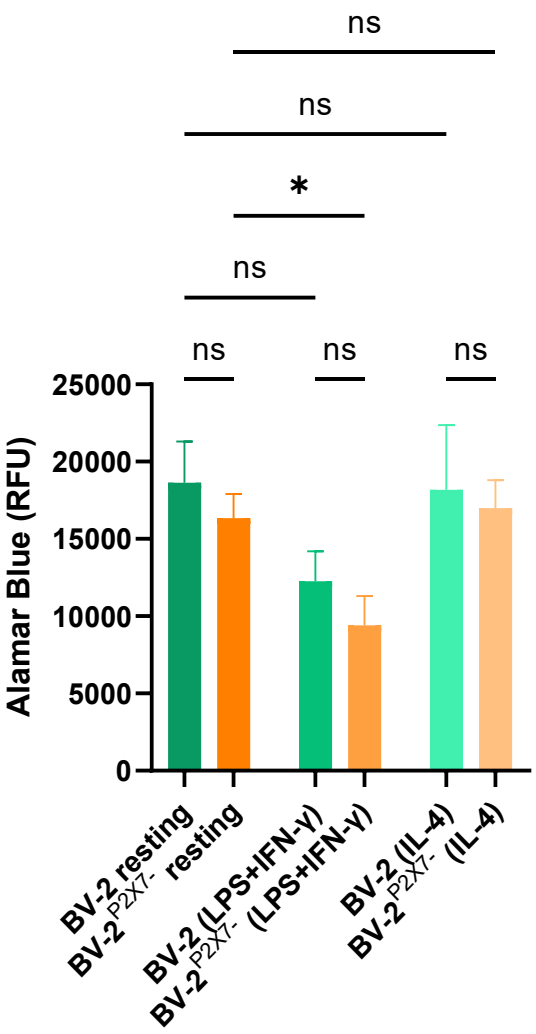

Figure 4.2 Metabolic activity of polarised cells in Alamar blue assay. *BV-2 and BV-2^{P2X7-} cells were plated in 0.5% serum-containing media at a starting density of 9000 cells/well in a 96-well plate. Classic activating factors were added to the media to polarise cells towards classical phenotypes. Cells were either unstimulated (resting) control; activated with LPS (100ng/mL) and IFN-γ (50 ng/mL); or activated with IL-4 (20 ng/mL). Cells were incubated for 48h and Alamar blue was performed as described in the method section. The data are an average of 3 independent experiments with 4 technical replicates for each condition. Analyzed with One-way ANOVA and Šídák's multiple comparisons test. (Statistical significance denoted by * p<0.05, ** p<0.01, *** p<0.001, ns not significant).*

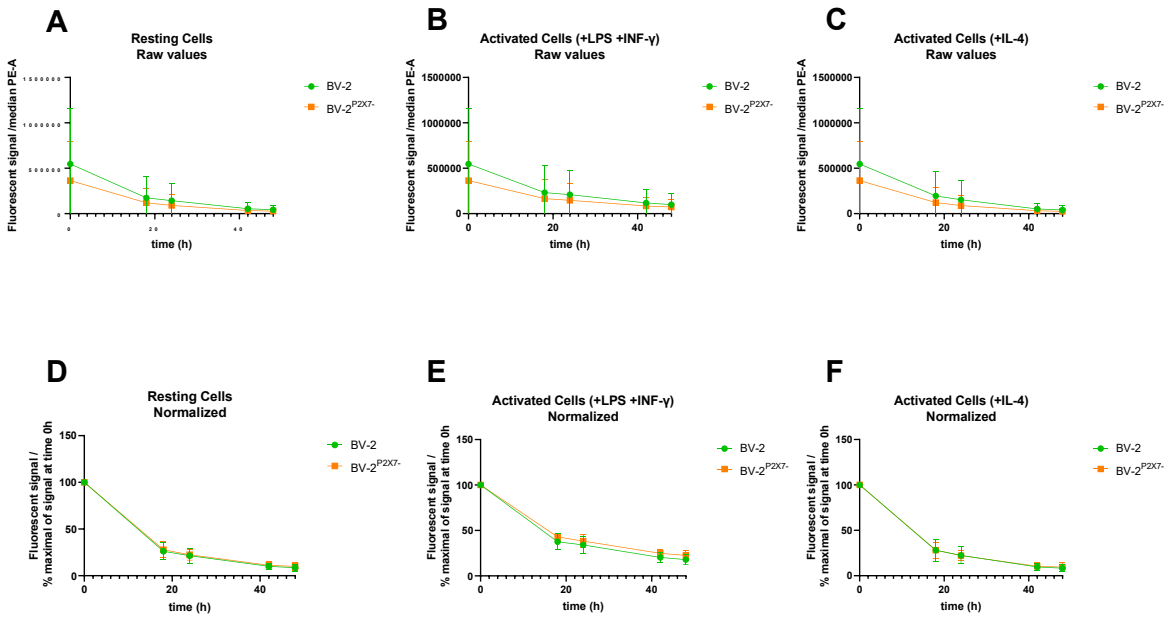

Figure 4.3 Effect of polarization on cell division over 48h of growth in reduced serum with classical activating factors. *BV-2 and BV-2^{P2X7-} cells were stained with CellTrace Yellow dye as described in the method section, washed, and plated in 24-well plates in 0.5% serum-containing media at the starting density 35640 and 53460 cells/well (equivalent to 6000 and 9000 cells/well in a 96-well plate). Activating factors were added to the media **A**, **D** nothing (unstimulated control); **B**, **E** +LPS (100 ng/mL) + IFN-γ (50 ng/mL); and **C**, **F** +IL-4 (20 ng/mL). The cells were then trypsinized out of the plate at different timepoints over the next 48h and fluorescence was measured by flow cytometry. Each point is an average of 3 independent experiments. **A**, **B**, **C** show dye retention depicted by fluorescence signal (raw data), and **D**, **E**, **F** show normalized data (percentage of maximum signal at time 0h) for each sample.*

CellTrace Yellow dilution experiments on polarized cells (Figure 4.3) show that dye retention, during the 48h exposure to polarising agents, is the same in the cells expressing or lacking P2X7. However, the initial dye uptake is higher in BV-2 cells expressing P2X7, and this is true regardless of the ongoing polarisation or its lack in the 'resting' cells. This higher initial dye uptake was first observed in Chapter 3. The CTY experiments above were run in pairs with the Alamar Blue repeats on polarized cells. This further supports the data in Alamar Blue Figure 4.3, showing that LPS +IFN-γ treatment slows down cell division, as the slopes of the curves in Figure 4.3 E are less steep. There, the dye retention in LPS + IFN-γ stimulated cells at 18h is approximately 50%, while in control and IL-4 stimulated cells (Figure 4.3 D and F, respectively) at the same time point, the dye retention is approximately 30%. In both figures, Figure 4.2 and Figure 4.3, the difference between BV-2^{P2X7-} and BV-2 cells stimulated with LPS +IFN-γ is slightly greater than between these cells in other states.

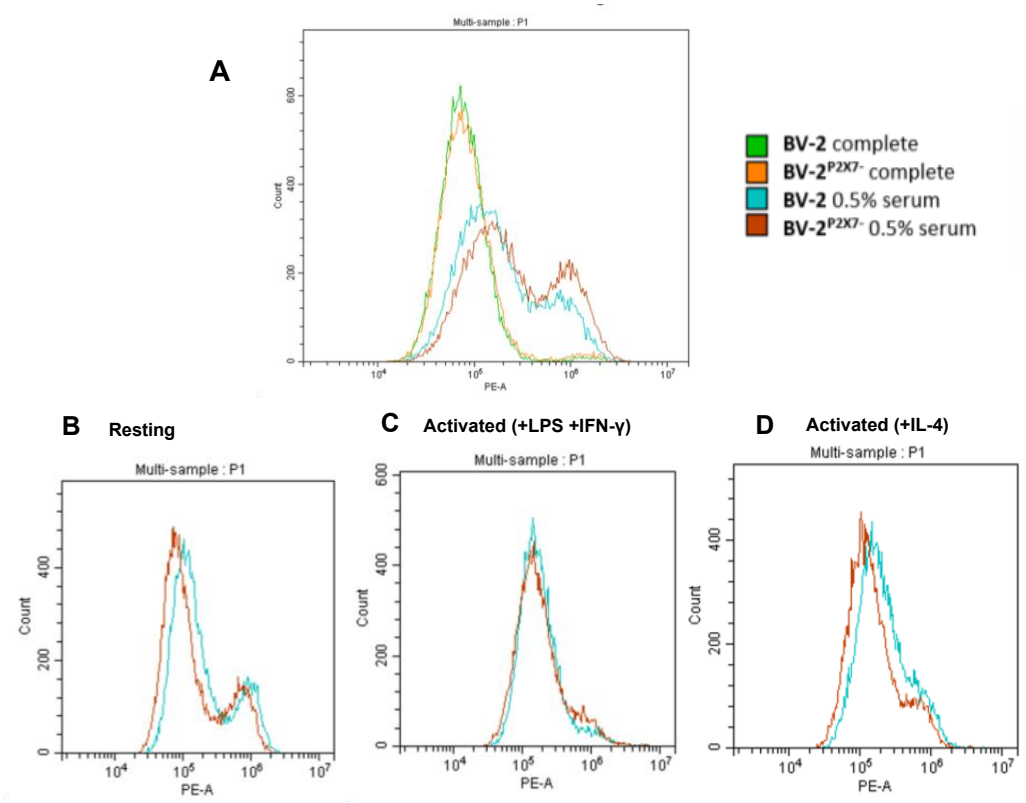

Figure 4.4 Effect of P2X7 expression on mitochondrial Superoxide levels. *The cells were stained with mitochondrial superoxide (MitoSOX) dye according to the manufacturer's protocol. The fluorescent signal was recorded by flow cytometry as described in the method section. The figures show histograms representative of a single experiment. Cells were pre-grown for 48h in 24-well plates at a starting density equivalent to 9000 cells/well in a 96-well plate, in either complete or 0.5% serum media. Cells were trypsinized out, and three wells were pulled together to achieve a larger pellet. Cells were stained with 20nM MitoSOX dye. Cells were pre-grown for 48h in 24-well plates at a starting density 53460 cells/well, in either complete or 0.5% serum media (**A**). Cells were subjected to classical activating factors or 'nothing' (control) in 0.5% serum media during the 48h incubation (**B,C,D**). Cells in media only (control) in resting state. **C** Cells exposed to 100 ng/mL LPS and 50 ng/mL IFN-γ (activated phenotype). **D** Cells exposed to 20 ng/mL IL-4 (activated phenotype). Cells were trypsinised out and three wells were pooled together to achieve a larger pellet.*

Activation induces an inflammatory profile in microglia and affects metabolic health, respiration, and mitochondrial ROS production (Norris & Kipnis, 2019; Timmerman et al., 2018). The expression of mitochondrial superoxide, a ROS species, was investigated in BV-2 and BV-2^{P2X7-} cells in different activated states (Figure 4.4). Cells were stained with MitoSOX dye and recorded using flow cytometry to determine the levels of mitochondrial superoxide in the microglia. Serum reduction resulted in a signal shift to the right, indicating an increase in superoxide levels. Polarisation did not produce a change in signal. The cells were affected in the same way, regardless of P2X7 expression.

Many molecules have the capacity to affect microglial function and morphology. In addition to the classical polarising factors in the combinations used in literature, various molecules such as pro-inflammatory cytokine IFN-γ on its own, bacterial LPS alone, and the viral mimetic Poly(I:C), as well as some endogenous hormones and neurosteroid compounds, were examined for a polarising effect on BV-2 cells by looking for morphological changes in the cells (Figure 4.5, Figure 4.6 and Figure 4.7, respectively). Cells were plated at a density of 9000 cells/well in 0.5% serum media and exposed to different potential activators for 48h or 72h. Morphological differences were compared to an unstimulated control. Microglia are highly heterogeneous and often show differentiated subpopulations within a large population of cells. X 10 and x 20 magnification were used to observe the extent of the response in the widest population image possible. LPS produced clear changes to the morphology of all cells, such as an enlarged cell body and a rounded shape (Figure 4.5 D,H). Several of the cells appeared very large. (This is further explored in Chapter 5 as Giant Multinucleated Cells). IFN-γ (Figure 4.5 C,G) and Poly (I:C) (Figure 4.5 B,F) also resulted in the occurrence of more numerous large ameboid cells, although some cells remained small and spindle-shaped.

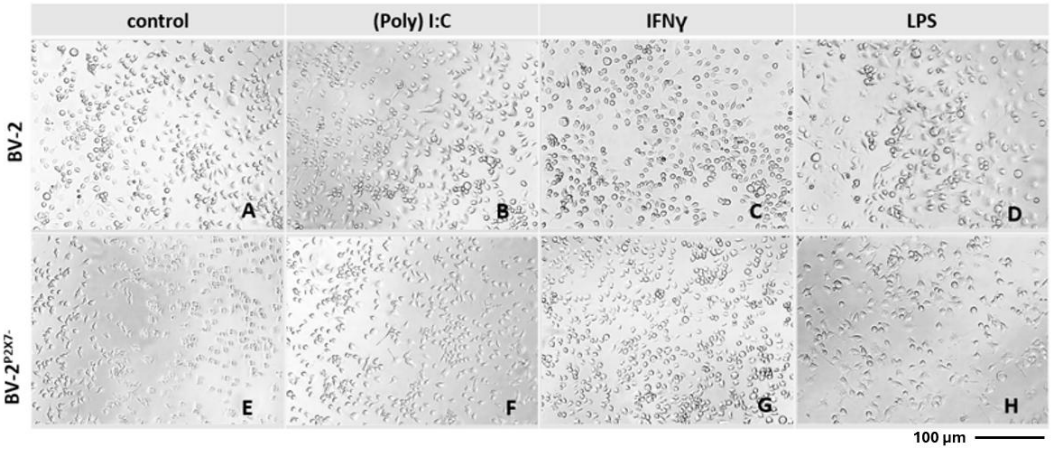

Figure 4.5 Effect of pro-inflammatory molecules on morphological polarisation of BV-2 and BV-2^{P2X7-} cells at 48h. *Cells were plated at density 9000 cells/well in 0.5% serum with various factors. After 48h of incubation representative images of each condition were taken using x 20 magnification on Nikon Eclipse Ti microscope. BV-2 cells are shown in images labelled **A**, **B**, **C**, **D**; and BV-2^{P2X7-}cells are represented by **E**, **F**, **G**, **H**, **A**, **E** represent control; **B**,**F** show Poly(I:C) 100 ng/mL; **C**,**G** show IFN-γ 50 ng/mL; and **D**,**H** show LPS 100 ng/mL. The images are a representative of each condition of a routinely done experiment.*

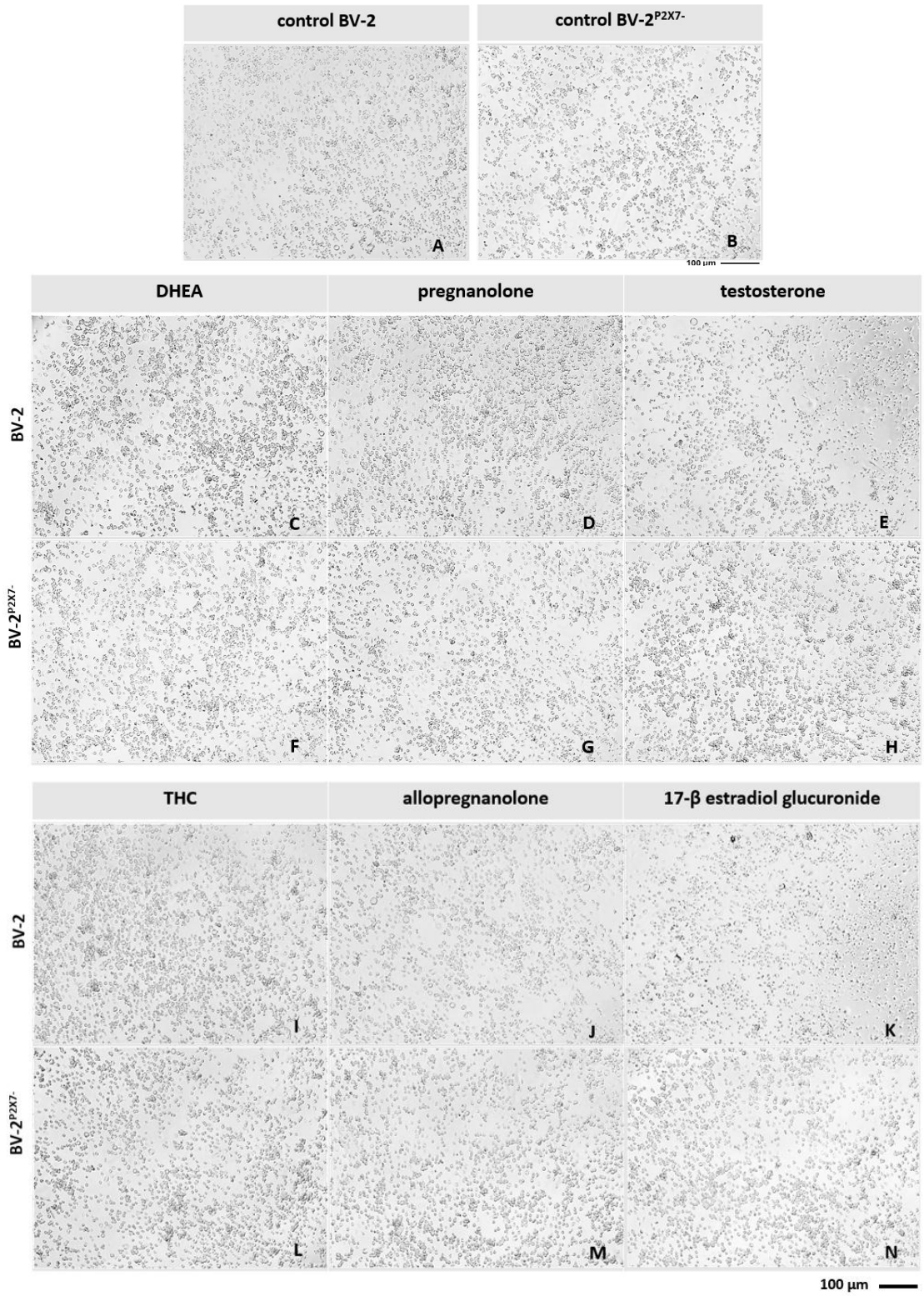

Figure 4.6 Effect of neurosteroids on morphological polarization of BV-2 and BV-2^{P2X7-} cells at 48h. *Cells were plated at density 9000 cells/well in 0.5% serum with various neurosteroids at concentration 10 µM. After 48h of incubation representative brightfield images of each condition were taken using x 10 magnification on Nikon Eclipse Ti microscope. BV-2 cells are shown in all images labelled **A**, **C**, **D**, **E**, **I**, **J**, **K** and BV-2^{P2X7-}cells are represented by **B**, **F**, **G**, **H**, **L**, **M**, **N**. (**A**,**B**) control, (**C**,**F**) DHEA, (**D**,**G**) pregnanolone, (**E**,**H**) testosterone, (**I**,**L**) THC, (**J**,**M**) allopregnanolone, (**K**,**N**) 17-β glucuronide. The images are a representative of each condition. Experiment was independently repeated twice.*

Neurosteroids did not influence the population as strongly and, in most cases, were unremarkable at the 48h time point (Figure 4.6 and Figure 4.7). Neurosteroids were further checked in a corresponding Alamar Blue cell viability experiment to quantify changes in cell density (Figure 4.8). Some conditions were also further investigated for morphological changes following 72h exposure to the factors. This is shown below in Figure 4.6.

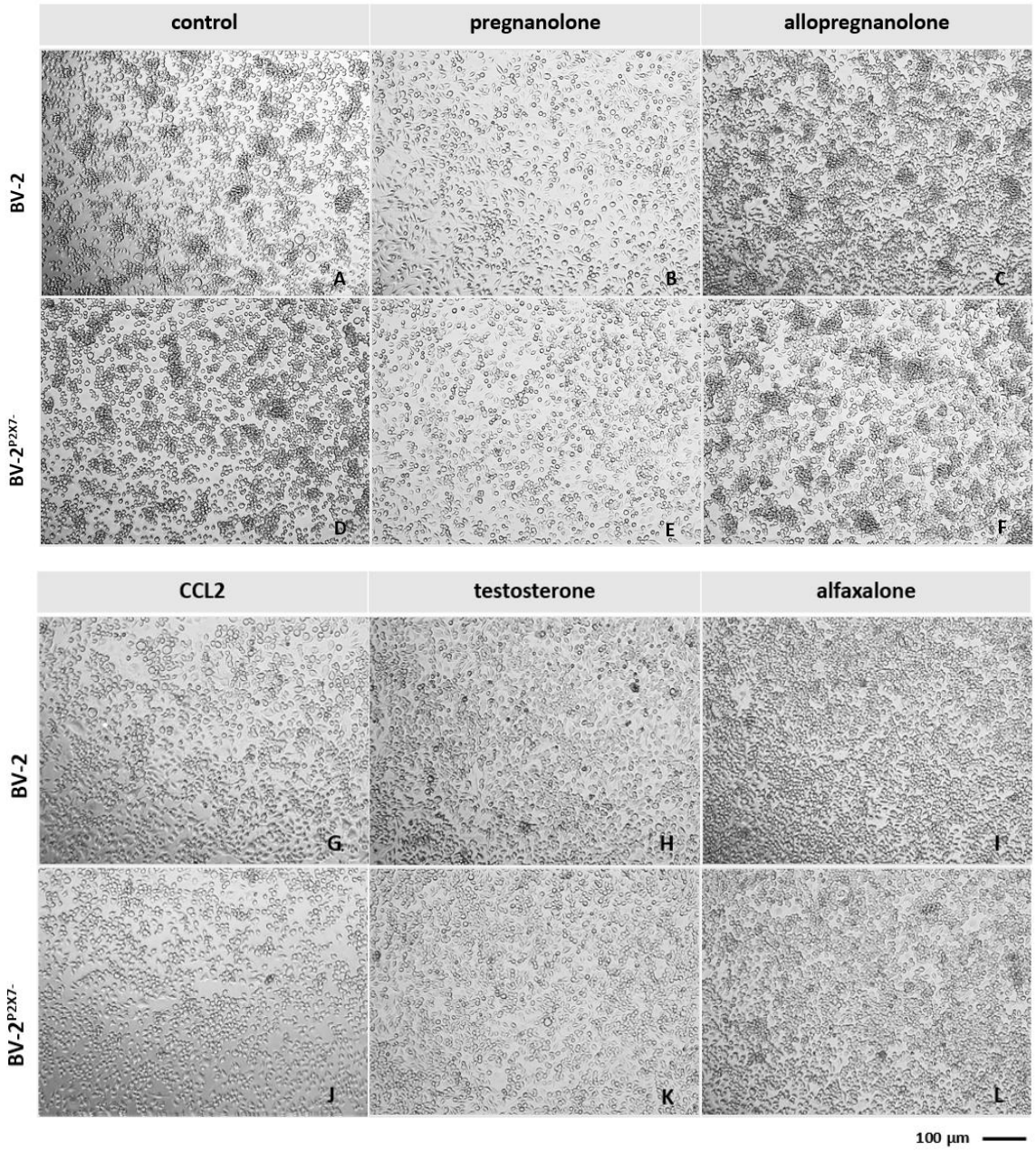

Figure 4.7 Effect of neurosteroids and cytokines on morphological polarization of BV-2 and BV-2^{P2X7-} cells at 72h. *Cells were plated at density 9000 cells/well in 0.5% serum with various neurosteroids at concentration 10 µM. After 48h of incubation representative brightfield images of each condition were taken using x 10 magnification of a Nikon Eclipse Ti microscope. BV-2 cells are shown in images labelled **A**,**B**,**C**,**G**,**H**,**I** and BV-2^{P2X7-}cells are represented by **D**,**E**,**F**,**J**,**K**,**L**. (**A**,**D**) control, (**B**,**E**) pregnanolone, (**C**,**F**) allopregnanolone, (**G**,**J**) CCL2, (**H**,**K**) testosterone, (**I**,**L**) Alfaxalone. The images are a representative of each condition, experiment was carried out once.*

The screened neurosteroids did not affect morphology or cell viability as seen in Figure 4.8, and this was not pursued with further replicates. The readings for pregnanolone, pregnenolone, and DHEA were slightly higher than control, while THC lowered the reading. It is possible that minor differences in the Alamar Blue assay were due to the metabolic activity of the cells, which could be interesting to pursue with more replicates in the future, as this experiment was only a single one. In all cases, the usual pattern was observed in Alamar Blue reading, where BV-2 cells showed slightly higher values than BV-2^{P2X7-} cells. Because no new differences were found between BV-2 and BV-2^{P2X7-} cells, the neurosteroids screening was not pursued further in terms of the ability of neurosteroids to polarize the cells or affect cell number.

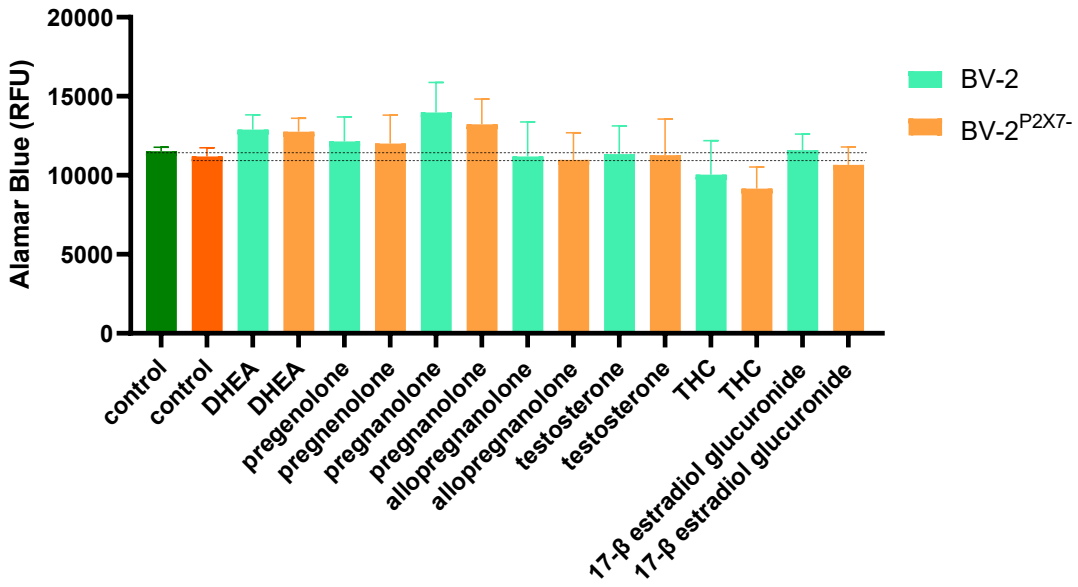

Figure 4.8 Alamar blue assay on cells exposed to neurosteroids for 48h. *BV-2 and BV-2^{P2X7-} cells were plated in 0.5% serum-containing media at a starting density 9000 cells/well in a 96-well plate. Neurosteroids were added to the media to the final concentration of 10 µM. Cells were incubated for 48h and Alamar Blue was performed as normal. Reading was taken after 2h of processing time. The data are the repeats of a single biological experiment with three technical replicates for each condition.*

The effect of Cytokines and Pro-inflammatory molecules on BV-2 and BV-2^{P2X7-} cells in the Alamar blue assay (Figure 4.9) was assessed in the same way as the neurosteroid compounds. The effect of polarizing cytokine IL-13 was the same as that of IL-4 and increased the RFU values compared to the control. LPS lowered all values, likely due to lower cell numbers per well, which was apparent in Figure 4.5, although the literature provides mixed evidence on LPS reducing or increasing proliferation rate in cells in different experimental models (Pan et al., 2023; Xie et al.,

2020; M. Zhang et al., 2023). When LPS was administered together with IFN-γ or TNF-α, the RFU remained lowered. IFN-γ on its own did not show a difference from control. TNFα showed a lower value compared to control in the Alamar blue assay for BV-2^{P2X7-} cells only, and a further reduction in RFU when co-administered with LPS. The difference between BV-2 and BV-2^{P2X7-} remained the same in the Alamar blue screen, regardless of cytokine addition. As cytokines were not contributing to this discrepancy, their effect was likely independent of P2X7 expression. The cytokines' effect on BV-2 polarization with respect to P2X7 was not pursued with further replicates.

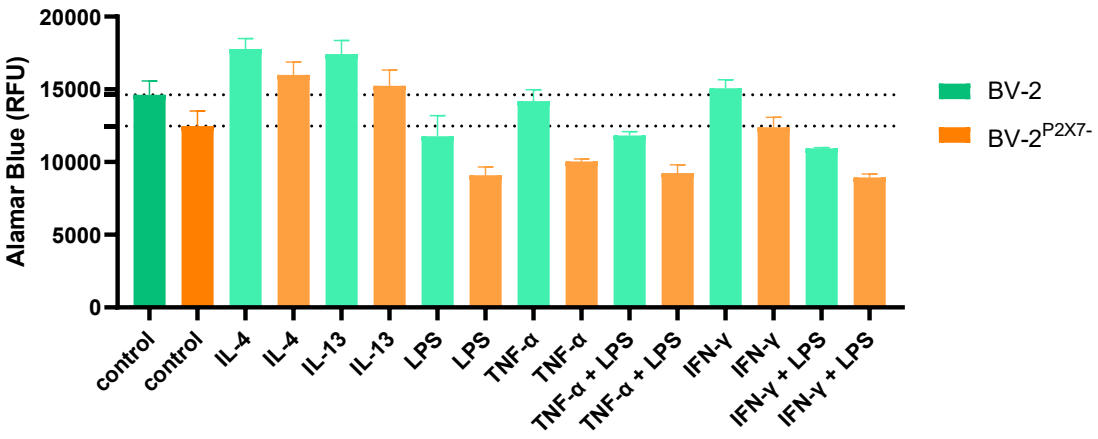

Figure 4.9 Alamar blue assay on cells exposed to cytokines and pro-inflammatory molecules for 48h. *BV-2 and BV-2^{P2X7-} cells were plated in 0.5% serum-containing media at a starting density of 9000 cells/well in a 96-well plate. The factors were added to the media to the final concentration LPS 100nM, IL-4 20 ng/mL, IL-13 20 ng/mL, TNF-α 50 ng/mL, IFN-γ 50 ng/mL. Cells were incubated for 48h, and Alamar Blue was performed as normal. Reading was taken after 2h of processing time. The data are the repeats of a single biological experiment with three technical replicates for each condition.*

4.2.3 Effect of neurosteroids on P2X7 signalling

Neurosteroids and steroid compounds are known to affect purinergic receptors (Sivcev et al., 2023). Selected neurosteroids and steroid compounds which were previously reported to affect microglia (Jolivel et al., 2021; Sivcev et al., 2023; Yilmaz et al., 2019) were tested on P2X7 ion channel activity. For this purpose, a series of steroid compounds was screened on HEK 293 cells which had been transfected with the human P2X7 receptor. P2X7 activity to its agonist ATP was measured by looking at channel pore opening and calcium signalling, in the presence of steroid

compounds, using two fluorometric assays (YOPRO-1 dye uptake and Fura-2 AM fluorescence) described below in more detail.

All steroid compounds were initially screened in a dye uptake assay, where a large YO-PRO-1 dye is used to indicate the opening of the P2X7 pore. YOPRO-1 dye only fluoresces when inside the cell and can only enter through the P2X7 macropore when P2X7 is activated. The results are shown in Figure 4.10. Due to the nature of the assay and the time taken by the plate reader to measure the responses across the plate (which is approximately 1h), the cells were allowed to pre-incubate with the compounds for 15 minutes to 1 hour. In each repeat, replicates were spread systematically across the plate to ensure a representative distribution of pre-incubation times in the collated data.

As seen in Figure 4.10, Pregnenolone, pregnanolone, and testosterone had the strongest inhibitory effect on the responses obtained, compared to the control solvent (DMSO). All three compounds lowered the maximal response and shifted the curve slightly to the right, meaning a higher concentration of ATP was now needed to evoke the same response in the presence of the hormone. Progesterone and the synthetic steroid Alfaxalone also shifted the curve to the right, but only decreased the maximal response subtly. Allopregnanolone, DHEA, THC, and 17-β-estradiol glucuronide did not have any effect on the dose-response curves, which indicates no impact on P2X7. The steroid compounds found to have an inhibitory effect on P2X7, namely testosterone, pregnenolone, and pregnanolone, were next evaluated in the Fura-2 AM assay, which measures calcium signalling (Figure 4.11).

Fura-2 AM is a dye that becomes fluorescent in the presence of Calcium ions and, therefore, is commonly used to measure calcium signalling in cells. The neurosteroids, which were found to have an inhibitory effect in the YO-PRO-1 screen, were assessed with the Fura-2 AM assay. Pregnanolone was the most inhibitory compound and decreased the maximal response and shifted the curve to the right, increasing the EC50 value (Figure 4.11 B). Pregnenolone and Testosterone had similar effects, but the decrease of maximal response and rightward shift was much more subtle.

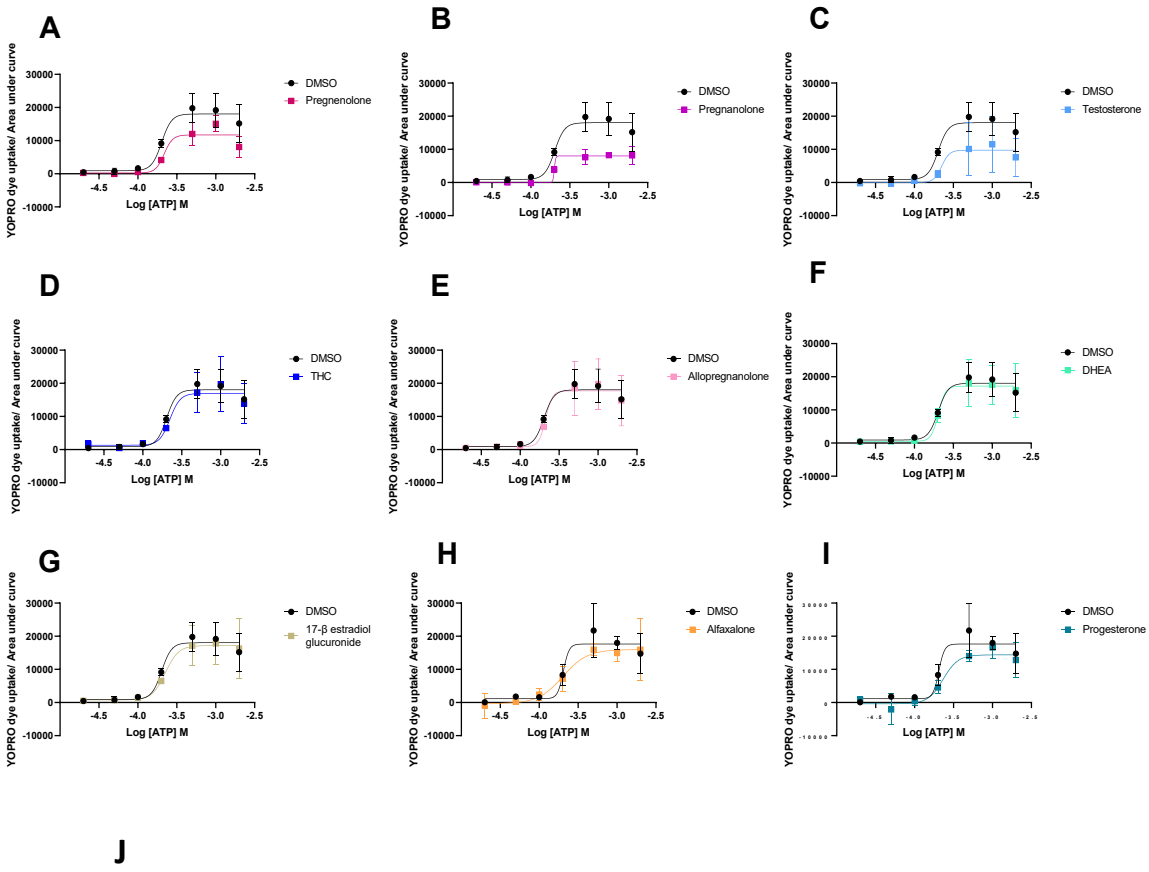

compound	EC50 (μM)	Confidence Interval (CI)
DMSO	202	148 to 265
pregnenolone	218	140 to ?
pregnanolone	200	?
testosterone	223	?
THC	*223*	129 to ?
allopregnanolone	212	121 to ?
DHEA	203	123 to 354
17-β estradiol glucuronide	226	128 to 423
alfaxalone	201	75 to 432
progesterone	232	170 to 361

Figure 4.10 Effect of neurosteroids on P2X7 pore activity in a YO-PRO-1 dye uptake assay as dose-response curves to P2X7 agonist ATP in HEK293^{hP2X7} cells. *Cells were plated on poly-D lysine-coated plates at a density 2x 10^5 cells/well and incubated overnight. Standard YO-PRO-1 protocol was followed on a confluent plate of HEK293^{hP2X7} cells. Responses were measured after pre-incubation with the compounds for 15 minutes to 1 hour. One to three independent experiments were performed (as indicated) with three technical replicates for each point. The locations of the conditions on the plates were varied for a representative result. An average of 1-3 experiments is shown. Neurosteroids were used at a final concentration of 10 μM vs DMSO solvent control. ATP range was 2 mM, 1 mM, 500 μM, 200 μM, 100 μM, 50 μM, 20 μM.* ***A*** *pregnenolone (n=3),* ***B*** *pregnanolone (n=3),* ***C*** *testosterone (n=3),* ***D*** *THC (n=2),* ***E*** *allopregnanolone (n=2),* ***F*** *Dehydroepiandrosterone (DHEA) (n=2),* ***G*** *17-β estradiol glucuronide (n=2),* ***H*** *Alfaxalone (n=1),* ***I*** *progesterone (n=1). EC50 was calculated from the plots and is shown in table* ***J****.*

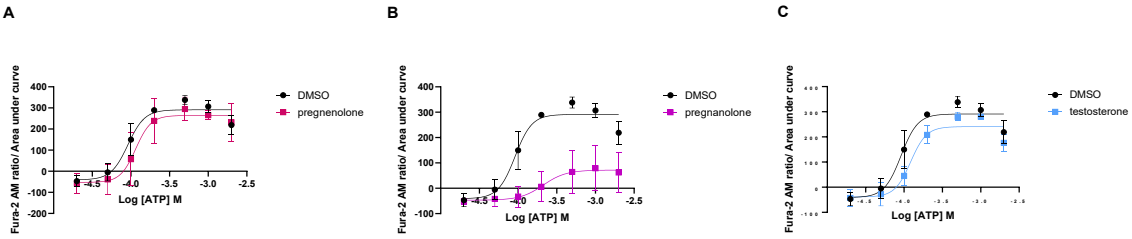

D

compound	EC50 (µM)	Confidence Interval (CI)
DMSO	91	66 to 115
pregnenolone	115	73 to ?
pregnanolone	211	?
testosterone	122	95 to 162

Figure 4.11 Effect of neurosteroids on P2X7 signalling as dose-response curves to P2X7 agonist ATP in Fura-2 AM assay in HEK293^{hP2X7} cells. *Cells were plated on poly-D lysine-coated plates at a density 2x 10^5 cells/well and incubated overnight. Standard Fura-2 AM protocol was followed on a confluent plate of HEK293^{hP2X7} cells. Cells were loaded with Fura-2 AM dye for 1h, and responses were measured after pre-incubation with the compounds for 15 minutes to 1 hour. ATP range used was 2 mM, 1 mM, 500 µM, 200 µM, 100 µM, 50 µM, 20 µM. Three independent experiments were performed while the locations of the conditions on the plates were varied for a representative result. An average of the three independent experiments is shown with three technical replicates for each condition. Neurosteroids were used at a final concentration of 10 µM vs DMSO solvent control (n=3).* ***A*** *pregnenolone (n=3),* ***B*** *pregnanolone (n=3),* ***C*** *testosterone (n=3).* ***D*** *EC50 was calculated from the plots.*

4.2.4 Cytokine secretion from BV-2 cells

One of the crucial functions of microglia is the ability to release cytokines in response to various stimuli. IL-1β is released from microglia upon stimulation in a pro-inflammatory cascade, and P2X7 is thought to initiate this via the activation of the NLRP3 inflammasome and supporting IL-1β maturation (Campagno et al., 2025; He et al., 2017b). BV-2 cells were assessed in an ELISA assay for secretion of IL-1β. The initial assay produced a normal standard curve (data not shown); however, the release of IL-1β was very low and was only present with ATP stimulation on top of LPS priming in BV-2 cells. The assay was attempted multiple times, with modifications to the protocol of the ELISA, trying different buffers and sera to block the plate, until optimization was achieved. However, overall, very little IL-1β release was observed from BV-2 cells. After several optimisations, the assay detected a low amount of 14.3 pg/mL of IL-1β released with LPS priming

and ATP 300 µM stimulation from BV-2 cells. Even nigericin (positive control) did not induce IL-1β release.

Expression of IL-1β was checked by qPCR in BV-2 and BV-2^{P2X7-} cells. Figure 4.12. shows that IL-1β upregulation was seen in both cell lines in response to LPS (over 360-fold upregulation). Some upregulation (8-fold) was seen in response to 1 mM ATP with P2X7 expression. 1 mM ATP stimulation did not induce any IL-1β upregulation in P2X7 knockout microglia.

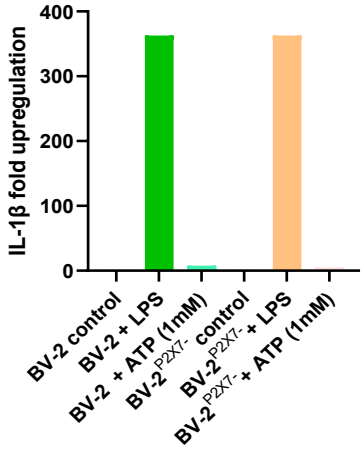

Figure 4.12 IL-1β Expression in BV-2 and BV-2^{P2X7-} cells. *Cells were plated in 0.5% serum at density 60 000 cells/well in 24-well plates for 24h. Cells were treated with LPS +/- ATP (1mM) for 4h. Cells were lysed in wells and harvested. RNA was extracted using Qiagen RNeasy kit and cDNA was synthesised using cDNA Tetro kit following manufacturers' protocols. qPCR was performed as described in the method section. The data shows an average of one experiment conducted with three technical replicates for each condition, normalized to internal control gene- beta actin. Data processed by Delta-delta Ct method to calculate fold change.*

CCL2 chemokine is a crucial signaling molecule in microglia, which is involved in the regulation of chemotaxis and migration. CCL2 release was linked to P2X7 activity by Shieh et al., 2014). CCL2 secretion from BV-2 and BV-2^{P2X7-} cells was assessed in an ELISA Assay. CCL2 ELISA was carried out on BV-2 and BV-2^{P2X7-} cells according to the manufacturer's protocol. No CCL2 was released from the cells in response to ATP alone (Figure 4.13). At the same time, constitutive release of CCL2 in control cells was relatively high and observed in all conditions. The BV-2 cell line cultured in a different serum (PanBiotech) – BV-2 (II) was used (Figure 4.13 C,D) to check the responses in the CCL2 ELISA assay. The baseline responses, compared to the original cell line, were indeed lower by almost a third, however so was the LPS positive control response. This indicated that the induced responses in Figure 4.13 A are still relative, proportional, and informative. Other than the

constitutive release, the pattern observed with BV-2 cells plus a P2X7 antagonist, Az106 (Figure 4.13 D), replicated exactly the pattern observed with BV-2^{P2X7-} knockout cell line (Figure 4.13 B).

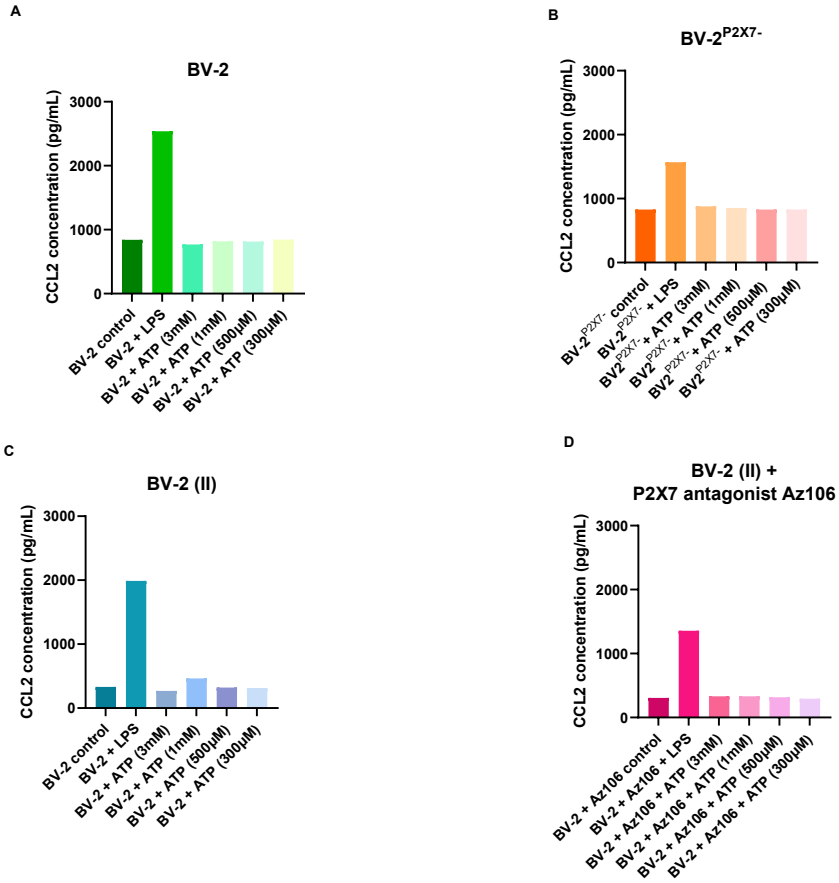

Figure 4.13 CCL2 Release in response to different stimuli in BV-2 vs BV-2^{P2X7-} cells. *Cells were plated in 24-well plates at a density 70 000 cells/well in 0.5% serum media and incubated for 48h. Next, the cells were stimulated with ATP (3mM, 1mM, 0.3mM) for 4 hours. LPS (100 ng/mL) was used as a positive control. Supernatants were used to perform an ELISA assay, as described in the method section.* ***A*** *and* ***B*** *shows the first experiment on BV-2/ BV-2^{P2X7-} cell line from our laboratory.* ***C*** *and* ***D*** *Shows the same experiment repeated on a cell line from a different laboratory with a different serum (Pan biotech) used in the growth media (BV-2 (II)) with Az106 used (P2X7 antagonist) instead of a knockout cell line. The data shows an average of duplicate technical repeats of one biological experiment.*

Optimisation of the assay was attempted to see if stronger responses could be observed with ATP stimulation. The CCL2 ELISA assay was repeated with longer exposure times to LPS positive control or to ATP- over 8h and 24h (Figure 4.14 A, B). Cell lysis was also added as an extra step to facilitate release of any CCL2 stored in intercellular vesicles or inside the cells (Figure 4.14 C,D). Finally, cells cultured in low glucose were used for the ELISA (Figure 4.14 E,F). All abovementioned modifications produced the same pattern where P2X7 expressing cells released slightly more

CCL2, but overall both cell lines released a high amount in response to LPS. High glucose concentration has been linked to an enhanced inflammatory response in BV-2 cells to LPS stimulation (Hung et al., 2022). The concentration of glucose in the culture and experimental media is 17 mM, which is considered high. This may be causing a high constitutive chemokine release, making other stimulations, such as ATP, difficult to induce a significant change in the assay. However, in this experiment, the chemokine release with ATP stimulation and LPS on BV-2 cells grown in 4 mM glucose for 2-3 passages was higher than that of the cells grown in 17 mM glucose. The difference between BV-2 and BV-2 + Az106 cells was not changed. LPS still introduced almost 5 times higher release of CCL2 than ATP.

As the cytokine release assay protocols were not producing much IL-1β or CCL2 with ATP stimulations, the viability of cells following the assay procedure was considered. The cells were plated in a 96-well plate and subjected to a handling procedure mimicking the steps of an ELISA assay to assess whether handling of the cells is impacting viability and thus cytokine release. Alamar Blue assay showed that viability is not affected by the ELISA procedure and the 4h long LPS, ATP (300 µM and 1 mM) +/- Az106 treatment. 3 mM ATP was used as a negative control, and cells were expected to die at this concentration. This is shown in Figure 4.15.

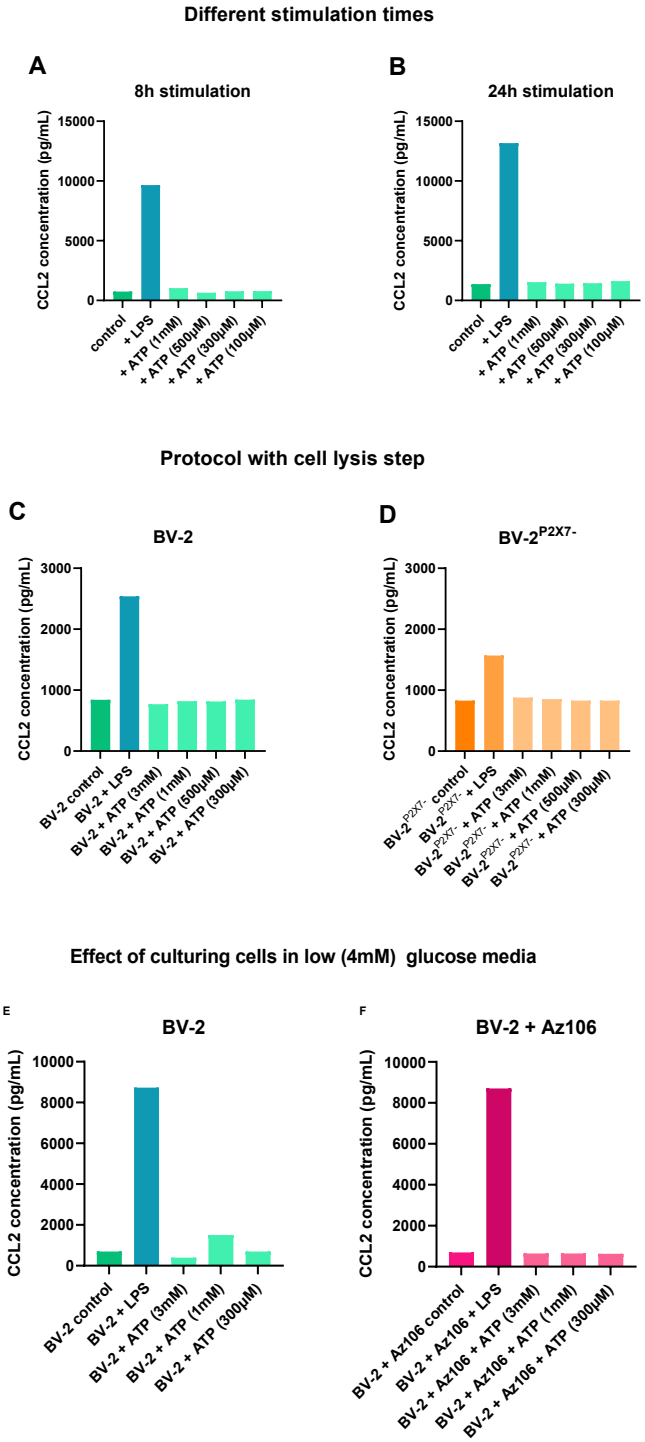

Figure 4.14 Modifications of the CCL2 ELISA protocol on BV-2 and BV-2^{P2X7-} cells. *Cells were plated in 24-well plates at a density 70 000 cells/well in 0.5% serum media and incubated for 48h. Next, the cells were stimulated with ATP (3 mM, 1 mM, 0.3 mM) for 8 hours (**A**), 24 hours (**B**), or 4 hours (**C**,**D**,**E**,**F**). LPS (100 ng/mL) was used as a positive control. Supernatants were used to perform an ELISA assay, as described in the method section. In **C** and **D** the cells were lysed with 1% Triton prior to supernatant collection. In **E** and **F** cells were cultured in low glucose (4 mM) media, and the stimulations were performed in low glucose (4 mM) media. **A** shows the release after stimulation for 8h. **B** shows the release after 24h stimulation. The data shows an average of duplicate technical repeats for each condition of one biological experiment.*

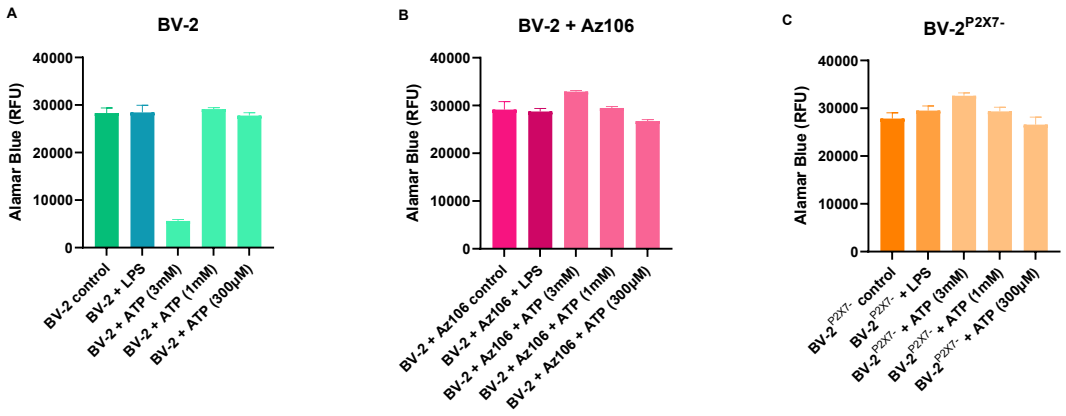

Figure 4.15 Viability in Alamar Blue Assay following cell handling in ELISA protocol. *Cells were plated in a 96-well plate in 0.5% serum media at 20 000 cells/ well to achieve high confluency required in ELISA assays. The cells were incubated for 48h. The standard protocol for supernatant collection for a CCL2 ELISA was followed. The cells were stimulated with ATP (3 mM, 1 mM, 0.3 mM) for 4 hours. LPS (100 ng/mL) was used as a positive control. Alamar blue assay was followed immediately using the standard protocol. The graphs represent one biological experiment with three technical replicates for each condition.*

Although CCL2 release in response to LPS positive control seemed slightly enhanced with P2X7 expression over the 4h stimulation, during a prolonged (8h or 24h) exposure, both cell lines would reach the same levels of secretion. Therefore, no direct evidence for P2X7 being involved in CCL2 secretion from resting BV-2 cells was observed. As P2X7 is upregulated with LPS and IFN-γ polarization, the CCL2 secretion was next evaluated in cells activated with the classic polarizing factors to see whether this may produce an enhanced release. Cells were next polarized for 48h, using the previously tested protocols, and then subjected to LPS or ATP treatment for 4 hours to stimulate CCL2 release (Figure 4.16). Interestingly, the constitutive release from resting (unpolarized) cells was much higher than that of the polarized cells, in both cell lines. ATP, compared to control, induced some more release on top of the high constitutive (approx. 90-100 pg/mL), 3 mM, giving the highest release, but also likely leading to cell death (Figure 4.15), and 1 mM ATP gave a small increase over the control. Again, the difference between BV-2 and BV-2^{P2X7-} was small, and ATP was still able to induce some release without P2X7 present, suggesting a different mechanism might be involved.

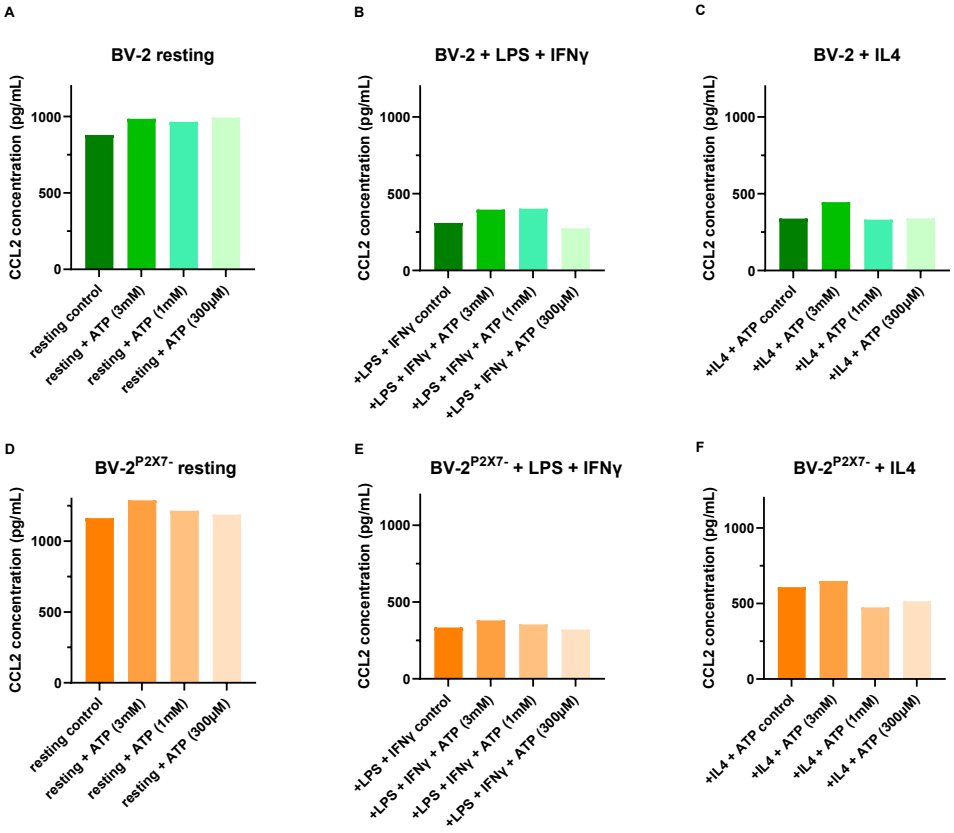

Figure 4.16 Effect of polarization states on CCL2 release. *Cells were plated in 24-well plates at a density 70 000 cells/well in 0.5% serum media and incubated for 48h with polarizing factors LPS 100 ng/mL + IFNg 50 ng/mL (**B**,**E**) or IL-4 20 ng/mL (**C**,**F**) or with 'nothing' (control) (**A**,**D**). Next, the cells were stimulated with ATP (3 mM, 1 mM, 0.3 mM) for 4h. LPS (100 ng/mL) was used as a positive control. Cells were lysed with 1% Triton. Supernatants were used to perform an ELISA assay, as described in the method section. **A**,**B**,**C** shows the release from BV-2 cells. **D**,**E**,**F** shows the release from BV-2^{P2X7-} cells. The data shows an average of duplicate technical repeats of one biological experiment.*

To see if a different purinergic receptor might be involved in the low ATP-induced release of CCL2 from BV-2^{P2X7-}cells, the effect of various nucleotides on CCL2 release was also investigated (Figure 4.17). Following LPS priming, only 3 mM AMP on the P2X7-deficient cell line increased CCL2 release, while majority of the nucleotides lowered the release below that of an unstimulated control. This was true in both cell lines. Interestingly, ADP was highly inhibitory on CCL2 release when P2X7 was present, but not in the knockout cell line. It is possible that there is a compensatory mechanism at play for CCL2 release from BV-2^{P2X7-} cells, although this preliminary data should be followed with more experimental repeats.

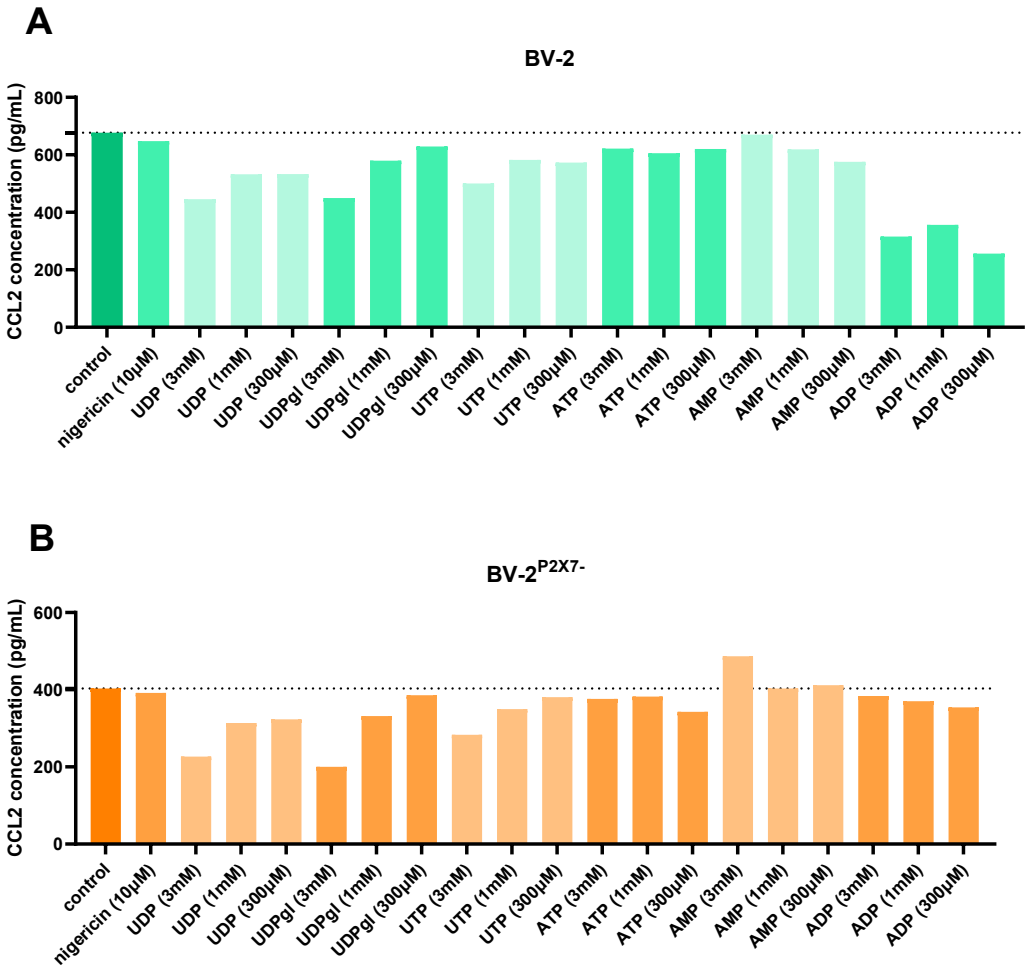

Figure 4.17 Effect of nucleotides on CCL2 release on BV-2 and BV-2^{P2X7-} cells. *Cells were plated in 24-well plates at a density 70 000 cells/well in 0.5% serum media and incubated for 48h. The cells were primed with LPS for 4 hours. Next, the cells were stimulated with a range of nucleotides (3 mM, 1 mM, 0.3 mM) for 30 minutes. Nigericin was used as a positive control. Supernatants were used to perform an ELISA assay, as described in the method section.* ***A*** *shows the release from BV-2 cells.* ***B*** *shows the release from BV-2^{P2X7-} cells. The data shows an average of duplicate technical repeats of one biological experiment.*

Finally, the expression of CCL2 was checked by qPCR in BV-2 and BV-2^{P2X7-} cells. CCL2 upregulation occurred in response to LPS, 32-fold in BV-2 cells, and 13-fold in BV-2^{P2X7-}. This is shown in Figure 4.18. The data shown represent the results from many months of investigations of CCL2 release in the BV-2 cell line with limited success. It was not possible to reproduce work from other groups, which suggest a robust involvement of P2X7 in CCL2 release (Shieh et al., 2014). The observed release of CCL2 in response to LPS positive control stimulation corroborates the groups that show this in BV-2 microglia (Bose et al., 2016; Y. Wang et al., 2022).

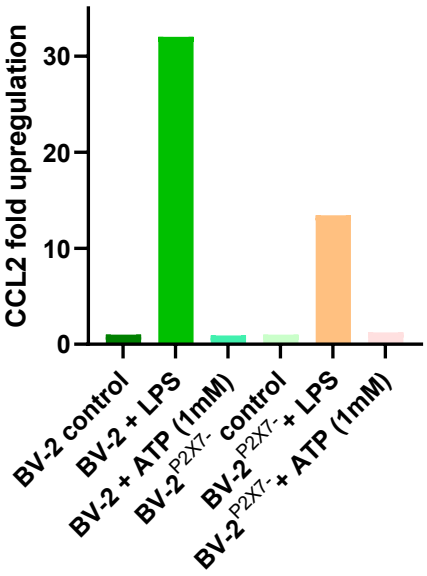

Figure 4.18 CCL2 Expression in BV-2 and BV-2^{P2X7-} cells. *Cells were plated in 0.5% serum at density 60 000 cells/well in 24-well plates for 24h. Cells were treated with 'nothing' (control, LPS 100 ng/mL, or ATP (1 mM) for 4h. Cells were lysed in wells and harvested. RNA was extracted using Qiagen RNeasy kit and cDNA was synthesised using cDNA Tetro kit following manufacturers' protocols. qPCR was performed as described in the method section. The data shows an average of three technical replicates for each condition of one biological experiment, normalized to internal control gene- beta actin. Data processed by Delta-delta Ct method to calculate fold change.*

4.2.5. Phagocytosis in BV-2 cells

Phagocytosis is an important ability of microglial cells throughout development, adulthood and aging. P2X7 has been implicated in regulating this activity as a scavenger receptor in microglia (Gu et al., 2011; Gu & Wiley, 2018). BV-2 and BV-2^{P2X7-} cells were compared in their ability to phagocytose various materials. First, the cells were assessed in their resting and activated phenotypes with fluorescent Zymosan particles (Figure 4.19 A) using flow cytometry. No difference was observed in the cells' ability to phagocytose fluorescent zymosan material regardless of P2X7 expression.

Next, *E. coli* pHrodo uptake was assessed in Figure 4.19 B. As the cells phagocytose the *E. coli* particles, pHrodo fluoresces due to the low pH of the lysosomal environment inside the cells. The fluorescence was the highest in the LPS-activated phenotype in both cell lines suggesting the highest phagocytic delivery to the lysosomal compartment. Although at 2h and 4h there was some variability in the data (data not shown), when measured at 6h, both cell lines had the same capacity to phagocytose the *E. coli* pHrodo particles (Figure 4.19 B).

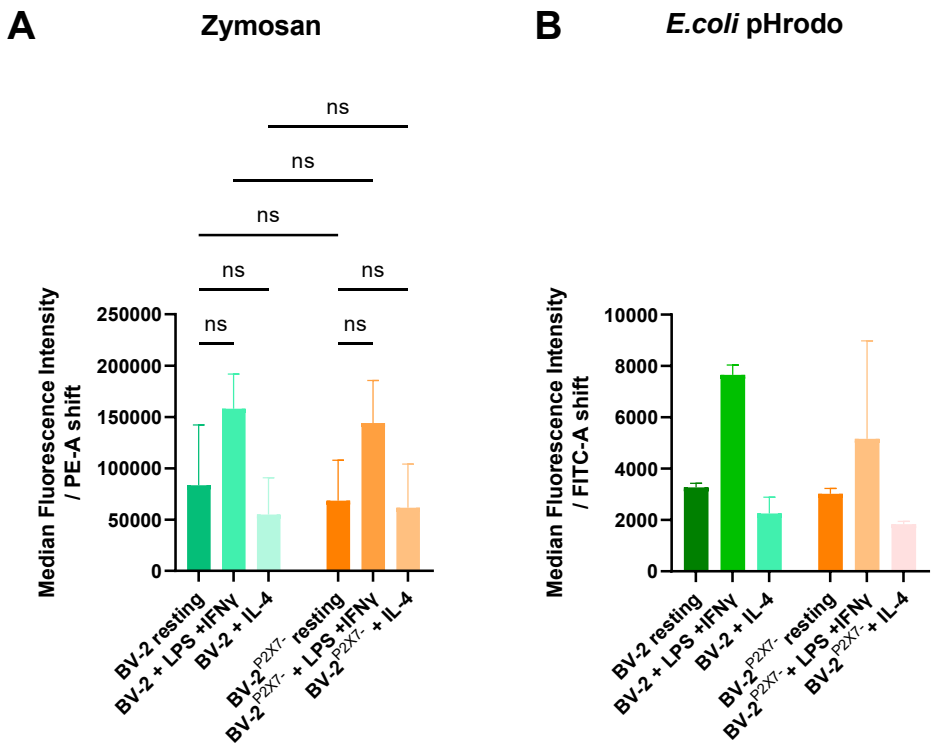

Figure 4.19 Uptake of Fluorescent Particles by BV-2 and BV-2^{P2X7-} cells in different polarised states. *Cells were seeded in 0.5% serum media in a 96-well plate at a density 9000 cells/well and incubated with 'nothing' (resting control), LPS 100ng/mL + IFNγ 50 ng/mL, or IL-4 20 ng/mL for 48h. Cells were fed Zymosan particles following the manufacturer's protocol and left in the incubator for 1h.* ***A*** *The average fluorescent signal of phagocytosed Zymosan particles recorded by flow cytometry as described in the method section. The data shows the median fluorescence shift away from respective controls as an average of three independent biological experiments conducted. Data analyzed by Ordinary One-way ANOVA and Šídák's multiple comparisons test. (Statistical significance ns = not significant).* ***B*** *The average fluorescent signal of phagocytosed E.coli pHrodo particles recorded by flow cytometry. The data shows average of two independent biological repeats (n=2).*

4.3. Discussion

Microglia constantly surveil their environment and respond to cues and stressors by targeted actions and tailored behaviour (Frank et al., 2019; Kettenmann et al., 2011). To allow for the high heterogeneity and plasticity required by their role, microglia exist on a spectrum of phenotypes and activation states (Frank et al., 2019; Korzhevskii & Kirik, 2016). Microglial activation has been well studied, and certain responses have been documented and replicated frequently enough to

become signature markers for polarisation (Korzhevskii & Kirik, 2016). Whether P2X7 affects the polarization and behaviour in activated BV-2 microglia is not clear.

Resting BV-2 microglia have been described in Chapter 3 as spindle-shaped cells. Reduction of serum activated the cells slightly, resulting in a more rounded appearance. LPS + IFN-γ treatment is known to promote a pro-inflammatory profile, while IL-4 and IL-13 can be used to induce alternatively activated cells (Jin et al., 2019; Orihuela et al., 2016; L. Wang, Liu, et al., 2019). BV-2 and BV-2^{P2X7-} cells polarised well in 0.5% serum over 48h. This was apparent in morphological changes observed in the cells, such as an enlarged and rounded appearance with LPS + IFN-γ stimulation, and a small clustering appearance in the presence of the interleukins. This is in line with the literature on BV-2 microglia (Henn et al., 2009; Yao & Fu, 2020). P2X7 did not appear to play a role in the cells' acquisition of the activated phenotypes. Presence of surface markers was measured by immunofluorescence staining and quantified by flow cytometry. The changes were recorded at 48h and appeared to follow the same pattern for P2X7-expressing and P2X7-lacking cells. P2X7 itself was highly expressed in LPS and IFN-γ-activated state, reflective of the inflammatory environment, and expressed on the surface of resting and interleukin-activated cells equally. The usual markers of microglial activation, CD11b and CD86 were upregulated with LPS + IFN-γ treatment. This corroborates with the work of Piano et al., (2023) on primary mouse microglia, which showed an upregulation of CD86 and CD11b to LPS, as well as a decrease of CD206 with LPS, which was also observed here. Interestingly, one paper on BV-2 cells (Qin et al., 2016) showed that CD11b does not change with LPS stimulation alone and showed upregulation of CD206 with LPS alone exposure, which was not observed here with LPS + IFN-γ stimulation. Finally, P2Y12 was also upregulated by LPS + IFN-γ in this work. With interleukin stimulation, the marker CD206 was upregulated, and it was downregulated with LPS + IFN-γ treatment, corroborating the literature (Jurga et al., 2020; Korzhevskii & Kirik, 2016; Orihuela et al., 2016; Pan et al., 2023).

In the CNS environment, there are many endogenous molecules present, capable of interacting with microglia and their receptors. Compounds with a steroidal and glycosidic structure have been shown to interact with P2X7 and affect ATP-induced calcium signaling and dye uptake (Stokes et al., 2020; Bidula et al., 2019). Cholesterol regulates P2X7 activation (Murrell-Lagnado, 2017; Robinson et al., 2014), and its metabolites may have a modulatory effect on P2X7 activity in microglia (Yilmaz et al., 2019). Endogenous progesterone and oestrogen (Jolivel et al., 2021; Yilmaz et al., 2019) have known neuroprotective properties, and some hormones may have anti-inflammatory properties and interact with microglia, and may even modulate the proliferation of

the cells (Yilmaz et al., 2019). Sivcev et al., (2023) reviews endogenous steroids that may act as allosteric modulators of P2X receptors. However, the authors say that specific modulators of P2X7 are not known among neurosteroids. The effect of neurosteroids was examined on BV-2 morphology by imaging. No remarkable features were observed, suggesting that the neurosteroids tested did not polarize the BV-2 or BV-2^{P2X7-} cells. However, when tested in a P2X7 activity assay measuring Calcium signaling (Fura-2 AM) and P2X7 pore-activation assay (YO-PRO-1 dye uptake), the endogenous steroid metabolites- pregnanolone, pregnenolone, testosterone, progesterone, and alfaxalone -a synthetic neuroactive steroid used as an anaesthetic in veterinary medicine- stood out as having an inhibitory effect on P2X7. It is therefore possible that these neurosteroids modulate microglial responses via inhibition of P2X7, even if the morphology of the cells does not change when tested *in vitro*. Pregnanolone had the highest inhibitory activity on both calcium signaling and pore activity of P2X7. This is an interesting finding, and modulation of P2X7 in microglia using endogenous molecules such as neurosteroids is worth exploring further in future work as a potential therapeutic approach in states of chronic neuroinflammation or gender differences in microglia.

Viability in Alamar Blue assay was not affected by polarization of microglia. BV-2 cells still showed an advantage over the P2X7-deficient clones. LPS slowed down the proliferation of the cells, and this made the difference between the two cell lines slightly more apparent. Following up with CellTrace Yellow dye retention assay, showed that the rates of cell division were still the same, regardless of polarized state at 48h and irrespective of P2X7 expression.

Microglia in their polarized state are reported to release specific cytokines. ELISA assays were used to measure the release of CCL2 and IL1β. CCL2 chemokine (also called MCP-1) is involved in the migration of microglia, and its key role in chemotaxis in the BV-2 cell line has been shown before (Bose et al., 2016). The release of CCL2 has been linked to ATP-activated P2X7 in mouse microglia by Shieh et al., (2014). In this work however, the ELISA assays demonstrated an apparent increase in CCL2 in response to LPS stimulation in both cell lines, regardless of P2X7 expression. During a 4h stimulation, the LPS-induced CCL2 release was higher when P2X7 was present. However, pharmacological blockage of P2X7 and the receptor knockout did not abolish CCL2 release from the cells completely. ATP had a limited scope of inducing a release of CCL2 from BV-2 cells expressing P2X7. 1mM ATP induced a five times lower response than the robust effect observed with LPS, and some CCL2 release was observed in response to ATP in BV-2^{P2X7-} cells. Even in unstimulated control wells, some CCL2 release was present. The high constitutive release could be linked to the media composition, which included high glucose. High glucose has been shown to enhance CCL2 expression (Quan et al., 2011; Takaishi et al., 2003) and increase the inflammatory response of BV-2 cells when stimulated with LPS (Hung et al., 2022). However, here

when the cells were cultured in low glucose for 2-3 passages, they actually released higher amounts of CCL2 in response to LPS, but showed comparable unstimulated constitutive release. The ELISA protocol underwent multiple optimization steps, including culturing cells in low glucose, cell lysis step and altering stimulation times; however, the results were not very different with the modifications. Although P2X7 expression in BV-2 cells appears to carry a slight advantage for CCL2 release in response to inflammatory stimulation with LPS and ATP, the knockout cell line, is also capable of releasing high levels of CCL2. This suggests there may be compensatory mechanisms involved in the BV-2^{P2X7-} cell line that include other receptors than P2X7. Shieh et al., (2014) showed in primary mouse microglial culture that stimulation with 500μM ATP increased CCL2 release significantly and induced upregulation of CCL2 gene expression, linking this to P2X7 activity, since a P2X7 knockout in their experiments completely abolished the ATP-induced chemokine release. This was not observed here. However, the same authors also observed a relatively high constitutive release of CCL2, without ATP or any stimulation present, as was observed in this work. qPCR confirmed the findings of ELISA assays and showed that in P2X7-expressing BV-2 cells, CCL2 upregulation was approximately twice as high as in P2X7-deficient cells. However, BV-2^{P2X7-} cells still responded with a strong upregulation of CCL2. ATP stimulation did not affect CCL2 gene expression in either cell line, even though it showed a slightly elevated chemokine release in the ELISA assays.

IL-1β, a pro-inflammatory cytokine that has been linked to P2X7 expression via the inflammasome activation, leading to the cytokine release (Campagno et al., 2025; Ferrari et al., 2006). There is a lot of evidence in the literature which shows that LPS stimulation leads to upregulation of IL-1β in microglia; however, some papers suggest that only with coupled LPS + ATP stimulation does IL-1β maturation and release occur (Ferrari et al., 2006; Mehta et al., 2001). A recent paper (Campagno et al., 2025) implicates P2X7 in the process of priming and the release of IL-1β from retinal microglia in primary mouse and rat cells. Although IL-1β release from murine microglia has been documented in the literature, only very low release was observed in ELISA assays in this work, in response to ATP stimulation in LPS-primed BV-2 cells. Low levels of ATP and viral Poly(I:C) stimulation were not effective at inducing IL-1β release from BV-2 cells (data not shown). qPCR was used to demonstrate the upregulation in IL-1β expression; however, it showed the same levels of upregulation regardless of P2X7 expression. Strangely, nigericin (commonly used in literature as a positive control in cytokine release) did not induce any cytokine release in the assays performed on BV-2 cells. This cell line might not be a good model for IL-1β assays.

Phagocytosis in microglia is thought to be enhanced and modified by polarization (Norden & Godbout, 2013; J. Wang et al., 2017; M. Wang et al., 2025). Furthermore, P2X7 unstimulated expression is thought to affect phagocytosis (Ou et al., 2018), and P2X7 activation is believed to

impact lysosomal health (Sekar, Huang, Hsieh, et al., 2018b). Phagocytic ability of BV-2 and BV-2^{P2X7-} cells was measured in different activated states vs resting cells. Although the impact of P2X7 on phagocytosis has been demonstrated on various cell lines (Campagno & Mitchell, 2021b), it is not clear whether P2X7 has this effect in BV-2 microglia. Both cell lines demonstrated the same ability to phagocytose fluorescent beads. In BV-2 cells, E. coli pHrodo uptake was doubled with LPS + IFNγ stimulation, and less pronounced but still showing the same pattern in BV-2^{P2X7-} cells. Zymosan uptake also reflected a similar pattern. This is in concordance with the literature on the effects of LPS on BV-2 cells, enhancing phagocytosis (Tawbeh et al., 2023). P2X7 expression does not appear to affect phagocytosis in the BV-2 model studied. However, the literature reports that expression of P2X7 is able to positively affect phagocytosis. Gu et al., (2011) showed that P2X7 silencing had a profound effect on phagocytosis in human monocytes. In mouse microglia here, however, P2X7 expression did not seem to affect the phagocytic ability of BV-2 cells.

It should be considered that Gu et al., (2012) researched in detail the effect of serum and its components on P2X7-induced phagocytosis and found it to be inhibitory. Although the experiments were carried out in low- 0.5% serum, it is possible that in serum-free media, a difference between BV-2 and BV-2^{P2X7-} cells would have become apparent. Unfortunately, complete serum removal negatively affected the cells' health; therefore, 48h polarization and subsequent phagocytosis experiments would not have been possible to carry out reliably. In the future, it would be interesting to explore a way to investigate phagocytic differences in P2X7 knockout microglia using serum-free media, perhaps in a different cell line which better handles complete serum deprivation.

Conclusions

P2X7 expression did not appear to affect BV-2 cells in terms of polarization, morphology, or function, such as phagocytosis or cytokine release, in the model tested here. The scope of markers of polarization was limited to only key markers selected, and focused on surface marker expression. Techniques such as qPCR could reveal more subtle changes to the polarized state in the upregulation of genes. This was indeed seen in qPCR revealing changes in CCL2 and IL-1β gene upregulation, that did not translate into robust secretion events. In the future work, it would be interesting to explore some of the assays in serum-free conditions, as there are reports on serum components having an inhibitory effect on P2X7-influenced functions such as phagocytosis. There may be an impact on other cytokines and chemokines, and future studies could exploit the use of the P2X7-deficient BV-2 line to identify other P2X7-regulated molecules and behavioural features of the microglia. One apparent difference in polarized morphology of the BV-2 vs BV-2^{P2X7-} cells,

was the presence of scattered giant cells, mostly round-shaped, when polarized with LPS alone for 72h. These giant cells were more prevalent when P2X7 was expressed. This finding was followed up separately in Chapter 5 as giant multinucleated cells.

Chapter 5 - P2X7 involvement in multinucleation and giant cell formation

5.1 Introduction

Giant Multinucleated Cell (GMC, or MGC in some literature) is a term adopted to describe giant cells of the macrophage/ monocytic or microglial origin that contain multiple nuclei (Ahmadzadeh et al., 2022). GMCs have been noted in numerous diseases and *in vitro* models; however, they remain poorly understood, with reports of these cells showing enhanced functional adaptations, as well as being a feature of a pathology (Ahmadzadeh et al., 2022). This chapter focuses on the role of the P2X7 receptor in supporting multinucleation and giant cell formation, focusing on BV-2 microglia. The work discusses microglial GMC phenotype, function, and activity. It compares these cells to some better-understood GMC models and giant cell subtypes described in the literature, commonly occurring under physiological and inflammatory conditions in macrophages and monocytes.

5.1.1 GMC subtypes

In macrophages and monocytes, GMCs arise via cell fusion (Sabe et al., 2024; Lösslein et al., 2021). However, other GMCs in mammalian organisms may also occur via endoreplication or abortion of the cell cycle (Hazra et al., 2023). During development, polyploid cells induced by endoreplication form an essential step for the normal development of tissues such as the placenta, liver, skin, and even blood (Fox & Duronio, 2013). For example, during platelet formation, megakaryocytes become polyploid cells before undergoing fragmentation. In pathologies, endoreplication is also a hallmark of certain cancers, for example, liver cancer (Fox & Duronio, 2013). Finally, GMCs are often observed as a feature of aging and a result of changes that happen in senescent cells (Kloc et al., 2022). It is crucial to consider that different pathways may lead to multinucleation in mammalian cells (Brooks et al., 2019). This chapter, however, focuses on microglial GMCs and their similarity to macrophage-derived GMCs and examines cell fusion as a possible multinucleation process in detail.

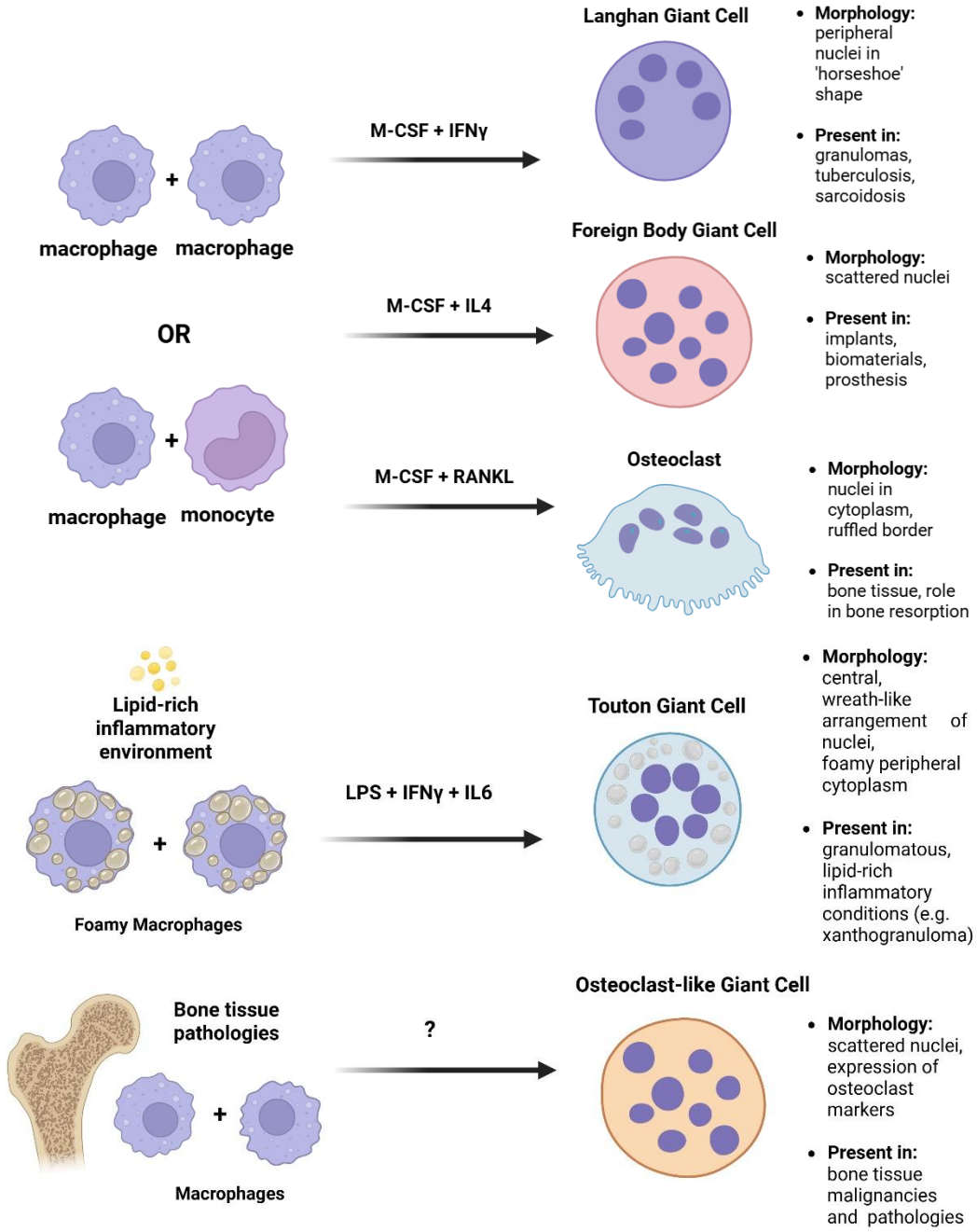

Figure 5.1 Macrophage-derived multinucleated giant cell subtypes. *Cell fusion of macrophages or macrophages and monocytes leads to GMC formation. The presence of Langhan's Giant Cells (LGCs) is noted in granulomatous diseases such as sarcoidosis and tuberculosis. Nuclei in LGCs are arranged in a horseshoe shape. M-CSF and IFN-γ can induce LGs in vitro. Foreign Body Giant Cells (FBGCs) are associated with the presence of non-biological material such as implants. FBGCs contain numerous dispersed nuclei. FBGCs can be induced by M-CSF and IL-4 signaling. Osteoclasts are highly specialized GMCs involved in bone resorption. They are characterized by a ruffled border and numerous nuclei either dispersed in cytoplasm, or located closely together. M-CSF and RANKL stimulation induces osteoclast formation in vitro. Osteoclast-like GMCs are similar to osteoclasts in expression of markers. They are seen in bone tissue pathologies. In lipid-rich inflammatory or granulomatous conditions Touton giant cells have been reported. They are characterized by a central, wreath-like arrangement of nuclei and a foamy appearance of cytoplasm. Figure generated in Biorender.*

GMCs described in macrophages

GMCs, which form from the fusion of macrophages or monocytes, are generally divided into three main subtypes (Ahmadzadeh et al., 2022), depending on morphological characteristics, function, and the multinucleation process (illustrated in Figure 5.1). Osteoclasts arise from RANKL and M-CSF signaling and are involved in bone tissue maintenance (McDonald, Kim, et al., 2021). They attain many characteristics, such as a ruffled border, where the cell attaches to the bone surface and secretes specified enzymes to degrade the material (Sabe et al., 2024). Foreign Body Giant Cells (FBGCs), as the name suggests, form in response to a prolonged presence of non-biological objects such as prostheses, implants, and biomaterials in the environment (Sheikh et al., 2015). These cells commonly arise during chronic inflammation. They can also form in response to inflammatory cytokine IFN-γ, interleukins such as IL-4 and IL-13, and in the presence of specific pathogens *in vitr*o. FBGCs can reach very large sizes with hundreds of nuclei in number, scattered throughout the cytoplasm (Mcnally & Anderson, 1995). They are characterized by a high phagocytic capacity and high expression of CD206 and CD11b (Milde et al., 2015;McNally & Anderson, 2015). The third subtype, Langhans Giant Cells (LGCs), form under specific conditions associated with granulomatous diseases, in sarcoidosis, and during infections such as tuberculosis. Here, the nuclei are arranged in a distinct horseshoe shape around the Golgi apparatus and can reach up to 20 in number (Ahmadzadeh et al., 2022). LGCs are generally round in shape, and ultrastructural studies show lysosomes evenly distributed throughout the cytoplasm in these cells (Sakai et al., 2012). They have been shown to arise from pro-inflammatory or epithelioid macrophages in the presence of IL-3, IFN-γ, GM-CSF, and TNF-α. There is some evidence indicating that DC-STAMP and CD40 are important for the formation of LGCs (Sakai et al., 2012). Theodor Langhan first described these cells in 1868, studying granulomas in tuberculosis (Lay et al., 2007). Multinucleated and giant cells in the body are often associated with very specific functions. LGCs seem to have a low phagocytic ability, reflected in low expression of the mannose receptor CD206 and CD11b; however, they have been shown to be able to isolate the pathogens in tuberculosis by surrounding them and fusing with macrophages, which have already taken up the pathogens (Wang et al., 2025). Different strains of pathogens seem to induce different LGCs that can contain higher or lower numbers of nuclei (Lay et al., 2007; Wang et al., 2025). While osteoclasts resorb bone tissue, other GMCs may participate in inflammatory responses by secreting cytokines, inflammatory mediators, and antigen presentation. Z. Wang et al., (2025) showed that in *Mycobacterium marinum* cutaneous infection in mice, LGCs limit the spread of granulomas, inhibit bacterial growth, and secrete inflammatory molecules IL-10 and IL-1β, as well as antimicrobial peptides. The authors suggested that LGCs could be useful in

cytotherapy. All GMCs may have some therapeutic potential, but their role in health and disease still needs to be better understood.

In certain pathologies, other less common types of GMCs of monocytic and macrophage origin have also been described. For example, Osteoclast-like giant cells have been described in inflammatory lesions associated with bone pathologies such as tumours, cherubism, and bone malignancies, but also occasionally with no proximity to the bone surface, in skin lesions (Ahmadi Moghaddam et al., 2018). These cells display some characteristics of osteoclasts, such as a large shape, multiple dispersed nuclei, and expression of osteoclast markers (Sabe et al., 2024).

Touton Giant cells are another lesser-known subtype, described in association with lipid-rich lesions and granulomatous inflammatory conditions such as lesions (Aramin et al., 2019; Jakobiec et al., 2018). These GMCs form via fusion of foamy macrophages, which, in turn, are associated with LPS and IFN-γ stimulation. Foam cells are typically macrophages that have accumulated high levels of lipids in their cytoplasm and thereby appear 'foamy' under the microscope. Fusion of foamy macrophages to form Touton GMCs has been linked to IL-6 signaling and inflammation-resolving behaviour (Ahmadzadeh et al., 2022), although more research is needed to support this. Because of the LPS association, their formation is thought to rely on TLR activation-induced changes (Ahmadzadeh et al., 2022; Aramin et al., 2019). Touton giant cells are histologically recognized by foamy cytoplasm in H&E staining, surrounding a circular wreath-like arrangement of nuclei with a homogenous cytoplasm centre (Aramin et al., 2019). Figure 5.1 summarizes the different types of GMCs and pathways leading to their formation.

Osteoclasts

Osteoclasts are by far the best described and studied GMC subtype. They contribute to bone remodeling throughout life by absorbing the bone matrix in balance with bone-laying osteoblasts (Teitelbaum, 2007). They are formed by the fusion of mononuclear macrophages and monocytes (Ahmadzadeh et al., 2022). Signaling pathways leading to this event involve the macrophage colony stimulating factor (M-CSF) and receptor activator of nuclear factor kappa B ligand (RANKL) stimulation (Sabe et al., 2024). The function of osteoclasts is reviewed by multiple writers (Jacome-Galarza et al., 2019; McDonald, Kim, et al., 2021; Teitelbaum, 2007). In summary, multiple nuclei and a giant cell body size allow them to perform their function better. Osteoclasts secrete a range of enzymes that degrade the bone tissue. Multiple nuclei in the cell render more transcription and translation capacity to allow for a high production of enzymes, and may even allow for the formation of larger lysosomes (Arnett & Orriss, 2018). A higher number of mitochondria per cell supports the high energy demand of the osteoclasts, which need to release

high amounts of enzymes at the resorption zone, maintain a low pH, and sustain the high demand for phagocytosis and engulfment of bone remnants (Arnett & Orriss, 2018). These cells express high levels of TRAP and MMP9, which are believed to be involved in bone resorption at the osteoclast ruffled border (Wittrant et al., 2003). The energy demand is thought to be met by the incorporation of additional nuclei. (Sabe et al., 2024; Teitelbaum, 2007; Xu & Teitelbaum, 2013).

In order for osteoclasts to form, cell fusion of precursors – macrophages or monocytes, must occur (Sabe et al., 2024). The precursors must first acquire a pro-fusion phenotype and express relevant receptors on the surface, induced by RANKL signaling, then the cells move close together and attach to each other (Xu & Teitelbaum, 2013). Fusogens expressed by the precursor cells facilitate membrane fusion by acting like catalysts to lower the energy barriers required in the process (Sabe et al., 2024).

Osteoclasts are generally thought to be terminally differentiated cells. A previously accepted theory that osteoclasts tend to undergo apoptosis within 2-4 weeks of formation is now challenged by studies showing that osteoclasts are able to incorporate new nuclei from mononucleated precursor macrophages under optimal conditions, which allows them to survive longer (Jacome-Galarza et al., 2019). McDonald & Khoo, et al., (2021) showed that under specific conditions, such as prolonged RANKL exposure, osteoclasts may even divide into osteomorphs—daughter cells.

5.1.2 Mechanism of cell fusion

Cell fusion is the main process leading to formation of Giant multinucleated cells arising from macrophages and is explored in this work as a possible pathway to formation of GMCs in P2X7 expressing microglia. Cell fusion is an active research topic and has been primarily informed by virus-cell fusion experiments (Sabe et al., 2024). (Hernández & Podbilewicz, 2017; Sabe et al., 2024) describe the process in their reviews and point out several conditions and principles that need to be met in order for cell fusion to occur. The process will have energy barriers that will need to be overcome, such as hydration force and deformation of the membranes. The process starts with structural rearrangement of the membranes which is energy demanding. Therefore, catalysis by proteins called fusogens, which lower this energy barrier is essential to initiate the fusion process by binding a receptor on the target cell (Nadav Segev et al., 2018). The energy released during a conformational change of the fusogen protein is used to pull the membranes closer together(Sabe et al., 2024).

Acquisition of a pro-fusion phenotype

With regards to viruses, numerous fusogens have been identified; however, in other, more complex eukaryotic cells, the fusion proteins and mechanisms remain more elusive (Nadav Segev et al., 2018).

In osteoclasts, the process is induced by signaling adaptor DNAX-activating protein 12 (DAP12) interaction with triggering receptor expressed on myeloid cells 2 (TREM2) (Helming et al., 2008). DAP12/TREM2 signaling has been shown to be required by all GMC precursor cells for multinucleation, with distinct downstream pathways resulting in various GMC subtypes (Ahmadzadeh et al., 2022).

In osteoclast precursors DAP12/TREM2 signaling leads to cytoplasmic spleen tyrosine Kinase (SYK) signaling which via the phospholipase C (PLC) and Ca^{2+} signalling enhances the key transcription factor in osteoclastogenesis, namely nuclear factor of activated T-cells c1 (NFATC1) (Humphrey & Nakamura, 2016).

In Foreign Body Giant Cells, IL-4 signaling, together with immunoreceptor tyrosine-based activation motif (ITAM), induce signal transducer and activator of transcription 6 (STAT6) which upregulates fusion protein expression such as E-cadherin, DC-STAMP, and MMP9 (Cai et al., 2024).

In LGC the pathways leading to multinucleation have not yet been fully elucidated; however signaling via NF-κβ and mitogen-activated protein kinases (MAPKs) is suspected to be involved in the final stages of cell fusion (Yasui et al., 2009).

Chemotaxis and adhesion

The second stage leading to fusion is chemotaxis (Hernández & Podbilewicz, 2017). In macrophages, this is mainly attributed to the chemokine CCL2 activity and its receptor (Sabe et al., 2024). Furthermore, CCL2 has been shown to induce expression of key proteins involved in cell fusion, such as DC-STAMP and MMP9, and activation of a cytoskeleton-regulating protein ras-related C3 botulinum toxin substrate 1 (RAC1), which may aid the cell in rearranging the internal structures required for cell fusion (Usman, 2010;Zhang et al., 2014)

Finally, cell-to-cell adhesion is required before the fusion can occur (Sabe et al., 2024). The homotypic cell-to-cell contacts are thought to be mostly mediated by E-cadherin and integrins (Fiorino & Harrison, 2016). E-cadherins are adhesion molecules dependent on Ca2+. They are essential for both initiation and maintenance of cell-to-cell contacts between neighboring cells by creating homophilic interactions, which create the initial tethering of the cells (Van Roy & Berx,

2008). The heterodimeric transmembrane receptors- integrins- promote not only cell-cell connections, but also matrix- cell adhesions (Bachmann et al., 2019). Some integrins noted in all fusing cells include CD9 and CD81 (Parthasarathy et al., 2009).

At the onset of cell fusion, SIRPα and its ligand CD47 are upregulated (X. Han et al., 2000; Sabe et al., 2024). The signal regulatory protein alpha (SIRPα), also known as macrophage fusion receptor, is a transmembrane protein of the immunoglobulin family. Its ligand, CD47, integrin-associated protein, with SIRPα also known as the 'don't eat me' signal, is an important immune checkpoint and is involved in many homeostatic tissue functions (Matlung et al., 2017).

Cytoskeletal reorganization

During all stages of the cell fusion process, including migration and adhesion, the cytoskeleton of the GMC precursors must reorganize itself to facilitate all the processes and changes (Sabe et al., 2024). This is observed in macrophages, which display characteristic actin protrusions from the cell membrane, as well as the formation of actin rings (Martin, 2016). (Lu et al., 2024) showed that impaired formation of actin membrane protrusions negatively impacts GMC formation.

Membrane reorganization

Phosphatidylserine (PS) externalization, facilitated by flippases and scramblases, which redistribute the lipid arrangement in the membrane bilayer, has been noted in multinucleating osteoclasts (J. H. Kang et al., 2020). Furthermore, (J. H. Kang et al., 2020; Verma et al., 2018) showed that PS externalization may be inhibited by anti-DC-STAMP antibodies and via inhibition of lipid transporters which in turn resulted in inhibition of osteoclast precursor formation.

Caspase 3 downstream of Cas 8 and RANKL signalling is thought to promote PS exposure and fusion of osteoclasts (Krishnacoumar et al., 2024). The nuclear RNA chaperone La protein may also be involved in PS externalization and it has been shown to be located at the cell surface of fusing osteoclasts (Whitlock et al., 2023). It has also been proposed as an off-switch signal for multinucleating cells, as in mature GMCs, La protein was observed to translocate from the cell surface to the nuclei of the osteoclasts (Whitlock et al., 2023). Phosphatidylethanolamine (PE) exposure may also be involved in cell fusion during the formation of osteoclasts (Irie et al., 2017). In FBGC formation, CD36 on precursor cells was hypothetised to localize to contact sites and interact with externalized PS to allow for cell fusion. Stewart et al., (2024) showed that

macrophages deficient in CD36 were not forming FBGCs effectively in response to IL-4 stimulation. However, CD36 was not essential to formation of osteoclasts.

Aside from DC-STAMP being a key fusogen in the final stages of the fusion process of FBGCs, LGCs and Osteoclasts (Sabe et al., 2024; C. Zhang et al., 2014), the involvement of tetraspanins CD9 and CD81 has also been shown, although whether they play a positive or negative role in regulating cell fusion is not clear based on contrasting evidence (Parthasarathy et al., 2009). Tetraspanins have the ability to interact with multiple molecules forming functional clusters at tetraspanin-rich membrane regions and therefore may be facilitating cell-to-cell interactions (Parthasarathy et al., 2009).

5.1.3 Giant cells in the CNS and multinucleated microglia

GMCs have also been observed in the CNS. A study by Shtaya et al., (2019) reports GMCs of microglial origin in postmortem human brains in spontaneous intracerebral hemorrhage, appearing after day 5 and through to day 12 of the incident. The study was based on immunohistochemical staining (Iba-1 labelling for microglia) and analysis of brain slice images. In a couple of images, the authors observe fusion of microglia to form a giant multinucleated microglial cell. The authors report a lack of ramified microglia in the insult sites, observing only ameboid, phagocytic, and reactive microglia, which, within a 2-3mm distance of the hemorrhage location, were clustering and fusing to form GMCs. A substantial limitation of the study is that Iba-1 does not conclusively differentiate microglia from macrophage or monocyte origin cells. Although the paper reports that cell fusion is observed in the images, the authors admit that disrupted and excessive demand for microglial proliferation could also potentially have led to the formation of the GMCs observed. A study by Wei et al., (2020) showed that GMCs of macrophage/microglia origin indeed form and can phagocytose hematomas during ischemic events in mice. The number of GMCs forming could be increased by anti-CD47 antibody injection (which suppresses the erythrocyte phagocytosis ‘don’t eat me’ signal of the induced hematoma) and eliminated by chlodronate liposomes (which are commonly used to eliminate macrophages and microglia in tissues). The authors reported strong phagocytic capacity of GMCs and surface expression of ‘M1-like’, as well as ‘M2-like’ activation markers. Here also, the authors were not able to distinguish the origin of the GMCs as distinctly macrophage, microglia or both, in their study. In their subsequent paper (Fu et al., 2024), the same group showed that GMC formation was reduced in mice lacking complement 3. Interestingly, in this study, the number of GMCs

forming in response to an ischemic event was found to be lower in aged mice; however, it was not dependent on the animals' gender.

In Microglia, the appearance of GMCs has been recorded, especially in connection with certain diseases (Kloc et al., 2022; Milde et al., 2015; Wei et al., 2020). These cells appear fully functional, have a high phagocytic ability, and can release cytokines and pro-inflammatory molecules (Milde et al., 2015). They have been noted in HIV associated dementia (Teo et al., 1997), in association with amyloid beta-induced angiitis (Rittner et al., 1999), and in Giant Cell Arteritis, in the inflammation of the arteries of the head. These diseases are associated with the accumulation of microglia at the inflammation site, and indeed, GMCs containing amyloid beta deposits were found in a study of an angiitis model (Danve et al., 2014). In a rat model of amyotrophic lateral sclerosis, induced by expression of a mutant Cu/Zn superoxide dismutase gene, GMCs were observed in the spinal cords of the animals (Fendrick et al., 2007). In a study by Moca et al., (2022) investigating microglial aging in mouse models, the authors reported clusters of microglial GMCs in Ventral Tegmental Area (VTA) and Substantia Nigra compacta (SNc), however, none in Nucleus Accumbens (NAc), which in all cases increased with aging. GMCs showed heterogeneity between those locations with larger GMCs in SNc. The authors postulated that this might be reflective of a greater inflammatory environment and phagocytic demand around the SNc dopaminergic neurons in a Parkinson's disease model. In Krabbe disease, which is a genetic lysosomal storage disorder resulting in an infantile-onset demyelination, via the impairment of the lysosomal galactosylceramidase enzyme, which causes lysosomal dysfunction and formation of multinucleated microglia named globoid cells (Wenger & Luzi, 2024). The lipid galactosyl ceramide and psychosine accumulation in the demyelinating loci, as a downstream effect of enzyme dysfunction, has been directly linked to globoid cell formation, and psychosine has been shown to cause multinucleation of healthy macrophages (Nicaise et al., 2016; Wenger & Luzi, 2024).

The mechanism of GMC formation in microglia is not fully understood and may share similarities with macrophages. An early paper by Suzumura et al., (1999) reports that multinucleation in microglia can be driven by IL-4 and IL-13. Hornik et al., (2014), however, showed that immortalized BV-2 and primary mouse GMC microglia *in vitro* form in response to inflammatory molecules such as LPS, amyloid beta, alpha synuclein, TNF-α, and IFN-γ. The authors showed that microglia may multinucleate as a failure to undergo cytokinesis via the PKC pathway under pro-inflammatory conditions, even though fusion was also possible via induction with Polyethylene glycol (PEG). They showed that this process can be reversed with PKC inhibition and initiated by Phorbol 12-myristate 13-acetate (PMA), a highly inflammatory triggering molecule and a PKC pathway stimulator. The authors further demonstrated that the resulting GMC microglia had a higher phagocytic capacity for dead cells than mononucleated cells did. Lee et al., (2024) generated

multinucleated microglia via Pyk2 inhibition and abscission of cell division in the cell cycle. These microglia were shown to be highly phagocytic for acutely infused β-amyloid.

Taken together, there is increasing evidence of GMCs of microglial origin in the CNS, however their exact function and formation in health and disease needs to be better studied.

5.1.4 P2X7 in support of GMC formation

Hornik et al., (2014) showed that in BV-2 microglia, multinucleation can occur via activation of the PKC pathway. PKCs are important facilitators of cytoplasmic signalling and the downstream cascades are involved in regulation of a variety of functions in microglia (Shiratori et al., 2010). P2X7-induced Ca^{2+} signalling has been shown to support the Ca^{2+}-dependent PKC pathway activation (Armstrong et al., 2009). The authors showed that PKC translocation was P2X7-dependent in osteoclasts.

P2X7 is implicated as a fusogen involved in multinucleation of macrophages, with a few studies linking P2X7 expression to FBGCs, LGCs and osteoclasts formation. However, there is also conflicting evidence showing that osteoclast formation in mice continues with P2X7 knocked out (Di et al., 2013; Irma Lemaire et al., 2006). Di Virgilio & Irma Lemaire et al., (2011) showed that macrophages expressing P2X7 in high levels, have a greater ability to form GMCs, while P2X7 antagonists inhibit GMC formation. Irma Lemaire et al., (2006) showed that rat alveolar macrophages, expressing native P2X7, as well as HEK293 cells transfected with P2X7, had an advantage at cell fusion and GMC formation over mock-transfected cells. The authors hypothesise that the unique ability of P2X7 to form a giant pore drives cell fusion by allowing the neighbouring cells to form cytoplasmic connections. The authors showed that a transfection with a truncated variant of P2X7 -lacking the pore-forming capacity- did not further increase the GMC-forming advantage when stimulated with P2X7 potentiator Polymyxin B, which was otherwise effective at potentiating cell fusion and GMC formation in other transfected variants.

The increase in intracellular Ca^{2+}, also driven by P2X7, as well as downstream activation of caspases via NLRP3 inflammasome, are also shown to correlate with GMC formation incidence. Whether P2X7 involvement in GMC formation allows for a specific fusion process or allows the cell to acquire a pro-fusion phenotype by expression of relevant fusion proteins is still unclear. For example, P2X7 may be linked to higher CCL2 and IL-1β secretion, which in turn may contribute to higher chemotaxis and fusing ability in GMC precursors, respectively. CCL2 increases migration and has been shown to increase GMC formation of all GMC subtypes (Khan et al., 2016; Kyriakides

et al., 2004). Increased IL-1β secretion has been shown to promote osteoclast precursor fusion and increase expression of osteoclast markers and fusion proteins in *in vitro* primary mouse cell cultures (Cao et al., 2016).

P2X7 has been previously linked to increased expression of surface receptor CD44, which is important in cell fusion of macrophages. CD44 has been linked to P2X7 as a pharmacological target in sarcoidosis treatment (Kaiser et al., 2019; Moura et al., 2015). Di Virgilio & Irma Lemaire et al., (2011) demonstrated in GM-CSF induced fusion of macrophages that not only P2X7 expression but also co-expression of Pannexin-1 are needed for GMC formation. They argued for GM-CSF-stimulated P2X7 pore formation driving cell fusion in rat alveolar macrophages, and that macrophages from P2X7 and Pannexin-1 knockout animals did not respond to GM-CFS. They also propose that extracellular ATP released locally via P2X7 is then metabolised to adenosine, which ultimately mediates the expression of CD44, which needs to be highly upregulated on the surface of cells acquiring a pro-fusion competency.

P2X7 is involved in PS exposure (Qu & Dubyak, 2009), which is thought to be important for cell fusion and membrane interaction of fusing macrophages forming FBGCs (Whitlock & Chernomordik, 2021). PS is normally located to the inner side of the membrane bilayer and is only externalized when the cell is about to undergo elimination by phagocytosis or fusion due to damage (Irie et al., 2017). External pH may be the discriminating factor for the cell's fate. Wu et al., (2019) notes that external acidic pH promotes cell fusion, while alkaline pH is associated with phagocytosis. Short time activity of P2X7 has been associated with a PS flip that was reversible, while the irreversible PS exposure associated with prolonged P2X7 activation initiates cell death (Mackenzie et al., 2005; Whitlock & Chernomordik, 2021). Blocking PS at the cell surface and inhibiting the scramblase TMEM16 inhibits osteoclast fusion (Whitlock & Chernomordik, 2021).

Finally, it has been proposed that P2X7 activity may play a role in lipid synthesis in macrophages, such as ceramide synthesis, which in turn may be affecting membrane composition and fluidity and thus indirectly, fusion capacity (Lépine et al., 2006; Raymond & Le Stunff, 2006).

In these ways, P2X7 expression by microglia or any GMC precursors, including macrophages, may in fact be supporting all key stages of GMC formation via cell fusion- phenotype acquisition, chemotaxis, cell contact and adhesion, and membrane fusion. While there is evidence in the literature to support both cell-fusion-mediated GMC formation and cytokinesis failure leading to multinucleation in microglia, it is likely that P2X7 expression contributes to the fusion competency of microglia. The pathways in which P2X7 expression may support GMC formation in microglia are shown in Fig.5.2.

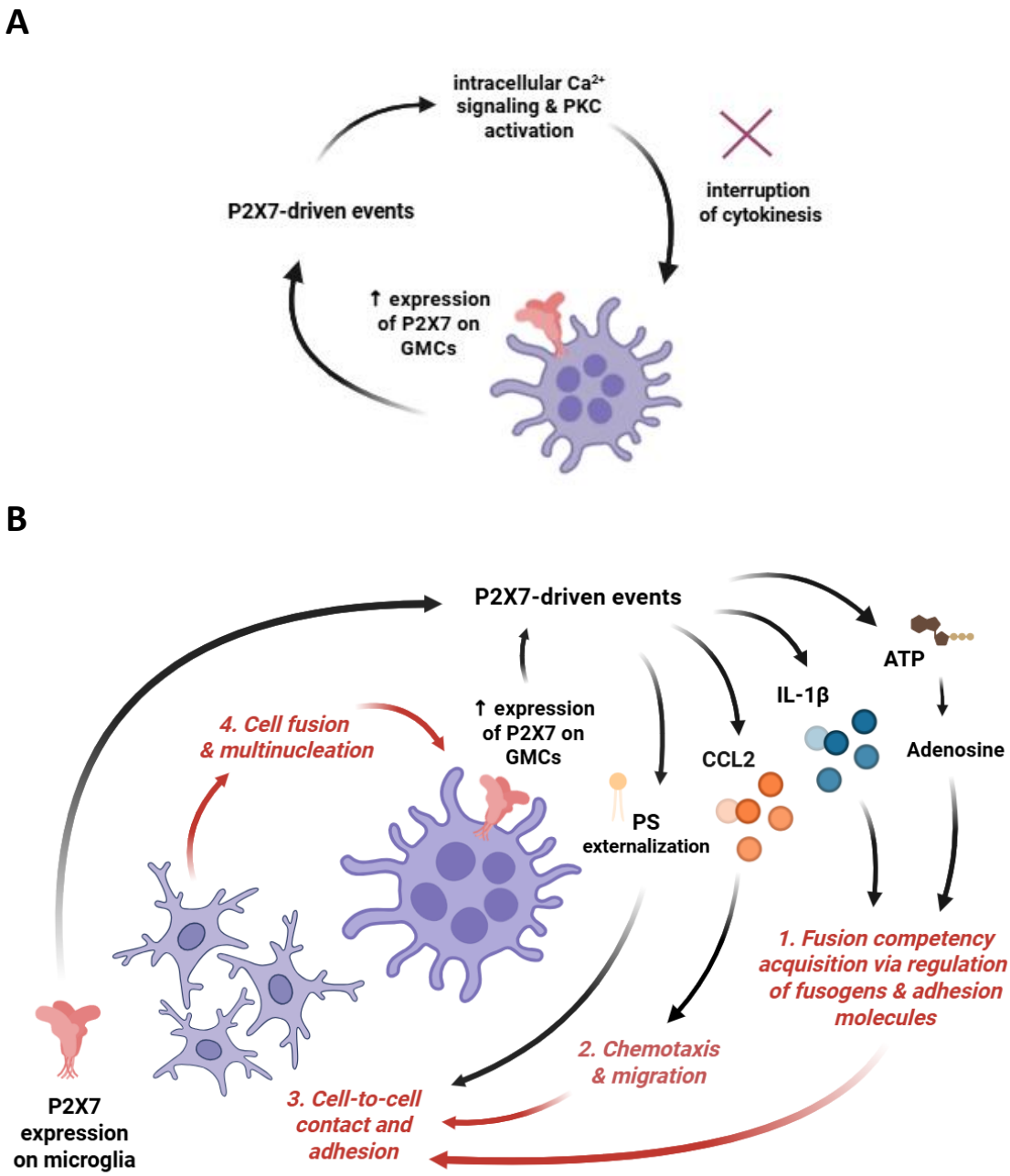

Figure 5.2 Ways in which P2X7 may support GMC formation. A *P2X7 may promote cytokinesis disruption via the PKC pathway.* ***B*** *P2X7 may be contributing to cell fusion. GMC formation via cell fusion requires four steps (pathway in red). 1. Acquisition of fusion competency; 2. Chemotaxis; 3. Cell-to-cell adhesion; 4. Cell fusion. P2X7 expression on microglia contributes to many local events (pathway in black), such as ATP, cytokine release, and PS externalization. ATP is metabolised to adenosine. Adenosine, as well as IL-1β, regulates the expression of fusion molecules, adhesion proteins, and integrins, which are important for the acquisition of a fusion-competent phenotype. CCL2 drives chemotaxis, which is essential for migration and interaction of mononucleated cells. P2X7 also affects PS exposure, which happens before cell membranes can fuse. Cell fusion occurs, and GMCs form, which highly express P2X7, completing the cycle. Figure generated in Biorender.*

5.2 Results

5.2.1 Effect of P2X7 expression on giant multinucleated cell formation in BV-2 and BV-2^{P2X7-}cells

During routine cell culture interesting morphological observations were made of BV-2 cells when grown to high confluency and when cultured with LPS stimulation. It became apparent that the cells were reaching very large sizes over the course of >72h. Upon staining with nuclear dye Hoechst 33342, multinucleation was observed in the large-sized cells (Fig.5.3). The sizes of the giant cells and the incidence of multinucleation appeared higher in the P2X7-expressing cells, compared to P2X7 deficient BV-2 clones. This was quantified in Fig.5.4.

Giant Multinucleated Cells (GMCs) are a phenomenon previously described in microglia (Hornik et al., 2014; Shtaya et al., 2019; Wenger & Luzi, 2024). The exact mechanism is still under dispute, but these cells are reported to form *in vitro* in response to prolonged stimulation with inflammatory molecules such as LPS, IL-13, TNF-α and IFN-γ, as well as in response to known multinucleating factor RANKL which is important in osteoclastogenesis in macrophages (Ahmadzadeh et al., 2022; Lösslein et al., 2021; Sabe et al., 2024). Hornik et al., (2014) described GMCs in BV-2 cell model and implicated failure of cytokinesis via the PKC as a pathway in their formation. P2X7 has never before been investigated in BV-2 cells as playing a role in multinucleation, although it has been investigated as driving GMC formation by cell fusion in transfected HEK cells and murine macrophages (Irma Lemaire et al., 2006). BV-2 and BV-2^{P2X7-} cells were tested for multinucleation under different conditions throughout this work and the effects of these stimulations are summarized in Table 5.1 later on in the chapter.

The size of the giant cells was measured using the image analysis software. The GMCs in images were highlighted, and the software was used to calculate the area of the cells. P2X7-expressing cells not only contained more numerous GMCs but also reached larger sizes within the 72h window. Morphological observations of cell cultures over 5-7 days suggest that both cell lines are capable of producing GMCs, which can reach even larger and comparable sizes if left for longer than 72h. Over 72h, spontaneous multinucleation would only occur in less than 2% of the total population, and with LPS induction, up to 16% of the total population would form GMCs.

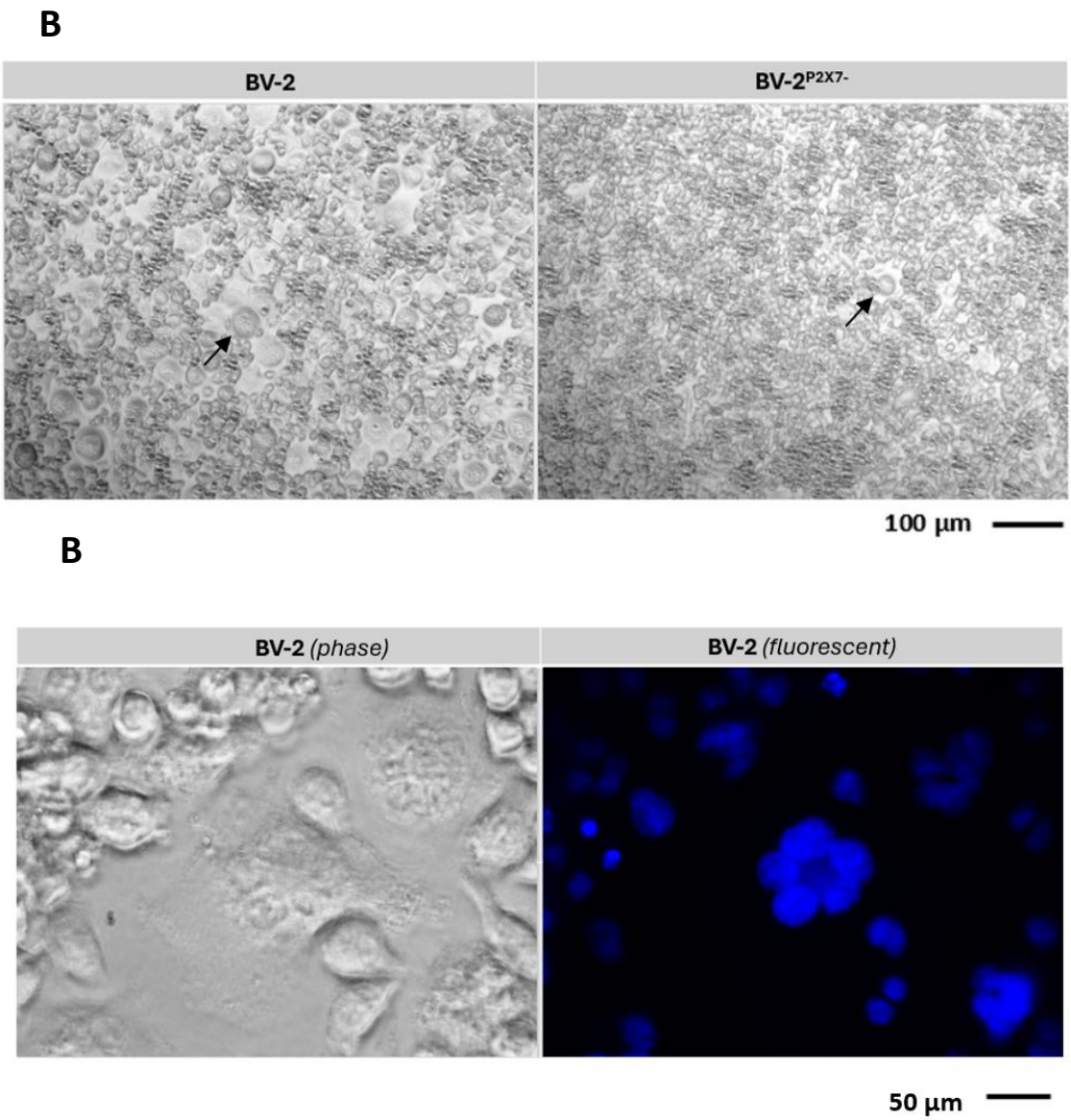

Figure 5.3 Giant multinucleated cell images in BV-2 and BV-2^{P2X7-} cells. *Giant cells spontaneously forming in confluent BV-2 cell cultures. Cells were left at high confluency without passaging but with feeding with fresh media for 72h.* ***A*** *Phase images taken with x10 objective of a light microscope. Black arrows show an example of a giant cell.* ***B*** *Images of Giant cells stained with Hoechst dye on a fluorescent microscope, as described in the method section. Images are representative of routine experiments.*

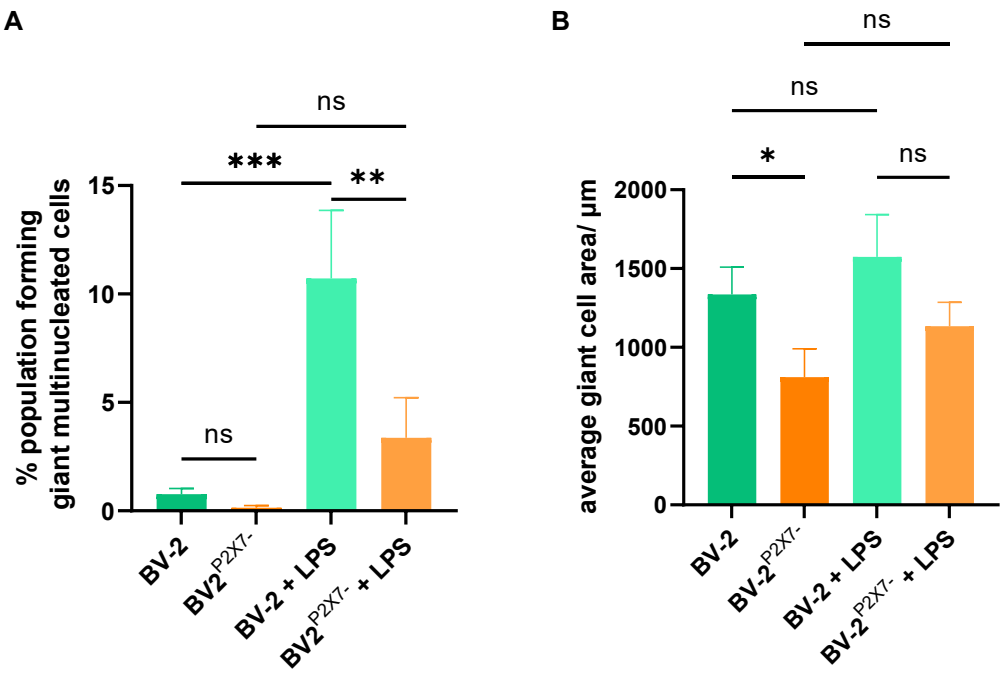

Figure 5.4 Quantification of formation of giant multinucleated cells in BV-2 and BV-2^{P2X7-} cells. *Cells were plated in 96-well plates with 0.5% serum-containing media for 72h with or without LPS (100 ng/mL). Cells were stained with Hoechst dye to stain the nuclei, as described in the method section.* ***A*** *GMC formation. Fluorescent and phase images were processed and counted as described in the method section.* ***B*** *Size of GMCs. The area of each cell was calculated using the software as described in the method section. Four largest cells were selected for each replicate and averaged. The data shows collated average of three independent experiments with three technical replicates for each condition. Analyzed with One-way ANOVA and Šídák's multiple comparisons test. (Statistical significance denoted by * p<0.05, ** p<0.01, *** p<0.001, ns not statistically significant).*

Hornik et al., (2014) showed that serum concentration does not affect multinucleation in BV-2 cells. It was also observed here that GMCs could form in low serum and high serum conditions. However, this was only briefly investigated here (data not shown), as it was observed that cells in complete media proliferated so quickly that it was difficult to calculate % of the GMC population due to overcrowding in the wells. It was, however, observed that multinucleation increased as the cells became older. This is shown in Figure 5.5. Both- spontaneously occurring GMCs and LPS-induced GMCs formed more readily in older cell cultures. Experiments were set up at different time points throughout the standard cell culture's life span, of approximately 12 weeks. Young cells set up under the same conditions formed visibly fewer giant cells than old and middle-aged cells.

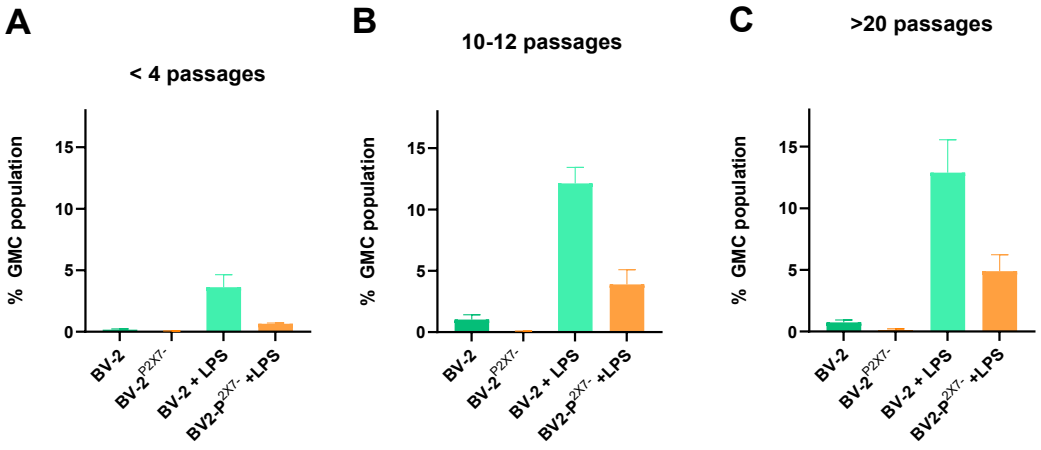

Figure 5.5 Multinucleation in BV-2 and BV-2^{P2X7-} over time in an aging cell population. *The graphs show results of three single experiments performed at different time points in cell culture life span.* ***A*** *Cells were young (passage number px 3).* ***B*** *Cells were in the middle of their life span (passage number px 11).* ***C*** *Cells were old and towards the end of their usage in cell culture and experiments (passage number px 20). Cells were seeded in 0.5% serum containing media in 96-well plates, with or without LPS 100 ng/mL present. Cells were incubated for 72h. Cells were stained with nuclear dye Hoechst and images were processed as described in the method section. The data shows collated average of three technical replicates of a single experiment for each age point representing a routine observation true over months of cell culture.*

The GMC formation in response to LPS exposure over 72h was further investigated by exposure to CLI-095, a TLR4 antagonist, to block the LPS response (Figure 5.6). In BV-2 cells, the LPS-induced morphological changes were abolished with the addition of 1µg/mL CLI-095, and multinucleation levels were comparable to the low numbers observed in unstimulated control wells- where a few sparse GMCs were still present. Lower concentration of CLI-095 was not as effective, but a reduced effect of LPS was observed. In BV-2^{P2X7-} cells, LPS-induced changes were abolished entirely in the presence of CLI-095, and only the treatment with LPS on its own showed GMC levels higher than control. This suggests that the P2X7-supported pathway may be independent of the LPS-induced pathway leading to GMC formation and the two might be occurring simultaneously in BV-2 microglia.

To better understand different induction pathways leading to GMC formation in BV-2 and BV-2^{P2X7-} cells, the effect of different factors on GMC formation was investigated by setting up 96-well plates with different stimulations in 0.5% serum media (Table 5.1. and Figure A.2 in Appendix). Wells were inspected daily for GMC formation, however, the only observable changes were noted at 72h, at which point images of the wells were taken. LPS stimulation was used as a positive control and a reference point for high GMC formation. Unstimulated control wells contained few GMCs.

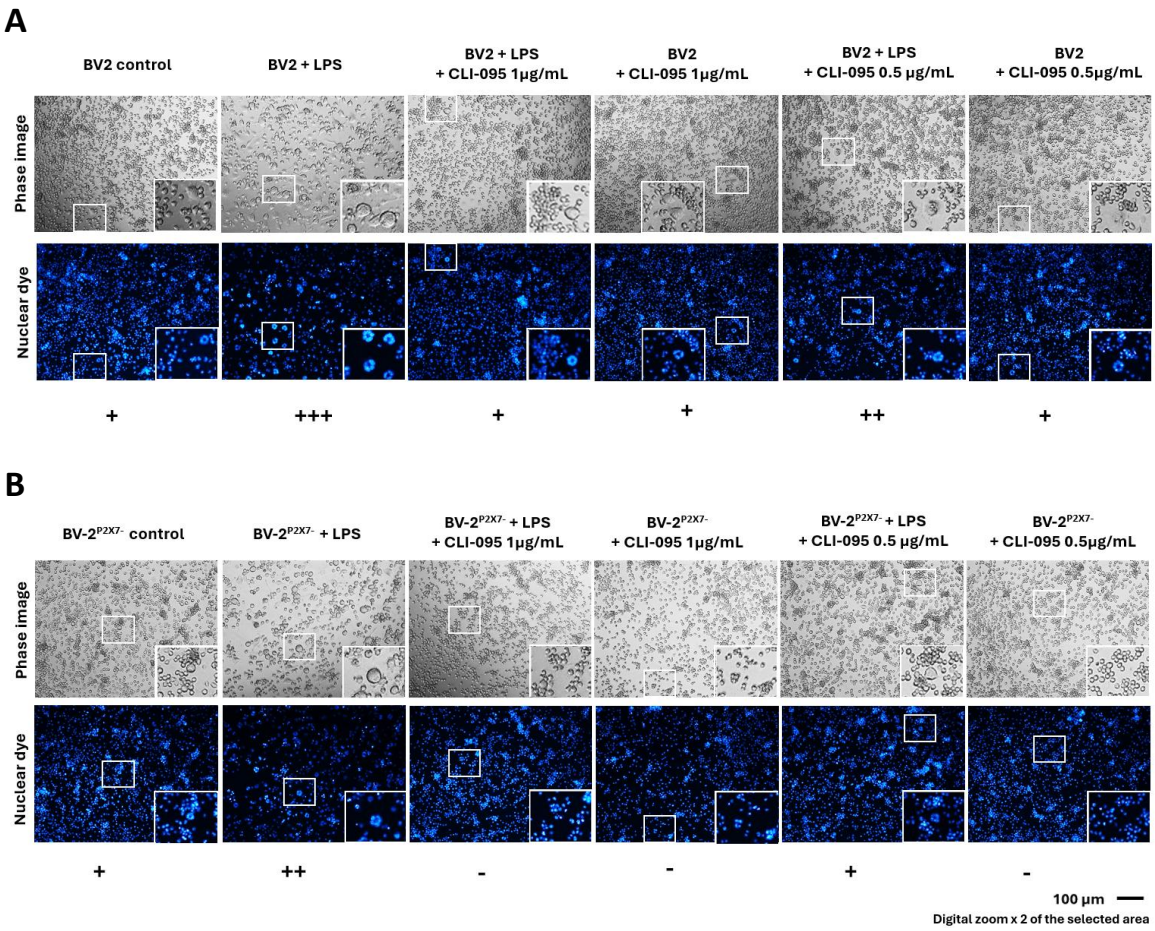

Figure 5.6 Effect of CLI-095 on LPS-induced GMC formation. *BV-2 cells (**A**) and BV-2^{P2X7-} (**B**) cells were seeded in 96-well plates at 9000 cells/well in 0.5% serum media +/- LPS 100ng/mL +/- CLI-095 at concentrations 1 µg/mL or 0.5 µg/mL and incubated for 72h. Hoechst nuclear dye 2 µg/mL was used to stain the nuclei in each well. Cells were photographed using the x10 objective for the most representative capture of the population in the well. Digital zoom x 2 of example areas with giant cells was done post-imaging. Phase images and Fluorescent nuclear images were assessed and scored for multinucleation (**-** none GMCs present, **+** few GMCs present, **++** some GMCs present, **+++** many GMCs present). The images shown are a representative of two independent experiments with three technical replicates for each condition.*

Some classical activators of microglia, such as chemokine CCL2, cytokines such as IL-13 and IL-4, TNF-α, and IFN-γ were previously reported in literature in relation to GMC formation (Cao et al., 2016; Hornik et al., 2014; Mcnally & Anderson, 1995; Sabe et al., 2024; Suzumura et al., 1999),and they were all tested in this work (Table 5.1. and Figure A.2 (Appendix)). Poly(I:C) was used as a stressor of a viral origin, but it did not have the same effect as bacterial LPS and did not induce GMC formation higher than the unstimulated control. LPS was tried at a higher concentration of 1µg/mL, and the previously used concentration of 100ng/mL. Higher concentration of LPS did not induce many more GMCs than the lower concentration; however, it did visibly slow down the proliferation of the cells even further. For the remainder of the experiments, LPS was used at the previously investigated lower level of 100ng/mL, which in Chapter 4 was shown to be sufficient to

induce an activated phenotype in the cells. P2X7 positive modulators such as polymyxin B, clemastine, and natural ginsenoside CK were also tested in combination with or without LPS. HEI3090 is a known positive modulator of the mouse P2X7 receptor. TNF-α, HEI3090, CK, and CCL2 were the only compounds which resulted in an observable change to GMC numbers, other than LPS. Some of the compounds such as polymyxin B and clemastine are known to interact with LPS (H. Kang et al., 2023; Padhy et al., 2024) and indeed when co-administered with LPS, instead of enhancing the P2X7-driven GMC formation, they reduced it, likely by counteracting the action of LPS. CCL2 also did not act in synergy with LPS.

A selection of neurosteroids, some of which were previously demonstrated to affect P2X7 activity (Chapter 4), were also tested for GMC induction over 72h. The neurosteroids did not increase GMC formation. Interestingly, however, in the presence of allopregnanolone and pregnanolone, no GMCs were observed at all. P2X7 antagonists, Az106 06120 and JNJ-47965567, were tested on their own and in combination with LPS to see if they could bring down GMC formation to the same level as in BV-2^{P2X7-} cells, however, they did not have an impact at the concentrations tested and did not lower the GMC formation. ATP was only tested at low concentrations of 10µM and 50µM, as higher concentrations over 72h had a negative effect on the BV-2 cell viability. Low concentrations of ATP did not increase GMC formation. Low glucose media (4mM) was also tested as an additional stressor to low serum, however the increase in GMCs was minor and inconsistent throughout the replicates.

As supported by images in Figure A.2 (Appendix), P2X7-expressing BV-2 cells in all conditions showed an advantage over the BV-2^{P2X7-} cells. Although LPS is by far the strongest inducer of GMCs, TNFα, CCL2, CK, polymyxin B, and HEI3090 also increased the number of GMCs in BV-2 cells above the control levels in the images.

AZ10606120 and JNJ-47965567 are both antagonists of P2X7 highly selective for this purinergic receptor that bind at allosteric sites of the receptor. The effect of Az10606120 and JNJ-47965567 on P2X7 responses in BV-2 cells was demonstrated in Figure A.1 (Appendix), where it was shown to effectively inhibit P2X7 activity in a dose-response curve to ATP. The effect of P2X7 antagonists Az10606120 and JNJ-47965567 was tested on GMC formation in BV-2 and BV-2^{P2X7} cell lines with and without LPS present. Pharmacological blockage of the receptor with antagonists was not able to reduce the spontaneous or LPS-induced GMC formation in BV-2 cells (Figure 5.7).

Table 5.1 Summary of various compounds tested for the induction of GMC formation on BV-2 and BV-2^{P2X7-} cell lines. *The table contains summarized information pooled from all experiments performed, including imaging data and GMC counts. For all experiments, the cells were plated in 96-well plates at density of 9000 cells/well, in 0.5% serum-containing media and incubated for 72h with the compounds at various concentrations (indicated in the table). The formation of GMCs is expressed relative to LPS (100 ng/mL) and positive control for each cell line respectively, without directly comparing BV-2 and BV-2^{P2X7-} cell lines.*

Common microglial activators, cytokines and GMC factors	BV-2	BV-2^{P2X7-}	Comments
Unstimulated (control)	+	+	Few GMCs visible (approx. 2%)
LPS 100 ng/mL (positive control)	+++	+++	Visibly more GMCs than control (approx. + 10%)
LPS 1 µg/mL	+++	+++	Visibly more GMCs than control (approx. + 10%)
IL-13 20 ng/mL	-	-	Cells were very small in size and round, migrating across wells and clumping together, many detaching from the surface. Fewer GMCs than in control wells (unstimulated) or none present.
IL-4 20 ng/mL	-	-	Cells were very small in size and round, migrating across wells and clumping together, many detaching from the surface. Fewer GMCs than in control wells (unstimulated) or none present.
IFN-γ 50 ng/mL	+	+	Few GMCs present
Poly(I:C) 100 ng/mL	+	+	Few GMCs present
TNFα 50 ng/mL	++	++	Visibly more GMCs
CCL2 10 µM	++	++	Visibly more GMCs
RANKL 100 ng/mL	++	++	Visibly more GMCs
PMA 50 ng/mL	++	++	GMCs present, however, some cell death, cells clumping together and phagocytosing each other. Not possible to take representative images to compare BV-2 and BV-2^{P2X7-} cell lines.
Low Glucose (4 mM) media	++	++	Some GMCs present, but inconsistent across replicates
Neurosteroids with possible activity on P2X7	BV-2	BV-2^{P2X7-}	Comments
Testosterone 10 µM	+	+	Some GMCs
Alfaxalone 10 µM	+	+	Some GMCs
Allopregnanolone 10 µM	-	-	Fewer GMCs than in control (unstimulated) or none present; cells are small in size.
Pregnanolone 10 µM	-	-	Fewer GMCs than in control (unstimulated) or none present; cells are small in size.
Positive modulators of P2X7	BV-2	BV-2^{P2X7-}	Comments
Clemastine 1 µM	+	+	Few GMCs
HEI3090 250 nM	++	+	Some GMCs, more in P2X7 expressing cells
CK 5 µM	++	+	Some GMCs, more in P2X7 expressing cells
ATP 10 µM (P2X7 agonist)	-	-	Fewer GMCs than in control (unstimulated) or none present
ATP 50 µM (P2X7 agonist)	-	-	Fewer GMCs than in control (unstimulated) or none present
Antagonists of P2X7	BV-2	BV-2^{P2X7-}	Comments
Az10606120 1 µM	+	+	Some GMCs, comparable to unstimulated control wells
Az10606120 1 µM + LPS 100 ng/mL	+++	+++	Visibly more GMCs than control (approx. + 10%), comparable to LPS control wells
JNJ-47965567 1 µM	+	+	Some GMCs, comparable to unstimulated control wells
JNJ-47965567 1 µM + LPS 100 ng/mL	+++	+++	Visibly more GMCs than control (approx. + 10%), comparable to LPS control wells

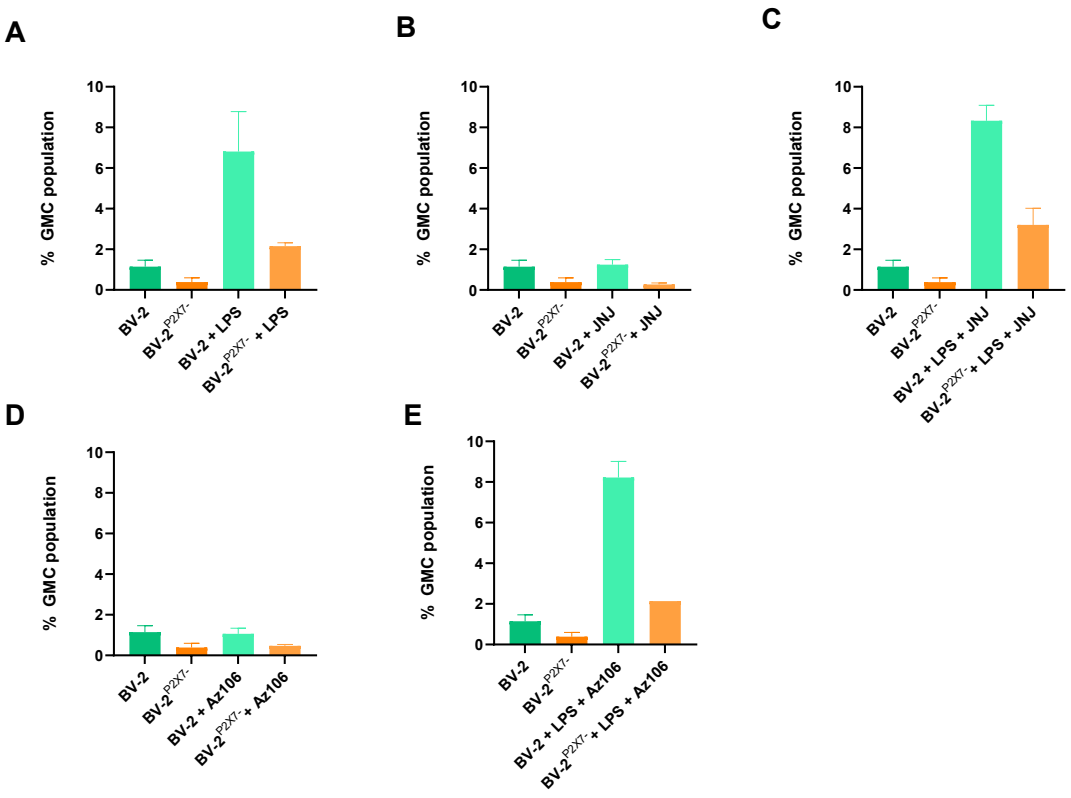

Figure 5.7 Effect of P2X7 antagonists on GMC formation. *Effect of P2X7 antagonists AZ10606120 (Az106) and JNJ-47965567 (JNJ) on multinucleation was quantified by counting GMCs in the images as percentage of total population. Cells were plated in 96-well plates at density 9000 cells/well, stimulated in 0.5% serum containing media and incubated for 72h with DMSO only (vehicle control), LPS 100 ng/mL (positive control) (**A**), JNJ 1 µM (**B**) or JNJ 1 µM + LPS 100 ng/mL (**C**) or Az106 1 µM (**D**) or Az106 1 µM + LPS 100 ng/mL (**E**). 10 x objective was used to capture the widest image. Three images were taken per well for accurate representation, as described in the method section. The data shows collated average of three technical replicates per condition in one experiment.*

CCL2 chemokine has been shown to be important for GMC formation in macrophages (Kyriakides et al., 2004). In Chapter 4, it was demonstrated that BV-2 and BV-2^{P2X7-}cells release CCL2 in abundance in response to LPS treatment. CCL2 may be part of the LPS-induced pathway leading to multinucleation in BV-2 microglia. The effect of CCL2 chemokine was quantified on GMC induction, with and without LPS present (Fig.5.8). CCL2 induced GMC formation slightly higher than control, although this was not statistically significant when quantified. Again, in BV-2^{P2X7-} cells, GMC formation remained similar to unstimulated control, and increased a little only when stimulated with LPS (positive control). CCL2 did not act in synergy with LPS and seemed to fully block its effect- when co-administered, the GMC numbers stayed as low as in the unstimulated control.

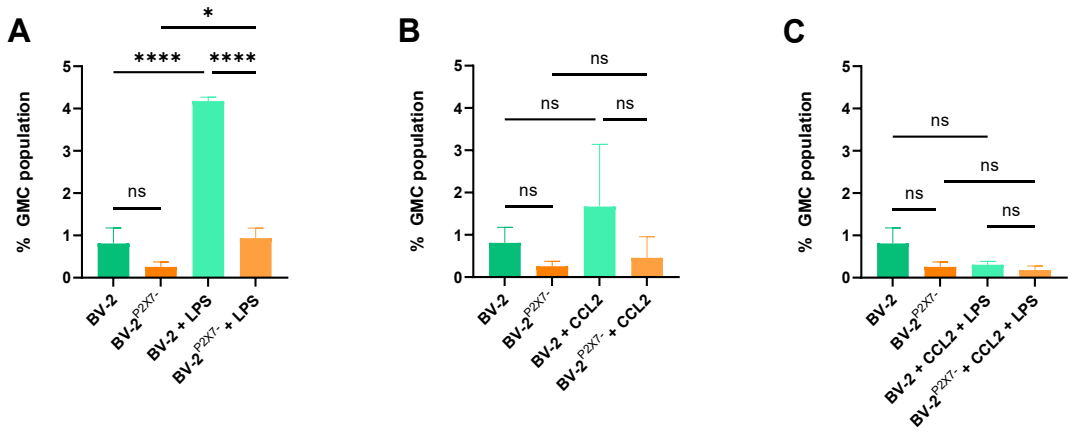

Figure 5.8 Effect of CCL2 on GMC formation. *Cells were plated in 96-well plates at density 9000 cells/well, stimulated in 0.5% serum containing media and incubated for 72h with DMSO only (vehicle control) (**A**), LPS 100 ng/mL (positive control) (**B**), CCL2 10 µM or CCL2 10 µM + LPS 100 ng/mL (**C**). Three images were taken per well for accurate representation and processed as described in the method section. The data shows GMCs as % population. Collated average of three independent experiments with three technical replicates for each condition. Analyzed with One-way ANOVA and Šídák's multiple comparisons test. (Statistical significance denoted by * p<0.05, **** p<0.0001, ns not statistically significant).*

HEI3090, Polymyxin B and CK are both effective positive allosteric modulators (PAMs) of P2X7. PAMs bind to a different site on the receptor than the agonist site and increase the receptor's affinity and response to the agonist. Effects of Polymyxin B, CK, and HEI3090 on GMC formation were further quantified by counting the GMCs in the images as a percentage of the total population (Fig.5.9, and Fig.5.10). Because the GMC formation was still relatively low in the presence of HEI3090 (Fig.5.9), and the increase was not statistically significant, Polymyxin B and CK were assessed on cells already stimulated with LPS to see if P2X7 PAMs could increase the multinucleation further. Polymyxin B and CK were also assessed on their own but the data was very variable and is not shown here. Some images are available in Figure A.2 (Appendix). CK + LPS and Polymyxin B + LPS resulted in GMC numbers significantly higher than those of the unstimulated control, but less than LPS alone- when co-administered with LPS, they both limited its effect (Figure 5.10). BV-2^{P2X7-} , when stimulated with P2X7 PAMs, showed no GMC formation. LPS on its own was the most effective stimulant for the induction of GMCs, and P2X7 modulators did not act in synergy with LPS, lowering its effect. Polymyxin B is thought to interact with LPS to exert its antimicrobial activity (Padhy et al., 2024). CK was shown to reduce the LPS-induced inflammatory gene profile in RAW 264.7 macrophages (H. Kang et al., 2023). CK + LPS was still effective at inducing multinucleation compared to unstimulated control, but the sizes of the multinucleated cells were generally not as large as those of LPS-induced GMC (Figure A.2 (Appendix)).

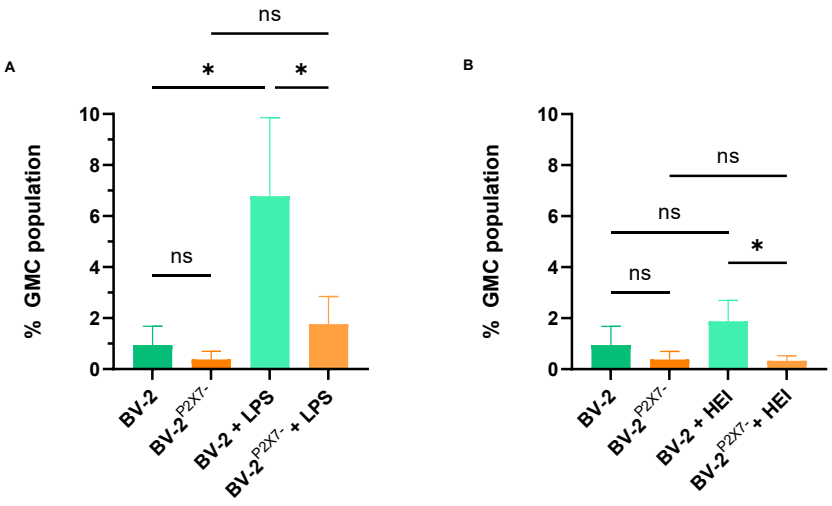

Figure 5.9 Effect of P2X7 positive modulator HEI13090 on GMC formation. *Cells were plated in 96-well plates at density 9000 cells/well, stimulated in 0.5% serum containing media and incubated for 72h with DMSO only (vehicle control) or LPS 100 ng/mL (positive control) (**A**) or HEI13090 250 nM (**B**). Three images were taken per well for accurate representation, and processed as described in the method section. The data shows GMCs as % population. Collated average of three independent experiments with three technical replicates per condition. Analyzed with One-way ANOVA and Šídák's multiple comparisons test. (Statistical significance denoted by * p<0.05, ns not statistically significant).*

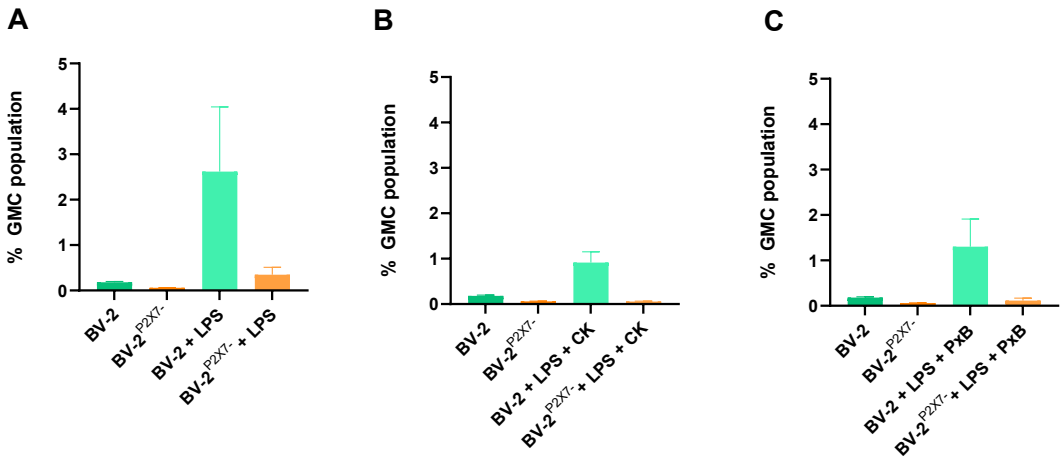

Figure 5.10 The effect of positive allosteric modulators, Polymyxin B and ginsenoside CK, on enhancing GMC formation with LPS. *Cells were plated in 96-well plates at density 9000 cells/well, stimulated in 0.5% serum containing media and incubated for 72h with DMSO only (vehicle control), LPS 100 ng/mL (positive control) (**A**), CK 1 µM (**B**) and Polymyxin B 10 ng/mL (**C**). Three images were taken per well and processed as described in the method section. The data shows collated average of two independent experiments with three technical replicates per condition. GMCs as % of total population.*

Denlinger et al., (2001); and Watters et al., (2001) showed that LPS may be interacting with P2X7 under certain optimal conditions and inhibiting its activity. It was next investigated whether LPS may directly affect the activation of P2X7 using a fura-2 assay to measure direct activation of the receptor (Figure 5.11). Dose-response curves to ATP were generated in the presence of a positive modulator of mP2X7 HEI3090 (1 µM) and LPS (100 ng/mL), to verify their activity at P2X7. Preincubation with HEI3090 1µM and LPS 100ng/mL resulted in a small shift of the dose-response curve to the left, demonstrating that a lower concentration of the agonist was now needed to evoke the response (EC50 changed from 251 µM with DMSO to 126 µM in the presence of HEI3090). LPS also resulted in a shift to the left (EC50 99 µM) and increased the maximal response to the agonist. HEI3090 250 nM was also trialled, but it did not change the immediate response of P2X7 away from the control at this concentration. The 250 nM concentration, however, would still be used in long exposure experiments with HEI3090, such as the 72h incubation timepoints.

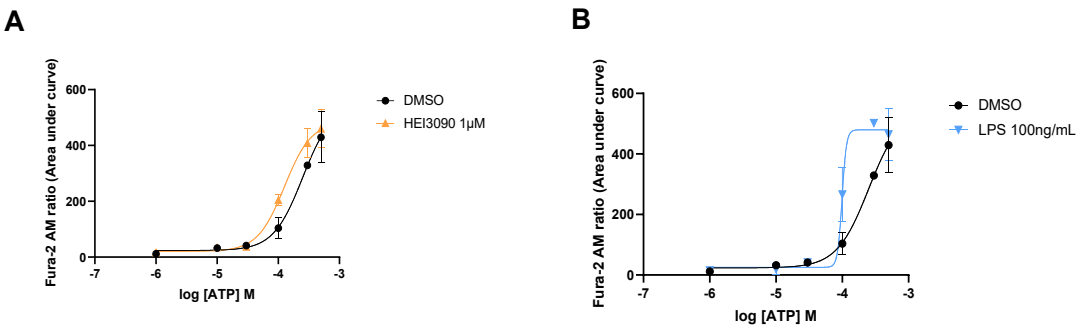

C

compound	EC50 (µM)	Confidence Interval (CI)
DMSO	251	152 to ?
HEI3090	126	97 to 262
LPS	99	? to 129

Figure 5.11 ATP dose-response curves of BV-2 cells in the presence of mP2X7 positive modulator HEI13090 and LPS vs vehicle control (DMSO). *Standard Fura-2 AM protocol was followed on a confluent plate of BV-2 cells. Cells were loaded with Fura-2-AM dye for 1h and responses were measured after pre-incubation with the compounds for 15-60 minutes. ATP concentrations used to obtain the dose-response curve were 1 mM, 500 µM, 300 µM, 100 µM, 50 µM, 30 µM. Three independent experiments were performed while the locations of the conditions on the plates were varied for a representative average. An average of the three independent experiments with three technical replicates per condition is shown .* ***A*** *HEII13090 at concentration 1 µM vs DMSO solvent control.* ***B*** *LPS 100 ng/mL vs DMSO control. EC50 was calculated from the plots (****C****).*

5.2.2 Activity and function of giant multinucleated microglia

Many theories have been proposed for the biological function of GMCs and the advantage of cell fusion ability. In osteoclasts, cell fusion supports the high energy demand by providing the GMC with a high number of active mitochondria (Teitelbaum, 2007). Mitochondrial mass in GMC BV-2 and BV-2^{P2X7-} cells was assessed to get a better understanding of GMCs mitochondrial numbers compared to small cells. MitoTracker dyes were used to investigate mitochondrial mass in different populations of BV-2 and BV-2^{P2X7-} cells, gated according to cell size using flow cytometry. Small and Giant cells, as well as a total population comprising different sizes, were compared. First, the cells from standard growth flasks were stained with MitoTracker Deep Red and compared to each other in a wide gate, which comprised all the large, small, and average-sized cells (Figure 5.12 A). Then the cell cultures rich in giant cell populations were stained and compared in the same way, with two gates set, one capturing small cells and one capturing the largest cells on the scatter plot (Figure 5.12 B). The data, together with Chapter 3 findings, corroborate the evidence that there is no difference in mitochondrial mass between P2X7-expressing or P2X7-deficient cells. However, the difference between a sample of small cells and giant cells is significant, and this is true for both cell lines, suggesting that giant cells are characterized by higher mitochondrial mass, proportional to their size.

This confirmation of different mitochondrial numbers, depending on cell size, prompted an experiment to see whether populations of BV-2 cells rich in giant cells process the Alamar Blue dye differently from small cells. To answer the question whether cultures rich in giant cells process the resazurin dye more efficiently, due to a higher number of mitochondria in giant cells, populations of normal and GMC-rich (GMC+) cultures of BV-2 and BV-2^{P2X7-} cells were used. Cells were set up at known densities of either 40,000 (Figure 5.13 B) or 20,000 cells/well (Figure 5.13 A) in a 96-well plate, and after allowing the cells to settle, given Alamar Blue dye to process in the usual assay protocol. The wells containing GMC+ populations in both cell lines gave much higher fluorescence readings, compared to the populations of 'normal' cells.

In Chapter 3, it was observed that Alamar blue processing was reflective of NQO1 activity in the cells. NQO1 activity in GMC+ populations was compared to a population from 'normal' flasks (Figure 5.14). Cells from both populations were plated at equal density in a 96-well plate, and NQO1 assay was performed according to the manufacturer's protocol. GMC+ populations scored higher values, showing higher levels of NQO1 activity compared to smaller cells (Figure 5.14). This was true for both BV-2 and BV-2^{P2X7-} cell lines, although the difference in BV-2 cells appeared greater.

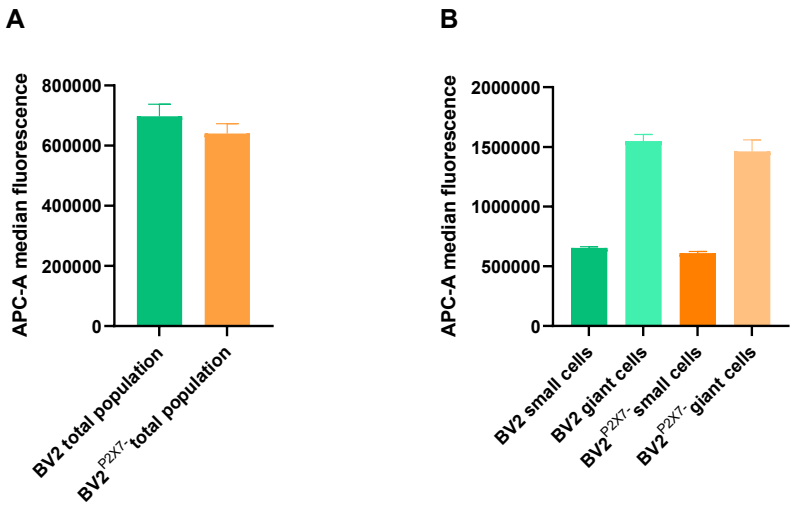

Figure 5.12 Mitochondrial mass in BV-2-derived GMCs vs Small Cells and total cell population. *Giant multinucleated cell-enriched populations (GMC+) were obtained from middle-aged cells which were cultured to high confluency and maintained by changing the media daily instead of passaging the flasks. Cells were pre-grown in complete media in growth flasks. Populations rich in GMCs were used. Cells were trypsinized out and stained with Mitotracker Deep Red dye according to the manufacturer's protocol. The fluorescent signal was recorded by flow cytometry using three different gated population of healthy cells – small cells, giant cells, and a total population comprising all cells in the sample.* ***A*** *total population* ***B*** *small vs giant cells. The data are an average of two independent experiments with four technical replicates for each condition.*

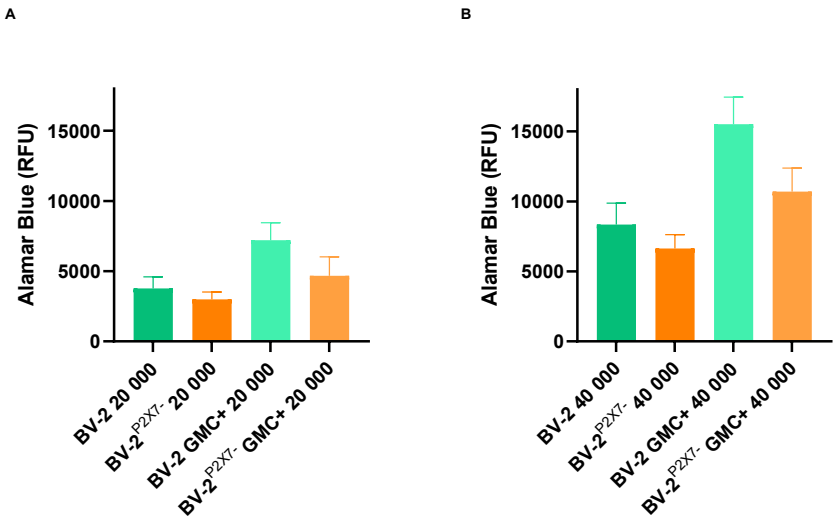

Figure 5.13 Processing of Alamar blue Resazurin dye in GMC enriched vs small cell cultures. *Giant Multinucleated Cell-enriched populations (GMC+) were obtained from middle-aged populations of cells, which were cultured to high confluency and maintained by changing the media daily instead of passaging the flasks. Cells were plated in 96-well plates in 0.5% serum media at densities of either 20,000 cells/well (**A**) or 40,000 cells/well (**B**). Cells were allowed to settle in the plate for 2 hours. Alamar Blue was performed according to the standard protocol and allowed to process for an additional 2h. The data are the average of two independent experiments with three technical replicates for each condition.*

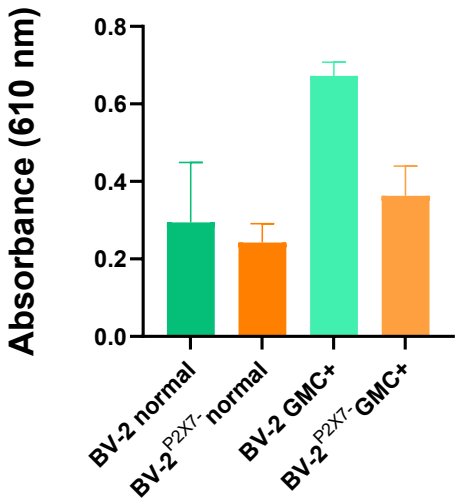

Figure 5.14 NQO1 Activity in GMC+ vs small cell cultures in BV-2 and BV-2^{P2X7-} cells. *Giant Multinucleated Cell-enriched populations (GMC+) were obtained from middle-aged populations of cells which were cultured to high confluency and maintained by changing the media daily instead of passaging the flasks. Cells from different cultures were seeded at 20 000 cells/ well in 0.5% serum media and incubated overnight (18h) before performing the assays. NQO1 assay ELISA protocol was followed according to the manufacturer's instructions, with extended processing time of 6h and absorbance was recorded using a plate reader. The data shows average of two independent experiments with three technical replicates per condition.*

It was next considered whether factors are secreted by GMCs that recruit and stimulate normal cells towards the GMC fate. This was investigated by exposing normal cell cultures to supernatants from GMC+ cultures and documented by imaging (Figure 5.15). Enhanced GMC formation in a fresh culture of BV-2 cells, as a result of the media swap for GMC+ culture supernatant, suggests that factors may be secreted into the media by GMCs that stimulate multinucleation further.

The wells which received GMC+ supernatants showed the most GMCs present. The wells which received conditioned media from normal BV-2 and BV-2^{P2X7-} cultures also scored higher than the control cells which received fresh media. BV2^{P2X7-} cells which received supernatant from BV-2 GMC+ cells (Figure 5.15) did not show enhanced GMC numbers compared to controls. This suggests that a P2X7-specific path may be involved.

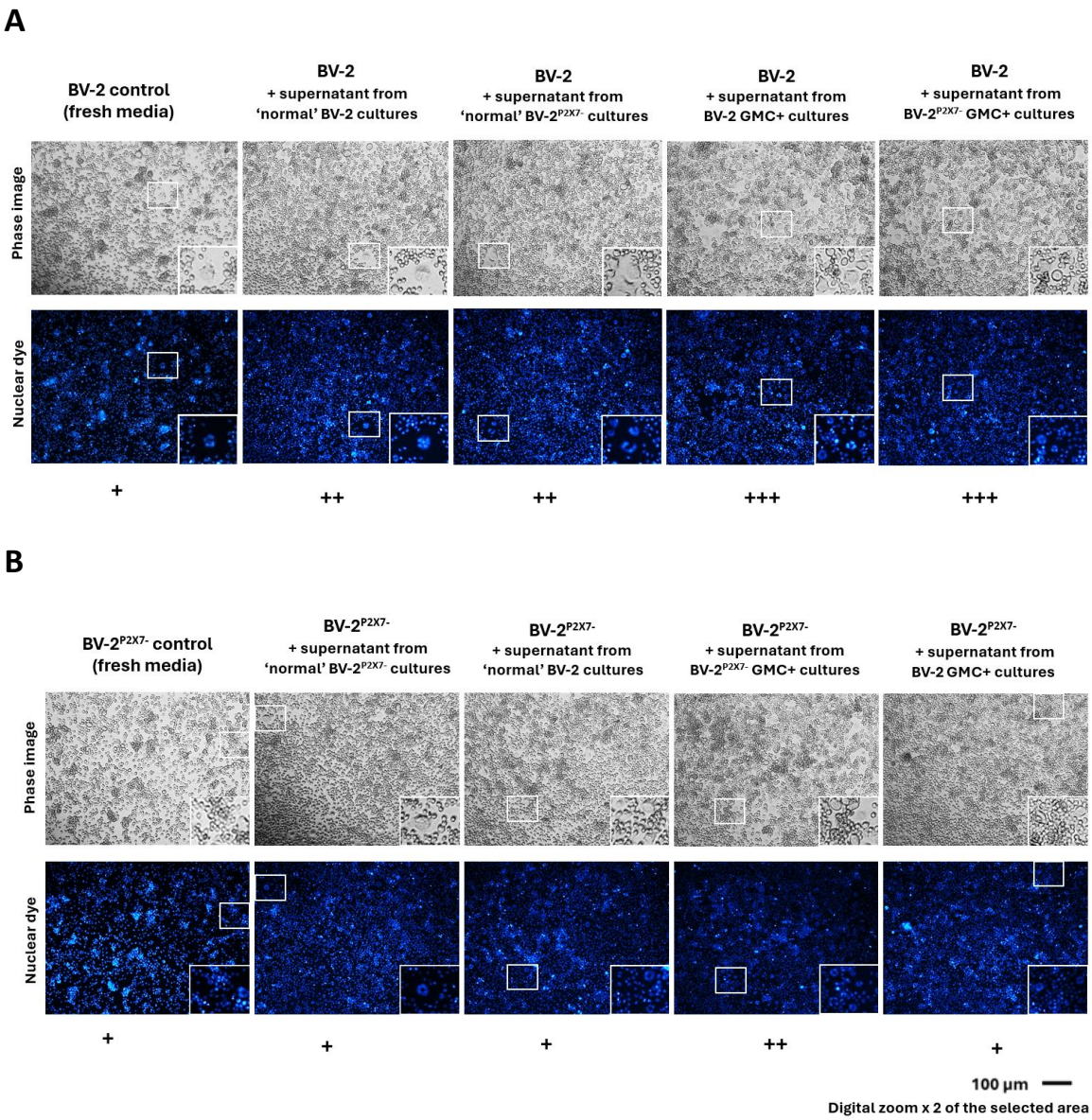

Figure 5.15 Effect of GMC+ culture supernatant on GMC formation in small cell culture cells in BV-2 and BV-2^{P2X7-} cells. *Giant Multinucleated Cell enriched populations (GMC+) were obtained from middle-aged populations of cells which were cultured to high confluency and maintained by changing the media daily instead of passaging the flasks. Cells from different cultures were seeded at 9000 cells/ well in 0.5% serum media and incubated overnight.* ***A*** *BV-2 cells.* ***B*** *BV-2^{P2X7-}cells. Media was carefully removed using a multichannel and swapped on the plates. Supernatant from GMC+ cultures was applied onto the wells or fresh media or supernatant from 'normal' small cell cultures. Cells were incubated for 72h and representative images were taken of the middle of the well for each condition on the plate and processed as described in the method section. Digital zoom x 2 of selected areas in the images were created post-imaging. Images were assessed and scored for multinucleation (***-*** none GMCs present,* ***+*** *few GMCs present,* ***++*** *some GMCs present,* ***+++*** *many GMCs present). Representative images of one biological experiment with three technical replicates per condition.*

It was investigated whether GMCs have a better ability to survive in challenging conditions. Serum deprivation and glucose deprivation result in cell death in all BV-2 populations. An experiment was set up where populations rich in spontaneously occurring GMCs (GMC+) were compared to

normal BV-2 cultures in extreme conditions of serum and glucose deprivation (GLC-/SFM) overnight (Figure 5.16). A standard Alamar blue assay experimental design was used across two plates for each cell line, on which GMC+ vs normal cells were seeded at the same densities. One plate had media changed over to GLC-/SFM, while the other plate did not (control). The plates were left overnight and photographed the next day before performing a Alamar blue viability assay. Data was presented as % of maximum survival (control unchallenged plate) to account for any differences in dye metabolism. GMC+ populations did not have an advantage over 'normal' cells in terms of viability in Alamar blue assay. However, in the images, it seems that many giant cells remain in the culture, retaining a healthy morphology, while the small cells look very shriveled (Figure 5.16 B). This would be interesting to follow by trypan blue staining in the culture following the GLC-/SFM challenge.

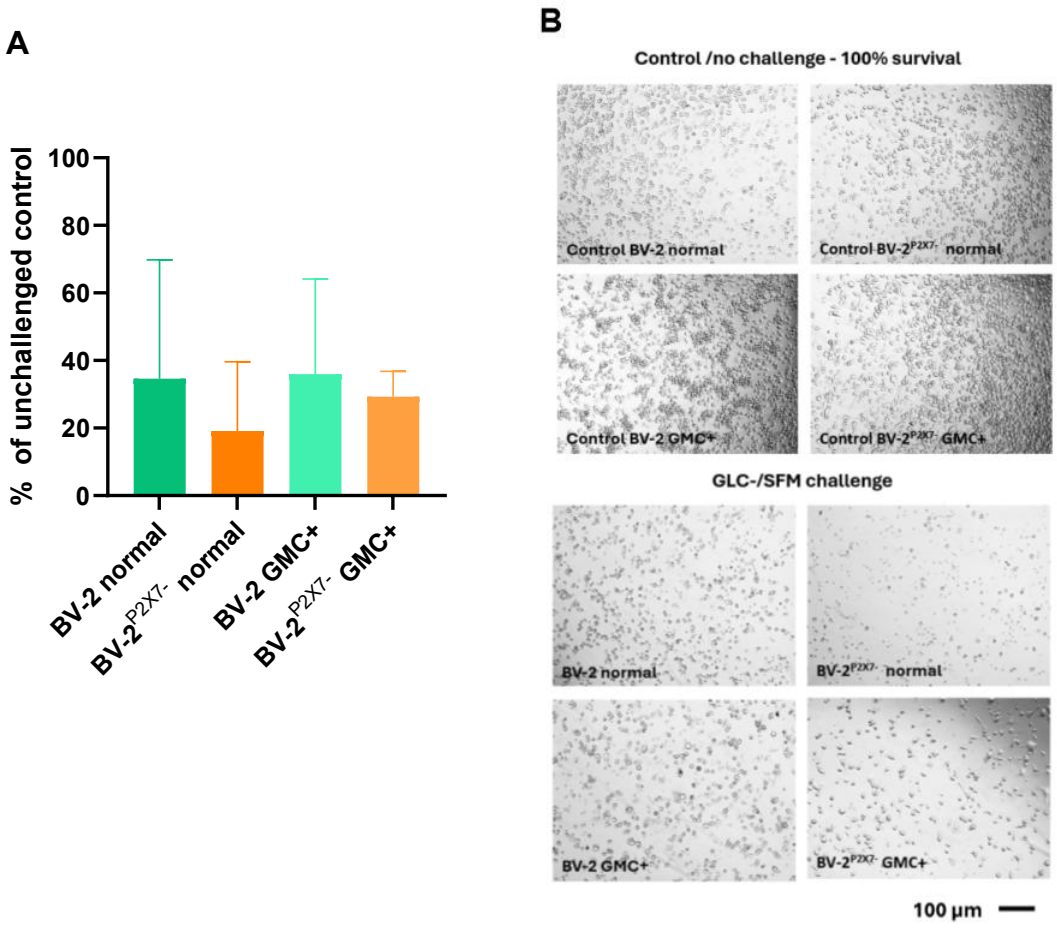

Figure 5.16 Survival to GLC-/SFM challenge in BV-2 and BV-2^{P2X7-} GMC+ populations. *Cells were plated at 9000 cells/well in complete media in two 96-well plates and allowed to incubate overnight. Cells were then subjected to a media swap using a multichannel pipette. One plate had media swapped for GLC-/SFM and the control plate had the media pipetted gently once up and down with a multichannel to mimic the swap. The plate was incubated for 24h. Images were taken at 24h (**B**) and a standard Alamar Blue assay (3h processing time) (**A**). For each cell line the data was normalized to the control plate where each condition was taken as the maximum survival. The figure shows average of two independent biological experiments with three technical replicates for each condition. X10 images were taken with Nikon Ti Eclipse microscope.*

GMCs may have a survival advantage to small mononucleated cells and appear to have a metabolic advantage in resazurin dye processing (Figure 5.13) due to higher mitochondrial mass per cell (Figure 5.12). In theory, the metabolic advantage visible in Alamar blue assay may also be partially due to a higher glycolytic metabolism in these cells. Highly glycolytic microglia upregulate expression of glucose transporters such as GLUT1 (L. Wang, Pavlou, et al., 2019). Therefore, their uptake of glucose should be higher. Glucose uptake was investigated in giant cells compared to small cells by flow cytometry using fluorescent 2-NBDG glucose, which is structurally similar to glucose and taken up through glucose transporters; however, it cannot be metabolized by the cells and thus accumulates inside. No difference was found between different populations of small, giant, or total cells of BV-2 and BV-2^{P2X7-} microglia, originating either from normal cell culture, LPS-stimulated or older GMC+ rich cultures. No difference was observed regardless of P2X7 presence. Figure 5.17 shows the same magnitude of shift away from control on the histograms obtained.

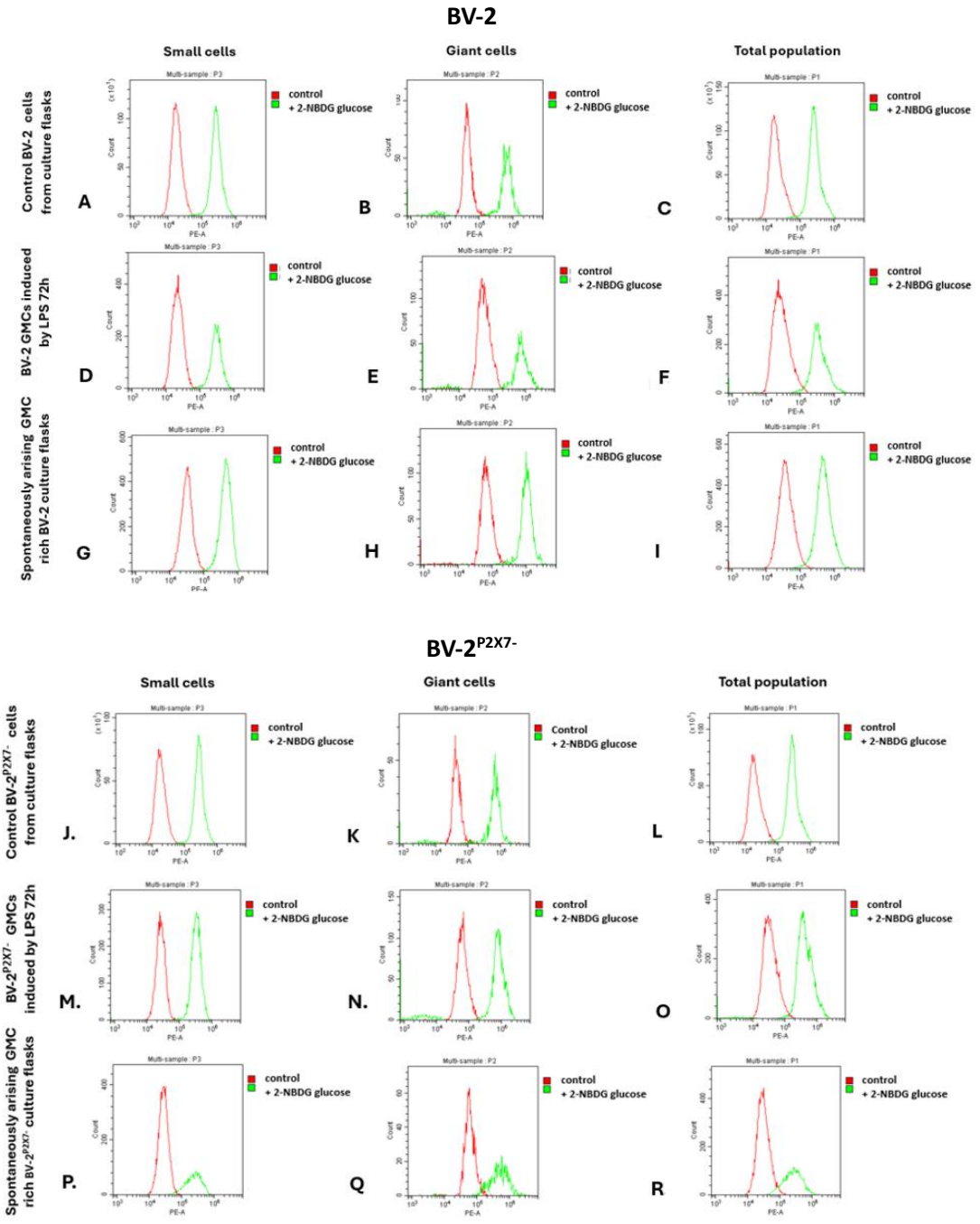

Figure 5.17 Glucose uptake by flow cytometry in BV-2 and BV-2^{P2X7-} populations of cells gated by size. *Cells were taken from three different culture setups- control- 'normal' unstimulated cells from the flasks BV-2 (**A**, **B**, **C**) and BV-2^{P2X7-} (**J**, **K**, **L**) , or cultures incubated with LPS 100 ng/mL for 72h to induce GMC formation in BV-2 cells (**M**, **N**, **O**) and BV-2^{P2X7-} (**D**, **E**, **F**) , and from cell cultures which accumulated more spontaneously arising GMCs in BV-2 cells (**G**, **H**, **I**) and BV-2^{P2X7-} (**P**, **Q**, **R**). Cells were exposed to 2-NBDG for 1h or to media only (control) and rinsed, according to the manufacturer's protocol. Fluorescence was measured by flow cytometry. Three populations of cells were gated 'small cells', 'giant cells' and 'total population'. The figure shows individual histograms of a single experiment representative of each condition.*

BV-2 and BV-2^{P2X7-} GMCs appear healthy and functional, express high levels of mitochondria, and show high NQO1 activity. Various functions of GMCs have been proposed in the literature. One theory often explored is that GMCs may have a capacity to phagocytose large-sized debris and dead cells, which could not be engulfed by average-sized microglia. At the same time, some types of GMCs, such as Langhan cells, are described as having low phagocytic ability. To investigate the phagocytic properties of GMCs in BV-2 cultures expressing or lacking P2X7, the cells were fed fluorescent zymosan particles and their uptake was recorded in images and measured by flow cytometry (Figure 5.18).

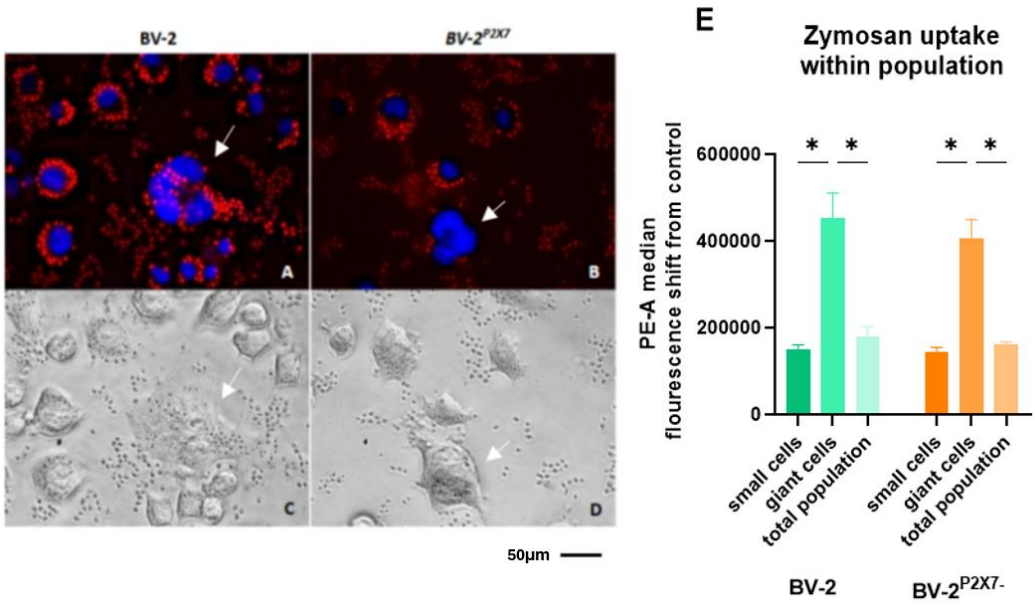

Figure 5.18 Uptake of fluorescent Zymosan particles by small and giant multinucleated BV-2 and BV-2^{P2X7-} cells. *Cells were seeded in 0.5% serum media in a 96-well plate to achieve 70% confluency and allowed to settle overnight. Cells were fed Zymosan particles following the manufacturer's protocol and left in the incubator for 1h. Cells were stained with nuclear dye Hoechst and processed as described in the method section.* ***A*** *(BV-2 cells) and* ***B*** *(BV-2^{P2X7-} cells) show an overlap of fluorescent images capturing Zymosan particles in red and cell nuclei in blue.* ***C*** *and* ***D*** *show a corresponding phase images.* ***E*** *Average fluorescent signal of phagocytosed Zymosan particles recorded by flow cytometry in different gated populations of cells 'small cells' only, 'giant cells' only, and total population of cells. The data shows the median fluorescence shift away from respective controls as an average of three independent biological experiments conducted. Data analyzed by Ordinary One-way ANOVA and Šídák's multiple comparisons test. (Statistical significance denoted by * p<0.05).*

The data in Figure 5.18 corroborates the findings from Chapter 4 that both BV-2 and BV-2^{P2X7-} microglia are capable of phagocytosing Zymosan particles with the same capacity. The images further demonstrate that Giant Multinucleated cells are capable of effectively taking up Zymosan beads. This also appears to be equally well done by GMCs expressing or lacking P2X7. This was

further supported by flow cytometry (Figure 5.18 E). Populations of cells were gated according to cell size, one gate capturing giant cells, and one- small cells. The average signal from the total population was also recorded. This data shows that phagocytosis is higher within a population of giant cells than in a population of small cells, as more beads per cell can be taken up due to the cells' large size.

Phagocytosis in GMC was also investigated by imaging and flow cytometry, using *E.coli* pHrodo particles, which give off a fluorescent signal due to a drop in pH induced by lysosomes of the phagocytosing cells (Figure 5.19). However, the pHrodo fluorescence in GMCs was poor in images and highly variable when measured by flow cytometry. The experiments were repeated to n=3 each time, however no consistency was observed in the recorded values. This could be down to fluorescence, overlapping of fluorospheres on the microscope, or possibly due to the pH of GMCs, rather than their ability to phagocytose the particles. Even with such high variability in readings, Figure 5.19 E clearly shows an advantage of giant cells over small cells in *E.coli* pHrodo uptake captured by flow cytometry.

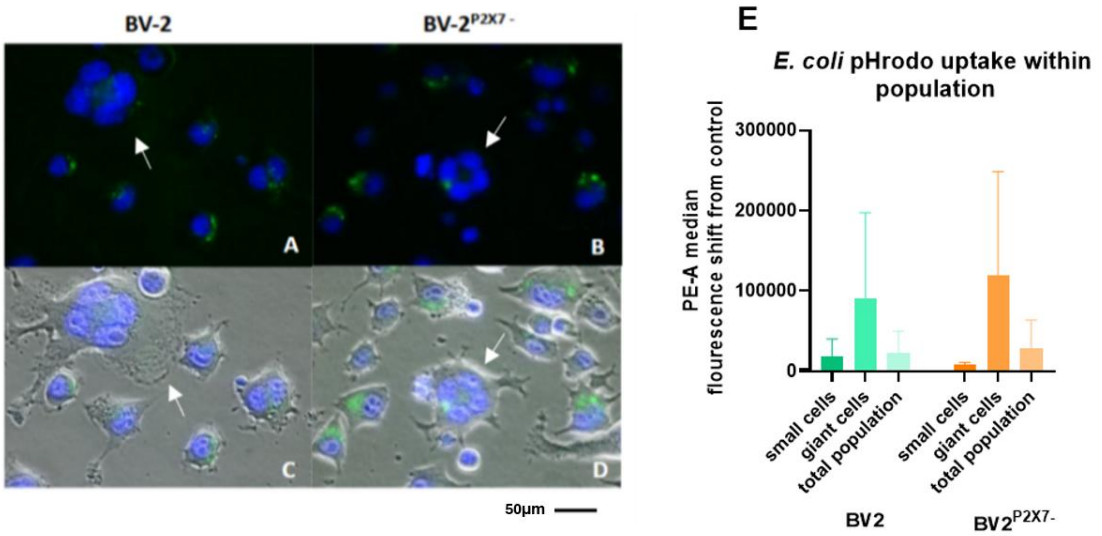

Figure 5.19 Uptake of Fluorescent E.coli pHrodo Particles by small and giant multinucleated BV-2 and BV-$^{2P2X7-}$ cells. *Cells were seeded in 0.5% serum media in a 96-well plate to achieve 70% confluency and allowed to settle overnight. Cells were fed E.coli pHrodo particles following the manufacturer's protocol and left in the incubator for 1h. Cells were stained with nuclear dye Hoechst and processed as described in the method section.* ***A*** *(BV-2 cells) and* ***B*** *(BV-2^{P2X7-} cells) show an overlap of fluorescent images capturing pHrodo particles in green and cell nuclei in blue.* ***C*** *and* ***D*** *show a corresponding phase images.* ***C*** *Average fluorescent signal of phagocytosed E.coli pHrodo particles recorded by flow cytometry in different gated populations of cells 'small cells' only, 'giant cells' only and total population of cells. The data shows the median fluorescence shift away from respective controls as an average of three independent biological experiments conducted. Data analyzed by Ordinary One-way ANOVA and Šídák's multiple comparisons test. Not statistically significant.*

The lack of a strong fluorescent signal from *E.coli* pHrodo particles in the images of GMCs compared to small cells, and the degree of variability in flow cytometry recordings were surprising.

To gain more insight into the activity of GMCs and their ability to express surface proteins, staining data from Chapter 4 were re-analyzed with respect to giant cells in the samples (Figure 5.21). The cells in their resting phenotype, challenged with 0.5% serum containing media for 48h, had been stained for classic microglia activation markers using anti-P2Y12, anti-CD11b, anti-CD86, anti-CD206 and anti-P2X7 antibodies and flow cytometry was used to quantify the expression as fluorescence signal shift away from the unstained control. The samples were gated to compare 'small cells' only to 'giant cells' only vs a total population comprising all cells in the sample. Giant cells showed higher levels of all the markers, and no difference was observed between P2X7-expressing or lacking GMCs, apart from P2X7 itself, which was highly expressed by BV-2 GMCs, but not the BV-2^{P2X7-} cells.

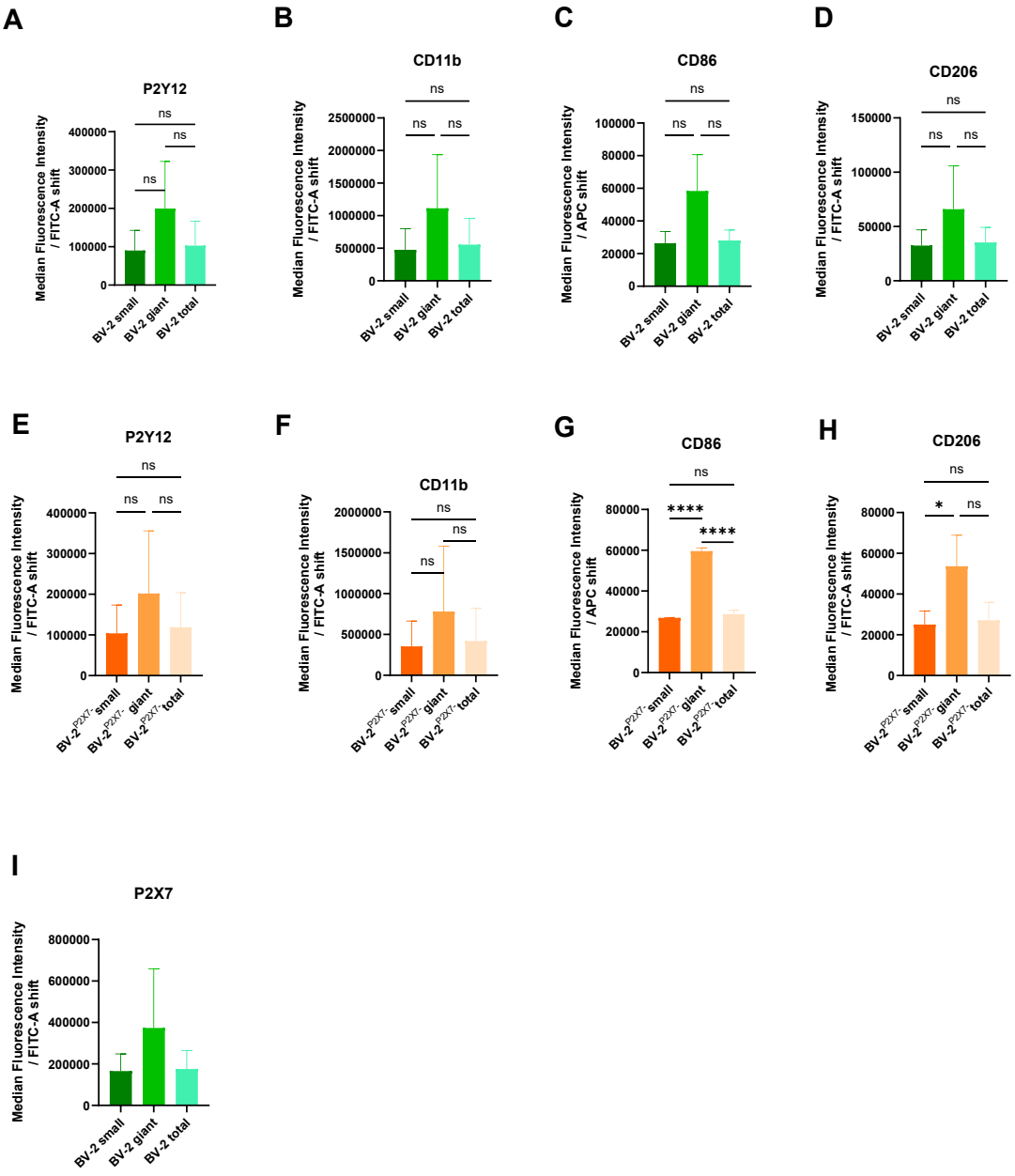

Figure 5.20 Analysis of staining for surface markers on BV-2 and BV-2^{P2X7-} by gating populations of different sizes. *Cells were plated in 24-well plates in 0.5% serum media at density 53460 cells/well and incubated for 48h. Cells were stained with antibodies for P2Y12, CD11b, CD86, CD206 and P2X7 as instructed in the manufacturers protocols. Fluorescence was recorded using flow cytometry. Populations of cells were gated according to size to include 'small cells' only, 'giant cells' only and total population of cells.* ***A***, ***B***, ***C***, ***D***, ***I*** *show P2Y12, CD11b, CD86, CD206 and P2X7, respectively, in BV-2 cells and* ***E***, ***F***, ***G***, ***H*** *show P2Y12, CD11b, CD86 and CD206, respectively, in BV-2^{P2X7-} cells. The data shows average of three independent biological experiments, apart from* ***I*** *which shows two independent biological experiments. Data analyzed by Ordinary One-way ANOVA and Šídák's multiple comparisons test. (Statistical significance denoted by * p<0.05, ** p<0.01, *** p<0.001, **** p<0.0001 ns not statistically significant).*

5.2.3. Cell fusion as a possible pathway in GMC formation

Cell fusion is how most GMCs, including osteoclasts, form in the body (Ahmadzadeh et al., 2022). Microglia, sharing many similarities with macrophages, may also have the capacity to fuse together to form GMCs. Although Hornik et al 2014 showed that in BV-2 cells, multinucleation in proinflammatory conditions likely arises via failure of cytokinesis, the significant advantage that P2X7-expressing cells possess in multinucleation may be due to the properties of P2X7 as a fusogen (Irma Lemaire et al., 2006; Pellegatti et al., 2011). Irma Lemaire et al., (2006) described P2X7 as a fusogen in transfected HEK293 and murine macrophage *in vitro* models.

In this thesis, it was hypothesized that more than one pathway may be at play in GMC formation in microglia, and P2X7 expression might also fuel the cell fusion capacity of GMC precursors in BV-2 cells. An experiment was designed to investigate whether BV-2 and BV-2^{P2X7-} cells form GMCs by fusion. The cells were trypsinised, and the pellet was divided into two samples stained with dyes of two different fluorescence spectra. Cells were counted and mixed in proportions 1:1. They were then plated in a usual experimental design of reduced serum, with or without LPS, for 72h to induce GMC formation. Fluorescent images were taken and overlapped. A lack of overlapping colours in LPS-stimulated cells indicated a lack of cell fusion occurring. The dyes were fading over time due to cell divisions, which meant that at 72h, a high proportion of cells was only very lightly fluorescent under the microscope. Images were taken in three independent experiments, and combinations of different dyes were tried. CFSE and CellTrace Far Red had the most visibility at 72h. Small, strongly fluorescent specks were observed inside cells, which could be remnants of phagocytosed cells. No overlap of the dyes was observed in LPS-treated wells of either cell line (Figure 5.22 A and B). Although, due to the faintness of the dyes at 72h, something might have been missed. In the unstimulated control wells of BV-2 cells, however, an overlap was observed, where a few GMC cells were spotted, showing the colours of both fluorescent dyes evenly spread across the cell body (Fig.5.22 C), suggesting that cell fusion might have occurred for this GMC to arise. It may be possible that cell fusion, as well as other processes, are occurring in BV-2 cells under low serum conditions, to generate GMCs, and while LPS is leading to GMCs arising from cytokinesis failure, spontaneous cell fusion also takes place, but to a much lower rate.

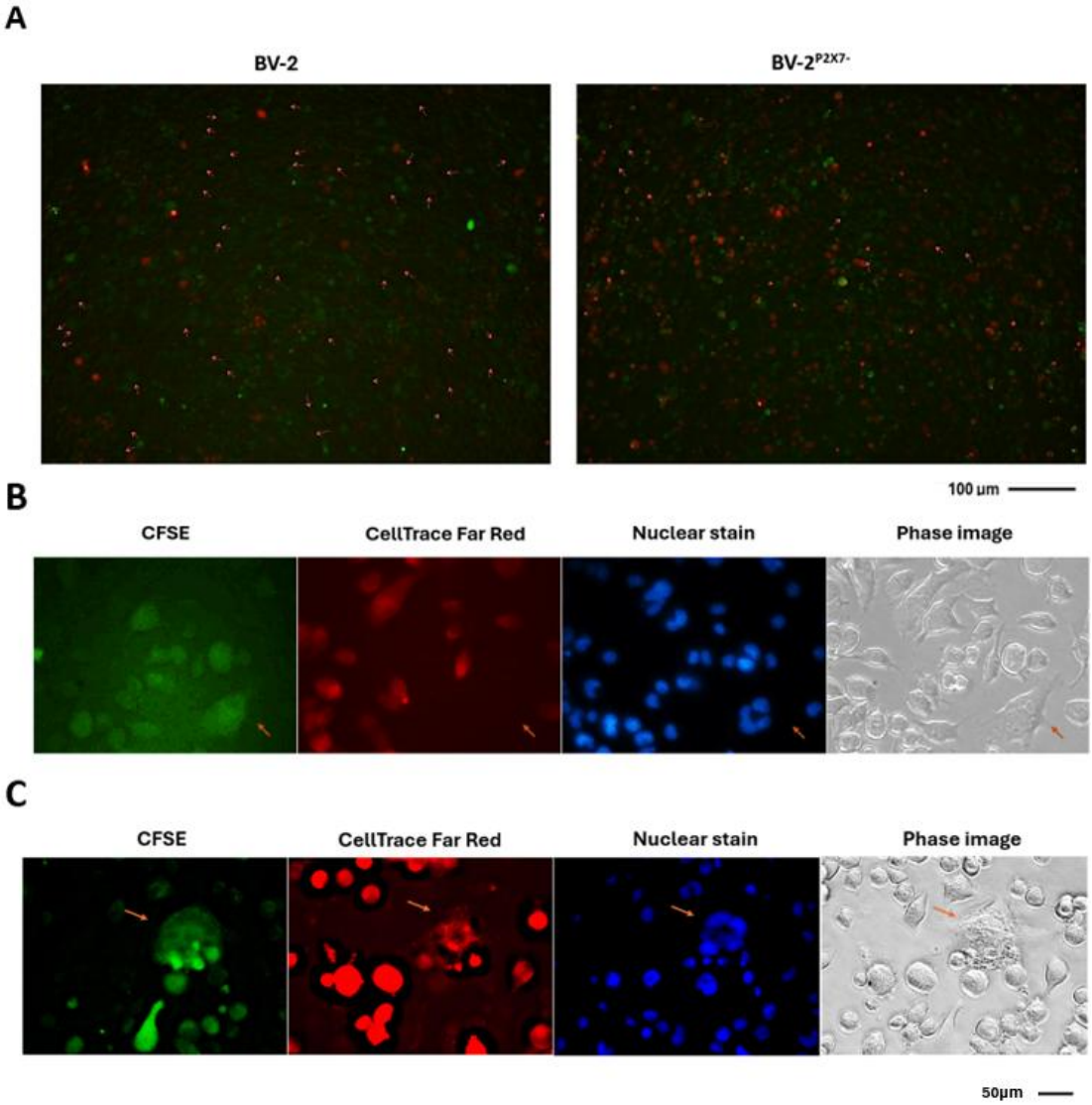

Figure 5.21 GMC formation and cell fusion in BV-2 and BV-2^{P2X7-} cells. *Cell Fusion was investigated by imaging. Cells were stained with two different dyes CellTrace Far Red (red) and CFSE (green) or CellTrace Yellow (green) according to the manufacturers' protocols. They were counted and mixed 1:1 in a bijoux in 0.5% ser media. Cells were then seeded at density of 12 000 cells/well in 0.5% serum media and stimulated with 'nothing' (spontaneous GMC formation) (**C**) or LPS 100 ng/mL (**A** and **B**) for 72h to induce GMC formation. Images were taken at 72h and processed as described in the method section. **A** shows x10 BV-2 and BV-2^{P2X7-} images. Cells mixed 1:1 stained with CellTrace Yellow (green) and CellTrace Deep Red (red) + LPS 100 ng/mL 72h, orange arrows show GMCs in the images. Lack of overlapping colours indicates lack of cell fusion during the formation of GMCs in the well. **B** BV-2 cells mixed 1:1 after staining with CFSE (green) and CellTrace Far Red (red) + LPS 100 ng/mL 72h, orange arrow show GMC in the images, x 60 objective. GMC stained with CFSE present, lack of CellTrace Far Red staining indicates lack of cell fusion. **C** BV-2 cells. Cells mixed 1:1 stained with CFSE (green) and CellTrace Far Red (red) unstimulated (spontaneously forming GMC), x 60 objective. GMC present with CFSE staining and with CellTrace Far Red indicates cell fusion. Representative images of three independent biological experiments with three technical replicates per condition.*

It has been shown in several studies that fusogens are important in GMC formation. l(Helming et al., 2008; Hernández & Podbilewicz, 2017; Sabe et al., 2024; C. Zhang et al., 2014). High expression of certain genes may also be ascribed to certain types of GMCs (Ahmadzadeh et al., 2022; Sabe et al., 2024). In order to investigate further whether cell fusion might be occurring in spontaneously forming GMCs, a qPCR experiment was designed, looking at the expression of various fusogens, which may be playing a role in GMC formation with or without LPS stimulation. Several markers were chosen to better understand the nature of the BV-2 GMCs. Cathepsin K, MMP9, and TRAP are all markers of terminally differentiated mature multinucleated osteoclasts (Ariffin et al., 2024; Humphrey & Nakamura, 2016; Jacome-Galarza et al., 2019). CD44, CD9, and CD81 integrins are adhesion molecules expressed by all cells that have the ability to fuse together (Hernández & Podbilewicz, 2017; Sabe et al., 2024). CD301 is important in cell fusion, together with DC-STAMP, which is also a marker of osteoclast differentiation (Brooks et al., 2021; Sabe et al., 2024). TREM2 and DAP12 interact with each other to initiate multinucleation in macrophage GMC precursor cells (Helming et al., 2008). Sirpα and CD47 interact to prevent phagocytosis on cells that express CD47 -the well-known 'don't eat me' signal (X. Han et al., 2000). Sirpα is also known as a macrophage fusion protein (Matlung et al., 2017; and Sabe et al., 2024). CCR2 is a chemokine receptor for CCL2 and so plays an important role in the migration of the cells (Khan et al., 2016; Kyriakides et al., 2004a). CCR2 has been implicated in multinucleation of almost all GMC subtypes (Ahmadzadeh et al., 2022). Finally, chemokine CCL2 and cytokine IL-1β were also of interest in cell cultures rich in spontaneous GMCs (Gschwandtner et al., 2019). Beta actin was used as a control to which all genes were normalized in data analysis. GAPDH was selected as a second housekeeping gene and a control for the experiments. RAW 264.7 mouse macrophages were used as a control model, as macrophages have been studied and evidenced in the literature with respect to GMC formation far more than microglia. It was confirmed via imaging that RAW 264.7 cells, following 72h with LPS, showed multinucleated giant cells (data not shown). RAW 264.7 expression profile, following a 72h exposure to LPS, showed downregulation of most genes (Figure 5.23). Expression of DC-STAMP, CD44, CD9, CD81, DAP12, TREM2 and CCR2 was downregulated by LPS, while CCL2 and IL-1β were highly upregulated. The remaining genes, such as CD47, Sirpα, CD301, TRAP, MMP9, and Cathepsin K, were unaffected by LPS, and their expression remained unchanged.

The effect of serum reduction to 0.5% on fusogen-related gene expression in BV-2 and BV-2^{P2X7-} cells was first investigated. In chapter 3, the sole act of serum reduction to 0.5% over 48h was shown to induce P2X7-dependent effects in BV-2 microglia (measured by Alamar blue processing). Figure 5.24 shows that serum reduction affected gene expression in BV-2 and BV-2^{P2X7-} cells differently. The expression of most genes in BV-2^{P2X7-} cells remained unchanged, with the exception of only MMP9 and IL-1β, which went down. Conversely in P2X7-expressing BV-2 cells,

upregulation of Cathepsin K, DC-STAMP and CD-44 was observed, while other genes stayed the same or showed marginal changes, and IL-1β was decreased. The serum-induced changes between the two cell lines were apparently different. Reduction to 0.5% serum hardly affected the gene expression in P2X7-deficient cells, but induced changes in the profile of several fusogens and adhesion proteins tested in BV-2 cells.

Next, the effect of LPS was investigated on BV-2 and BV-2^{P2X7-} cells. Cells were exposed to LPS in low serum (0.5%) for 72h. LPS induced downregulation of many proteins and receptors tested (Figure 5.25). DC-STAMP, CD9, CD81, DAP12, TREM2, and CCR2 were all downregulated compared to expression levels of unstimulated control. The same genes were downregulated in RAW cells stimulated with LPS for 72h. TRAP was upregulated in both cell lines. Similar to the effect of serum reduction, only $BV2^{P2X7-}$ cells showed an upregulation of MMP9. CCL2 and IL-1β were highly upregulated in both cell lines in concordance with findings of Chapter 4.

Finally, BV-2 and BV-2^{P2X7-} cell cultures rich in GMCs were subjected to the same experiment and the expression of the same panel of genes was investigated with respect to P2X7 and GMC+ populations vs small cell populations low in GMCs (Figure 5.26). Osteoclast markers Cathepsin K, MMP9, and TRAP were upregulated in both GMC+ populations, compared to control small cells. Furthermore, P2X7-expressing cells showed higher levels of upregulation in those genes than the P2X7-deficient clones. CCR2 in GMC+ populations was downregulated in BV-2 cells only, and CD44 was upregulated in P2X7-expressing BV-2 GMC+ cells only. Both BV-2 and BV-2^{P2X7-} GMC+ populations showed slightly higher levels of TREM2, marginal DAP12, and CCL2.

The expression levels of proteins of interest in GMCs from this experiment are summarized in Figure 5.26.

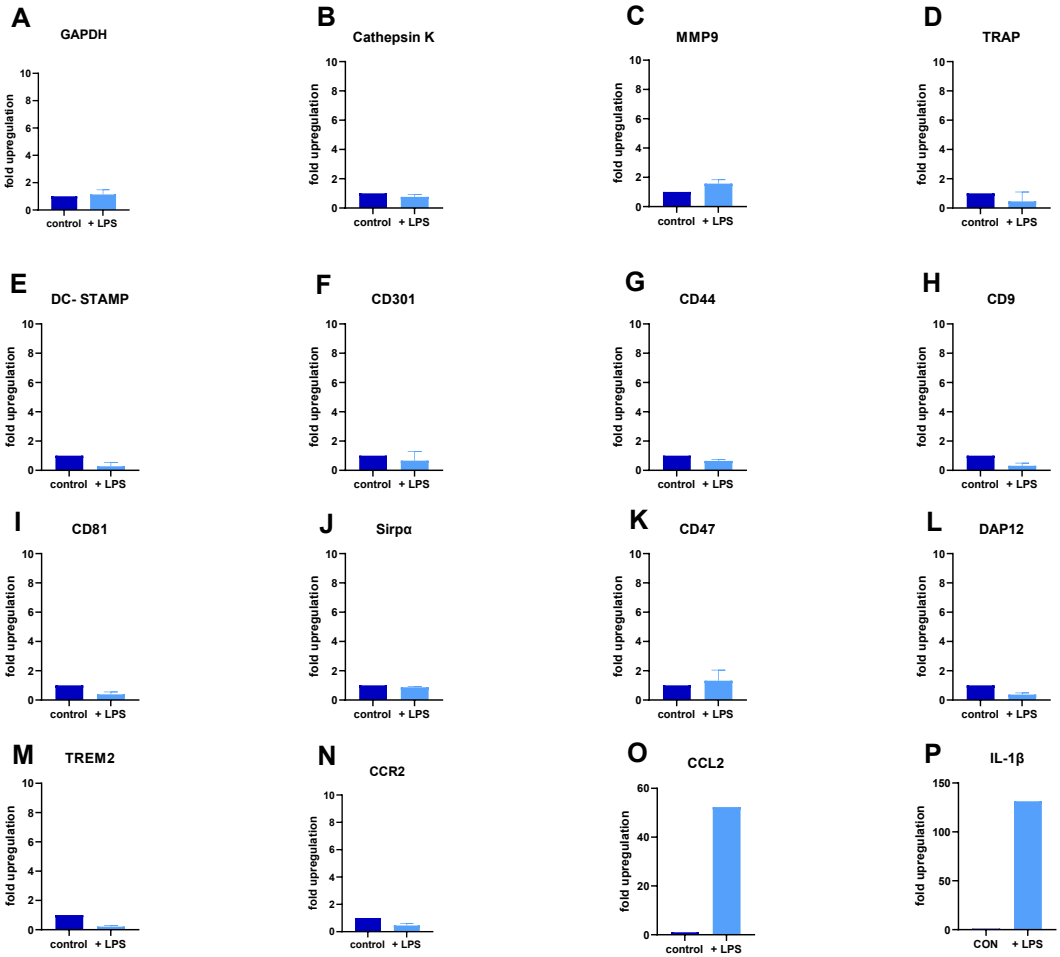

Figure 5.22 Expression of GMC fusogens and markers by in RAW264.7 cells stimulated with LPS for 72h to induce multinucleation vs unstimulated control cells. *Cells were plated in 0.5% serum +/- LPS 100 ng/mL at density 53460 cells/well in 24-well plates for 72h. RNA extraction and qPCR was performed as described in the method section. The data shows an average of two independent biological experiments conducted with three technical replicates per condition, apart from CCL2 and IL-1β, which came from a single biological experiment with three technical replicates per condition. All data was normalized to internal control gene- beta actin. Data processed by Delta-delta Ct method to calculate fold change.*

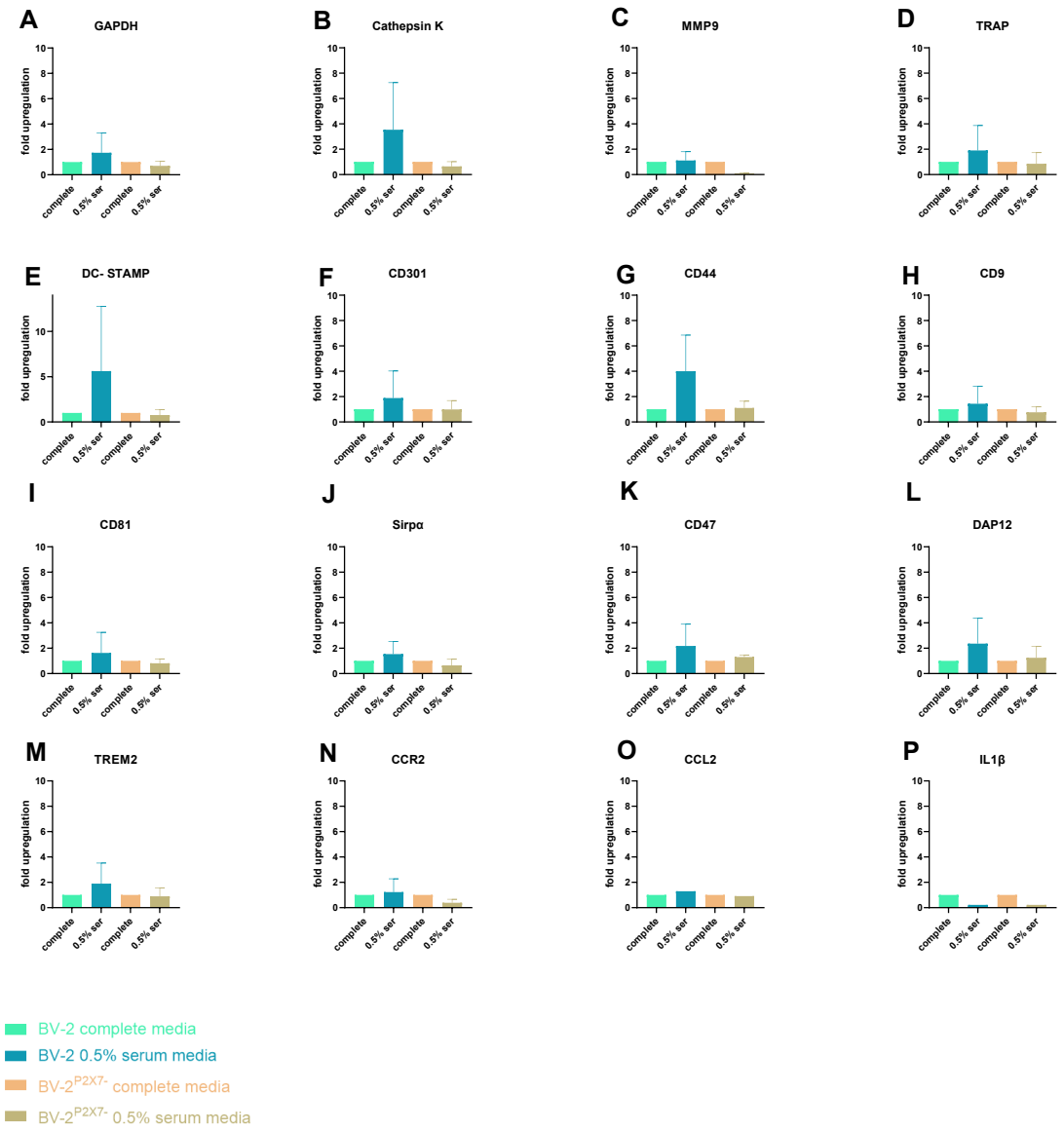

Figure 5.23 Expression of GMC fusogens and markers in BV-2 and BV-2^{P2X7-} cells cultured in complete vs 0.5% ser media for 72h. *Cells were plated in 0.5% serum or complete media at density 53460 cells/well in 24-well plates for 72h. RNA extraction and qPCR was performed as described in the method section. The data shows an average of two independent biological experiments conducted with three technical replicates per condition, apart from CCL2 and IL-1β, which came from a single biological experiment with three technical replicates per condition, normalized to internal control gene- beta actin. Data processed by Delta-delta Ct method to calculate fold change.*

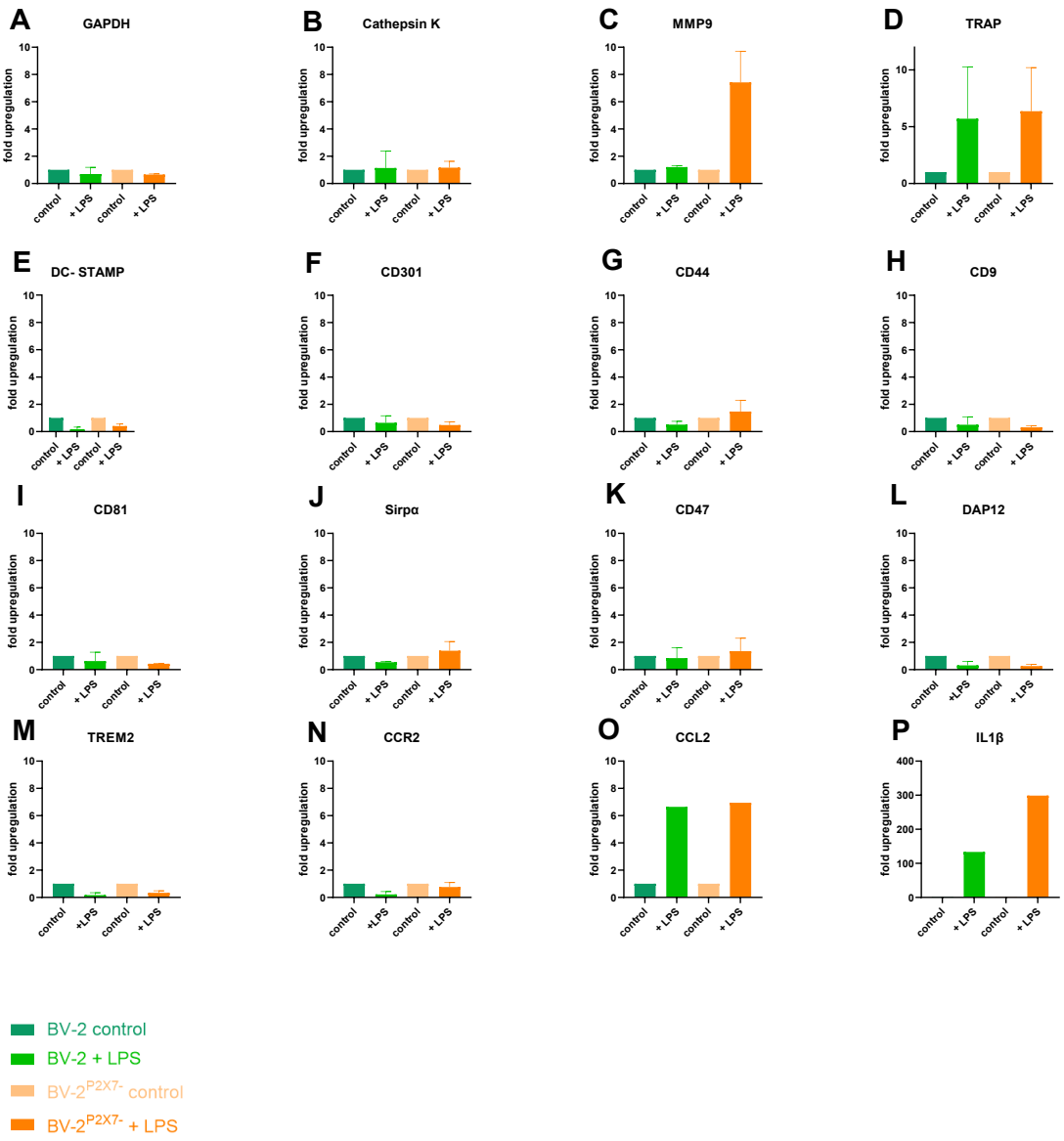

Figure 5.24 Expression of GMC fusogens and markers in BV-2 and BV-2^{P2X7-} cells grown in 0.5% ser media + LPS for 72h. *Cells were plated in 0.5% serum +/- LPS 100ng/mL at density 53460 cells/well in 24-well plates for 72h. RNA extraction and qPCR was performed as described in the method section. The data shows an average of two independent biological experiments conducted with three technical replicates per condition, apart from CCL2 and IL-1β, which came from a single biological experiment with three technical replicates per condition. All data normalized to internal control gene- beta actin. Data processed by Delta-delta Ct method to calculate fold change.*

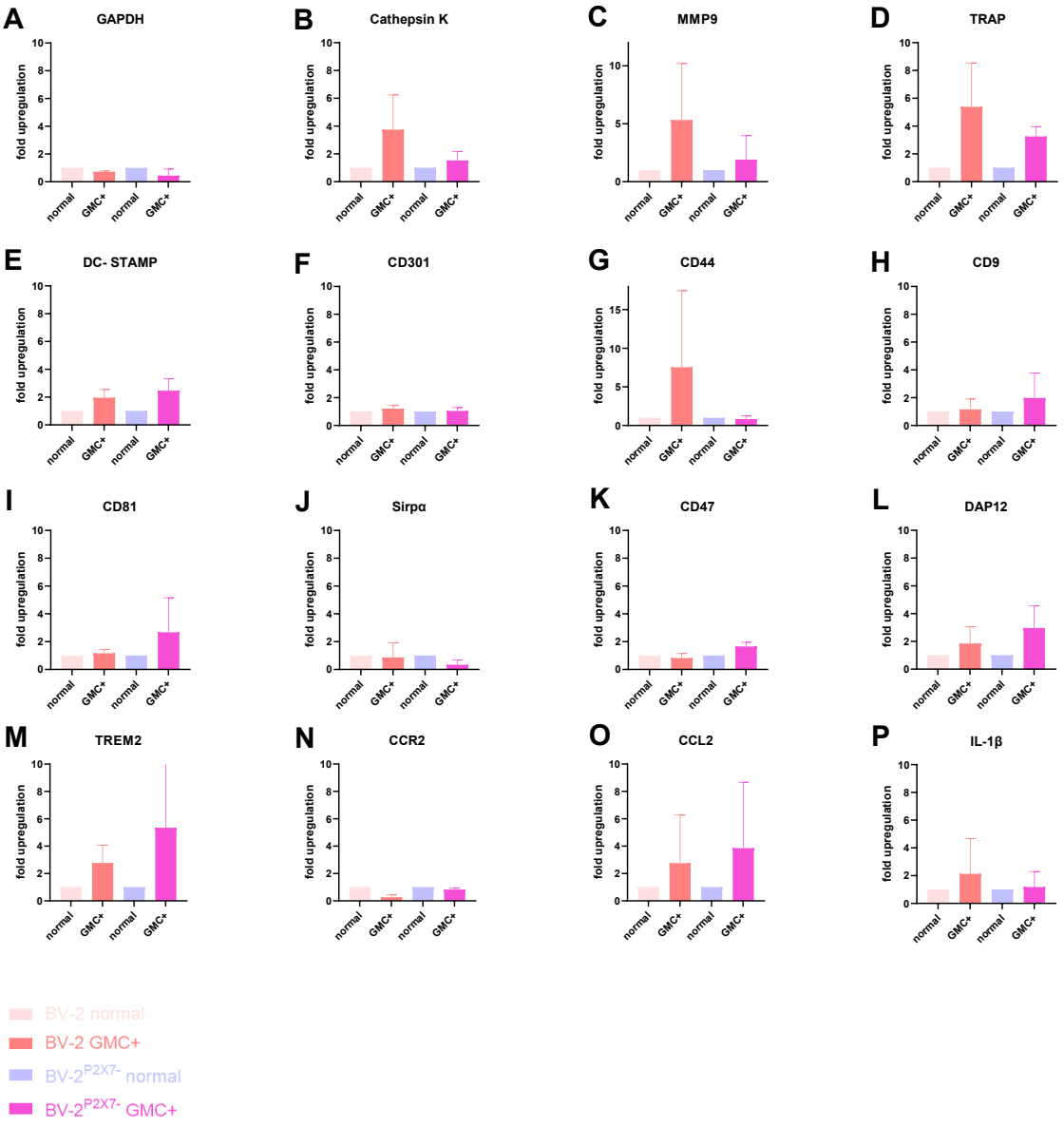

Figure 5.25 Expression of GMC fusogens and markers in BV-2 and BV-2^{P2X7-} cells rich in GMCs (GMC+) vs normal cell culture. *Cells were plated in complete media at density 70 x 10^4 cells/ well in 6-well plates for 72h. RNA extraction and qPCR was performed as described in the method section. The data shows an average of two independent biological experiments conducted with three technical replicates per condition, apart from CCL2 and IL-1β, which came from a single biological experiment with three technical replicates per condition. All data normalized to internal control gene- beta actin. Data processed by Delta-delta Ct method to calculate fold change.*

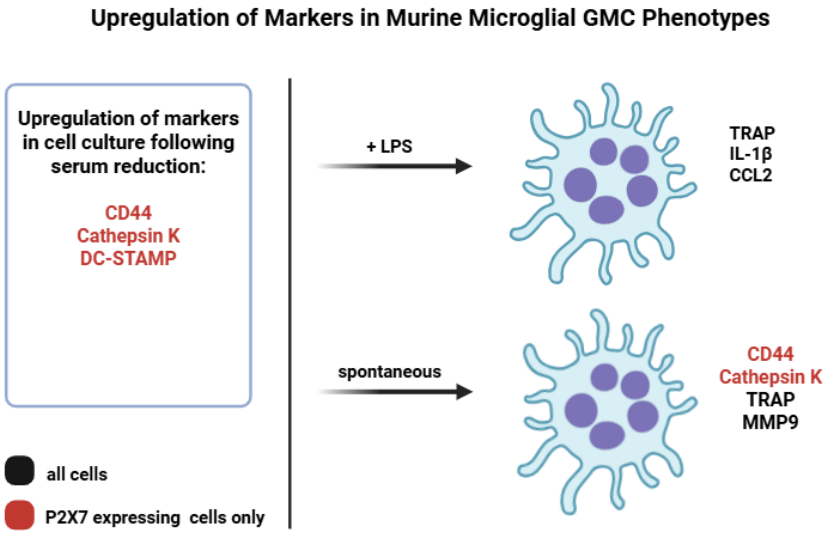

Figure 5.26 Summary of the expression of GMC fusogens and markers by qPCR in BV-2 and BV-2^{P2X7-} cells stimulated with LPS for 72h to induce multinucleation vs unstimulated spontaneously arising GMCs. *LPS and spontaneously forming GMCs have a different profile of protein expression. Spontaneously arising GMCs upregulate osteoclast markers Cathepsin K, TRAP, MMP9 and fusion protein CD44, while LPS induces downregulation of most markers associated with osteoclasts and cell fusion. Serum reduction upregulates a similar profile of GMC markers in P2X7-expressing cells. Changes observed in all cells are shown in black and changes observed only in P2X7-expressing cells are shown in red. Figure created in Biorender.*

While macrophage-derived GMCs have been described well, with clearly defined subtypes, the identity of microglial GMCs is not clear. The qPCR experiment revealed some similarity in genetic profile to osteoclast-like cells. The identity of BV-2 GMCs was further investigated by looking at cell morphology.

Certain GMC subtypes are characterized by specific morphologies and structural characteristics. Actin rings have been previously reported as a morphological feature observed in multinucleated macrophages and *in vitro* models of osteoclasts (G. Han et al., 2019; Martin, 2016) . If microglia were forming osteoclast-like giant cells, similar internal organization of F-actin would be observed. Actin staining was used to observe the GMCs morphology in BV-2 and BV-2^{P2X7-} microglia, and J774 mouse macrophages using phalloidin-Alexa Fluor 488. GMCs were induced by exposure to LPS and RANK ligand (RANKL).

J774-derived GMC cells stained well and showed a strong outline of actin at the edge of the cell, when stimulated with LPS, and more evenly distributed actin, with no ring, when stimulated with RANKL (Figure 5.28 C, and Figure 5.28 D, respectively). BV-2 and BV-2^{P2X7-} cells showed central accumulation of actin, and an even distribution throughout the cell body and protrusions. No actin rings were observed, regardless of P2X7 expression, neither with LPS or RANKL stimulation (Figure

5.28 A and B and Figure 5.29 B and C, respectively), nor with spontaneously occurring GMCs (Figure 5.29 A). No striking features were observed between the P2X7-expressing or lacking cells or between GMCs induced by various methods. RAW 264.7 cells failed to multinucleate in the presence of RANKL and were not used in this experiment, although they did show multinucleation with LPS. J774 macrophages were used instead. Many of the BV-2 and BV-2^{P2X7-} GMCs showed actin-rich extensions reaching out to neighboring cells. These could be described as filopodia and lamellipodia, frequently observed with microglia (Figure 28 A and B, Figure 5.29, and Figure 30). The morphologies of GMCs could be very variable depending on the ongoing interactions with neighbouring cells, the only constant feature remaining the central wreath-like arrangement of nuclei with an actin rich middle. J774 macrophages showed centrally collected nuclei but not in a circular fashion.

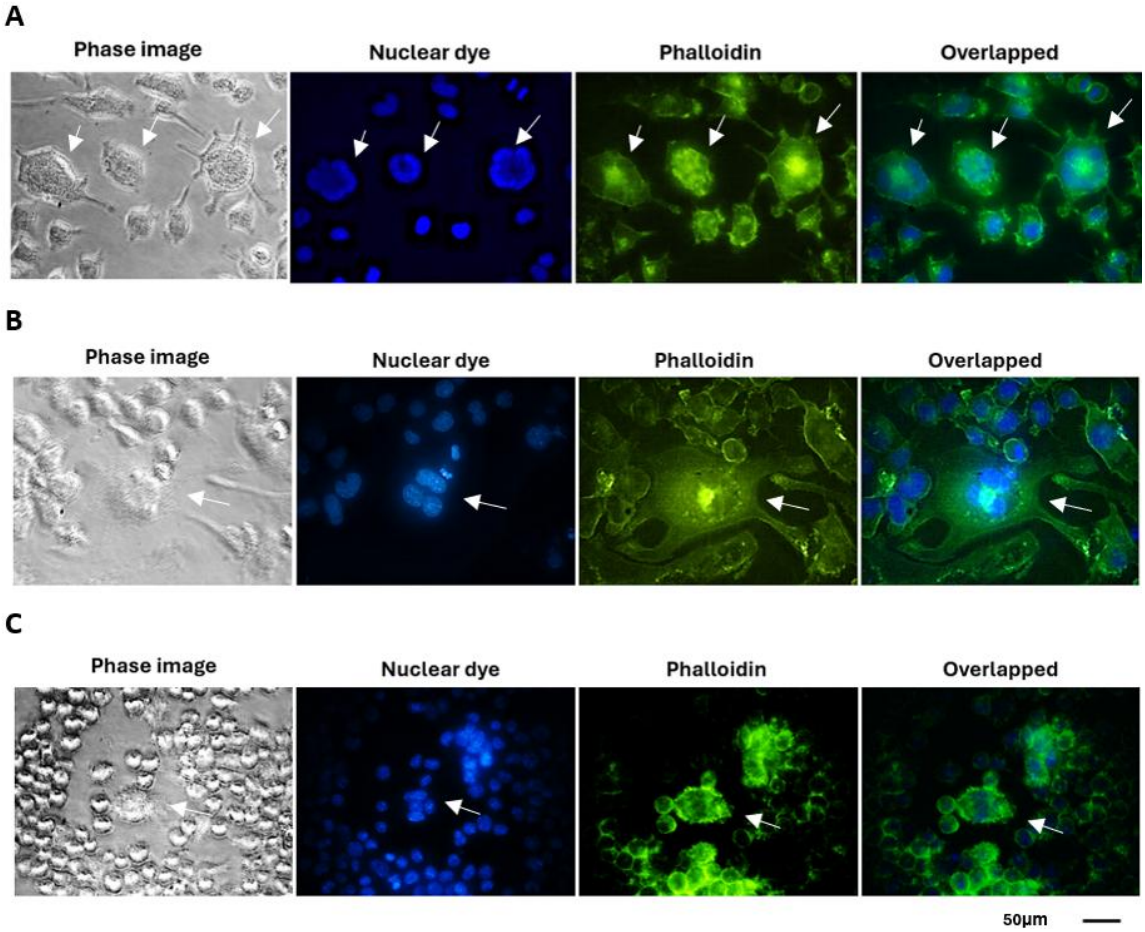

Figure 5.27 Phalloidin staining showing actin distribution in BV-2 and BV-2^{P2X7-} cells and control staining of RAW264 macrophages. *Cells were stained with phalloidin to fluorescently label actin (green) and nuclear dye Hoechst (blue). Cells were plated in 0.5% serum containing media + LPS 100 ng/L in wells of a dark 96-well plate and incubated for 72h to induce GMC formation. Stained with phalloidin in PBS for 30 mins after formaldehyde fixation, following the manufacturer's protocol and Hoechst nuclear dye. Images were taken using x60 objective and processed as described in the method section.* ***A*** *BV-2 cells,* ***B*** *BV-2^{P2X7-}cells,* ***C*** *J774 macrophages. The images are a representative of three independent biological experiments.*

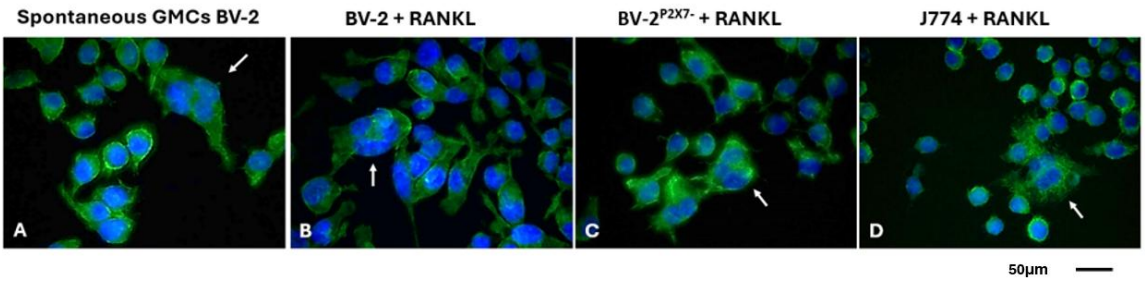

Figure 5.28 Phalloidin staining showing actin distribution in BV-2 and BV-2^{P2X7-} cells in spontaneously forming GMCs and following RANKL stimulation. *Cells were stained with phalloidin to fluorescently label actin (green) and nuclear dye Hoechst (blue). White arrows indicate GMCs. Cells were grown on coverslips in 0.5% serum media and stimulated with RANKL 100 ng/mL or 'nothing' (spontaneous GMCs) in a 24-well plate and incubated for 72h to induce GMC formation. Stained with phalloidin in PBS for 30 mins after formaldehyde fixation, and with Hoechst nuclear dye. Images were taken using x60 objective and processed as described in the method section.* ***A*** *spontaneous GMCs in BV-2 cells,* ***B*** *BV-2 + RANKL,* ***C*** *BV-2^{P2X7-}+ RANKL,* ***D*** *J774 + RANKL. The images are a representative of two independent biological experiments.*

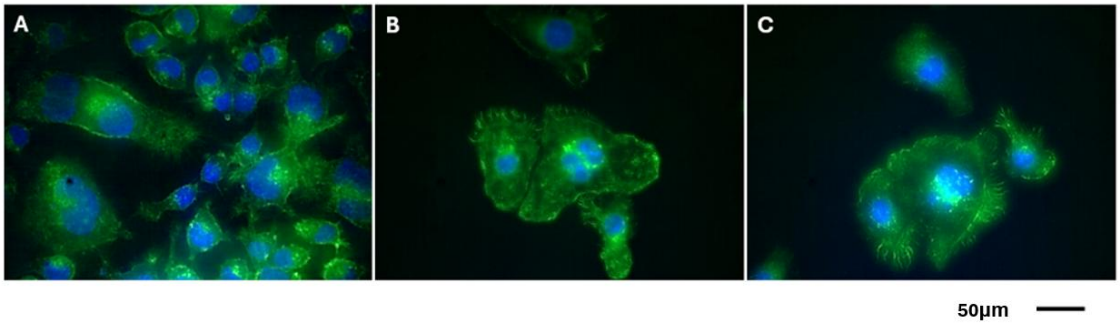

Figure 5.29 Phalloidin staining showing different morphologies observed in BV-2 LPS-induced GMC cells. *Cells were stained with phalloidin to fluorescently label actin (green) and nuclear dye Hoechst (blue). Cells were grown in 0.5% serum media and stimulated with LPS 100 ng/mL for 72h.* ***A*** *Cells were grown in plastic wells of a 96-well plate.* ***B*** *Cells were grown in plastic wells of a 24-well plate, scraped, transferred to glass coverslips and allowed to settle for 3h. Stained with phalloidin in PBS for 30 mins after formaldehyde fixation. Stained with Hoechst nuclear dye. Images were taken using x60 objective and processed as described in the method section. The images are a representative of two independent biological experiments.*

5.3 Discussion

5.3.1 GMC formation in BV-2 and BV-2^{P2X7-} microglia

P2X7 function as a fusogen has been previously proposed in HEK293 and murine macrophage models (Di et al., 2013; Irma Lemaire et al., 2006), however in direct relation to microglia and BV-2 cells, this has never been explored. The clear advantage of P2X7-expressing BV-2 cells in GMC formation, demonstrated in this work, may reveal multiple pathways at play in GMC formation. Although failure of cytokinesis has been demonstrated by some authors as a multinucleation pathway in microglia, P2X7 needs to be considered as a contributor to microglial multinucleation by cell fusion. Figures 5.3 and 5.4 clearly show the consistent advantage P2X7-expressing BV-2 cells have in terms of GMC formation. This is true with LPS stimulations, and also where GMCs form spontaneously, without the presence of any agents. Although over time, both cell lines can reach very large sizes, when compared to each other over a 72h period, P2X7 expressing BV-2 cells form larger GMCs, as well as more numerous (Figure.5.4).

The LPS-initiated induction of GMCs could be inhibited completely by CLI-096, a TLR4 receptor antagonist, in BV-2^{P2X7-} cells, but not in BV-2 cells expressing the receptor (Figure.5.6). This suggests a separate pathway at play which relies on P2X7 expression. While LPS induces a more robust GMC formation (up to 16% of the population), the advantage carried by P2X7 is more subtle (up to 2%) and may be occurring in parallel and independently of the LPS-induced pathway.

Different cytokines and pro-inflammatory factors were tested for their ability to induce GMCs. According to the literature, in GMC formation in macrophages and monocytes, cytokines manipulate the cells towards different phenotypic differentiation profiles, which then result in various types of GMCs. Ahmadzadeh et al., (2022) suggests that thefusion of alternatively activated (IL-4/IL-13 activated) macrophages *in vitro* produces FBGCs, while the fusion of LPS and IFN-γ or TNFα-activated macrophages, or using TLR pathways leads to LGCs. RANKL and M-CSF stimulation induces osteoclasts (Ahmadzadeh et al., 2022). The identity of the BV-2 microglia was investigated by looking at responses to cytokines.

Suzumura et al., (1999) showed that GMCs can occur as a result of microglia stimulation with IL-4 and IL-13. However, in BV-2 and BV-2^{P2X7-} cells under conditions investigated here, IL-4 and IL-13 did not induce any GMC formation. In fact, the cells assumed a smaller size, unlike the cells stimulated with LPS, and while they clustered together, they did not appear to be fusing, and no multinucleation was observed when the cells were stained with nuclear dye Hoechst. This is in concordance with Hornik et al., (2014) who also did not record any multinucleation with murine

BV-2 microglia or primary microglia with IL-4. Both IL-4 and IL-13 cytokines increase CD206 expression on cell surface of BV-2 and BV-2^{P2X7-} cells, which was shown in Chapter 4, and CD206 has been shown to contribute to FBGC formation. However, since neither cytokine led to GMC formation in microglia cultures, the resulting BV-2 giant cells are not likely to be FBGC-like.

BV-2 microglia responded to LPS and RANKL with GMC formation and their identity as osteoclast-like cells, LGC or Touton-like GMCs was considered in further experiments.

Hornik et al., (2014) showed that serum has no effect on GMC formation during GMC induction. Contrary to this paper, this work finds a clear effect of serum deprivation on the expression levels of many proteins important for facilitating cell fusion. DC-STAMP, CD44, and Cathepsin K were all upregulated by serum reduction exclusively in the P2X7-expressing cells. This provides more basis for investigating cell fusion as a possible pathway in GMC formation in microglia.

Images were taken of cells stained with different dyes and incubated for 72h with and without LPS. Images were carefully inspected for any overlap of fluorescent dyes at the end of the incubation period, which would indicate cell fusion. No evidence of cell fusion was observed in the LPS-stimulated cultures, neither in BV-2 nor BV-2^{P2X7-} cells. In BV-2 unstimulated cultures, a couple of giant cells were observed with an overlapping fluorescence of two different dyes. It is possible that this overlap was the result of cell fusion, as both dyes were evenly spread across the cell body. Because the cells were not stimulated with LPS, only 1-2% of the population was forming GMCs. This made it difficult to record more events. It is also possible that cells of the same colour could have fused together, which would make them indistinguishable from non-fusing cells in this experiment.

Cell fusion was explored as an additional pathway to GMC formation in BV-2 and BV-2^{P2X7-} cells, where P2X7 expression is an advantage. P2X7 has been previously described as a fusogen. (Lemaire et al., 2006) showed that P2X7 transfection in HEK cells leads to enhanced GMC formation. Their study, as well as other work on osteoclasts *in vitro* and *in vivo*, shows that P2X7 is not essential for GMC formation to occur, but rather its expression enhances cell fusion capacity and GMC incidence. This is very much reflected in this work, and the collected data on BV-2 vs BV-2^{P2X7-} cells. It is important to note that there are species differences at play. Irma Lemaire et al., (2006) used rat alveolar macrophages. Our studies on HEK cells transfected with different species variants of P2X7 (data not shown) indicate that rat P2X7 carries an enhanced GMC-forming capacity, higher than that of human or mouse variants.

P2X7 sole expression- not just signaling- allows for an advantage in GMC formation in BV-2 cells. Experiments with Az10606120 and JNJ-47965567 shown in Appendix (Figure A.1), show clearly that these antagonists effectively reduce P2X7 activity, in the Fura-2 AM assay, which measures

calcium signaling. Figure 5.7 shows that incubation for 72h with the P2X7 antagonists does not reduce GMC formation when incubated with or without LPS. Rather, the P2X7-expressing cells retain their advantage in GMC formation over the P2X7-deficient cells. This suggests it is the presence of the receptor in the membrane, regardless of its activation state, that allows for enhanced GMC production. However, P2X7 allosteric positive modulators such as CK, clemastine, HEI33090 and PxB were able to slightly potentiate the GMC formation compared to unstimulated control (as seen in images Figure A.2, Appendix). PxB has been previously investigated by (Di et al., 2013; Lemaire et al., 2006) in transfected P2X7 HEK cell model forming GMCs by cell fusion, however CK, a naturally occurring P2X7 allosteric modulator, has not been previously investigated in GMC formation. It is possible that P2X7 affects the membrane composition or allows for cytoplasmic contact and exchange in its active and inactive state, perhaps through the same property that allows for the giant pore formation, which had been previously linked to multinucleation by (Di et al., 2013; Lemaire et al., 2006) in transfected HEK cells, to allow for the mechanics of cell fusion. P2X7 expression may support both the LPS-induced process, which may be occurring via cytokinesis failure as demonstrated by Hornik et al., (2013), and it may support spontaneous GMC formation in unstimulated culture, which may be happening via cell fusion. Perhaps the activity of P2X7 is not important in terms of calcium signaling; however, positive allosteric modulation, which allows for even more potentiated giant pore formation, might have a further positive effect on GMC incidence.

Lemaire et al., (2006) performed their experiments on P2X7 in cell fusion on cells in serum-free conditions, rather than stimulating the cell culture with LPS or cytokines. Although Hornik et al., (2014) showed no difference in GMC formation between BV-2 cells grown in complete or serum-free media, the data gathered here on protein expression under reduced serum conditions supports the link between P2X7, cell fusion capacity, and serum levels.

Expression of genes in differently induced GMCs

The qPCR experiment showed that 'LPS induction' and 'spontaneous formation' in BV-2 cell culture are likely two different pathways that result in GMCs that express distinct panels of surface markers and receptors. It is possible that GMCs form via different routes, and while LPS may be inducing GMC formation via failure of cytokinesis, as shown by Hornik et al, the spontaneous GMCs may be arising from cell fusion supported by P2X7 expression.

Stimulation of RAW cells with LPS resulted in downregulation of many proteins associated with cell fusion, and BV-2 and BV-2^{P2X7} cells mirrored that pattern.

In spontaneously forming GMCs, the opposite of LPS-induced changes happened, although only slight upregulation was observed in some cases. Markers such as CD44, Cathepsin K, and MMP9, and TRAP were upregulated. This supports the idea that a different pathway utilizing cell fusion may be leading to the formation of Osteoclast-like GMCs. Expression of the transmembrane protein DC-STAMP, especially, has been implicated in enabling cell fusion of osteoclasts and FBGCs. In this work DC-STAMP was only marginally upregulated in spontaneously forming GMCs and more repeats should follow on this experiment. All GMCs showed elevated TRAP levels. Literature suggests that TRAP marks all GMCs including FBGCs, LGCs, and Osteoclasts(Ahmadzadeh et al., 2022; Sabe et al., 2024). All GMC+ cultures showed slightly increased levels of CCL2 and IL1β, compared to normal small cell cultures, indicating that GMCs may be contributing to functions such as the release of cytokines in cell culture. Furthermore, spontaneously forming giant cells highly express all key surface markers relevant to phenotypic activation in microglia, as investigated in Figure 5.21, including higher expression of P2X7 on giant cells compared to 'small' control cells.

A major observation from examining the gene expression panel was that P2X7-deficient cells did not show a high degree of change in their profile of fusogens and markers. Regardless of the stimulation or GMC induction process, their expression of the genes remained relatively stable, compared to the control. When P2X7 was present, however, upregulation and downregulation of different markers were apparent. It is likely that P2X7 expression supports the regulation of markers and contributes to the cells' plasticity needed to acquire different phenotypes and respond to environmental cues flexibly. For example, serum reduction to 0.5% was enough to induce a series of changes in BV-2 cells but not BV-2^{P2X7-}microglia. Cathepsin K, DC-STAMP, and CD44 were upregulated. Interestingly, this pattern mirrored the changes to the profile of GMC+ cell cultures compared to normal cell cultures, where Cathepsin K, TRAP, CD44, and MMP9 were the key upregulated markers, and these changes were greater in P2X7-expressing cells, especially with respect to Cathepsin K, TRAP, and CD44. These markers may be the key to the relationship between P2X7 expression and GMC formation. The literature on mouse osteoclast formation shows that TRAP, DC-STAMP, and Cathepsin K are all upregulated in IL-1β-supported cell fusion of osteoclast precursors (myeloid blasts) (Cao et al., 2016). P2X7 expression over 72h of incubation or in cell culture may be supporting local IL-1β signaling, allowing for the acquisition of a pro-fusion phenotype. Furthermore, local ATP release by P2X7 over the 72h may be increasing local adenosine, which could be upregulating CD44 expression, which is thought to be a key surface protein for macrophage fusion leading to GMC formation (Sterling et al., 1998).

Consistent with the qPCR findings of upregulated adhesion molecules in P2X7-expressing cells, the microglial GMCs were highly adherent to the bottom of the well or flask. Indeed, on occasion

they needed to be scraped as enzymatic treatment with Trypsin-EDTA was not enough to detach the cells. This corroborates the observation from Chapter 3 that BV-2 cells were generally much more adherent than BV-2^{P2X7-} cells. Literature suggests that cell adhesion is important for cell fusion in GMC formation, and expression of CD44, especially, is important for the acquisition of the fusing properties of GMC precursor cells (Sabe et al., 2024).

It was observed that GMC formation in cell culture increases gradually over time, regardless of stimulation. Once a few GMCs are present, more are shortly observed in their vicinity. A patchy appearance of GMC-rich areas in cell culture suggests that local factors are at play to sustain and stimulate spontaneous multinucleation. Secreted factors or cell-to-cell contact and stimulation might be important for GMC formation. In Figure 5.15 it was observed that small cells exposed to supernatants from GMC-rich cultures result in more GMC formation than when fresh media or supernatant from normal 'small' cell culture was used. Factors such as IL1β or CCL2 release may be relevant to this process, given that qPCR detected the genes for production of these cytokines to be slightly upregulated in spontaneous GMC+ cell culture, compared to normal cell culture. Increased expression of surface proteins involved in cell contact and fusion ability, such as CD44, seen in spontaneous GMCs, which is potentiated by serum reduction, may also be relevant to cell-cell contact and induction of neighbouring cells as the cells deplete the media over time. During cell culture it was observed that one simple way to increase GMCs in the plate wells or growth flasks was to select for adherent cells by using an altered passaging protocol. Shorter exposure to trypsin-EDTA or 'rinsing off' the less adherent cells from the bottom of the flask with media results in the selection of adherent cells which remain in the cell culture. Passaging cells this way increases the population of GMCs in the flasks. This again suggests the importance of adhesion molecules for spontaneous GMC formation and the likelihood of cell fusion occurring.

5.3.2 Morphology, identity, and function of BV-2 and BV-2^{P2X7-} GMCs

BV-2 microglia appear to share some similarities with the existing better-described macrophage-derived GMC subtypes. Regardless of P2X7 expression, or mode of GMC induction, different numbers of nuclei per cell were observed. The nuclei were always arranged centrally in the cell, like a wreath, in a symmetrical or geometrically organized manner. It can be said with certainty that the cells did not resemble FBGCs because of the organized nuclear arrangement and due to the lack of GMC induction with IL-4 and IL-13. In terms of the nuclei, the cells best resembled the centrally organized LGCs and Touton cells. However, the BV-2 cells were actively phagocytic, unlike the LGCs described in the literature (Ahmadzadeh et al., 2022; Lay et al., 2007). To determine

whether the spontaneous BV-2 GMCs are like Touton GMCs, H&E, Giemsa, or lipid staining could be employed in the future to see whether lipid droplets or vesicles are present on the periphery of the central circle of nuclei, giving the GMCs a foamy appearance.

Many of the GMCs had a very large flattened cell body. Some studies on senescence suggest that multinucleation, a large cell body, and a flattened appearance are characteristics of aged cells (Kloc et al., 2022) . It is possible that GMCs, which indeed accumulate with aging in cell culture, are the result of senescence. The aged cells would likely display more pro-inflammatory characteristics, which is consistent with BV-2 GMCs showing upregulated IL-1β and CCL2 gene expression and high marker expression for CD86 and P2X7. However, other hallmarks of senescence in cells include poor nuclear envelope integrity, with chromatin becoming condensed into dense senescence-associated heterochromatin foci, and the release of chromatin fragments into the cytoplasm is frequently observed. In BV-2 GMCs, nuclear staining was always limited to the nuclei, which had a smooth, rounded appearance with diffuse and evenly distributed Hoechst stain, which suggests a healthy, youthful appearance. The presence of large vacuoles and large lysosomes is also commonly noted in aging or degenerating cells, and lysosomal function has been linked to aging in microglia (Moca et al., 2022) and neurodegeneration (Udayar et al., 2022). It would be of interest to investigate the lysosomal health in GMCs compared to mononucleated cells. No vacuoles were observed in BV-2 GMCs. This was true regardless of P2X7 expression and regardless of stimulation or GMC induction method. According to (Kloc et al., 2022) another sign of aging cells is mitochondrial impairment and reduced oxidative phosphorylation, while a higher number of mitochondria is observed, due to reduced mitophagy and impaired mitostasis. Ultimately, this results in enhanced ROS production. ROS production in GMCs has been reported, but it was not investigated here. It would be an interesting path to explore in future work. BV-2 and BV-2^{P2X7-} cells stained with Mitotracker Deep Red, indeed, reveal higher numbers of mitochondria in GMCs, which appears to correspond to a higher metabolic outcome in the Alamar Blue assay. A glucose uptake into BV-2 and BV-2^{P2X7-} GMCs vs small cells was measured by flow cytometry. No increased glucose uptake was observed, which could have otherwise been indicative of a higher glycolytic demand due to poor oxidative phosphorylation. NQO1 activity levels in microglial GMC-rich cultures were also found to be higher compared to the small cells. NQO1 is thought to be an important regulator of senescence in aging cells and in tumorigenesis. However, in the functional and viability assays performed, GMC+ cultures showed a high phagocytic function and similar viability to small cells. If indeed P2X7-expressing cells result in more senescence in cell culture and accumulation of GMCs as a result of aging, this may explain some hallmarks observed in HEK cells; however, BV-2 GMCs appeared as healthy and functional as the small cells of the same passage number in terms of phagocytosis, nuclear health.

Rather than resulting from senescence, the microglial GMCs may be sharing similarity with osteoclast-like GMCs. Spontaneously arising GMCs were shown by qPCR to express higher levels of osteoclast markers such as Cathepsin K, TRAP, MMP9, and fusion protein DC-STAMP, and these were upregulated in P2X7-expressing cells only. This may suggest that some of the GMCs forming in microglial cultures share similarities with macrophages and osteoclast-like giant cells. Osteoclasts are also known to have a high number of mitochondria to support their high energy demand. BV-2 cells in spontaneously occurring GMC+ populations had higher mitochondrial mass than small cells. In those ways spontaneous BV-2 microglial GMCs could be similar to Osteoclast-like GMCs, rather than resulting from senescence.

GMCs arising from macrophages in cell culture were described in the literature as possessing certain structural characteristics. GMCs in mouse macrophages *in vitro* show a similar centrally organized arrangement of nuclei, although it is not always 'wreath-like', which was observed in BV-2 cells, and characteristic actin rings on the borders of the multinucleated macrophages are commonly noted. Fusion of macrophages has also been described to happen via specialized fusopodia- thick filopodia rich in actin. BV-2 and BV-2^{P2X7-} GMCs were stained for actin using fluorescent phalloidin; however, no actin rings were observed in the microglial cells. This was true for both LPS, RANKL-induced, and spontaneously arising GMCs, regardless of P2X7 expression. In microglial GMCs, actin was evenly distributed across the cell body, accumulating in the center between the nuclei, and present in the larger protrusions concentrated on the ends- these may have been acting as fusopodia. These structures, rich in short bundles of actin filaments, are involved in chemosensing, attraction, and cell-to-cell adhesion. In osteoclasts and FBGCs these have been shown to be crucial for the cell fusion process, and PE phosphatidylethanolamide dynamics in fusopodia were shown to mediate the fusion of the membranes (Irie et al., 2017). One study confirmed that PS externalization and its detection by CD36 plays a role in cytokine-induced (especially IL-4) fusion of macrophages (Helming et al, 2009), however, CD36 was described as redundant in osteoclastogenesis, and was not investigated here due to a lack of IL-4-induced GMC formation to begin with. However, P2X7 is known to be involved in the control of phosphatidylserine (PS) exposure and PS flip to the outer membrane (J. H. Kang et al., 2020). PS flip preceding cell fusion depletes cholesterol from the cell membrane, increasing its fluidity (Verma et al., 2018). Phosphatidylethanolamine (PE) is also believed to be important. Its immobilization in the membrane was shown to inhibit filopodia formation, which initiates cell fusion in macrophages (Irie et al., 2017).

Conclusions

This chapter demonstrated the involvement of P2X7 in GMC formation in BV-2 microglia. While failure of cytokinesis via PKC in BV-2 GMCs has been proposed as a pathway involving LPS and inflammatory stimulation, P2X7 must also be considered as a fusogen contributing to a fusion path in GMC formation. P2X7 expression results in spontaneous GMC formation in up to 2% of the population in cell culture, however this can increase further under the right conditions as existing GMCs appear to 'recruit' other cells. Spontaneously occurring GMCs showed a different profile of gene expression than LPS-induced GMCs. This included upregulation of signature markers of osteoclasts and serum reduction was sufficient to induce these changes in P2X7-expressing cells, but not in P2X7 deficient clones. GMCs themselves were shown to display high levels of P2X7 which is considered a fusogen. P2X7 may be involved in expression of other fusogens via increasing local ATP and IL-1β levels and by influencing membrane flexibility (Ma et al., 2022a; Pellegatti et al., 2011). IL-1β induces monocyte and macrophage fusion in osteoclasts (Cao et al., 2016) and P2X7 expression may be further supporting the process of GMC formation simply by contributing to higher IL-1β secretion (Cao et al., 2016). Plasma membrane permeabilization is believed to be supported by P2X7 (Karasawa et al., 2017; Qu & Dubyak, 2009). In a study on RAW264.7 macrophages P2X7 silencing negatively impacted osteoclast size and functioning and resulted in lower expression of Cathepsin K (Ma et al., 2022).

BV-2 GMCs were found to be healthy and functional. While microglial GMCs share similarities with other subtypes of macrophage-originating GMCs, they also possess unique characteristics and appear to be a new and separate GMC type. More studies are needed to understand their behaviour in health and disease.

It was not determined whether multinucleation observed is occurring with nuclear fusion as the final step of the process. Throughout the work, some distinctively large nuclei were observed in giant cells in both BV-2 and HEK cultures. The presence of uneven numbers of multiple nuclei, as well as their very large size, may suggest that these cells did not form from failed cell division, but rather via cell fusion, which may have included nuclear fusion or ejection of a nucleus from the cell. For the purposes of this work, no cells with two nuclei or one nuclei were included in the cell counts for GMCs in the images, regardless of the nucleus size and the cell size. It is therefore possible that the resulting figures were a slight underestimate of the multinucleation events occurring, and the actual number of syncytia forming is higher because it ultimately includes synkaryons, as well as homokaryons. Interestingly, Shtaya et al., (2019) in their histological analysis of human intracerebral hemorrhage images, reports observing giant cells that did not contain any nuclei at all. In any future work it would be important to determine whether the giant cells with

two or less nuclei also had the same properties as multinucleated giant cells and whether they should be classified as the same type of cell.

Literature suggests that scavenger receptor CD36 then recognizes PS and CD36 has been shown to be important in GMCs but not in osteoclasts, and limited to IL-4 and IL-13 induced GMCs. Since no GMC formation was observed in response to IL-4 and IL-13, CD36 was not selected as a primary protein of interest in the qPCR experiment. Still, this might be interesting to pursue in any future work, especially in terms of identifying unifying markers of GMCs. Similarly, E-cadherin, which appears to be important in GMC formation and cell fusion (Fiorino & Harrison, 2016; Van Roy & Berx, 2008), was attempted in the qPCR experiment, but multiple sets of primers did not work. It would be interesting to gain insight into E-cadherin expression in the future and its relationship with P2X7.

Chapter 6 - General discussion

Microglia are a dynamic, heterogenous, and self-renewing population of brain-resident macrophages (Kettenmann et al., 2011). As such, they perform vital tasks in the CNS that require high adaptability and flexibility. The regulation of microglial behaviour comprises many intricate mechanisms and a synchronized interplay between the expression and activity of cells' receptors, their interaction with neighbouring microglia, astrocytes, and neurons, and the integration of microenvironmental cues(Kettenmann et al., 2011). The mechanisms regulating microglial function are not yet fully understood. The aim of this thesis was to examine the impact of the P2X7 receptor on microglial health and function. P2X7 is highly expressed by microglia and has been reported to affect microglial behaviour in many ways (He et al., 2017b; T. Jiang et al., 2015b; Monif et al., 2010; von Mücke-Heim et al., 2023). For example, activation of P2X7 with ATP has been linked in microglia to cytokine release and upregulation of pro-inflammatory transcription factors (Shieh et al., 2014). P2X7, in its unstimulated form, has been proposed to act as a scavenger receptor, driving phagocytosis (Gu et al., 2010); basal expression of this receptor in transfected HEK cells, and an *in vitro* model of microglia cells, was reported to aid survival and allow for proliferation in challenging conditions (Monif et al., 2010); and in macrophages P2X7 has been reported as a fusogen and an important player in osteoclast formation via fusion of macrophage and monocyte progenitors into multinucleated cells (Di et al., 2013; Irma Lemaire et al., 2006).

For the purpose of this thesis, BV-2 murine immortalized microglial cells were used. BV-2 cells endogenously expressing P2X7 were compared to a CRISPR-generated BV-2^{P2X7-} line. BV-2 cells are a good model for this type of research, as they are extensively used in other laboratories around the world and are well described in the literature (Henn et al., 2009). Using this model, any activity in relation to P2X7 expression could be easily examined and validated. There are obvious species-related differences between a mouse and a human cell line to be considered (Das et al., 2016; Henn et al., 2009); however, as a screening tool for implicating P2X7 signaling in microglial behaviour, this was a convenient model. Human P2X7 and mouse P2X7 respond in a very similar way to ATP stimulation and classic antagonists, with minor sensitivity differences (Hibell et al., 2000). Mouse and human microglia are similarly highly heterogeneous and plastic across different brain regions, demonstrating specialized morphologies, activities and functions in development and population remodelling (Sharma et al., 2021), however, this work would benefit from being validated in a human cell line to verify the P2X7 dependent activity of microglia relevant to advancing medical research, or validation in primary microglia over an immortalized cell line-especially in the work addressing proliferation.

In Chapter 3, the putative trophic activity of P2X7 was thoroughly examined. Various assays measuring cell viability, cell number, cycle divisions, and proliferation were employed to compare BV-2 and BV-2^{P2X7-} cell numbers following a 48h challenge of low serum and/or low glucose. No evidence was found for a proliferative advantage of P2X7-expressing cells. However, the Alamar blue assay consistently demonstrated what was interpreted to be a metabolic difference with respect to P2X7 expression (since Alamar blue is processed intracellularly by reductases such as diaphorases (O'Brien et al., 2000)). P2X7-dependent Alamar blue processing may be due to metabolic changes in the cells, or the presence of more numerous giant multinucleated cells in the P2X7-expressing cell line, which were linked to P2X7 expression in Chapter 5. Amoroso et al., (2012) showed that P2X7 plays an important role in the metabolic switch, similar to the Warburg effect displayed by cancer cells. In future work, it would be interesting to use more sensitive tools such as Seahorse assay, to examine any differences that occur in the metabolism of P2X7-expressing or P2X7-deficient cells, and whether these are exacerbated in giant multinucleated cells that were shown to highly express P2X7 in Chapter 5.

Activation and phenotypic differentiation of BV-2 and BV-2^{P2X7-} microglia were examined in Chapter 4. P2X7 expression did not affect polarization of the cells; however, a small advantage was found in CCL2 and IL-1β production with P2X7 expression, with LPS stimulation. Overall, the IL-1β ELISA assay did not detect major release of the cytokine, in contrast to what is reported for microglia in the literature, and it was noted that BV-2 cells, in the experimental setup used in this work, may not have been a good model for measuring IL-1β release. Similarly, CCL2 release ELISA, despite the optimisation efforts, did not reproduce the literature suggesting robust release via P2X7 with ATP stimulation (Shieh et al., 2014). However, other cytokines linked to P2X7 expression, such as IL-6 and TNF-α, may be of interest to test in the BV-2 vs BV-2^{P2X7-} model in the future. IL-1β and CCL2 ELISA assays may also prove to be useful in human microglia models over murine cells. Various cytokines and pro-inflammatory molecules were tested for their ability to influence BV-2 activation and polarization. The classical activators described previously in literature, such as LPS, IFN-γ, and IL-4, were equally capable of inducing activation morphological changes, regardless of P2X7 expression, and were able to alter surface receptor expression in concordance with the literature describing classic signs of polarization in microglia (Orihuela et al., 2016; L. Wang, Liu, et al., 2019). Neurosteroids were also examined as possible endogenous modulators of microglial activity via P2X7; however, no major morphological or proliferative changes were observed. Nevertheless, testosterone, pregnanolone, pregnenolone, and synthetic steroid Alfaxalone inhibited P2X7-induced Ca^{2+} signalling and macropore formation in fluorometric assays. Interestingly, allopregnanolone and pregnanolone also prevented giant cell formation in BV-2 cells, which was observed in Chapter 5. Endogenous steroid compounds such

as hormones and cholesterol metabolites are interesting to explore as possible endogenous modulators of microglial behaviour. The levels of cholesterol and its metabolites may be altered in various disease states, impacting neuroinflammation. Furthermore, hormonal profiles can vary between genders, age groups, and lifestyles, and are important to consider when developing pharmacological tools and treatments. This topic could be further explored in future work involving P2X7 and microglia.

Many of the Chapter 4 experiments would have benefited from more technical and biological replicates and power calculations to be able to better examine statistically significant differences.

In the literature, P2X7 was linked to phagocytic activity in microglia (Fairbairn et al., 2001b; Gu & Wiley, 2018). In this work, no difference was observed between BV-2 and BV-2^{P2X7-} cells in their ability to phagocytose small fluorescent particles such as *E-coli* or zymosan fluorescent bioparticles. A high capability for phagocytosis, however, was noted in GMCs described in Chapter 5.

Chapter 5 investigated the enhanced multinucleation and giant cell formation in BV-2 cell populations in relation to P2X7 expression. The basic activity, health, and function of GMCs were examined by looking at BV-2 and BV-2^{P2X7-} populations rich in GMCs. Nuclei and lysosome labelling did not reveal any signs associated with senescence in GMCs. The GMC cells appeared fully functional, expressing the same surface protein activation markers as small mononucleated BV-2 cells, but at a higher level compared to small cells, in the quiescent state, and upregulated P2X7 in BV-2 cells. The markers investigated included CD86, CD206, CD11b, and P2Y12 and P2X7. Spontaneously generated GMC BV-2 and BV-2^{P2X7-} cells were capable of phagocytosing large quantities of fluorescent particles such as Zymosan and *E. coli* pHrodo. Flow cytometry was used to quantify the phagocytosis in gated populations of small vs giant cells. It showed that the capacity of giant cells to phagocytose beads per cell was proportionally higher than that of small cells, likely simply due to the size of the cells. Milde et al., (2015) showed that GMCs and mononuclear cells are equally capable of phagocytosis of small particles up to a certain size. After 10µm diameter, however, GMCs had a clear advantage. It would be interesting to explore in any future work if larger particles were effectively phagocytosed by giant multinucleated BV-2 cells. One theory proposed for the function of GMCs in the brain is that they may be capable of phagocytosing large pieces of debris and dead cells. Wei et al., (2020) showed that in mice with induced ischemic events, GMCs accumulate in areas of stroke and contain pieces of the induced hematoma. It would be interesting to investigate whether factors associated with a haemorrhagic environment (for example, glucose/oxygen deprivation, hemoglobin or heme exposure can induce GMC formation in microglia *in vitro*. Lee et al., (2024) showed that Pyk2-induced GMC microglia

were more phagocytic for acute infusion of β-amyloid particles than mononucleated microglia. It would be very relevant to explore the role of GMCs in Alzheimer's models and any neurodegenerative diseases where the accumulation of protein aggregates causes neurotoxicity. In fact, GMCs induced clinically could be explored as a new way of removing large deposits in all neurodegenerative diseases, where the capacity of mononucleated microglia is simply not enough.

(J. Liu et al., 2024) showed that GMCs, such as osteoclasts, contain high levels of highly active mitochondria to meet the energy demands of these cells. In BV-2 microglia, GMCs were found to contain high levels of healthy mitochondria. Using flow cytometry, it was shown that giant cells contain a higher mitochondrial mass than small cells. Comparing the total populations of BV-2 and BV-2^{P2X7-} cells did not reveal any differences in terms of mitochondrial mass in Chapter 3. However, Chapter 5 shows that giant cells contain more mitochondria than small cells. Furthermore, P2X7-expressing cells contain higher populations of GMCs, and this means that the overall metabolic capacity of that cell line may be slightly higher than that of P2X7-deficient cells simply due to the number of mitochondria. Indeed, the Alamar blue assay carried out on populations of small cells vs GMC-rich populations of BV-2 and BV-2^{P2X7-} cells shows that GMC+ populations have a higher capacity to reduce the Resazurin dye. The differences between BV-2 and BV-2^{P2X7-} cells observed in Chapter 3 in all Alamar Blue figures may therefore be explained by the higher presence of GMCs in P2X7-expressing cells. The NQO1 assay comparing GMC+ populations to small cell populations of BV-2 and BV-2^{P2X7-} cells shows a similar advantage with respect to giant cells. It would be interesting to use more assays and tools to examine the ability of GMCs to release cytokines such as CCL-2 and IL-1β, compared to small cells, and with regard to P2X7 expression. The specific mechanisms of GMC formation under different conditions should be further confirmed in different P2X7-expressing cell lines to conclusively prove that cell fusion is occurring under physiological conditions, and whether LPS-induced GMC formation may be happening via a different pathway, such as inhibition of cell division.

The identity of microglial GMCs appeared to be unique, although they shared some similarities with osteoclast-like and Touton GMCs differentiated from macrophages in the periphery in certain diseases and inflammatory conditions. The spontaneous formation of GMCs in cell culture should be investigated further. Whether GMCs are a physiologically occurring, beneficial mechanism or the result of an underlying pathology is a controversial topic (Ahmadzadeh et al., 2022). Currently, there is not enough evidence to conclusively support either theory with respect to microglia. GMC numbers have been linked to aging by some authors (Kloc et al., 2022) and, indeed, were shown to accumulate with aging *in vitro* in this work. GMC relevance to neurodegenerative diseases

associated with aging should be further explored, along with the role of P2X7 in multinucleation and giant cell formation.

Conclusions

There are many mechanisms at play regulating microglial activity in health and disease throughout the lifespan. This work helped to further unravel the role P2X7 plays in microglial function and behaviour.

- P2X7 was not found to exert a trophic effect on the BV-2 cell line in challenging conditions of serum reduction and low glucose. The literature implying this trophic effect is uniform in all models and cell lines should be treated with care.
- P2X7 expression did not affect microglial activation in BV-2 cells, although the receptor itself was upregulated with inflammatory stimuli.
- P2X7 was found to enhance giant cell formation and multinucleation in BV-2 microglia, which in turn may enhance certain functions, such as dye-reducing capacity in the metabolic assay Alamar blue. Phagocytic activity of GMCs, especially, appears as an interesting target to pursue in research in the field of neurodegenerative diseases. Cytokine release from GMCs should also be explored in future work.
- BV-2 GMCs were shown to express different genes, depending on the mode of induction of multinucleation.
- How P2X7 drives GMC formation in microglia via cell fusion should be further confirmed by live imaging in future work.

Appendix

A

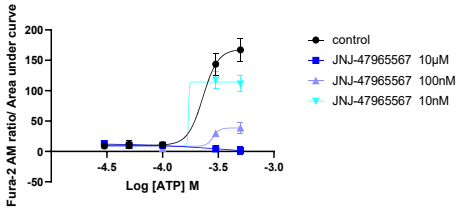

B

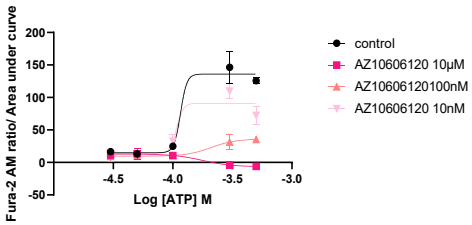

C

compound	**EC50 (µM)**	Confidence Interval (CI)
DMSO control for JNJ-47965567	230	164 to ?
JNJ-47965567 10nM	?	?
JNJ-47965567 100nM	284	?
JNJ-47965567 10µM	458	?
DMSO control for AZ10606120	116	?
AZ10606120 10nM	209	?
AZ10606120 100nM	209	108 to ?
AZ10606120 10µM	177	?

Figure A.1 Dose-response curves to P2X7 agonist ATP in Fura-2AM assay in BV-2 cells. *Standard Fura-2 AM protocol was followed on a confluent plate of BV-2 cells. Cells were loaded with Fura-2-AM dye for 1h and responses were measured after pre-incubation with the compounds for 15 mins-1h depending on the location on the plate. The concentration of ATP used was 1 mM, 500 µM, 300 µM, 100 µM, 50 µM, 30 µM. Antagonists were tested at 10 nM, 100 nM, and 10 µM. An average of one experiment, with three technical replicates per condition, is shown. Antagonists were used at concentration 10 µM vs DMSO solvent control. EC50 was calculated from the plots together with confidence intervals for each value (**C**.). (**A**) Effect of JNJ-47965567 on cells pre-cultured in 4mM glucose; (**B**) Effect of AZ10606120 on cells cultured in 17mM glucose.*

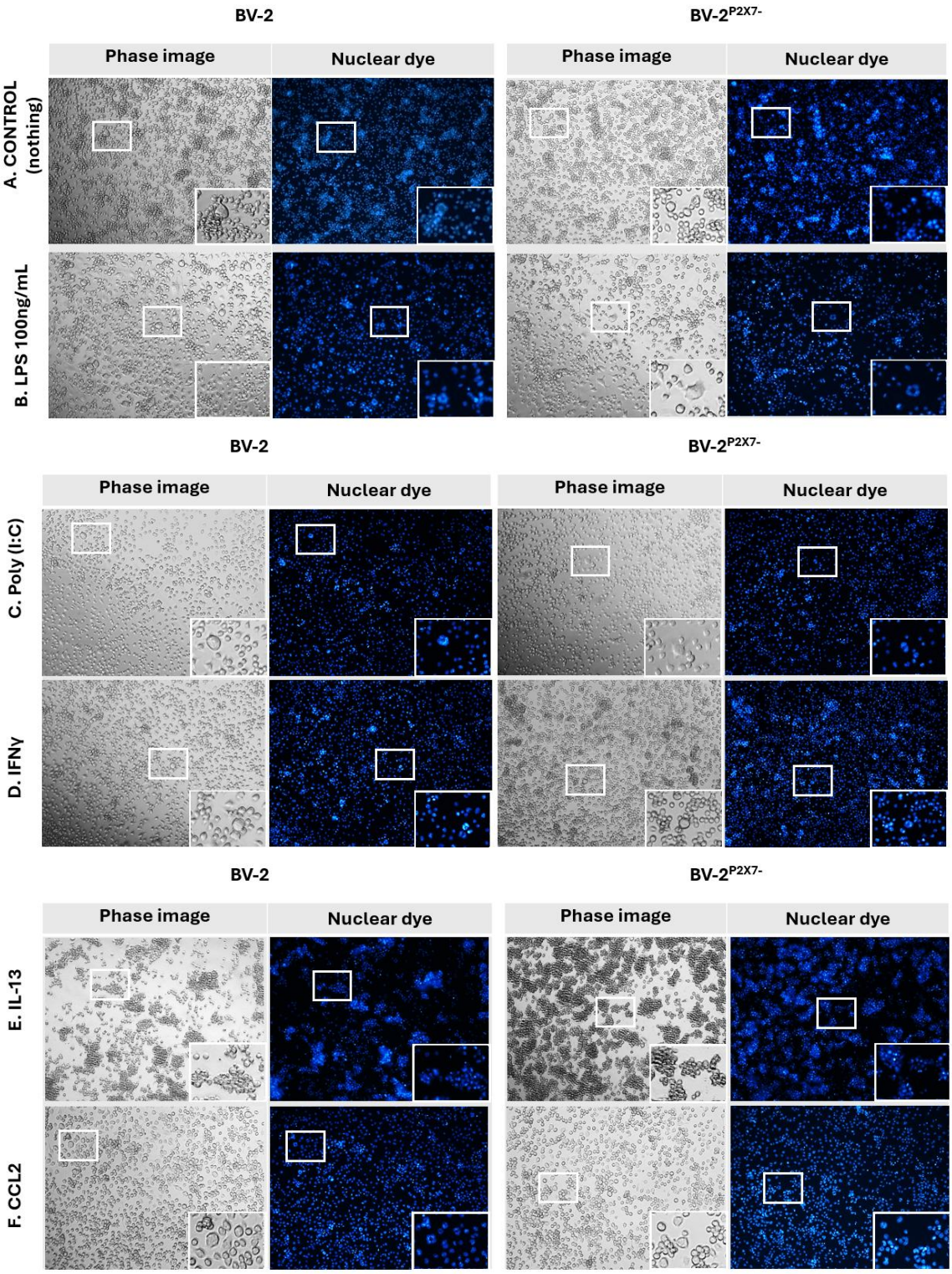
BV-2
BV-2P2X7-
Phase image
Nuclear dye
A. CONTROL (nothing)
B. LPS 100ng/mL
C. Poly (I:C)
D. IFNγ
E. IL-13
F. CCL2

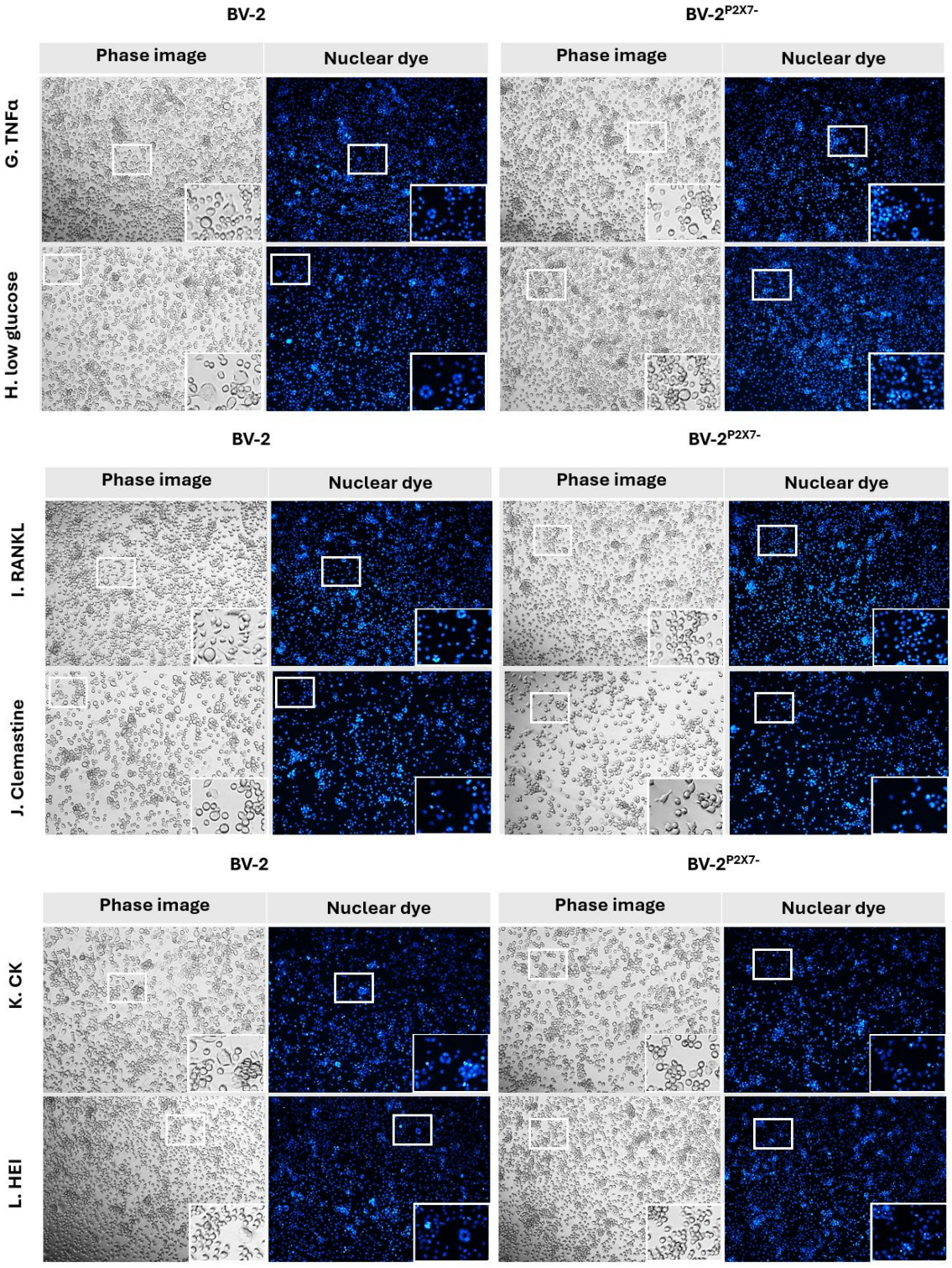
BV-2
BV-2P2X7-
Phase image
Nuclear dye
G. TNFα
H. low glucose
I. RANKL
J. Clemastine
K. CK
L. HEI

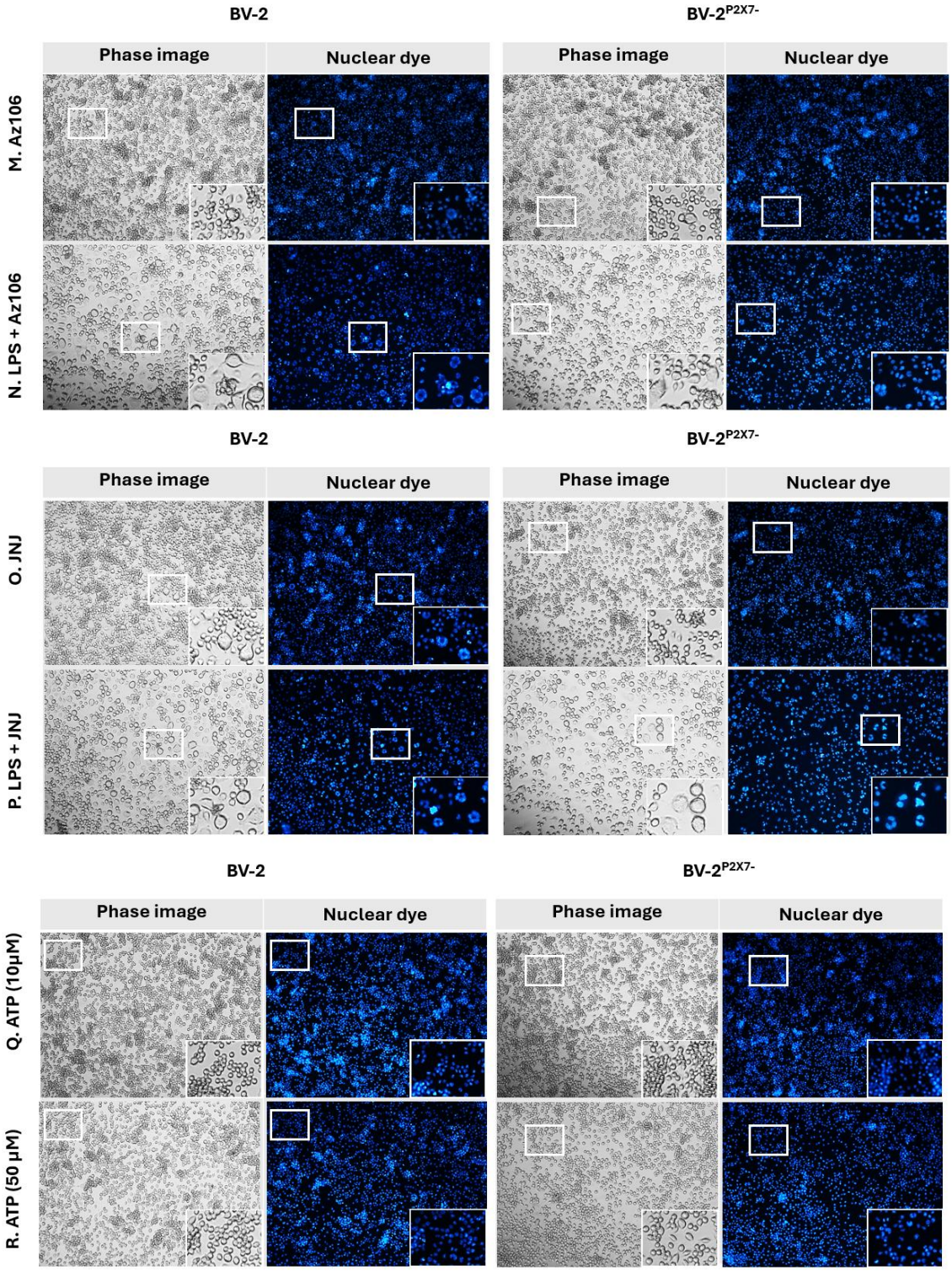
BV-2
BV-2P2X7-
Phase image
Nuclear dye
M. Az106
N. LPS + Az106
O. JNJ
P. LPS + JNJ
Q. ATP (10μM)
R. ATP (50 μM)

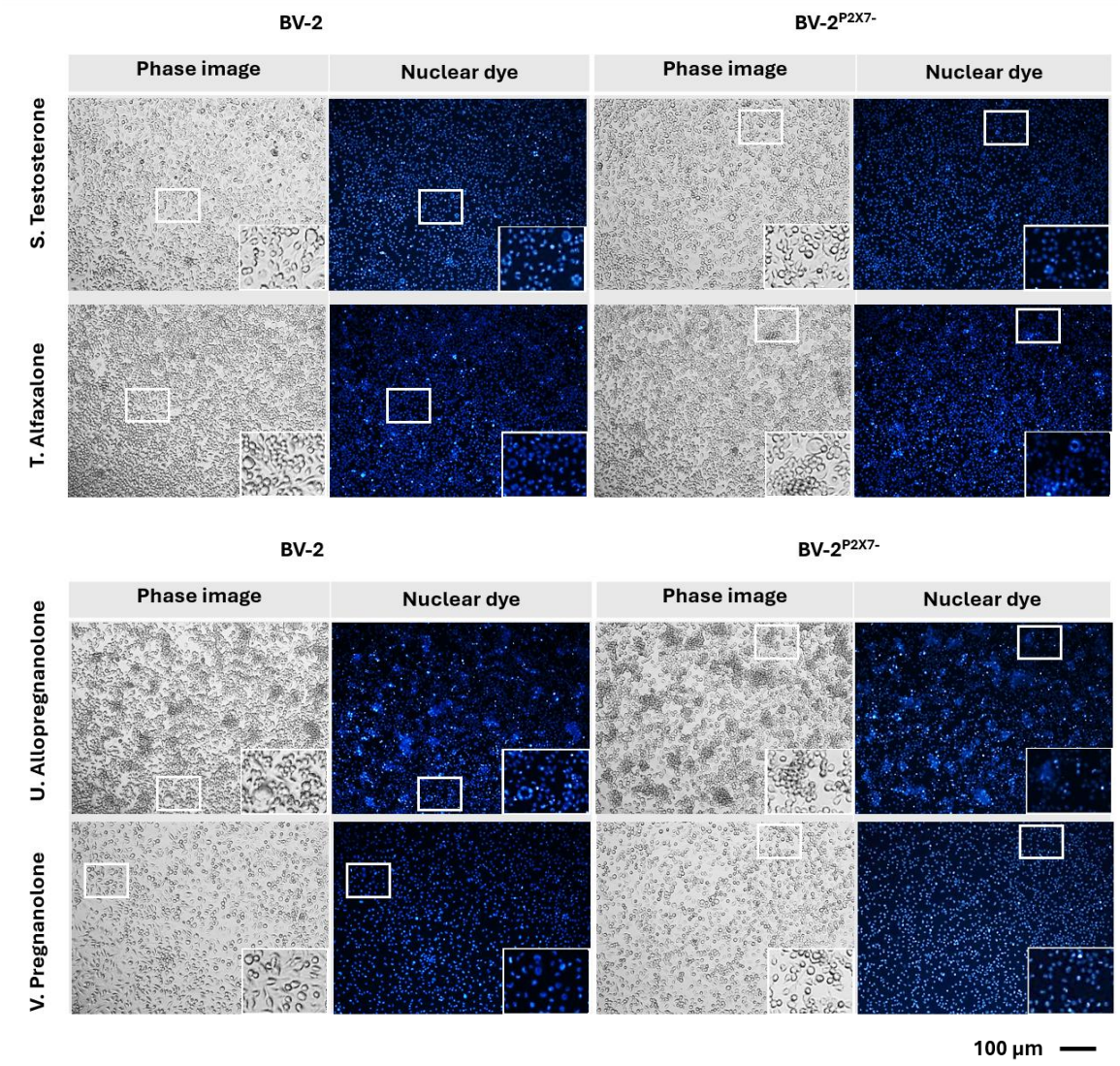

Figure A.2 Images of screening of various compounds for ability to induce GMC formation in BV-2 and BV-2^{P2X7-} cells. *Cells were plated in 96-well plates at density 9000 cells/well, stimulated in 0.5% serum containing media and incubated for 72h with different compounds. Nikon Ti Eclipse microscope together with Nikon NIS Elements software were used to obtain and edit the images. (**A**. control ('nothing'), **B.** LPS 100ng/mL, **C**. Poly (I:C) 100 ng/mL, **D**. IFNγ 50 ng/mL, **E**. IL-13 20 ng/mL, **F.** CCL2 10 ng/mL, **G**. TNFα 50 ng/mL, **H.** 5 mM glucose media, **I**. RANK ligand 100 ng/mL, **J.** Clemastine 1 µM, **K**. CK 5 µM, **L.** HEI 250 nM, **M**. Az106 1 µM, **N.** LPS 100 ng/mL + Az106 1 µM, **O**. JNJ 1 µM, **P**. LPS 100 ng/mL + JNJ 1 µM, **Q**. ATP 10 µM, **R**. ATP 50 µM, **S.** testosterone 10 µM, **T**. Alfaxalone 10 µM, **U**. Allopregnanolone 10 µM, **V.** Pregnanolone 10 µM). The formation of GMCs was inspected daily and photographs were taken at 72h. Due to cells ability to migrate across the plate 10 x objective was used to capture the widest image field. Three images were taken per well for accurate representation. A representative image of the middle of the well is shown for each condition. Digital zoom box shows x2 selected area. Giant cells were observed in phase images and corresponding nuclear dye images were used to confirm the presence of multiple nuclei. Any cell with three or more nuclei was considered multinucleated.Two independent experiments were performed.*

References

Adinolfi, E., Giulia Callegari, M., Ferrari, D., Bolognesi, C., Minelli, M., Wieckowski, M. R., Pinton, P., Rizzuto, R., & Di Virgilio, F. (2005). Basal Activation of the P2X 7 ATP Receptor Elevates Mitochondrial Calcium and Potential, Increases Cellular ATP Levels, and Promotes Serum-independent Growth. *Molecular Biology of the Cell*, *16*(16), 3260–3272. https://doi.org/10.1091/mbc.E04

Adrian, M., Weber, M., Tsai, M. C., Glock, C., Kahn, O. I., Phu, L., Cheung, T. K., Meilandt, W. J., Rose, C. M., & Hoogenraad, C. C. (2023). Polarized microtubule remodeling transforms the morphology of reactive microglia and drives cytokine release. *Nature Communications*, *14*(1). https://doi.org/10.1038/s41467-023-41891-6

Ahmadi Moghaddam, P., Singh, R., Mahmoodi, M., Mehrotra, M., Benaim, G., Luthra, R., & Paniz-Mondolfi, A. (2018). Poorly differentiated osteoclast-like giant cell variant of cutaneous squamous cell carcinoma: Uncovering its mutational landscape through massive parallel sequencing. *Pathology Research and Practice*, *214*(11), 1898–1903. https://doi.org/10.1016/j.prp.2018.08.017

Ahmadzadeh, K., Vanoppen, M., Rose, C. D., Matthys, P., & Wouters, C. H. (2022). Multinucleated Giant Cells: Current Insights in Phenotype, Biological Activities, and Mechanism of Formation. In *Frontiers in Cell and Developmental Biology* (Vol. 10). Frontiers Media S.A. https://doi.org/10.3389/fcell.2022.873226

Aldana, B. I. (2019). Microglia-Specific Metabolic Changes in Neurodegeneration. In *Journal of Molecular Biology* (Vol. 431, Number 9, pp. 1830–1842). Academic Press. https://doi.org/10.1016/j.jmb.2019.03.006

Allsopp, R. C., & Evans, R. J. (2015). Contribution of the juxtatransmembrane intracellular regions to the time course and permeation of ATP-gated P2X7 Receptor Ion Channels. *Journal of Biological Chemistry*, *290*(23), 14556–14566. https://doi.org/10.1074/jbc.M115.642033

Amoroso, F., Falzoni, S., Adinolfi, E., Ferrari, D., & Di Virgilio, F. (2012). The P2X7 receptor is a key modulator of aerobic glycolysis. *Cell Death and Disease*, *3*(8). https://doi.org/10.1038/cddis.2012.105

Antignano, I., Liu, Y., Offermann, N., & Capasso, M. (2023). Aging microglia. In *Cellular and Molecular Life Sciences* (Vol. 80, Number 5). Springer Science and Business Media Deutschland GmbH. https://doi.org/10.1007/s00018-023-04775-y

Antonio, L. S., Stewart, A. P., Xu, X. J., Varanda, W. A., Murrell-Lagnado, R. D., & Edwardson, J. M. (2011). P2X4 receptors interact with both P2X2 and P2X7 receptors in the form of homotrimers. *British Journal of Pharmacology*, *163*(5), 1069–1077. https://doi.org/10.1111/j.1476-5381.2011.01303.x

Aramin, H., Zaleski, M., Prieto, V. G., & Aung, P. P. (2019). Skin and superficial soft tissue neoplasms with multinucleated giant cells: Clinical, histologic, phenotypic, and molecular differentiating features. In *Annals of Diagnostic Pathology* (Vol. 42, pp. 18–32). W.B. Saunders. https://doi.org/10.1016/j.anndiagpath.2019.06.013

Ariffin, S. H. Z., Wahab, R. M. A., Razak, M. A., Yazid, M. D., Shahidan, M. A., Miskon, A., & Abidin, I. Z. Z. (2024). Evaluation of in vitro osteoblast and osteoclast differentiation from stem cell: a systematic review of morphological assays and staining techniques. *Peer Journal*, *12*(7). https://doi.org/10.7717/peerj.17790

Armstrong, S., Pereverzev, A., Dixon, S. J., & Sims, S. M. (2009). Activation of P2X7 receptors causes isoform-specific translocation of protein kinase C in osteoclasts. *Journal of Cell Science*, *122*(1), 136–144. https://doi.org/10.1242/jcs.031534

Arnett, T. R., & Orriss, I. R. (2018). Metabolic properties of the osteoclast. In *Bone* (Vol. 115, pp. 25–30). Elsevier Inc. https://doi.org/10.1016/j.bone.2017.12.021

Bachmann, M., Kukkurainen, S., Hytönen, V. P., & Wehrle-Haller, B. (2019). Cell adhesion by integrins. *Physiol Rev*, *99*, 1655–1699. https://doi.org/10.1152/physrev.00036.2018.-Integrins

Banati, R. B., Egensperger, R., Maassen, A., Hager, G., Kreutzberg, G. W., Manuel, B., & Graeber. (2004). Mitochondria in activated microglia in vitro. *Journal of Neurocytology*, *33*(5), 535–541. https://doi.org/10.1007/s11068-004-0515-7

Barbieri, R., Alloisio, S., Ferroni, S., & Nobile, M. (2008). Differential crosstalk between P2X7 and arachidonic acid in activation of mitogen-activated protein kinases. *Neurochemistry International*, *53*(6–8), 255–262. https://doi.org/10.1016/j.neuint.2008.05.001

Beiter, R. M., Sheehan, P. W., & Schafer, D. P. (2024). Microglia phagocytic mechanisms: Development informing disease. In *Current Opinion in Neurobiology* (Vol. 86). Elsevier Ltd. https://doi.org/10.1016/j.conb.2024.102877

Bernier, L. P., York, E. M., Kamyabi, A., Choi, H. B., Weilinger, N. L., & MacVicar, B. A. (2020). Microglial metabolic flexibility supports immune surveillance of the brain parenchyma. *Nature Communications*, *11*(1). https://doi.org/10.1038/s41467-020-15267-z

Bernier, L. P., York, E. M., & MacVicar, B. A. (2020). Immunometabolism in the Brain: How Metabolism Shapes Microglial Function. In *Trends in Neurosciences* (Vol. 43, Number 11, pp. 854–869). Elsevier Ltd. https://doi.org/10.1016/j.tins.2020.08.008

Bhattacharya, A., Wang, Q., Ao, H., Shoblock, J. R., Lord, B., Aluisio, L., Fraser, I., Nepomuceno, D., Neff, R. A., Welty, N., Lovenberg, T. W., Bonaventure, P., Wickenden, A. D., & Letavic, M. A. (2013). Pharmacological characterization of a novel centrally permeable P2X7 receptor antagonist: JNJ-47965567. *British Journal of Pharmacology*, *170*(3), 624–640. https://doi.org/10.1111/bph.12314

Bianco, F., Ceruti, S., Colombo, A., Fumagalli, M., Ferrari, D., Pizzirani, C., Matteoli, M., Di Virgilio, F., Abbracchio, M. P., & Verderio, C. (2006). A role for P2X 7 in microglial proliferation. *Journal of Neurochemistry*, *99*(3), 745–758. https://doi.org/10.1111/j.1471-4159.2006.04101.x

Bose, S., Kim, S., Oh, Y., Moniruzzaman, M., Lee, G., & Cho, J. (2016). Effect of CCL2 on BV2 microglial cell migration: Involvement of probable signaling pathways. *Cytokine*, *81*, 39–49. https://doi.org/10.1016/j.cyto.2016.02.001

Bradford, M. D., & Soltoff, S. P. (2002). P2X 7 receptors activate protein kinase D and p42/p44 mitogen-activated protein kinase (MAPK) downstream of protein kinase C. In *Biochem. J* (Vol. 366).

Brooks, P. J., Glogauer, M., & McCulloch, C. A. (2019). An Overview of the Derivation and Function of Multinucleated Giant Cells and Their Role in Pathologic Processes. In *American Journal of Pathology* (Vol. 189, Number 6, pp. 1145–1158). Elsevier Inc. https://doi.org/10.1016/j.ajpath.2019.02.006

Brooks, P. J., Wang, Y., Magalhaes, M. A., Glogauer, M., & McCulloch, C. A. (2021). CD301 mediates fusion in IL-4-driven multinucleated giant cell formation. *Journal of Cell Science*, *133*(24). https://doi.org/10.1242/jcs.248864

Brown, G. C., & Neher, J. J. (2014). Microglial phagocytosis of live neurons. *Nature Reviews Neuroscience*, *15*(4), 209–216. https://doi.org/10.1038/nrn3710

Bruttger, J., Karram, K., Wörtge, S., Regen, T., Marini, F., Hoppmann, N., Klein, M., Blank, T., Yona, S., Wolf, Y., Mack, M., Pinteaux, E., Müller, W., Zipp, F., Binder, H., Bopp, T., Prinz, M., Jung, S., & Waisman, A. (2015). Genetic Cell Ablation Reveals Clusters of Local Self-Renewing Microglia in the Mammalian Central Nervous System. *Immunity*, *43*(1), 92–106. https://doi.org/10.1016/j.immuni.2015.06.012

Buell, G. N., & Rassendren, F. (1998). P2X: The ionotropic receptor for extracellular ATP. *Drug Development Research*, *45*(3–4), 125–129. https://doi.org/10.1002/(SICI)1098-2299(199811/12)45:3/4<125::AID-DDR6>3.0.CO;2-I

Burnstock, G. (2018). Purine and purinergic receptors. *Brain and Neuroscience Advances*, *2*, 239821281881749. https://doi.org/10.1177/2398212818817494

Burnstock, G., & Knight, G. E. (2018). The potential of P2X7 receptors as a therapeutic target, including inflammation and tumour progression. In *Purinergic Signalling* (Vol. 14, Number 1). Springer Netherlands. https://doi.org/10.1007/s11302-017-9593-0

Cai, F., Jiang, B., & He, F. (2024). Formation and biological activities of foreign body giant cells in response to biomaterials. In *Acta Biomaterialia* (Vol. 188, pp. 1–26). Acta Materialia Inc. https://doi.org/10.1016/j.actbio.2024.08.034

Campagno, K. E., Lu, W., Sripinun, P., Albalawi, F., Cenaj, A., & Mitchell, C. H. (2025). Priming and release of cytokine IL-1β in microglial cells from the retina. *Experimental Eye Research*, *252*. https://doi.org/10.1016/j.exer.2025.110246

Campagno, K. E., & Mitchell, C. H. (2021). The P2X7 Receptor in Microglial Cells Modulates the Endolysosomal Axis, Autophagy, and Phagocytosis. In *Frontiers in Cellular Neuroscience* (Vol. 15). Frontiers Media S.A. https://doi.org/10.3389/fncel.2021.645244

Campbell, J. N., & Meyer, R. A. (2006). Mechanisms of Neuropathic Pain. In *Neuron* (Vol. 52, Number 1, pp. 77–92). https://doi.org/10.1016/j.neuron.2006.09.021

Cao, Y., Jansen, I. D. C., Sprangers, S., Stap, J., Leenen, P. J. M., Everts, V., & de Vries, T. J. (2016). IL-1β differently stimulates proliferation and multinucleation of distinct mouse bone marrow osteoclast precursor subsets. *Journal of Leukocyte Biology*, *100*(3), 513–523. https://doi.org/10.1189/jlb.1a1215-543r

Cargnello, M., & Roux, P. P. (2011). Activation and Function of the MAPKs and Their Substrates, the MAPK-Activated Protein Kinases. *Microbiology and Molecular Biology Reviews*, *75*(1), 50–83. https://doi.org/10.1128/mmbr.00031-10

Chessell, I. P., Hatcher, J. P., Bountra, C., Michel, A. D., Hughes, J. P., Green, P., Egerton, J., Murfin, M., Richardson, J., Peck, W. L., Grahames, C. B. A., Casula, M. A., Yiangou, Y., Birch, R.,

Anand, P., & Buell, G. N. (2005). Disruption of the P2X7 purinoceptor gene abolishes chronic inflammatory and neuropathic pain. *Pain*, *114*(3), 386–396. https://doi.org/10.1016/j.pain.2005.01.002

Collado-Díaz, V., Martinez-Cuesta, M. Á., Blanch-Ruiz, M. A., Sánchez-López, A., García-Martínez, P., Peris, J. E., Usach, I., Ivorra, M. D., Lacetera, A., Martín-Santamaría, S., Esplugues, J. V., & Alvarez, A. (2021). Abacavir Increases Purinergic P2X7 Receptor Activation by ATP: Does a Pro-inflammatory Synergism Underlie Its Cardiovascular Toxicity? *Frontiers in Pharmacology*, *12*. https://doi.org/10.3389/fphar.2021.613449

Costa-Junior, H. M., Vieira, F. S., & Coutinho-Silva, R. (2011). C terminus of the P2X7 receptor: Treasure hunting. In *Purinergic Signalling* (Vol. 7, Number 1, pp. 7–19). Kluwer Academic Publishers. https://doi.org/10.1007/s11302-011-9215-1

Danve, A., Grafe, M., & Deodhar, A. (2014). Amyloid Beta-Related Angiitis-A Case Report and Comprehensive Review of Literature of 94 Cases. In *Seminars in Arthritis and Rheumatism* (Vol. 44, Number 1, pp. 86–92). W.B. Saunders. https://doi.org/10.1016/j.semarthrit.2014.02.001

Das, A., Kim, S. H., Arifuzzaman, S., Yoon, T., Chai, J. C., Lee, Y. S., Park, K. S., Jung, K. H., & Chai, Y. G. (2016). Transcriptome sequencing reveals that LPS-triggered transcriptional responses in established microglia BV2 cell lines are poorly representative of primary microglia. *Journal of Neuroinflammation*, *13*(1). https://doi.org/10.1186/s12974-016-0644-1

Deczkowska, A., Keren-Shaul, H., Weiner, A., Colonna, M., Schwartz, M., & Amit, I. (2018). Disease-Associated Microglia: A Universal Immune Sensor of Neurodegeneration. In *Cell* (Vol. 173, Number 5, pp. 1073–1081). Cell Press. https://doi.org/10.1016/j.cell.2018.05.003

Denlinger, L. C., Fisette, P. L., Sommer, J. A., Watters, J. J., Prabhu, U., Dubyak, G. R., Proctor, R. A., & Bertics, P. J. (2001). *Cutting Edge: The Nucleotide Receptor P2X7 Contains Multiple Protein-and Lipid-Interaction Motifs Including a Potential Binding Site for Bacterial Lipopolysaccharide1*. https://academic.oup.com/jimmunol/article/167/4/1871/8025618

Dhuna, K., Felgate, M., Bidula, S. M., Walpole, S., Bibic, L., Cromer, B. A., Angulo, J., Sanderson, J., Stebbing, M. J., & Stokes, L. (2019). Ginsenosides act as positive modulators of P2X4 receptors. *Molecular Pharmacology*, *95*(2), 210–221. https://doi.org/10.1124/mol.118.113696

Di, F., Zhang, V., Pellegatti, P., Adinolfi, E., Chiozzi, P., Lemaire, I., Falzoni, S., & Leduc, N. (2013). Involvement of the Purinergic Receptor P2X7 in the Formation of Giant Multinucleated Cells. In *J Immunol References The Journal of Immunology at Pennsylvania State Univ on February* (Vol. 177). http://www.jimmunol.org/content/177/10/7257http://www.jimmunol.org/content/177/10/7257.full#ref-list-1http://www.aai.org/ji/copyright.htmlhttp://jimmunol.org/cgi/alerts/etochttp://jimmunol.org/

Di Virgilio, F., Ferrari, D., & Adinolfi, E. (2009). P2X7: A growth-promoting receptor - Implications for cancer. *Purinergic Signalling*, *5*(2), 251–256. https://doi.org/10.1007/s11302-009-9145-3

Di Virgilio, F., Ferrari, D., Idzko, M., Panther, E., Norgauer, J., La Sala, A., & Girolomoni, G. (2003). Extracellular ATP, P2 receptors, and inflammation. *Drug Development Research*, *59*(1), 171–174. https://doi.org/10.1002/ddr.10191

Di Virgilio Irma Lemaire, F., Falzoni, S., & Zhang, B. (2011). The P2X7 Receptor and Pannexin-1 Are Both Required for the Promotion of Multinucleated Macrophages by the Inflammatory Cytokine GM-CSF. *J Immunol References*, *187*, 3878–3887. https://doi.org/10.4049/jimmunol.1002780

Divangahi, M., Aaby, P., Khader, S. A., Barreiro, L. B., Bekkering, S., Chavakis, T., van Crevel, R., Curtis, N., DiNardo, A. R., Dominguez-Andres, J., Duivenwoorden, R., Fanucchi, S., Fayad, Z., Fuchs, E., Hamon, M., Jeffrey, K. L., Khan, N., Joosten, L. A. B., Kaufmann, E., … Netea, M. G. (2021). Trained immunity, tolerance, priming and differentiation: distinct immunological processes. In *Nature Immunology* (Vol. 22, Number 1, pp. 2–6). Nature Research. https://doi.org/10.1038/s41590-020-00845-6

Douguet, L., Janho dit Hreich, S., Benzaquen, J., Seguin, L., Juhel, T., Dezitter, X., Duranton, C., Ryffel, B., Kanellopoulos, J., Delarasse, C., Renault, N., Furman, C., Homerin, G., Féral, C., Cherfils-Vicini, J., Millet, R., Adriouch, S., Ghinet, A., Hofman, P., & Vouret-Craviari, V. (2021). A small-molecule P2RX7 activator promotes anti-tumor immune responses and sensitizes lung tumor to immunotherapy. *Nature Communications*, *12*(1). https://doi.org/10.1038/s41467-021-20912-2

Drill, M., Jones, N. C., Hunn, M., O'brien, T. J., & Monif, M. (2021). *Antagonism of the ATP-gated P2X7 receptor: a potential therapeutic strategy for cancer*. (17), 215–227. https://doi.org/10.1007/s11302-021-09776-9/Published

Duque-Prata, A., Serpa, C., & Caridade, P. J. S. B. (2024). Theoretical Evaluation of Fluorinated Resazurin Derivatives for In Vivo Applications. *Molecules*, *29*(7). https://doi.org/10.3390/molecules29071507

Escoubas, C. C., Dorman, L. C., Nguyen, P. T., Lagares-Linares, C., Nakajo, H., Anderson, S. R., Barron, J. J., Wade, S. D., Cuevas, B., Vainchtein, I. D., Silva, N. J., Guajardo, R., Xiao, Y., Lidsky, P. V., Wang, E. Y., Rivera, B. M., Taloma, S. E., Kim, D. K., Kaminskaya, E., … Molofsky, A. V. (2024). Type-I-interferon-responsive microglia shape cortical development and behavior. *Cell*, *187*(8), 1936-1954.e24. https://doi.org/10.1016/j.cell.2024.02.020

Fairbairn, I. P., Stober, C. B., Kumararatne, D. S., & Lammas, D. A. (2001a). ATP-Mediated Killing of Intracellular Mycobacteria by Macrophages Is a P2X7-Dependent Process Inducing Bacterial Death by Phagosome-Lysosome Fusion. *The Journal of Immunology*, *167*(6), 3300–3307. https://doi.org/10.4049/jimmunol.167.6.3300

Fairbairn, I. P., Stober, C. B., Kumararatne, D. S., & Lammas, D. A. (2001b). *ATP-Mediated Killing of Intracellular Mycobacteria by Macrophages Is a P2X7-Dependent Process Inducing Bacterial Death by Phagosome-Lysosome Fusion1*. https://academic.oup.com/jimmunol/article/167/6/3300/8017367

Falzoni, S., Chiozzi, P., Ferrari, D., Buell, G., & Di Virgilio, F. (2000). P2X 7 Receptor and Polykarion Formation. In *Molecular Biology of the Cell* (Vol. 11).

Felgate, M. (2019). *P2X7 Receptor Function in Microglia in Relation to Glaucoma*. PhD thesis. University of East Anglia

Fendrick, S. E., Xue, Q. S., & Streit, W. J. (2007). Formation of multinucleated giant cells and microglial degeneration in rats expressing a mutant Cu/Zn superoxide dismutase gene. *Journal of Neuroinflammation*, *4*. https://doi.org/10.1186/1742-2094-4-9

Ferrari, D., Pizzirani, C., Adinolfi, E., Forchap, S., Sitta, B., Turchet, L., Falzoni, S., Minelli, M., Baricordi, R., & Di Virgilio, F. (2004). The Antibiotic Polymyxin B Modulates P2X 7 Receptor Function . *The Journal of Immunology*, *173*(7), 4652–4660. https://doi.org/10.4049/jimmunol.173.7.4652

Ferrari, D., Pizzirani, C., Adinolfi, E., Lemoli, R. M., Curti, A., Idzko, M., Panther, E., & Di Virgilio, F. (2006). The P2X 7 Receptor: A Key Player in IL-1 Processing and Release . *The Journal of Immunology*, *176*(7), 3877–3883. https://doi.org/10.4049/jimmunol.176.7.3877

Ferrari, D., Stroh, C., & Schulze-Osthoff, K. (1999). P2X7/P2Z purinoreceptor-mediated activation of transcription factor NFAT in microglial cells. *Journal of Biological Chemistry*, *274*(19), 13205–13210. https://doi.org/10.1074/jbc.274.19.13205

Filiano, A. J., Gadani, S. P., & Kipnis, J. (2017). How and why do T cells and their derived cytokines affect the injured and healthy brain? In *Nature Reviews Neuroscience* (Vol. 18, Number 6, pp. 375–384). Nature Publishing Group. https://doi.org/10.1038/nrn.2017.39

Fiorino, C., & Harrison, R. E. (2016). E-cadherin is important for cell differentiation during osteoclastogenesis. *Bone*, *86*, 106–118. https://doi.org/10.1016/j.bone.2016.03.004

Flowers, A., Bell-Temin, H., Jalloh, A., Stevens, S. M., & Bickford, P. C. (2017). Proteomic anaysis of aged microglia: Shifts in transcription, bioenergetics, and nutrient response. *Journal of Neuroinflammation*, *14*(1). https://doi.org/10.1186/s12974-017-0840-7

Fox, D. T., & Duronio, R. J. (2013). Endoreplication and polyploidy: Insights into development and disease. *Development (Cambridge)*, *140*(1), 3–12. https://doi.org/10.1242/dev.080531

Franceschini, A., Capece, M., Chiozzi, P., Falzoni, S., Sanz, J. M., Sarti, A. C., Bonora, M., Pinton, P., & Di Virgilio, F. (2015). The P2X7 receptor directly interacts with the NLRP3 inflammasome scaffold protein. *FASEB Journal*, *29*(6), 2450–2461. https://doi.org/10.1096/FJ.14-268714

Frank, M. G., Fonken, L. K., Watkins, L. R., & Maier, S. F. (2019). Microglia: Neuroimmune-sensors of stress. In *Seminars in Cell and Developmental Biology* (Vol. 94, pp. 176–185). Elsevier Ltd. https://doi.org/10.1016/j.semcdb.2019.01.001

Fu, X., Wang, M., Wan, Y., Hua, Y., Keep, R. F., & Xi, G. (2024). Formation of Multinucleated Giant Cells after Experimental Intracerebral Hemorrhage: Characteristics and Role of Complement C3. *Biomedicines*, *12*(6). https://doi.org/10.3390/biomedicines12061251

Fujiwara, M., Ohbori, K., Ohishi, A., Nishida, K., Uozumi, Y., & Nagasawa, K. (2017). Species Difference in Sensitivity of Human and Mouse P2X7 Receptors to Inhibitory Effects of Divalent Metal Cations. In *Biol. Pharm. Bull* (Vol. 40, Number 3).

Ghosh, S., Castillo, E., Frias, E. S., & Swanson, R. A. (2018). Bioenergetic regulation of microglia. In *GLIA* (Vol. 66, Number 6, pp. 1200–1212). John Wiley and Sons Inc. https://doi.org/10.1002/glia.23271

Giannasi, C., Niada, S., Della Morte, E., Casati, S. R., De Palma, C., & Brini, A. T. (2023). Serum starvation affects mitochondrial metabolism of adipose-derived stem/stromal cells. *Cytotherapy*, *25*(7), 704–711. https://doi.org/10.1016/j.jcyt.2023.03.004

Gil, B., Smith, J., Tang, Y., Illes, P., & Engel, T. (2022). Beyond Seizure Control: Treating Comorbidities in Epilepsy via Targeting of the P2X7 Receptor. In *International Journal of Molecular Sciences* (Vol. 23, Number 4). MDPI. https://doi.org/10.3390/ijms23042380

Gimeno-Bayón, López-López, J., Mj, R., & Mahy N. (2014). *Title: Glucose pathways adaptation supports acquisition of activated microglia phenotype*.

Giuliani, A. L., Colognesi, D., Ricco, T., Roncato, C., Capece, M., Amoroso, F., Wang, Q. G., De Marchi, E., Gartland, A., Di Virgilio, F., & Adinolfi, E. (2014). Trophic activity of human P2X7 receptor isoforms A and B in osteosarcoma. *PLOS ONE*, *9*(9). https://doi.org/10.1371/journal.pone.0107224

Giuliani, A. L., Sarti, A. C., Falzoni, S., & Di Virgilio, F. (2017). The P2X7 receptor-interleukin-1 liaison. In *Frontiers in Pharmacology* (Vol. 8, Number MAR). Frontiers Research Foundation. https://doi.org/10.3389/fphar.2017.00123

Grol, M. W., Panupinthu, N., Korcok, J., Sims, S. M., & Dixon, S. J. (2009). Expression, signaling, and function of P2X7 receptors in bone. In *Purinergic Signalling* (Vol. 5, Number 2, pp. 205–221). https://doi.org/10.1007/s11302-009-9139-1

Gschwandtner, M., Derler, R., & Midwood, K. S. (2019). More Than Just Attractive: How CCL2 Influences Myeloid Cell Behavior Beyond Chemotaxis. In *Frontiers in Immunology* (Vol. 10). Frontiers Media S.A. https://doi.org/10.3389/fimmu.2019.02759

Gu, B. J., Duce, J. A., Valova, V. A., Wong, B., Bush, A. I., Petrou, S., & Wiley, J. S. (2012). P2X7 receptor-mediated scavenger activity of mononuclear phagocytes toward non-opsonized particles and apoptotic cells is inhibited by serum glycoproteins but remains active in cerebrospinal fluid. *Journal of Biological Chemistry*, *287*(21), 17318–17330. https://doi.org/10.1074/jbc.M112.340885

Gu, B. J., Rathsam, C., Stokes, L., Mcgeachie, A. B., & Wiley, J. S. (2009). Extracellular ATP dissociates nonmuscle myosin from P2X 7 complex: this dissociation regulates P2X 7 pore formation. *Am J Physiol Cell Physiol*, *297*, 430–439. https://doi.org/10.1152/ajpcell.00079.2009.-The

Gu, B. J., Saunders, B. M., Jursik, C., & Wiley, J. S. (2010). The P2X 7-nonmuscle myosin membrane complex regulates phagocytosis of nonopsonized particles and bacteria by a pathway attenuated by extracellular ATP. *Blood*, *115*, 1621–1631. https://doi.org/10.1182/blood-2009-11

Gu, B. J., Saunders, B. M., Petrou, S., & Wiley, J. S. (2011). P2X7 Is a Scavenger Receptor for Apoptotic Cells in the Absence of Its Ligand, Extracellular ATP. *The Journal of Immunology*, *187*(5), 2365–2375. https://doi.org/10.4049/jimmunol.1101178

Gu, B. J., & Wiley, J. S. (2018). P2X7 as a scavenger receptor for innate phagocytosis in the brain. In *British Journal of Pharmacology* (Vol. 175, Number 22, pp. 4195–4208). John Wiley and Sons Inc. https://doi.org/10.1111/bph.14470

Guan, Z., Kuhn, J. A., Wang, X., Colquitt, B., Solorzano, C., Vaman, S., Guan, A. K., Evans-Reinsch, Z., Braz, J., Devor, M., Abboud-Werner, S. L., Lanier, L. L., Lomvardas, S., & Basbaum, A. I. (2015). Injured sensory neuron-derived CSF1 induces microglial proliferation and DAP12-dependent pain. *Nature Neuroscience*, *19*(1), 94–101. https://doi.org/10.1038/nn.4189

Gutiérrez, I. L., Martín-Hernández, D., MacDowell, K. S., García-Bueno, B., Caso, J. R., Leza, J. C., & Madrigal, J. L. M. (2025). CX3CL1 Regulation of Gliosis in Neuroinflammatory and

Neuroprotective Processes. In *International Journal of Molecular Sciences* (Vol. 26, Number 3). Multidisciplinary Digital Publishing Institute (MDPI). https://doi.org/10.3390/ijms26030959

Hambardzumyan, D., Gutmann, D. H., & Kettenmann, H. (2015). The role of microglia and macrophages in glioma maintenance and progression. In *Nature Neuroscience* (Vol. 19, Number 1, pp. 20–27). Nature Publishing Group. https://doi.org/10.1038/nn.4185

Han, G., Zuo, J., & Holliday, L. S. (2019). Specialized roles for actin in osteoclasts: Unanswered questions and therapeutic opportunities. In *Biomolecules* (Vol. 9, Number 1). MDPI AG. https://doi.org/10.3390/biom9010017

Han, X., Sterling, H., Chen, Y., Saginario, C., Brown, E. J., Frazier, W. A., Lindberg, F. P., & Vignery, A. (2000). CD47, a ligand for the macrophage fusion receptor, participates in macrophage multinucleation. *Journal of Biological Chemistry*, *275*(48), 37984–37992. https://doi.org/10.1074/jbc.M002334200

Hanisch, U. K. (2002). Microglia as a source and target of cytokines. In *Glia* (Vol. 40, Number 2, pp. 140–155). https://doi.org/10.1002/glia.10161

Hattori, Y. (2022). The behavior and functions of embryonic microglia. In *Anatomical Science International* (Vol. 97, Number 1). Springer. https://doi.org/10.1007/s12565-021-00631-w

Hazra, S., Kalyan Dinda, S., Kumar Mondal, N., Hossain, S. R., Datta, P., Yasmin Mondal, A., Malakar, P., & Manna, D. (2023). Giant cells: multiple cells unite to survive. In *Frontiers in Cellular and Infection Microbiology* (Vol. 13). Frontiers Media SA. https://doi.org/10.3389/fcimb.2023.1220589

He, Y., Taylor, N., Fourgeaud, L., & Bhattacharya, A. (2017). The role of microglial P2X7: modulation of cell death and cytokine release. *Journal of Neuroinflammation*, *14*(1). https://doi.org/10.1186/s12974-017-0904-8

Healy, L. M., Zia, S., & Plemel, J. R. (2022). Towards a definition of microglia heterogeneity. *Communications Biology*, *5*(1). https://doi.org/10.1038/s42003-022-04081-6

Helming, L., Tomasello, E., Kyriakides, T. R., Martinez, F. O., Takai, T., Gordon, S., & Vivier, E. (2008). *Essential Role of DAP12 Signaling in Macrophage Programming into a Fusion-Competent State*. www.SCIENCESIGNALING.org

Henn, A., Lund, S., Hedtjärn, M., Schrattenholz, A., Pörzgen, P., & Leist, M. (2009). *The Suitability of BV2 Cells as Alternative Model System for Primary Microglia Cultures or for Animal Experiments Examining Brain Inflammation*.

Hermann, D. M., & Gunzer, M. (2021). Modulating Microglial Cells for Promoting Brain Recovery and Repair. *Frontiers in Cellular Neuroscience*, *14*. https://doi.org/10.3389/fncel.2020.627987

Hernández, J. M., & Podbilewicz, B. (2017). The hallmarks of cell-cell fusion. In *Development (Cambridge)* (Vol. 144, Number 24, pp. 4481–4495). Company of Biologists Ltd. https://doi.org/10.1242/dev.155523

Hibell, A. D., Kidd, E. J., Chessell, I. P., Humphrey, P. P. A., & Michel, A. D. (2000). Apparent species differences in the kinetic properties of P2X7 receptors. *British Journal of Pharmacology*, *130*(1), 167–173. https://doi.org/10.1038/sj.bjp.0703302

Hoeffel, G., Chen, J., Lavin, Y., Low, D., Almeida, F. F., See, P., Beaudin, A. E., Lum, J., Low, I., Forsberg, E. C., Poidinger, M., Zolezzi, F., Larbi, A., Ng, L. G., Chan, J. K. Y., Greter, M., Becher, B., Samokhvalov, I. M., Merad, M., & Ginhoux, F. (2015). C-Myb+ Erythro-Myeloid Progenitor-Derived Fetal Monocytes Give Rise to Adult Tissue-Resident Macrophages. *Immunity*, *42*(4), 665–678. https://doi.org/10.1016/j.immuni.2015.03.011

Hornik, T. C., Neniskyte, U., & Brown, G. C. (2014). Inflammation induces multinucleation of Microglia via PKC inhibition of cytokinesis, generating highly phagocytic multinucleated giant cells. *Journal of Neurochemistry*, *128*(5), 650–661. https://doi.org/10.1111/jnc.12477

Huang, P., Zhang, Z., Zhang, P., Feng, J., Xie, J., Zheng, Y., Liang, X., Zhu, B., Chen, Z., Feng, S., Wang, L., Lu, J., Liu, Y., & Zhang, Y. (2023). TREM2 Deficiency Aggravates NLRP3 Inflammasome Activation and Pyroptosis in MPTP-Induced Parkinson's Disease Mice and LPS-Induced BV2 Cells. *Molecular Neurobiology*, *61*(5), 2590–2605. https://doi.org/10.1007/s12035-023-03713-0

Humphrey, M. B., & Nakamura, M. C. (2016). A Comprehensive Review of Immunoreceptor Regulation of Osteoclasts. In *Clinical Reviews in Allergy and Immunology* (Vol. 51, Number 1, pp. 48–58). Humana Press Inc. https://doi.org/10.1007/s12016-015-8521-8

Hung, H. C., Tsai, S. F., Sie, S. R., & Kuo, Y. M. (2022). High glucose enhances lipopolysaccharide-induced inflammation in cultured BV2 microglial cell line. *Immunity, Inflammation and Disease*, *10*(5). https://doi.org/10.1002/iid3.610

Idzko, M., Ferrari, D., & Eltzschig, H. K. (2014). Nucleotide signalling during inflammation. In *Nature* (Vol. 509, Number 7500, pp. 310–317). Nature Publishing Group. https://doi.org/10.1038/nature13085

Irie, A., Yamamoto, K., Miki, Y., & Murakami, M. (2017). Phosphatidylethanolamine dynamics are required for osteoclast fusion. *Scientific Reports*, *7*. https://doi.org/10.1038/srep46715

Irma Lemaire, Simonetta Falzoni, Natacha Leduc, Bin Zhang, Patrizia Pellegatti, Elena Adinolfi, Paola Chiozzi, & Francesco Di Virgilio. (2006). Involvement of the Purinergic P2X7 Receptor in the Formation of Multinucleated Giant Cells. *The Journal of Immunology*, *177*(10), 7257–7265.

Iwata, M., Ota, K. T., Li, X. Y., Sakaue, F., Li, N., Dutheil, S., Banasr, M., Duric, V., Yamanashi, T., Kaneko, K., Rasmussen, K., Glasebrook, A., Koester, A., Song, D., Jones, K. A., Zorn, S., Smagin, G., & Duman, R. S. (2016). Psychological stress activates the inflammasome via release of adenosine triphosphate and stimulation of the purinergic type 2X7 receptor. *Biological Psychiatry*, *80*(1), 12–22. https://doi.org/10.1016/j.biopsych.2015.11.026

Jacome-Galarza, C. E., Percin, G. I., Muller, J. T., Mass, E., Lazarov, T., Eitler, J., Rauner, M., Yadav, V. K., Crozet, L., Bohm, M., Loyher, P. L., Karsenty, G., Waskow, C., & Geissmann, F. (2019). Developmental origin, functional maintenance and genetic rescue of osteoclasts. *Nature*, *568*(7753), 541–545. https://doi.org/10.1038/s41586-019-1105-7

Jakobiec, F. A., Ma, L., Wolkow, N., Sutula, F. C., & Freitag, S. K. (2018). The Significance of Extracellular Cholesterol Crystals or a Cholesterol Granuloma in Xanthelasma. *Ocular Oncology and Pathology*, *4*(6). https://doi.org/10.1159/000486532

Jiang, D., Burger, C. A., Akhanov, V., Liang, J. H., Mackin, R. D., Albrecht, N. E., Andrade, P., Schafer, D. P., & Samuel, M. A. (2022). Neuronal signal-regulatory protein alpha drives

microglial phagocytosis by limiting microglial interaction with CD47 in the retina. *Immunity*, *55*(12), 2318-2335.e7. https://doi.org/10.1016/j.immuni.2022.10.018

Jiang, T., Hoekstra, J., Heng, X., Kang, W., Ding, J., Liu, J., Chen, S., & Zhang, J. (2015a). P2X7 receptor is critical in α-synuclein-mediated microglial NADPH oxidase activation. *Neurobiology of Aging*, *36*(7), 2304–2318. https://doi.org/10.1016/j.neurobiolaging.2015.03.015

Jiang, T., Hoekstra, J., Heng, X., Kang, W., Ding, J., Liu, J., Chen, S., & Zhang, J. (2015b). P2X7 receptor is critical in α-synuclein-mediated microglial NADPH oxidase activation. *Neurobiology of Aging*, *36*(7), 2304–2318. https://doi.org/10.1016/j.neurobiolaging.2015.03.015

Jin, X., Liu, M.-Y., Zhang, D.-F., Zhong, X., Du, K., Qian, P., Gao, H., & Wei, M.-J. (2019). Natural products as a potential modulator of microglial polarization in neurodegenerative diseases. *Pharmacological Research*, *145*, 104253. https://doi.org/10.1016/j.phrs.2019.104253

Jolivel, V., Brun, S., Binamé, F., Benyounes, J., Taleb, O., Bagnard, D., De Sèze, J., Patte-Mensah, C., & Mensah-Nyagan, A.-G. (2021). Microglial Cell Morphology and Phagocytic Activity Are Critically Regulated by the Neurosteroid Allopregnanolone: A Possible Role in Neuroprotection. *Cells*, *10*(3), 698. https://doi.org/10.3390/cells10030698

Jung, J., Zeng, H., & Horng, T. (2019). Metabolism as a guiding force for immunity. In *Nature Cell Biology* (Vol. 21, Number 1, pp. 85–93). Nature Publishing Group. https://doi.org/10.1038/s41556-018-0217-x

Jurga, A. M., Paleczna, M., & Kuter, K. Z. (2020). Overview of General and Discriminating Markers of Differential Microglia Phenotypes. *Frontiers in Cellular Neuroscience*, *14*. https://doi.org/10.3389/fncel.2020.00198

Kaczmarek-Hájek, K., Lörinczi, É., Hausmann, R., & Nicke, A. (2012). Molecular and functional properties of P2X receptors-recent progress and persisting challenges. *Purinergic Signalling*, *8*(3), 375–417. https://doi.org/10.1007/s11302-012-9314-7

Kahali, S., Baisya, R., Das, S., & Datta, A. (2025). Simultaneous Live Mapping of pH and Hydrogen Peroxide Fluctuations in Autophagic Vesicles. *JACS Au*, *5*(1), 343–352. https://doi.org/10.1021/jacsau.4c01021

Kaiser, Y., Eklund, A., & Grunewald, J. (2019). Moving target: Shifting the focus to pulmonary sarcoidosis as an autoimmune spectrum disorder. In *European Respiratory Journal* (Vol. 54, Number 1). European Respiratory Society. https://doi.org/10.1183/13993003.021532018

Kan, L. K., Drill, M., Jayakrishnan, P. C., Sequeira, R. P., Galea, E., Todaro, M., Sanfilippo, P. G., Hunn, M., Williams, D. A., O'Brien, T. J., Drummond, K. J., & Monif, M. (2023). P2X7 receptor antagonism by AZ10606120 significantly reduced in vitro tumour growth in human glioblastoma. *Scientific Reports*, *13*(1). https://doi.org/10.1038/s41598-023-35712-5

Kan, L. K., Drill, M., Jayakrishnan, P. C., Sequeira, R. P., Sanfilippo, P. G., McLean, C., Hunn, M., Williams, D. A., O'Brien, T. J., Drummond, K. J., & Monif, M. (2024). P2X7 receptor antagonism by AZ10606120 significantly depletes glioblastoma cancer stem cells in vitro. *Brain Research Bulletin*, *215*. https://doi.org/10.1016/j.brainresbull.2024.110996

Kan, L. K., Williams, D., Drummond, K., O'Brien, T., & Monif, M. (2019). The role of microglia and P2X7 receptors in gliomas. *Journal of Neuroimmunology*, *332*(January), 138–146. https://doi.org/10.1016/j.jneuroim.2019.04.010

Kang, H., Kim, S., Lee, J. Y., & Kim, B. (2023). Inhibitory Effects of Ginsenoside Compound K on Lipopolysaccharide-Stimulated Inflammatory Responses in Macrophages by Regulating Sirtuin 1 and Histone Deacetylase 4. *Nutrients*, *15*(7). https://doi.org/10.3390/nu15071626

Kang, J. H., Ko, H. M., Han, G. D., Lee, S. Y., Moon, J. S., Kim, M. S., Koh, J. T., & Kim, S. H. (2020). Dual role of phosphatidylserine and its receptors in osteoclastogenesis. *Cell Death and Disease*, *11*(7). https://doi.org/10.1038/s41419-020-2712-9

Karasawa Akira, Michalski Kevin, Mikhelzon Polina, & Kawate Toshimitsu. (2017). *The P2X7 receptor forms a dye- permeable pore independent of its intracellular domain but dependent on membrane lipid composition*. https://doi.org/10.7554/eLife.31186.001

Karavis, M. Y., Siafaka, I., Vadalouca, A., & Georgoudis, G. (2023). Role of microglia in neuropathic pain. *Cureus*. https://doi.org/10.7759/cureus.43555

Kettenmann, H., Hanisch, U.-K., Noda, M., & Verkhratsky, A. (2011). Physiology of Microglia. *Physiological Reviews*, *91*(2), 461–553. https://doi.org/10.1152/physrev.00011.2010

Khan, U. A., Hashimi, S. M., Bakr, M. M., Forwood, M. R., & Morrison, N. A. (2016). CCL2 and CCR2 are Essential for the Formation of Osteoclasts and Foreign Body Giant Cells. *Journal of Cellular Biochemistry*, *117*(2), 382–389. https://doi.org/10.1002/jcb.25282

Kierdorf, K., Erny, D., Goldmann, T., Sander, V., Schulz, C., Perdiguero, E. G., Wieghofer, P., Heinrich, A., Riemke, P., Hölscher, C., Müller, D. N., Luckow, B., Brocker, T., Debowski, K., Fritz, G., Opdenakker, G., Diefenbach, A., Biber, K., Heikenwalder, M., … Prinz, M. (2013). Microglia emerge from erythromyeloid precursors via Pu.1-and Irf8-dependent pathways. *Nature Neuroscience*, *16*(3), 273–280. https://doi.org/10.1038/nn.3318

Kipnis, J. (2016). Multifaceted interactions between adaptive immunity and the central nervous system. In *Science* (Vol. 353, Number 6301, pp. 766–771). American Association for the Advancement of Science. https://doi.org/10.1126/science.aag2638

Kloc, M., Uosef, A., Subuddhi, A., Kubiak, J. Z., Piprek, R. P., & Ghobrial, R. M. (2022). Giant Multinucleated Cells in Aging and Senescence—An Abridgement. In *Biology* (Vol. 11, Number 8). MDPI. https://doi.org/10.3390/biology11081121

Kodakandla, G., Akimzhanov, A. M., & Boehning, D. (2023). Regulatory mechanisms controlling store-operated calcium entry. In *Frontiers in Physiology* (Vol. 14). Frontiers Media SA. https://doi.org/10.3389/fphys.2023.1330259

Kong, L., Wang, Z., Liang, X., Wang, Y., Gao, L., & Ma, C. (2019). Monocarboxylate transporter 1 promotes classical microglial activation and pro-inflammatory effect via 6-phosphofructo-2-kinase/fructose-2, 6-biphosphatase 3. *Journal of Neuroinflammation*, *16*(1). https://doi.org/10.1186/s12974-019-1648-4

Konishi, H., & Kiyama, H. (2018). Microglial TREM2/DAP12 signaling: A double-edged sword in neural diseases. In *Frontiers in Cellular Neuroscience* (Vol. 12). Frontiers Media S.A. https://doi.org/10.3389/fncel.2018.00206

Kopp, R., Krautloher, A., Ramírez-Fernández, A., & Nicke, A. (2019). P2X7 Interactions and Signaling – Making Head or Tail of It. *Frontiers in Molecular Neuroscience*, *12*(August), 1–25. https://doi.org/10.3389/fnmol.2019.00183

Korzhevskii, D. E., & Kirik, O. V. (2016). Brain Microglia and Microglial Markers. *Neuroscience and Behavioral Physiology*, *46*(3), 284–290. https://doi.org/10.1007/s11055-016-0231-z

Kouba, B. R., Gil-Mohapel, J., & Ana, A. L. (2023). NLRP3 Inflammasome: From Pathophysiology to Therapeutic Target in Major Depressive Disorder. In *International Journal of Molecular Sciences* (Vol. 24, Number 1). MDPI. https://doi.org/10.3390/ijms24010133

Krishnacoumar, B., Stenzel, M., Garibagaoglu, H., Omata, Y., Sworn, R. L., Hofmann, T., Ipseiz, N., Czubala, M. A., Steffen, U., Maccataio, A., Stoll, C., Böhm, C., Herrmann, M., Uderhardt, S., Jenkins, R. H., Taylor, P. R., Grüneboom, A., Zaiss, M. M., Schett, G., … Scholtysek, C. (2024). Caspase-8 promotes scramblase-mediated phosphatidylserine exposure and fusion of osteoclast precursors. *Bone Research*, *12*(1). https://doi.org/10.1038/s41413-024-00338-4

Kusner, D. J., & Barton, J. A. (2001). *ATP Stimulates Human Macrophages to Kill Intracellular Virulent Mycobacterium tuberculosis Via Calcium-Dependent Phagosome-Lysosome Fusion1*. https://academic.oup.com/jimmunol/article/167/6/3308/8016919

Kwak, S. H., Shin, S., Lee, J. H., Shim, J. K., Kim, M., Lee, S. D., Lee, A., Bae, J., Park, J. H., Abdelrahman, A., Müller, C. E., Cho, S. K., Kang, S. G., Bae, M. A., Yang, J. Y., Ko, H., Goddard, W. A., & Kim, Y. C. (2018). Synthesis and structure-activity relationships of quinolinone and quinoline-based P2X7 receptor antagonists and their anti-sphere formation activities in glioblastoma cells. *European Journal of Medicinal Chemistry*, *151*, 462–481. https://doi.org/10.1016/j.ejmech.2018.03.023

Kyriakides, T. R., Foster, M. J., Keeney, G. E., Tsai, A., Giachelli, C. M., Clark-Lewis, I., Rollins, B. J., & Bornstein, P. (2004). The CC Chemokine Ligand, CCL2/MCP1, Participates in Macrophage Fusion and Foreign Body Giant Cell Formation. In *Cell Cycle Molecules*.

Lauro, C., & Limatola, C. (2020). Metabolic Reprograming of Microglia in the Regulation of the Innate Inflammatory Response. In *Frontiers in Immunology* (Vol. 11). Frontiers Media S.A. https://doi.org/10.3389/fimmu.2020.00493

Lay, G., Poquet, Y., Salek-Peyron, P., Puissegur, M. P., Botanch, C., Bon, H., Levillain, F., Duteyrat, J. L., Emile, J. F., & Altare, F. (2007). Langhans giant cells from M. Tuberculosis-induced human granulomas cannot mediate mycobacterial uptake. *Journal of Pathology*, *211*(1), 76–85. https://doi.org/10.1002/path.2092

Lee, J. W., Mizuno, K., Watanabe, H., Lee, I. H., Tsumita, T., Hida, K., Yawaka, Y., Kitagawa, Y., Hasebe, A., Iimura, T., & Kong, S. W. (2024). Enhanced phagocytosis associated with multinucleated microglia via Pyk2 inhibition in an acute β-amyloid infusion model. *Journal of Neuroinflammation*, *21*(1). https://doi.org/10.1186/s12974-024-03192-7

Lépine, S., Le Stunff, H., Lakatos, B., Sulpice, J. C., & Giraud, F. (2006). ATP-induced apoptosis of thymocytes is mediated by activation of P2X7 receptor and involves de novo ceramide synthesis and mitochondria. *Biochimica et Biophysica Acta - Molecular and Cell Biology of Lipids*, *1761*(1), 73–82. https://doi.org/10.1016/j.bbalip.2005.10.001

Li, Y., Long, W., Gao, M., Jiao, F., Chen, Z., Liu, M., & Yu, L. (2021). Trem2 regulates high glucose-induced microglial inflammation via the nlrp3 signaling pathway. *Brain Sciences*, *11*(7). https://doi.org/10.3390/brainsci11070896

Lin, S. S., Tang, Y., Illes, P., & Verkhratsky, A. (2021). The Safeguarding Microglia: Central Role for P2Y12 Receptors. *Frontiers in Pharmacology*, *11*. https://doi.org/10.3389/fphar.2020.627760

Liu, J., Zhang, X., Hou, H., Ouyang, J., & Dai, J. (2024). Advances in Osteoblast and Mitochondrial Dynamics and Their Transfer in Osteoporosis. In *Journal of Cellular and Molecular Medicine* (Vol. 28, Number 24). John Wiley and Sons Inc. https://doi.org/10.1111/jcmm.70299

Liu, X., Jiang, N., & Zhou, W. (2023). Various Energetic Metabolism of Microglia in Response to Different Stimulations. *Molecules*, *28*(11). https://doi.org/10.3390/molecules28114501

Liu, X., Li, Y., Huang, L., Kuang, Y., Wu, X., Ma, X., Zhao, B., & Lan, J. (2024). Unlocking the therapeutic potential of P2X7 receptor: a comprehensive review of its role in neurodegenerative disorders. In *Frontiers in Pharmacology* (Vol. 15). Frontiers Media SA. https://doi.org/10.3389/fphar.2024.1450704

Liu, X., Ma, W., Surprenant, A., & Jiang, L. H. (2009). Identification of the amino acid residues in the extracellular domain of rat P2X 7 receptor involved in functional inhibition by acidic pH. *British Journal of Pharmacology*, *156*(1), 135–142. https://doi.org/10.1111/j.1476-5381.2008.00002.x

Lösslein, A. K., Lohrmann, F., Scheuermann, L., Gharun, K., Neuber, J., Kolter, J., Forde, A. J., Kleimeyer, C., Poh, Y. Y., Mack, M., Triantafyllopoulou, A., Dunlap, M. D., Khader, S. A., Seidl, M., Hölscher, A., Hölscher, C., Guan, X. L., Dorhoi, A., & Henneke, P. (2021). Monocyte progenitors give rise to multinucleated giant cells. *Nature Communications*, *12*(1). https://doi.org/10.1038/s41467-021-22103-5

Loureiro, A. V., Moura-Neto, L. I., Martins, C. S., Silva, P. I. M., Lopes, M. B. S., Leitão, R. F. C., Coelho-Aguiar, J. M., Moura-Neto, V., Warren, C. A., Costa, D. V. S., & Brito, G. A. C. (2022). Role of Pannexin-1-P2X7R signaling on cell death and pro-inflammatory mediator expression induced by Clostridioides difficile toxins in enteric glia. *Frontiers in Immunology*, *13*. https://doi.org/10.3389/fimmu.2022.956340

Lu, Y., Walji, T., Ravaux, B., Pandey, P., Yang, C., Li, B., Luvsanjav, D., Lam, K. H., Zhang, R., Luo, Z., Zhou, C., Habela, C. W., Snapper, S. B., Li, R., Goldhamer, D. J., Schmidtke, D. W., Pan, D., Svitkina, T. M., & Chen, E. H. (2024). Spatiotemporal coordination of actin regulators generates invasive protrusions in cell–cell fusion. *Nature Cell Biology*, *26*(11), 1860–1877. https://doi.org/10.1038/s41556-024-01541-5

Luis Marín-Teva, J., Dusart, I., Colin, C., Gervais, A., Van Rooijen, N., & Mallat, M. (2004). Microglia Promote the Death of Developing Purkinje Cells of specific cell components by caspase-3 is essential for the morphological and biochemical changes that characterize apoptosis of developing neurons, including. In *Neuron* (Vol. 41).

Ma, Y., Di, R., Zhao, H., Song, R., Zou, H., & Liu, Z. (2022). P2X7 receptor knockdown suppresses osteoclast differentiation by inhibiting autophagy and Ca2+/calcineurin signaling. *Molecular Medicine Reports*, *25*(5). https://doi.org/10.3892/mmr.2022.12677

Mackenzie, A. B., Young, M. T., Adinolfi, E., & Surprenant, A. (2005). Pseudoapoptosis induced by brief activation of ATP-gated P2X7 receptors. *Journal of Biological Chemistry*, *280*(40), 33968–33976. https://doi.org/10.1074/jbc.M502705200

Maeda, T., Inagaki, M., Fujita, Y., Kimoto, T., Tanabe-Fujimura, C., Zou, K., Liu, J., Liu, S., & Komano, H. (2016). ATP increases the migration of microglia across the brain endothelial cell monolayer. *Bioscience Reports*, *36*(2). https://doi.org/10.1042/BSR20160054

Maher, P. (2021). Investigations into the Role of Metabolism in the Inflammatory Response of BV2 Microglial Cells. *Antioxidants*, (109), 1–13. https://doi.org/10.3390/antiox

Majumdar, A., Cruz, D., Asamoah, N., Buxbaum, A., Sohar, I., Lobel, P., & Maxfield, F. R. (2007). Activation of Microglia Acidifies Lysosomes and Leads to Degradation of Alzheimer Amyloid Fibrils. *Molecular Biology of the Cell*, *18*, 1490–1496. https://doi.org/10.1091/mbc.E06

Mamad, O., Heiland, M., Lindner, A. U., Hill, T. D. M., Ronroy, R. M., Rentrup, K., Sanz-Rodriguez, A., Langa, E., Heller, J. P., Moreno, O., Llop, J., Bhattacharya, A., Palmer, J. A., Ceusters, M., Engel, T., & Henshall, D. C. (2023). Anti-seizure effects of JNJ-54175446 in the intra-amygdala kainic acid model of drug-resistant temporal lobe epilepsy in mice. *Frontiers in Pharmacology*, *14*. https://doi.org/10.3389/fphar.2023.1308478

Marschallinger, J., Iram, T., Zardeneta, M., Lee, S. E., Lehallier, B., Haney, M. S., Pluvinage, J. V., Mathur, V., Hahn, O., Morgens, D. W., Kim, J., Tevini, J., Felder, T. K., Wolinski, H., Bertozzi, C. R., Bassik, M. C., Aigner, L., & Wyss-Coray, T. (2020). Lipid-droplet-accumulating microglia represent a dysfunctional and proinflammatory state in the aging brain. *Nature Neuroscience*, *23*(2), 194–208. https://doi.org/10.1038/s41593-019-0566-1

Marshall, J. S., Warrington, R., Watson, W., & Kim, H. L. (2018). An introduction to immunology and immunopathology. In *Allergy, Asthma and Clinical Immunology* (Vol. 14). BioMed Central Ltd. https://doi.org/10.1186/s13223-018-0278-1

Martin, S. G. (2016). Role and organization of the actin cytoskeleton during cell-cell fusion. In *Seminars in Cell and Developmental Biology* (Vol. 60, pp. 121–126). Academic Press. https://doi.org/10.1016/j.semcdb.2016.07.025

Matlung, H. L., Szilagyi, K., Barclay, N. A., & van den Berg, T. K. (2017). The CD47-SIRPα signaling axis as an innate immune checkpoint in cancer. In *Immunological Reviews* (Vol. 276, Number 1, pp. 145–164). Blackwell Publishing Ltd. https://doi.org/10.1111/imr.12527

Matyśniak, D., Chumak, V., Nowak, N., Kukla, A., Lehka, L., Oslislok, M., & Pomorski, P. (2022). P2X7 receptor: the regulator of glioma tumor development and survival. *Purinergic Signalling*, *18*(1), 135–154. https://doi.org/10.1007/s11302-021-09834-2

McDonald, M. M., Khoo, W. H., Ng, P. Y., Xiao, Y., Zamerli, J., Thatcher, P., Kyaw, W., Pathmanandavel, K., Grootveld, A. K., Moran, I., Butt, D., Nguyen, A., Warren, S., Biro, M., Butterfield, N. C., Guilfoyle, S. E., Komla-Ebri, D., Dack, M. R. G., Dewhurst, H. F., … Phan, T. G. (2021). Osteoclasts recycle via osteomorphs during RANKL-stimulated bone resorption. *Cell*, *184*(5), 1330-1347.e13. https://doi.org/10.1016/j.cell.2021.02.002

McDonald, M. M., Kim, A. S., Mulholland, B. S., & Rauner, M. (2021). New Insights Into Osteoclast Biology. In *JBMR Plus* (Vol. 5, Number 9). John Wiley and Sons Inc. https://doi.org/10.1002/jbm4.10539

Mcnally, A. K., & Anderson, J. M. (1995). Interleukin-4 Induces Foreign Body Giant Cells from Human Monocytes/Macrophages Differential Lymphokine Regulation of Macrophage Fusion Leads to Morphological Variants of Multinucleated Giant Cells. In *American Journal of Pathology* (Vol. 147, Number 5).

McNally, A. K., & Anderson, J. M. (2015). Phenotypic expression in human monocyte-derived interleukin-4-induced foreign body giant cells and macrophages in vitro: Dependence on material surface properties. *Journal of Biomedical Materials Research - Part A*, *103*(4), 1380–1390. https://doi.org/10.1002/jbm.a.35280

Mehta, V. B., Hart, J., & Wewers, M. D. (2001). ATP-stimulated Release of Interleukin (IL)-1β and IL-18 Requires Priming by Lipopolysaccharide and Is Independent of Caspase-1 Cleavage. *Journal of Biological Chemistry*, *276*(6), 3820–3826. https://doi.org/10.1074/jbc.M006814200

Metzger, M. W., Walser, S. M., Aprile-Garcia, F., Dedic, N., Chen, A., Holsboer, F., Arzt, E., Wurst, W., & Deussing, J. M. (2017). Genetically dissecting P2rx7 expression within the central nervous system using conditional humanized mice. *Purinergic Signalling*, *13*(2), 153–170. https://doi.org/10.1007/s11302-016-9546-z

Milde, R., Ritter, J., Tennent, G. A., Loesch, A., Martinez, F. O., Gordon, S., Pepys, M. B., Verschoor, A., & Helming, L. (2015). Multinucleated Giant Cells Are Specialized for Complement-Mediated Phagocytosis and Large Target Destruction. *Cell Reports*, *13*(9), 1937–1948. https://doi.org/10.1016/j.celrep.2015.10.065

Minhas, P. S., Latif-Hernandez, A., McReynolds, M. R., Durairaj, A. S., Wang, Q., Rubin, A., Joshi, A. U., He, J. Q., Gauba, E., Liu, L., Wang, C., Linde, M., Sugiura, Y., Moon, P. K., Majeti, R., Suematsu, M., Mochly-Rosen, D., Weissman, I. L., Longo, F. M., … Andreasson, K. I. (2021). Restoring metabolism of myeloid cells reverses cognitive decline in ageing. *Nature*, *590*(7844), 122–128. https://doi.org/10.1038/s41586-020-03160-0

Mithaiwala, M. N., Santana-Coelho, D., Porter, G. A., & O'connor, J. C. (2021). Neuroinflammation and the Kynurenine pathway in CNS disease: Molecular mechanisms and therapeutic implications. In *Cells* (Vol. 10, Number 6). MDPI. https://doi.org/10.3390/cells10061548

Moca, E. N., Lecca, D., Hope, K. T., Etienne, F., Schaler, A. W., Espinoza, K., Chappell, M. S., Gray, D. T., Tweedie, D., Sidhu, S., Masukawa, L., Sitoy, H., Mathew, R., Saban, D. R., Greig, N. H., & De Biase, L. M. (2022). Microglia Drive Pockets of Neuroinflammation in Middle Age. *Journal of Neuroscience*, *42*(19), 3896–3918. https://doi.org/10.1523/JNEUROSCI.1922-21.2022

Monier, A., Adle-Biassette, H., Delezoide, A.-L., Evrard, P., Gressens, P., & Verney, C. (2007). *Entry and Distribution of Microglial Cells in Human Embryonic and Fetal Cerebral Cortex*. https://academic.oup.com/jnen/article/66/5/372/2916860

Monif, M., Burnstock, G., & Williams, D. A. (2010). Microglia: Proliferation and activation driven by the P2X7 receptor. *The International Journal of Biochemistry & Cell Biology*, *42*(11), 1753–1756. https://doi.org/10.1016/j.biocel.2010.06.021

Monif, M., Reid, C. A., Powell, K. L., Smart, M. L., & Williams, D. A. (2009). The P2X7 receptor drives microglial activation and proliferation: A trophic role for P2X7R pore. *Journal of Neuroscience*, *29*(12), 3781–3791. https://doi.org/10.1523/JNEUROSCI.5512-08.2009

Moon Eun-Yi. (2008). Serum Deprivation Enhances Apoptotic Cell Death by Increasing Mitochondrial Enzyme Activity. *Biomolecules & Therapeutics*, (16), 1–8.

Mou, Y. J., Li, F. M., Lou, J. T., Tu, H. Y., Zhu, Y., Sheng, R., Zhang, Z. L., Zhao, Y. Z., Ji, F. H., Wu, J. C., & Qin, Z. H. (2025). NADPH acts as an endogenous P2X7 receptor modulator to gate

neuroinflammatory responses of microglia. *Acta Pharmacologica Sinica*. https://doi.org/10.1038/s41401-025-01638-z

Moura, G. E. D. D., Lucena, S. V., Lima, M. A., Nascimento, F. D., Gesteira, T. F., Nader, H. B., Paredes-Gamero, E. J., & Tersariol, I. L. S. (2015). P2X7 receptor activity regulation: The role of CD44 proteoglycan GAG chains. In *Cell Death and Disease* (Vol. 6, Number 11). Nature Publishing Group. https://doi.org/10.1038/cddis.2015.340

Müller, C. E., & Namasivayam, V. (2022). Agonists, Antagonists, and Modulators of P2X7 Receptors. In A. Nicke (Ed.), *The P2X7 Receptor: Methods and Protocols* (pp. 31–52). Springer US. https://doi.org/10.1007/978-1-0716-2384-8_2

Murray, P. J., Allen, J. E., Biswas, S. K., Fisher, E. A., Gilroy, D. W., Goerdt, S., Gordon, S., Hamilton, J. A., Ivashkiv, L. B., Lawrence, T., Locati, M., Mantovani, A., Martinez, F. O., Mege, J. L., Mosser, D. M., Natoli, G., Saeij, J. P., Schultze, J. L., Shirey, K. A., … Wynn, T. A. (2014). Correction tp Macrophage activation and polarization: Nomenclature and experimental guidelines [Immunity, 41, 2014 (14-20)]. In *Immunity* (Vol. 41, Number 2, pp. 339–340). Cell Press. https://doi.org/10.1016/j.immuni.2014.07.009

Murrell-Lagnado, R. D. (2017). Regulation of P2X Purinergic Receptor Signaling by Cholesterol. *Current Topics in Membranes*, *80*, 211–232. https://doi.org/10.1016/BS.CTM.2017.05.004

Nadav Segev, Ori Avinoam, & Benjamin Podbilewicz. (2018). *Fusogens*.

Nair, S., Sobotka, K. S., Joshi, P., Gressens, P., Fleiss, B., Thornton, C., Mallard, C., & Hagberg, H. (2019). Lipopolysaccharide-induced alteration of mitochondrial morphology induces a metabolic shift in microglia modulating the inflammatory response in vitro and in vivo. *GLIA*, *67*(6), 1047–1061. https://doi.org/10.1002/glia.23587

Nicaise, A. M., Bongarzone, E. R., & Crocker, S. J. (2016). A microglial hypothesis of globoid cell leukodystrophy pathology. In *Journal of Neuroscience Research* (Vol. 94, Number 11, pp. 1049–1061). John Wiley and Sons Inc. https://doi.org/10.1002/jnr.23773

Nicke, A. (2008). Homotrimeric complexes are the dominant assembly state of native P2X7 subunits. *Biochemical and Biophysical Research Communications*, *377*(3), 803–808. https://doi.org/10.1016/j.bbrc.2008.10.042

Niraula, A., Sheridan, J. F., & Godbout, J. P. (2017). Microglia Priming with Aging and Stress. In *Neuropsychopharmacology* (Vol. 42, Number 1, pp. 318–333). Nature Publishing Group. https://doi.org/10.1038/npp.2016.185

Nopparat, C., Boontor, A., Kutpruek, S., & Govitrapong, P. (2023). The role of melatonin in amyloid beta-induced inflammation mediated by inflammasome signaling in neuronal cell lines. *Scientific Reports*, *13*(1). https://doi.org/10.1038/s41598-023-45220-1

Norden, D. M., & Godbout, J. P. (2013). Review: Microglia of the aged brain: Primed to be activated and resistant to regulation. In *Neuropathology and Applied Neurobiology* (Vol. 39, Number 1, pp. 19–34). https://doi.org/10.1111/j.1365-2990.2012.01306.x

Nörenberg, W., Hempel, C., Urban, N., Sobottka, H., Illes, P., & Schaefer, M. (2011). Clemastine potentiates the human P2X7 receptor by sensitizing it to lower ATP concentrations. *Journal of Biological Chemistry*, *286*(13), 11067–11081. https://doi.org/10.1074/jbc.M110.198879

Nörenberg, W., Sobottka, H., Hempel, C., Plötz, T., Fischer, W., Schmalzing, G., & Schaefer, M. (2012). Positive allosteric modulation by ivermectin of human but not murine P2X7

receptors. *British Journal of Pharmacology*, *167*(1), 48–66. https://doi.org/10.1111/j.1476-5381.2012.01987.x

Norris, G. T., & Kipnis, J. (2019). Immune cells and CNS physiology: Microglia and beyond. In *Journal of Experimental Medicine* (Vol. 216, Number 1, pp. 60–70). Rockefeller University Press. https://doi.org/10.1084/jem.20180199

O'Brien, J., Wilson, I., Orton, T., & Pognan, F. (2000). Investigation of the Alamar Blue (resazurin) fluorescent dye for the assessment of mammalian cell cytotoxicity. *European Journal of Biochemistry*, *267*(17), 5421–5426. https://doi.org/10.1046/j.1432-1327.2000.01606.x

Ochocka, N., & Kaminska, B. (2021). Microglia diversity in healthy and diseased brain: Insights from single-cell omics. In *International Journal of Molecular Sciences* (Vol. 22, Number 6, pp. 1–26). MDPI AG. https://doi.org/10.3390/ijms22063027

Orihuela, R., McPherson, C. A., & Harry, G. J. (2016). Microglial M1/M2 polarization and metabolic states. In *British Journal of Pharmacology* (Vol. 173, Number 4, pp. 649–665). John Wiley and Sons Inc. https://doi.org/10.1111/bph.13139

Orioli, E., De Marchi, E., Giuliani, A. L., & Adinolfi, E. (2017). P2X7 Receptor Orchestrates Multiple Signalling Pathways Triggering Inflammation, Autophagy and Metabolic/Trophic Responses. *Current Medicinal Chemistry*, *24*(21), 2261–2275. https://doi.org/10.2174/0929867324666170303161659

Orriss, I. R., Key, M. L., Brandao-Burch, A., Patel, J. J., Burnstock, G., & Arnett, T. R. (2012). The regulation of osteoblast function and bone mineralisation by extracellular nucleotides: The role of P2X receptors. *Bone*, *51*(3), 389–400. https://doi.org/10.1016/j.bone.2012.06.013

Ou, A., Gu, B. J., & Wiley, J. S. (2018). The scavenger activity of the human P2X7 receptor differs from P2X7 pore function by insensitivity to antagonists, genetic variation and sodium concentration: Relevance to inflammatory brain diseases. *Biochimica et Biophysica Acta (BBA) - Molecular Basis of Disease*, *1864*(4), 1051–1059. https://doi.org/10.1016/j.bbadis.2018.01.012

Ousingsawat, J., Wanitchakool, P., Schreiber, R., Wuelling, M., Vortkamp, A., & Kunzelmann, K. (2015). Anoctamin-6 controls bone mineralization by activating the calcium transporter NCX1. *Journal of Biological Chemistry*, *290*(10), 6270–6280. https://doi.org/10.1074/jbc.M114.602979

Padhy, I., Dwibedy, S. K., & Mohapatra, S. S. (2024). A molecular overview of the polymyxin-LPS interaction in the context of its mode of action and resistance development. In *Microbiological Research* (Vol. 283). Elsevier GmbH. https://doi.org/10.1016/j.micres.2024.127679

Pan, M. L., Ahmad Puzi, N. N., Ooi, Y. Y., Ramasamy, R., & Vidyadaran, S. (2023). Response Profiles of BV2 Microglia to IFN-γ and LPS Co-Stimulation and Priming. *Biomedicines*, *11*(10). https://doi.org/10.3390/biomedicines11102648

Paolicelli, R. C., Sierra, A., Stevens, B., Tremblay, M. E., Aguzzi, A., Ajami, B., Amit, I., Audinat, E., Bechmann, I., Bennett, M., Bennett, F., Bessis, A., Biber, K., Bilbo, S., Blurton-Jones, M., Boddeke, E., Brites, D., Brône, B., Brown, G. C., … Wyss-Coray, T. (2022). Microglia states and nomenclature: A field at its crossroads. In *Neuron* (Vol. 110, Number 21, pp. 3458–3483). Cell Press. https://doi.org/10.1016/j.neuron.2022.10.020

Parthasarathy, V., Martin, F., Higginbottom, A., Murray, H., Moseley, G. W., Read, R. C., Mal, G., Hulme, R., Monk, P. N., & Partridge, L. J. (2009). Distinct roles for tetraspanins CD9, CD63 and CD81 in the formation of multinucleated giant cells. *Immunology*, *127*(2), 237–248. https://doi.org/10.1111/j.1365-2567.2008.02945.x

Pellegatti, P., Falzoni, S., Donvito, G., Lemaire, I., & Di Virgilio, F. (2011). P2X7 receptor drives osteoclast fusion by increasing the extracellular adenosine concentration. *The FASEB Journal*, *25*(4), 1264–1274. https://doi.org/10.1096/fj.10-169854

Pérez-Flores, G., Lévesque, S. A., Pacheco, J., Vaca, L., Lacroix, S., Pérez-Cornejo, P., & Arreola, J. (2015). The P2X7/P2X4 interaction shapes the purinergic response in murine macrophages. *Biochemical and Biophysical Research Communications*, *467*(3), 484–490. https://doi.org/10.1016/j.bbrc.2015.10.025

Perez-Pouchoulen, M., VanRyzin, J. W., & McCarthy, M. M. (2015). Morphological and phagocytic profile of microglia in the developing rat cerebellum. *ENeuro*, *2*(4). https://doi.org/10.1523/ENEURO.0036-15.2015

Perregaux, D., & Gabels, C. A. (1994). Interleukin-lP Maturation and Release in Response to ATP and Nigericin EVIDENCE THAT POTASSIUM DEPLETION MEDIATED BY THESE AGENTS IS A NECESSARY AND COMMON FEATURE O F THEIR ACTMTY*. In *THE JOURNAL OF BIOLOGICAL CHEMISTRY* (Vol. 269, Number 21).

Peverini, L., Beudez, J., Dunning, K., Chataigneau, T., & Grutter, T. (2018). New Insights Into Permeation of Large Cations Through ATP-Gated P2X Receptors. *Frontiers in Molecular Neuroscience*, *11*. https://doi.org/10.3389/fnmol.2018.00265

Piano, I., Votta, A., Colucci, P., Corsi, F., Vitolo, S., Cerri, C., Puppi, D., Lai, M., Maya-Vetencourt, J. F., Leigheb, M., Gabellini, C., & Ferraro, E. (2023). Anti-inflammatory reprogramming of microglia cells by metabolic modulators to counteract neurodegeneration; a new role for Ranolazine. *Scientific Reports*, *13*(1). https://doi.org/10.1038/s41598-023-47540-8

Piyasirananda, W., Beekman, A., Ganesan, A., Bidula, S., & Stokes, L. (2021). Insights into the Structure-Activity Relationship of Glycosides as Positive Allosteric Modulators Acting on P2X7 Receptors. *Molecular Pharmacology*, *99*(2), 163–174. https://doi.org/10.1124/molpharm.120.000129

Prinz, M., Tay, T. L., Wolf, Y., & Jung, S. (2014). Microglia: Unique and common features with other tissue macrophages. In *Acta Neuropathologica* (Vol. 128, Number 3, pp. 319–331). Springer Verlag. https://doi.org/10.1007/s00401-014-1267-1

Qin, Y., Sun, X., Shao, X., Hu, M. X., Feng, J., Chen, Z., Sun, J., Zhou, Z., Duan, Y., & Cheng, C. (2016). Lipopolysaccharide Preconditioning Induces an Anti-inflammatory Phenotype in BV2 Microglia. *Cellular and Molecular Neurobiology*, *36*(8), 1269–1277. https://doi.org/10.1007/s10571-015-0324-1

Qu, Y., & Dubyak, G. R. (2009). P2X7 receptors regulate multiple types of membrane trafficking responses and non-classical secretion pathways. In *Purinergic Signalling* (Vol. 5, Number 2, pp. 163–173). https://doi.org/10.1007/s11302-009-9132-8

Quan, Y., Jiang, C. T., Xue, B., Zhu, S. G., & Wang, X. (2011). High glucose stimulates TNFα and MCP-1 expression in rat microglia via ROS and NF-κB pathways. *Acta Pharmacologica Sinica*, *32*(2), 188–193. https://doi.org/10.1038/aps.2010.174

Rampersad, S. N. (2012). Multiple applications of alamar blue as an indicator of metabolic function and cellular health in cell viability bioassays. *Sensors (Switzerland)*, *12*(9), 12347–12360. https://doi.org/10.3390/s120912347

Rani, V., Verma, R., Kumar, K., & Chawla, R. (2023). Role of pro-inflammatory cytokines in Alzheimer's disease and neuroprotective effects of pegylated self-assembled nanoscaffolds. *Current Research in Pharmacology and Drug Discovery*, *4*. https://doi.org/10.1016/j.crphar.2022.100149

Raymond, M. N., & Le Stunff, H. (2006). Involvement of de novo ceramide biosynthesis in macrophage death induced by activation of ATP-sensitive P2X7 receptor. *FEBS Letters*, *580*(1), 131–136. https://doi.org/10.1016/j.febslet.2005.11.066

Recourt, K., de Boer, P., van der Ark, P., Benes, H., van Gerven, J. M. A., Ceusters, M., van Nueten, L., Drevets, W. C., Bhatacharya, A., Browning, M., & Jacobs, G. E. (2023). Characterization of the central nervous system penetrant and selective purine P2X7 receptor antagonist JNJ-54175446 in patients with major depressive disorder. *Translational Psychiatry*, *13*(1). https://doi.org/10.1038/s41398-023-02557-5

Réu, P., Khosravi, A., Bernard, S., Mold, J. E., Salehpour, M., Alkass, K., Perl, S., Tisdale, J., Possnert, G., Druid, H., & Frisén, J. (2017). The Lifespan and Turnover of Microglia in the Human Brain. *Cell Reports*, *20*(4), 779–784. https://doi.org/10.1016/j.celrep.2017.07.004

Rezaie, P., Dean, A., Male, D., & Ulfig, N. (2005). Microglia in the cerebral wall of the human telencephalon at second trimester. *Cerebral Cortex*, *15*(7), 938–949. https://doi.org/10.1093/cercor/bhh194

Rittner, H. L., Kaiser, M., Brack, A., Szweda, L. I., Goronzy, J. J., & Weyand, C. M. (1999). *Tissue-Destructive Macrophages in Giant Cell Arteritis*. http://www.circresaha.org

Robinson, L. E., Shridar, M., Smith, P., & Murrell-Lagnado, R. D. (2014). Plasma membrane cholesterol as a regulator of human and rodent P2X7 receptor activation and sensitization. *Journal of Biological Chemistry*, *289*(46), 31983–31994. https://doi.org/10.1074/jbc.M114.574699

Ross, D., & Siegel, D. (2004). *[8] NAD(P)H:Quinone Oxidoreductase 1 (NQO1, DT-Diaphorase), Functions and Pharmacogenetics*. http://www.infobiogen.fr/

Rusiecka, O. M., Tournier, M., Molica, F., & Kwak, B. R. (2022). Pannexin1 channels—a potential therapeutic target in inflammation. In *Frontiers in Cell and Developmental Biology* (Vol. 10). Frontiers Media S.A. https://doi.org/10.3389/fcell.2022.1020826

Sabe, H., Yahara, Y., & Ishii, M. (2024). Cell fusion dynamics: mechanisms of multinucleation in osteoclasts and macrophages. In *Inflammation and Regeneration* (Vol. 44, Number 1). BioMed Central Ltd. https://doi.org/10.1186/s41232-024-00360-3

Sakai, H., Okafuji, I., Nishikomori, R., Abe, J., Izawa, K., Kambe, N., Yasumi, T., Nakahata, T., & Heike, T. (2012). The CD40-CD40L axis and IFN-γ play critical roles in Langhans giant cell formation. *International Immunology*, *24*(1), 5–15. https://doi.org/10.1093/intimm/dxr088

Santana, P. T., Benjamim, C. F., Martinez, C. G., Kurtenbach, E., Takiya, C. M., & Coutinho-Silva, R. (2015). The P2X7 Receptor Contributes to the Development of the Exacerbated Inflammatory Response Associated with Sepsis. *Journal of Innate Immunity*, *7*(4), 417–427. https://doi.org/10.1159/000371388

Santos, S. A. C. S., Persechini, P. M., Henriques-Santos, B. M., Bello-Santos, V. G., Castro, N. G., Costa de Sousa, J., Genta, F. A., Santiago, M. F., Coutinho-Silva, R., Savio, L. E. B., & Kurtenbach, E. (2022). P2X7 Receptor Triggers Lysosomal Leakage Through Calcium Mobilization in a Mechanism Dependent on Pannexin-1 Hemichannels. *Frontiers in Immunology*, *13*. https://doi.org/10.3389/fimmu.2022.752105

Sanz, J. M., Chiozzi, P., & Di Virgilio, F. (1998). Tenidap enhances P2Z/P2X7 receptor signalling in macrophages. *European Journal of Pharmacology*, *355*(2–3), 235–244. https://doi.org/10.1016/S0014-2999(98)00482-8

Sarti, A. C., Vultaggio-Poma, V., Falzoni, S., Missiroli, S., Giuliani, A. L., Boldrini, P., Bonora, M., Faita, F., Di Lascio, N., Kusmic, C., Solini, A., Novello, S., Morari, M., Rossato, M., Wieckowski, M. R., Giorgi, C., Pinton, P., & Di Virgilio, F. (2021a). Mitochondrial P2X7 Receptor Localization Modulates Energy Metabolism Enhancing Physical Performance. *Function*, *2*(2). https://doi.org/10.1093/function/zqab005

Sarti, A. C., Vultaggio-Poma, V., Falzoni, S., Missiroli, S., Giuliani, A. L., Boldrini, P., Bonora, M., Faita, F., Di Lascio, N., Kusmic, C., Solini, A., Novello, S., Morari, M., Rossato, M., Wieckowski, M. R., Giorgi, C., Pinton, P., & Di Virgilio, F. (2021b). Mitochondrial P2X7 Receptor Localization Modulates Energy Metabolism Enhancing Physical Performance. *Function*, *2*(2). https://doi.org/10.1093/function/zqab005

Saucier, J., Comeau, D., Robichaud, G., & Chamard-Witkowski, L. (2023). Reactive gliosis and neuroinflammation as prime suspects in neuropasc pathophysiology. *Journal of the Neurological Sciences*, *455*, 122575. https://doi.org/10.1016/j.jns.2023.122575

Savio, L. E. B., Mello, P. de A., da Silva, C. G., & Coutinho-Silva, R. (2018). The P2X7 receptor in inflammatory diseases: Angel or demon? *Frontiers in Pharmacology*, *9*(FEB). https://doi.org/10.3389/fphar.2018.00052

Sekar, P., Huang, D. Y., Hsieh, S. L., Chang, S. F., & Lin, W. W. (2018a). AMPK-dependent and independent actions of P2X7 in regulation of mitochondrial and lysosomal functions in microglia. *Cell Communication and Signaling*, *16*(1). https://doi.org/10.1186/s12964-018-0293-3

Sekar, P., Huang, D. Y., Hsieh, S. L., Chang, S. F., & Lin, W. W. (2018b). AMPK-dependent and independent actions of P2X7 in regulation of mitochondrial and lysosomal functions in microglia. *Cell Communication and Signaling*, *16*(1). https://doi.org/10.1186/s12964-018-0293-3

Sekar, P., Huang, D.-Y., Chang, S.-F., & Lin, W.-W. (2018). Coordinate effects of P2X7 and extracellular acidification in microglial cells. In *Oncotarget* (Vol. 9, Number 16). www.impactjournals.com/oncotarget

Sharma, K., Bisht, K., & Eyo, U. B. (2021). A Comparative Biology of Microglia Across Species. In *Frontiers in Cell and Developmental Biology* (Vol. 9). Frontiers Media S.A. https://doi.org/10.3389/fcell.2021.652748

Sheikh, Z., Brooks, P. J., Barzilay, O., Fine, N., & Glogauer, M. (2015). Macrophages, foreign body giant cells and their response to implantable biomaterials. In *Materials* (Vol. 8, Number 9, pp. 5671–5701). MDPI AG. https://doi.org/10.3390/ma8095269

Shieh, C. H., Heinrich, A., Serchov, T., van Calker, D., & Biber, K. (2014). P2X7-dependent, but differentially regulated release of IL-6, CCL2, and TNF-α in cultured mouse microglia. *GLIA*, *62*(4), 592–607. https://doi.org/10.1002/glia.22628

Shiratori, M., Tozaki-Saitoh, H., Yoshitake, M., Tsuda, M., & Inoue, K. (2010). P2X7 receptor activation induces CXCL2 production in microglia through NFAT and PKC/MAPK pathways. *Journal of Neurochemistry*, *114*(3), 810–819. https://doi.org/10.1111/j.1471-4159.2010.06809.x

Shtaya, A., Bridges, L. R., Esiri, M. M., Lam-Wong, J., Nicoll, J. A. R., Boche, D., & Hainsworth, A. H. (2019). Rapid neuroinflammatory changes in human acute intracerebral hemorrhage. *Annals of Clinical and Translational Neurology*, *6*(8), 1465–1479. https://doi.org/10.1002/acn3.50842

Sivcev, S., Kudova, E., & Zemkova, H. (2023). Neurosteroids as positive and negative allosteric modulators of ligand-gated ion channels: P2X receptor perspective. *Neuropharmacology*, *234*, 109542. https://doi.org/10.1016/J.NEUROPHARM.2023.109542

Sivcev, S., Slavikova, B., Ivetic, M., Knezu, M., Kudova, E., & Zemkova, H. (2020). Lithocholic acid inhibits P2X2 and potentiates P2X4 receptor channel gating. *Journal of Steroid Biochemistry and Molecular Biology*, *202*. https://doi.org/10.1016/j.jsbmb.2020.105725

Smith, J. A., Das, A., Ray, S. K., & Banik, N. L. (2012). Role of pro-inflammatory cytokines released from microglia in neurodegenerative diseases. In *Brain Research Bulletin* (Vol. 87, Number 1, pp. 10–20). https://doi.org/10.1016/j.brainresbull.2011.10.004

Sommer, A., Kordowski, F., Büch, J., Maretzky, T., Evers, A., Andrä, J., Düsterhöft, S., Michalek, M., Lorenzen, I., Somasundaram, P., Tholey, A., Sönnichsen, F. D., Kunzelmann, K., Heinbockel, L., Nehls, C., Gutsmann, T., Grötzinger, J., Bhakdi, S., & Reiss, K. (2016). Phosphatidylserine exposure is required for ADAM17 sheddase function. *Nature Communications*, *7*. https://doi.org/10.1038/ncomms11523

Soteros, B. M., & Sia, G. M. (2022). Complement and microglia dependent synapse elimination in brain development. In *WIREs Mechanisms of Disease* (Vol. 14, Number 3). John Wiley and Sons Inc. https://doi.org/10.1002/wsbm.1545

Soto-Heredero, G., Gómez de las Heras, M. M., Gabandé-Rodríguez, E., Oller, J., & Mittelbrunn, M. (2020). Glycolysis – a key player in the inflammatory response. In *FEBS Journal* (Vol. 287, Number 16, pp. 3350–3369). Blackwell Publishing Ltd. https://doi.org/10.1111/febs.15327

Squarzoni, P., Oller, G., Hoeffel, G., Pont-Lezica, L., Rostaing, P., Low, D., Bessis, A., Ginhoux, F., & Garel, S. (2014a). Microglia Modulate Wiring of the Embryonic Forebrain. *Cell Reports*, *8*(5), 1271–1279. https://doi.org/10.1016/j.celrep.2014.07.042

Squarzoni, P., Oller, G., Hoeffel, G., Pont-Lezica, L., Rostaing, P., Low, D., Bessis, A., Ginhoux, F., & Garel, S. (2014b). Microglia Modulate Wiring of the Embryonic Forebrain. *Cell Reports*, *8*(5), 1271–1279. https://doi.org/10.1016/j.celrep.2014.07.042

Sterling, H., Saginario, C., & Vignery, A. (1998). CD44 Occupancy Prevents Macrophage Multinucleation. In *The Journal of Cell Biology* (Vol. 143, Number 3). http://www.jcb.org

Stewart, C. L., Hook, A. L., Zelzer, M., Marlow, M., & Piccinini, A. M. (2024). Cellular and microenvironmental cues that promote macrophage fusion and foreign body response. *Frontiers in Immunology*, *15*. https://doi.org/10.3389/fimmu.2024.1411872

Stojilkovic, S. S., Leiva-Salcedo, E., Rokic, M. B., & Coddou, C. (2014). Regulation of ATP-gated P2X channels: From redox signaling to interactions with other proteins. In *Antioxidants and Redox Signaling* (Vol. 21, Number 6, pp. 953–970). Mary Ann Liebert Inc. https://doi.org/10.1089/ars.2013.5549

Stokes, L., Spencer, S. J., & Jenkins, T. A. (2015). Understanding the role of P2X7 in affective disorders—are glial cells the major players? *Frontiers in Cellular Neuroscience*, *9*(JULY), 1–6. https://doi.org/10.3389/fncel.2015.00258

Sun, R., & Jiang, H. (2024). Border-associated macrophages in the central nervous system. In *Journal of Neuroinflammation* (Vol. 21, Number 1). BioMed Central Ltd. https://doi.org/10.1186/s12974-024-03059-x

Suzuki, T., Hide, I., Ido, K., Kohsaka, S., Inoue, K., & Nakata, Y. (2004). Production and Release of Neuroprotective Tumor Necrosis Factor by P2X 7 Receptor-Activated Microglia. *Journal of Neuroscience*, *24*(1), 1–7. https://doi.org/10.1523/JNEUROSCI.3792-03.2004

Suzumura, A., Tamaru, T., Yoshikawa, M., & Takayanagi, T. (1999). Multinucleated giant cell formation by microglia: induction by interleukin Ž. IL-4 and IL-13. In *Brain Research* (Vol. 849). www.elsevier.comrlocaterbres

Tafani, M., Schito, L., Pellegrini, L., Villanova, L., Marfe, G., Anwar, T., Rosa, R., Indelicato, M., Fini, M., Pucci, B., & Russo, M. A. (2011). Hypoxia-increased RAGE and P2X7R expression regulates tumor cell invasion through phosphorylation of Erk1/2 and Akt and nuclear translocation of NF-κB. *Carcinogenesis*, *32*(8), 1167–1175. https://doi.org/10.1093/carcin/bgr101

Takaishi, H., Taniguchi, T., Takahashi, A., Ishikawa, Y., & Yokoyama, M. (2003). High glucose accelerates MCP-1 production via p38 MAPK in vascular endothelial cells. *Biochemical and Biophysical Research Communications*, *305*(1), 122–128. https://doi.org/10.1016/S0006-291X(03)00712-5

Takenouchi, T., Fujita, M., Sugama, S., Kitani, H., & Hashimoto, M. (2009). The role of the P2X7 receptor signaling pathway for the release of autolysosomes in microglial cells. In *Autophagy* (Vol. 5, Number 5, pp. 723–724). Taylor and Francis Inc. https://doi.org/10.4161/auto.5.5.8478

Tawbeh, A., Raas, Q., Tahri-Joutey, M., Keime, C., Kaiser, R., Trompier, D., Nasser, B., Bellanger, E., Dessard, M., Hamon, Y., Benani, A., Di Cara, F., Cunha Alves, T., Berger, J., Weinhofer, I., Mandard, S., Cherkaoui-Malki, M., Andreoletti, P., Gondcaille, C., & Savary, S. (2023). Immune response of BV-2 microglial cells is impacted by peroxisomal beta-oxidation. *Frontiers in Molecular Neuroscience*, *16*. https://doi.org/10.3389/fnmol.2023.1299314

Taylor, A. M. W., Mehrabani, S., Liu, S., Taylor, A. J., & Cahill, C. M. (2017). Topography of microglial activation in sensory- and affect-related brain regions in chronic pain. *Journal of Neuroscience Research*, *95*(6), 1330–1335. https://doi.org/10.1002/jnr.23883

Teitelbaum, S. L. (2007). Osteoclasts: What do they do and how do they do it? *American Journal of Pathology*, *170*(2), 427–435. https://doi.org/10.2353/ajpath.2007.060834

Teixeira, J. M., Oliveira, M. C. G., Parada, C. A., & Tambeli, C. H. (2010). Peripheral mechanisms underlying the essential role of P2X7 receptors in the development of inflammatory hyperalgesia. *European Journal of Pharmacology*, *644*(1–3), 55–60. https://doi.org/10.1016/j.ejphar.2010.06.061

Teo, I., Veryard, C., Barnes, H., An, S. F., Jones, M., Lantos, P. L., Luthert, P., & Shaunak, S. (1997). Circular Forms of Unintegrated Human Immunodeficiency Virus Type 1 DNA and High Levels of Viral Protein Expression: Association with Dementia and Multinucleated Giant Cells in the Brains of Patients with AIDS. In *JOURNAL OF VIROLOGY* (Vol. 71, Number 4). http://hiv-web.lanl.gov.],

Timmerman, R., Burm, S. M., & Bajramovic, J. J. (2018). An overview of in vitro methods to study microglia. In *Frontiers in Cellular Neuroscience* (Vol. 12). Frontiers Media S.A. https://doi.org/10.3389/fncel.2018.00242

Torres-Platas, S. G., Cruceanu, C., Chen, G. G., Turecki, G., & Mechawar, N. (2014). Evidence for increased microglial priming and macrophage recruitment in the dorsal anterior cingulate white matter of depressed suicides. *Brain, Behavior, and Immunity*, *42*, 50–59. https://doi.org/10.1016/j.bbi.2014.05.007

Troubat, R., Barone, P., Leman, S., Desmidt, T., Cressant, A., Atanasova, B., Brizard, B., El Hage, W., Surget, A., Belzung, C., & Camus, V. (2021). Neuroinflammation and depression: A review. *European Journal of Neuroscience*, *53*(1), 151–171. https://doi.org/10.1111/ejn.14720

Tsuda, M. (1959). Review Microglia-Mediated Regulation of Neuropathic Pain: Molecular and Cellular Mechanisms. In *Biol. Pharm. Bull* (Vol. 42, Number 12).

Usman, A., & Research Online, G. (2010). *Comparison of Foreign Body Giant Cells and Osteoclasts and the Role of CCL2, CCR2 and OC-STAMP in their Formation Thesis Type Rights statement*. https://doi.org/10.25904/1912/2343

Van Roy, F., & Berx, G. (2008). The cell-cell adhesion molecule E-cadherin. In *Cellular and Molecular Life Sciences* (Vol. 65, Number 23, pp. 3756–3788). https://doi.org/10.1007/s00018-008-8281-1

Verma, S. K., Leikina, E., Melikov, K., Gebert, C., Kram, V., Young, M. F., Uygur, B., & Chernomordik, L. V. (2018). Cell-surface phosphatidylserine regulates osteoclast precursor fusion. *Journal of Biological Chemistry*, *293*(1), 254–270. https://doi.org/10.1074/jbc.M117.809681

Vieira-da-Silva, B., & Castanho, M. A. R. B. (2023). Resazurin Reduction-Based Assays Revisited: Guidelines for Accurate Reporting of Relative Differences on Metabolic Status. *Molecules*, *28*(5). https://doi.org/10.3390/molecules28052283

Vilalta, A., & Brown, G. C. (2014). Deoxyglucose prevents neurodegeneration in culture by eliminating microglia. *Journal of Neuroinflammation*, *11*. https://doi.org/10.1186/1742-2094-11-58

Vilhardt, F. (2005). Microglia: Phagocyte and glia cell. In *International Journal of Biochemistry and Cell Biology* (Vol. 37, Number 1, pp. 17–21). Elsevier Ltd. https://doi.org/10.1016/j.biocel.2004.06.010

Volobоueva, L. A., Emery, J. F., Sun, X., & Giffard, R. G. (2013). Inflammatory response of microglial BV-2 cells includes a glycolytic shift and is modulated by mitochondrial glucose-regulated protein 75/mortalin. *FEBS Letters*, *587*(6), 756–762. https://doi.org/10.1016/j.febslet.2013.01.067

von Mücke-Heim, I. A., Martin, J., Uhr, M., Ries, C., & Deussing, J. M. (2023). The human P2X7 receptor alters microglial morphology and cytokine secretion following

immunomodulation. *Frontiers in Pharmacology*, *14*. https://doi.org/10.3389/fphar.2023.1148190

Walker, J. M. (2022). *Methods in Molecular Biology* (Anette Nicke, Ed.; 5210th ed.). Humana Press. http://www.springer.com/series/7651

Wang, H., He, Y., Sun, Z., Ren, S., Liu, M., Wang, G., & Yang, J. (2022). Microglia in depression: an overview of microglia in the pathogenesis and treatment of depression. In *Journal of Neuroinflammation* (Vol. 19, Number 1). BioMed Central Ltd. https://doi.org/10.1186/s12974-022-02492-0

Wang, J., Yang, C., Zhao, Q., Zhu, Z., Li, Y., & Yang, P. (2017). Microglia activation induced by serum of SLE patients. *Journal of Neuroimmunology*, *310*, 135–142. https://doi.org/10.1016/j.jneuroim.2017.07.010

Wang, L., Liu, Q., Zhang, Y., Chen, L., Hu, S., Zhang, Z., Wang, J., Cai, X., Jia, H., & He, X. (2019). Establishment of BV2 microglia polarization model and its effect on Toxoplasma gondii proliferation. *Research in Veterinary Science*, *125*, 382–389. https://doi.org/10.1016/j.rvsc.2019.08.002

Wang, L., Pavlou, S., Du, X., Bhuckory, M., Xu, H., & Chen, M. (2019a). Glucose transporter 1 critically controls microglial activation through facilitating glycolysis. *Molecular Neurodegeneration*, *14*(1). https://doi.org/10.1186/s13024-019-0305-9

Wang, M., Jin, G., Duan, T., Li, R., Gao, Y., Yu, M., & Xu, Y. (2025). Microglial phagocytosis and regulatory mechanisms: Key players in the pathophysiology of depression. In *Neuropharmacology* (Vol. 271). Elsevier Ltd. https://doi.org/10.1016/j.neuropharm.2025.110383

Wang, W. Y., Tan, M. S., Yu, J. T., & Tan, L. (2015). Role of pro-inflammatory cytokines released from microglia in Alzheimer's disease. In *Annals of Translational Medicine* (Vol. 3, Number 10). AME Publishing Company. https://doi.org/10.3978/j.issn.2305-5839.2015.03.49

Wang, Y., Jin, S., Sonobe, Y., Cheng, Y., Horiuchi, H., Parajuli, B., Kawanokuchi, J., Mizuno, T., Takeuchi, H., & Suzumura, A. (2014). Interleukin-1β induces blood-brain barrier disruption by downregulating sonic hedgehog in astrocytes. *PLoS ONE*, *9*(10). https://doi.org/10.1371/journal.pone.0110024

Wang, Y., Qi, Y., Qi, J., Wu, J., Lin, F., Cui, X., Ge, J., & Liu, Z. (2022). Activin A is a novel chemoattractant for migration of microglial BV2 cells. *Journal of Neuroimmunology*, *371*. https://doi.org/10.1016/j.jneuroim.2022.577929

Wang, Y., Szretter, K. J., Vermi, W., Gilfillan, S., Rossini, C., Cella, M., Barrow, A. D., Diamond, M. S., & Colonna, M. (2012). IL-34 is a tissue-restricted ligand of CSF1R required for the development of Langerhans cells and microglia. *Nature Immunology*, *13*(8), 753–760. https://doi.org/10.1038/ni.2360

Wang, Z., Bo, H., Cheng, C., Gan, T., Peng, J., Zou, Y., Jiang, H., & Wang, H. (2025). Analysis of the efficacy of Langhans giant cells in controlling cutaneous Mycobacterium marinum infections. *International Immunopharmacology*, *148*. https://doi.org/10.1016/j.intimp.2024.114003

Watters, J. J., Sommer, J. A., Fisette, P. L., Pfeiffer, Z. A., Aga, M., Prabhu, U., Guerra, A. N., Denlinger, L. C., & Bertics, P. J. (2001). P2X7 nucleotide receptor: Modulation of LPS-

induced macrophage signaling and mediator production. *Drug Development Research*, *53*(2–3), 91–104. https://doi.org/10.1002/ddr.1176

Wei, J., Wang, M., Jing, C., Keep, R. F., Hua, Y., & Xi, G. (2020). Multinucleated Giant Cells in Experimental Intracerebral Hemorrhage. *Translational Stroke Research*, (11), 1095–1102. https://doi.org/10.1007/s12975-020-00790-4/Published

Wenger, D. A., & Luzi, P. (2024). Krabbe disease: globoid cell leukodystrophy. In *Rosenberg's Molecular and Genetic Basis of Neurological and Psychiatric Disease, Seventh Edition: Volume 1* (Vol. 1, pp. 593–603). Elsevier. https://doi.org/10.1016/B978-0-443-19041-4.00043-1

Whitlock, J. M., & Chernomordik, L. V. (2021). Flagging fusion: Phosphatidylserine signaling in cell–cell fusion. In *Journal of Biological Chemistry* (Vol. 296). American Society for Biochemistry and Molecular Biology Inc. https://doi.org/10.1016/j.jbc.2021.100411

Whitlock, J. M., Leikina, E., Melikov, K., De Castro, L. F., Mattijssen, S., Maraia, R. J., Collins, M. T., & Chernomordik, L. V. (2023). Cell surface-bound La protein regulates the cell fusion stage of osteoclastogenesis. *Nature Communications*, *14*(1). https://doi.org/10.1038/s41467-023-36168-x

Wittrant, Y., Theoleyre, S., Couillaud, S., Dunstan, C., Heymann, D., & Rédini, F. (2003). Regulation of osteoclast protease expression by RANKL. *Biochemical and Biophysical Research Communications*, *310*(3), 774–778. https://doi.org/10.1016/j.bbrc.2003.09.084

Wu, H., Yin, Y., Hu, X., Peng, C., Liu, Y., Li, Q., Huang, W., & Huang, Q. (2019). Effects of Environmental pH on Macrophage Polarization and Osteoimmunomodulation. *ACS Biomaterials Science and Engineering*, *5*(10), 5548–5557. https://doi.org/10.1021/acsbiomaterials.9b01181

Xia, C. Y., Guo, Y. X., Lian, W. W., Yan, Y., Ma, B. Z., Cheng, Y. C., Xu, J. K., He, J., & Zhang, W. K. (2023). The NLRP3 inflammasome in depression: Potential mechanisms and therapies. In *Pharmacological Research* (Vol. 187). Academic Press. https://doi.org/10.1016/j.phrs.2022.106625

Xie, Y., Qian, Y., Wang, Y., Liu, K., & Li, X. (2020). Mechanical stretch and LPS affect the proliferation, extracellular matrix remodeling and viscoelasticity of lung fibroblasts. *Experimental and Therapeutic Medicine*, *20*(5), 1–1. https://doi.org/10.3892/etm.2020.9133

Xu, F., & Teitelbaum, S. L. (2013). Osteoclasts: New Insights. In *Bone Research* (Vol. 1, pp. 11–26). Sichuan University. https://doi.org/10.4248/BR201301003

Yan, X., Hu, Y., Wang, B., Wang, S., & Zhang, X. (2020). Metabolic Dysregulation Contributes to the Progression of Alzheimer's Disease. In *Frontiers in Neuroscience* (Vol. 14). Frontiers Media S.A. https://doi.org/10.3389/fnins.2020.530219

Yang, D., He, Y., Muñoz-Planillo, R., Liu, Q., & Núñez, G. (2015). Caspase-11 Requires the Pannexin-1 Channel and the Purinergic P2X7 Pore to Mediate Pyroptosis and Endotoxic Shock. *Immunity*, *43*(5), 923–932. https://doi.org/10.1016/j.immuni.2015.10.009

Yang, S. J., Shao, G. F., Chen, J. L., & Gong, J. (2018). The NLRP3 Inflammasome: An Important Driver of Neuroinflammation in Hemorrhagic Stroke. In *Cellular and Molecular Neurobiology* (Vol. 38, Number 3, pp. 595–603). Springer New York LLC. https://doi.org/10.1007/s10571-017-0526-9

Yao, Y., & Fu, K. Y. (2020). Serum-deprivation leads to activation-like changes in primary microglia and BV-2 cells but not astrocytes. *Biomedical Reports*, *13*(5), 1–8. https://doi.org/10.3892/br.2020.1358

Yasui, K., Yashiro, M., Nagaoka, Y., Manki, A., Wada, T., Tsuge, M., Kondo, Y., & Morishima, T. (2009). Thalidomide prevents formation of multinucleated giant cells (Langhans-type) from cultured monocytes: possible pharmaceutical applications for granulomatous disorders. In *INTERNATIONAL JOURNAL OF IMMUNOPATHOLOGY AND PHARMACOLOGY* (Vol. 22, Number 3).

Yilmaz, C., Karali, K., Fodelianaki, G., Gravanis, A., Chavakis, T., Charalampopoulos, I., & Alexaki, V. I. (2019). Neurosteroids as regulators of neuroinflammation. In *Frontiers in Neuroendocrinology* (Vol. 55). Academic Press Inc. https://doi.org/10.1016/j.yfrne.2019.100788

Yirmiya, R., Rimmerman, N., & Reshef, R. (2015). Depression as a Microglial Disease. In *Trends in Neurosciences* (Vol. 38, Number 10, pp. 637–658). Elsevier Ltd. https://doi.org/10.1016/j.tins.2015.08.001

Zengeler, K. E., & Lukens, J. R. (2021). Innate immunity at the crossroads of healthy brain maturation and neurodevelopmental disorders. In *Nature Reviews Immunology* (Vol. 21, Number 7, pp. 454–468). Nature Research. https://doi.org/10.1038/s41577-020-00487-7

Zhan, L., Krabbe, G., Du, F., Jones, I., Reichert, M. C., Telpoukhovskaia, M., Kodamaid, L., Wangid, C., Cho, S. H., Sayed, F., Li, Y., Leid, D., Zhou, Y., Shen, Y., West, B., & Gan, L. (2019). Proximal recolonization by self-renewing microglia re-establishes microglial homeostasis in the adult mouse brain. *PLoS Biology*, *17*(2). https://doi.org/10.1371/journal.pbio.3000134

Zhang, C., Dou, C., Xu, J., & Dong, S. (2014). DC-STAMP, the key fusion-mediating molecule in osteoclastogenesis. *Journal of Cellular Physiology*, *229*(10), 1330–1335. https://doi.org/10.1002/jcp.24553

Zhang, H., Li, F., Yang, Y., Chen, J., & Hu, X. (2015). SIRP/CD47 signaling in neurological disorders. In *Brain Research* (Vol. 1623, pp. 74–80). Elsevier B.V. https://doi.org/10.1016/j.brainres.2015.03.012

Zhang, J., Gao, L., Zhang, Y., Wang, H., Sun, S., & Wu, L. an. (2024). Involvement of microglial P2X7 receptor in pain modulation. In *CNS Neuroscience and Therapeutics* (Vol. 30, Number 1). John Wiley and Sons Inc. https://doi.org/10.1111/cns.14496

Zhang, M., Sun, Y., Zhang, Y., Wang, Z., Wang, Z. Y., Ming, X. Y., & Guo, Z. D. (2023). Lipopolysaccharide and lipoteichoic acid regulate the PI3K/AKT pathway through osteopontin/integrin β3 to promote malignant progression of non-small cell lung cancer. *Journal of Thoracic Disease*, *15*(1), 168–185. https://doi.org/10.21037/jtd-22-1825

Zubova, S. G., Suvorova, I. I., & Karpenko, M. N. (2022). Macrophage and microglia polarization: Focus on autophagy-dependent reprogramming. In *Frontiers in Bioscience - Scholar* (Vol. 14, Number 1). Bioscience Research Institute. https://doi.org/10.31083/J.FBS1401003